LATERAL DYNAMICS AND CONTROL OF RAIL VEHICLES

by

ROBERT LEE JEFFCOAT

S.B., S.M., Mech. E., Massachusetts Institute of Technology
(1972)

SUBMITTED IN PARTIAL FULFILLMENT
OF THE REQUIREMENTS FOR THE
DEGREE OF

DOCTOR OF PHILOSOPHY

at the

MASSACHUSETTS INSTITUTE OF TECHNOLOGY

OCTOBER, 1974
b.c. February 1975

Signature redacted

Signature of Author . . . . . .
Department of Mechanical Engineering, September 30, 1974

Signature redacted

Certified by . . . . . .
Thesis Supervisor

Signature redacted

Accepted by . . . . . .
Chairman, Department Committee on Graduate Students

ARCHIVES
MASS. INST. TECH.
MAR 3 1975
LIBRARIES

LATERAL DYNAMICS AND CONTROL OF RAIL VEHICLES

by

Robert Lee Jeffcoat

Submitted to the Department of Mechanical Engineering on September 30, 1974, in partial fulfillment of the requirements for the degree of Doctor of Philosophy.

ABSTRACT

An analytical investigation of the lateral dynamic behavior of two-truck railway vehicles using steel wheels and steel rails is described. Measures used to assess dynamic performance are maximum stable operating speed and, for a specified rail roughness input, power spectral density of lateral acceleration in the passenger compartment (ride quality) and the RMS lateral tracking error. Static suspension performance is measured by the lateral tracking error produced by steady curving. Linear, lumped-parameter models are used to represent the carbody and trucks. Trucks are modelled as rigid in the plane of the rails. Two models for the carbody are employed: a rigid body with translational and yaw freedom and with a truck at each end, and a translational mass with no yaw freedom and a single truck. The latter model is simpler, and is shown to be a useful approximation to the former in predicting the influence of suspension parameters. Inclusion of yaw freedom introduces further vibrational modes of the carbody which can reduce ride quality or cause instability.

Vehicles with conventional rigid trucks, having opposite wheels connected by rigid axles, are subject to lightly damped lateral oscillations ("hunting") which may become unstable even at low speeds. The effects of various suspension parameters on hunting are discussed. An automatic controller is defined to supplement the action of the secondary suspension. Two special cases of the general controller (active steering, and asymmetry in the passive suspension) are examined in detail and both shown to be capable of improving all three measures of dynamic performance significantly; both, however, can degrade steady curving ability.

The use of rigid trucks with independently rotating wheels, ground to a concave tread profile to provide guidance, is evaluated and found to be highly beneficial in improving ride quality, and to eliminate the cause of hunting instability. Such trucks exhibit less tracking error due to steady curving at low speeds than do conventional trucks, but more at high speeds.

Thesis Supervisor: David N. Wormley
Title: Associate Professor of Mechanical Engineering

ACKNOWLEDGEMENTS

The author gratefully acknowledges the support of the National Science Foundation, which, through a Graduate Fellowship, made this work possible. Thanks are also due to the Association of American Railroads for both technical and financial assistance.

To his supervisor, Professor David Wormley, and to the other members of his thesis committee, Professors Huw Davies, Herbert Richardson, Richard Sidell, and David Wilson, the author is especially indebted for their patience and sound advice.

Numerous conversations with Dr. Herbert Weinstock and his colleagues in the Transportation Systems Center of the U. S. Department of Transportation have been most helpful. Professor Joel Moses and Dr. Richard Bogen of Project MAC have also offered valuable suggestions.

From his fellow students at M. I. T. the author has enjoyed a constant flow of information, ideas, encouragement, and friendship. Particular appreciation goes to Ashok Boghani, Nikos Dagalakis, Woodie Flowers, Arnold Gilchrist, Larry Hare, Stanley Knutson, Douglas Limbert, Michael Lynch, Octavio Maizza Neto, Donald Margolis, Takeshi Ono, Bulent Platin, John Polley, Steven Rock, Sergio Simunovic, Edward Snyder, Larry Sweet, Masayoshi Tomizuka, Marc Weinberg, and David Wilson.

The author is deeply grateful to his parents and to his wife Marjorie for their unflagging interest and support.

TABLE OF CONTENTS

Abstract 2
Acknowledgements 3
Table of Contents 4
Symbols and Abbreviations 8

BACKGROUND

1. Introduction and Summary 13

1. Place of Rail Systems in Ground Transportation 13
2. Special Problems of the Rail Lateral Guidance System 16
3. Design Considerations for Lateral Suspensions 23
4. High-Speed Rail Systems Proposed or In Service 26
5. Scope and Summary of This Work 28

2. Survey of Prior Research 31

1. Fundamental Studies of Wheel-Rail Interactions 31
2. Properties of Track 35
3. Curving Analyses 36
4. Dynamic Models 37
5. Novel Designs 41
6. Automatic Control 42
7. Systems Studies 43
8. Overview; Gaps in the Literature 44

BEHAVIOR OF UNCONTROLLED VEHICLES

3. Component and System Models 47

1. Vehicle Subsystems and Coordinate System 48
2. Modelling Assumptions 51
3. Carbody Models 53
4. Secondary Suspension Models 57
5. Truck Models 59
6. Equations of Motion: LMO Complete Vehicle 68
7. Equations of Motion: RPB Complete Vehicle 72
8. Acceleration Transfer Functions 75
9. Baseline Parameter Values 80
10. Importance of Finite-Mass Vehicle Body Models 86
11. Characterization of Rail Profile 91

4. Performance of Conventional Vehicle with Lateral-Mass-Only Carbody, Uncontrolled 93

1. Stability 93
2. Ride Quality 101
3. Phasing of Inputs 112
4. Tracking Error 115
5. K-B-Series Yaw Secondary 117
6. Overview 122

5. Performance of Vehicle with Lateral-Mass-Only Carbody and Rigid Truck with Independently-Rotating Wheels 124

1. Equivalent RIW-LMO Mechanical System 124
2. Stability 127
3. Ride Quality 128
4. Tracking Error 129
5. Overview 136

PERFORMANCE IMPROVEMENT WITH CONTROL

6. Model for an Automatically Controlled Secondary Suspension 138

1. Rationale 138
2. Controller Definition 139
3. Special Cases 141
4. Equations of Motion -- LMO Carbody 146
5. Equations of Motion -- RPB Carbody 147
6. Acceleration Transfer Function: LMO Complete Vehicle 147
7. Control Power 147
8. Other Practical Considerations 156

7. Performance of Actively Steered Conventional Vehicle with Lateral-Mass-Only Carbody 160

1. Controller Notation and Operation 160
2. Stability 163
3. Ride Quality 166
4. Tracking Error 171
5. Control Power 171
6. Overview 174

8. Performance of Conventional Vehicle Model with Lateral-Mass-Only Carbody and Asymmetric Secondary Suspension 177

1. Physical Constraints 177
2. Notation 180
3. Stability 180
4. Ride Quality 182
5. Tracking Error 185
6. Overview 185

FULL VEHICLE PERFORMANCE

9. Performance of Vehicles Using Rigid-Plane-Body Carbody Model 189

1. Response of a Symmetric Plane Body 189
2. Behavior of a Conventional Vehicle 194
3. Behavior of Vehicle with Independently-Rotating Wheels 199
4. Behavior of Actively Steered RC-RPB Vehicle 199
5. Behavior of RC-RPB Vehicle with Passive Asymmetric Secondary 209
6. Discussion 212

10. Tracking Error due to Steady Curving 214

1. Simplifying Assumptions 214
2. Governing Equations 217
3. RC Curving with Conventional Suspension 223
4. RIW Curving with Conventional Suspension 223
5. RC Curving with Steering Control 229
6. RC Curving with Asymmetric Secondary 229
7. Other Effects 231
8. Observations on Steady Curving 233

- - -

11. Conclusions and Recommendations 235

1. Usefulness of the LMO Carbody Model 235
2. Modifications to Conventional Suspension 237
3. The RC Truck with Active Steering Control 238
4. The RC Truck with Asymmetric Secondary 239
5. The RIW Truck 239
6. Improvement of Models 240
7. Further Control Studies 241
8. Design and Experiment 242

List of References 244

APPENDICES

A. Gravitational Stiffness 250

1. Idealized Wheel-Rail Contact Geometry 250
2. Forces at the Interface 252
3. Choice of Initial Displacement 253
4. Sensitivity to Initial Displacement 253
5. Degree of Nonlinearity in Lateral Force Relationship 253
6. Yaw Gravitational Stiffness 256

B. Matrix Methods for Frequency-Domain Analysis 258

1. System Representation in State Variable Form 258
2. Compressed Matrices 259
3. Solution for Transfer Functions 260
4. Implementation of Symbolic Transfer Functions Using MACSYMA 261

Biographical Note 264

SYMBOLS AND ABBREVIATIONS

In the following list of symbols, ι represents a numerical subscript.

A	rail roughness parameter
$\underline{A}$	system characteristic matrix, Laplace transformed
$\hat{\underline{A}}$	compressed and Laplace transformed characteristic matrix
$\underline{a}$	characteristic matrix
B_b	secondary suspension yaw damping
B_c	secondary suspension lateral damping
$\underline{B}$	system input matrix, Laplace transformed
$\hat{\underline{B}}$	input matrix, compressed and Laplace transformed
$\underline{b}$	input matrix
D_ι	control gains (Equations 6.2.1 and 6.2.2)
e	base of the natural logarithms
F	any force
F_b	passive lateral secondary force
F_{bc}	active lateral secondary force
f	creep coefficient
G	any transfer function
G_a	carbody lateral acceleration transfer function
G_{TE}	truck center lateral tracking error transfer function
g_ι	parameter groups (Table 3-1)
g_5	$4f/(m_b V)$
H	any transfer function
h	half rail gauge

I_b truck moment of inertia around center of mass

I_c carbody moment of inertia around center of mass

$\bar{I}_c$ $I_c/(2m_cL^2)$, normalized carbody inertia

$\vec{i}$ unit vector, forward direction

j $\sqrt{-1}$

$\vec{j}$ unit vector, lateral direction

K_b secondary suspension yaw stiffness

K_c secondary suspension lateral stiffness

K_L linearized lateral gravitational stiffness, per wheel

k ratio of wheelbase to gauge

k_s k^2 for independently rotating wheels; k^2+1 for rigid wheelsets

L half carbody length between truck attachment points

ℓ_b distance to outboard truck dampers

ℓ_k distance to outboard truck springs

m_b truck mass

m_c half carbody mass

n order of system

P time derivative operator

q_ℓ m_bL/I_c

R radius of steady curving

R_w wheel tread radius of curvature

R_r railhead radius of curvature

r wheel rolling radius

r_0 nominal or centered wheel rolling radius

S_l parameter group (Table 3-2)

$\underline{S}$ matrix of Laplace variables (Appendix B)

s Laplace variable

T any torque

T_b passive secondary yaw torque

T_{bc} active secondary yaw torque

t time

V forward speed

V_c critical speed, at which lateral motions become unstable

v any lateral speed, $=\dot{y}$

v_b $\dot{y}_b$

v_c $\dot{y}_c$

x distance along direction of forward motion

y any lateral displacement from track nominal centerline

y_b lateral displacement of truck center of mass

y_c lateral displacement of carbody center of mass

y_{rf} lateral displacement of actual rail centerline at front wheels

y_{rb} lateral displacement of actual rail centerline at rear wheels

y_0 initial lateral displacement of profiled wheels (Appendix A)

α effective conicity

$\Delta[]$ pure delay operator

ΔR $R_w - R_r$

δ^+ $(1+e^{-\tau s})/2$

δ^- $(1-e^{-\tau s})/2$

δ^L $e^{-\tau_L s}$

ε $(\varepsilon_1, \varepsilon_2, \varepsilon_3)$, the list of active steering gains

ε_i active steering control gains (Equations 7.1.4 - 7.1.6)

ξ damping ratio

κ (σ_k,σ_b), the list of asymmetries

λ a wavelength

μ coefficient of sliding friction

ν frequency (circular)

π 3.141...

ρ_m m_b/m_c

ρ_{bb} $B_b V/(4fh^2k_s)$

ρ_{bc} $B_c V/(4f)$

σ_b secondary damper asymmetry

σ_k secondary stiffness asymmetry

τ 2kh/V, wheelbase time delay

τ_L 2L/V, carbody time delay

Φ_i any input power spectral density

Φ_o any output power spectral density

Φ_{yy} power spectral density of rail lateral centerline roughness

ϕ_b yaw angle of truck

ϕ_c yaw angle of carbody

Ω V/r_0, rotational speed of axle

ω_b $\dot{\phi}_b$

ω_c $\dot{\phi}_c$

ω_k kinematic hunting frequency (radian), $V\cdot\sqrt{\alpha/k_s r_0 h}$

Abbreviations

A.S.D.	acceleration power spectral density in the carbody, lateral
HFA	high-frequency asymptote of A.S.D.
HFE	envelope of HFA, neglecting out-of-phase contributions
LFA	low-frequency asymptote of A.S.D.
LMO	lateral-mass-only carbody (lateral freedom only)
RC	rigid conventional truck (rigid axles)
RIW	rigid truck with independently rotating wheels
RPB	rigid-plane-body (lateral and yaw freedom)

Subscripts

$()_b$	truck (or bogie) at center of mass; pertaining to dampers
$()_c$	carbody, at center of mass
$()_{cb}$	carbody, at truck attachment point
$()_{cr}$	due to creep forces
$()_g$	due to gravitational forces
$()_i$	arbitrary numerical index; or input
$()_k$	pertaining to springs
$()_L$	pertaining to carbody length
$()_o$	output
$()_r$	rail

CHAPTER 1

INTRODUCTION AND SUMMARY

Rail systems occupy an important place among ground transportation modes. They also exhibit certain unique dynamic characteristics which have constrained high-speed operation. With the increasing demand for faster, more comfortable ground transportation, railway technology is being seriously re-examined in an effort to relax these constraints. Essentially conventional systems in Europe, Japan, and the United States are operating in or planned for a speed range around 150 miles per hour; but such speeds are attained only with elaborate suspensions and over exceptionally good track. The research described herein was undertaken to discover how the performance of rail vehicles may be enhanced by the use of unconventional design approaches -- especially automatic control techniques. Emphasis is on passenger vehicles, but much of this work is also applicable to high-speed freight cars.

1. Place of Rail Systems in Ground Transportation. The railroad was historically the first machine-powered means of ground transportation, and it has risen to a position of major importance in the century since its invention. The bulk of land freight is moved by rail, at least along some of its route, since this mode offers reasonable speed together with an excellent ratio of payload to power. Passenger service by rail has declined in recent years, however, in the face of the automobile's greater flexibility and the airplane's higher

speed; the drop has been especially severe in the United States, where affluence and long travel distances have encouraged the shift to the latter modes.

Recent studies [1,2]* have indicated, however, that there would be a significant demand for intercity passenger service which would be competitive with air in speed, cost, comfort, convenience, and safety. Cruise speeds in the range of 100 - 300 mph would be required for successful intercity operation. Another important and growing application of tracked ground transportation is in urban rapid transit systems, where speeds are moderate but other operating requirements (curve negotiation, braking, and passenger comfort, for example) are severe.

Other systems besides rails are suitable for tracked vehicles. Rubber tires [3] offer a smooth ride, good tolerance to guideway irregularities, and low "footprint" pressure (with correspondingly low guideway wear). Tires, however, are subject to thermal deterioration due to flexural deformations and appear unsuitable for high-speed operation. Their use in rapid transit installations has been plagued by high maintenance costs. Two types of non-contacting suspensions appear to offer great promise for high-speed applications.

---

*Numbers in square brackets refer to the List of References at the end of this thesis.

By the use of air cushions [4] or magnetic levitation [5], friction at the vehicle-guideway interface can be greatly reduced. The advantages of low footprint pressure mentioned in connection with rubber tires are more significant in these cases, where the cushion or magnet may be several feet in extent. The disadvantages of air cushion or magnetic suspensions lies in their use of power to produce levitation. To keep power requirements down, they must be designed to operate with very small gaps; but small suspension gaps require smooth guideway surfaces in order to prevent contact with and possible damage to the suspension.

Steel wheels rolling on steel rails provide both support and guidance passively; no levitation power is required. The rolling friction is quite low for steel surfaces, unlike rubber on pavement. The railroad guideway is not especially inexpensive -- at least when designed for 200 mph operation -- but it is geometrically simple and largely prefabricated. The small area of the rail contact surface is subject to high stress and wear, but less liable to crippling accumulations of ice and snow than the broad, flat guideways required for air cushions or repulsive magnetic suspensions.

Perhaps most important, there already exists an extensive network of railroads and a large investment in railway equipment. If steel wheel / steel rail technology can be adapted to the needs of high-speed ground transportation, and if care is given to the requirements of compatibility between the new and old systems, the transition may be done in stages (staged introduction of fast service may be seen

in the cases of the Metroliner and TurboTrain in this country).

2. Special Problems of the Rail Lateral Guidance System. The use of flanged wheels to guide a vehicle along a track is familiar and perhaps obvious, but the resulting system shows a type of behavior not found with other forms of guidance. Certain concepts essential to an understanding of railway guidance will be introduced here.

Early systems used cylindrical wheels, and relied upon flanges inside each rail to limit lateral displacement of the wheel and thus to guide the vehicle along the track. It was later recognized that by making the running surface of each wheel conical -- the apices outside the rails as in Figure 1-1 -- a self - centering action was obtained. Conical wheels significantly reduced rail wear by suppressing the tendency of cylindrical wheels to run with one flange continually against the rail, but they introduced a phenomenon called hunting.

Hunting is a self - excited, speed - dependent sinuous motion of the wheelset along the track. The hunting motion of a single, unrestrained wheelset (i.e., two wheels connected by a rigid axle) is illustrated in Figure 1-2. Assuming pure rolling contact and a cone half - angle of α, a lateral displacement y of the wheelset from its centered position results in the radii of the two wheels being changed from the centered (nominal) radius of r_0 to:

$$r_+ = r_0 + \alpha y \quad \text{for the left wheel, and} \quad (1.2.1)$$

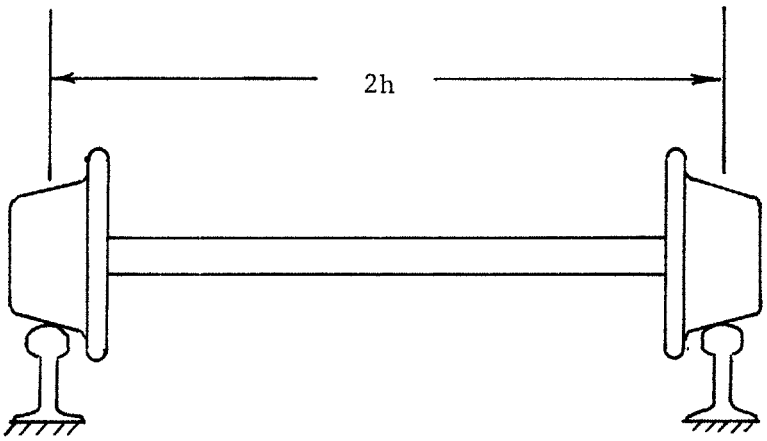

(a)

View of Coned Wheelset

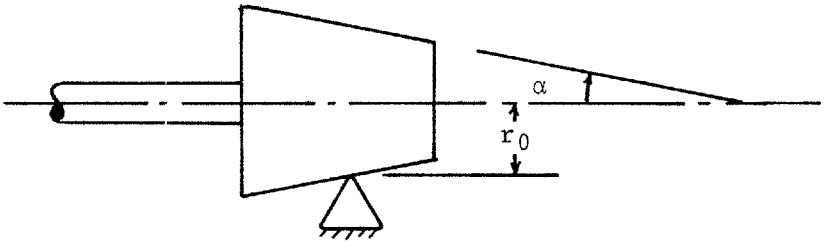

(b)

Simplified Wheel - Rail Contact Geometry

FIGURE 1-1

Rigid Wheelset Geometry

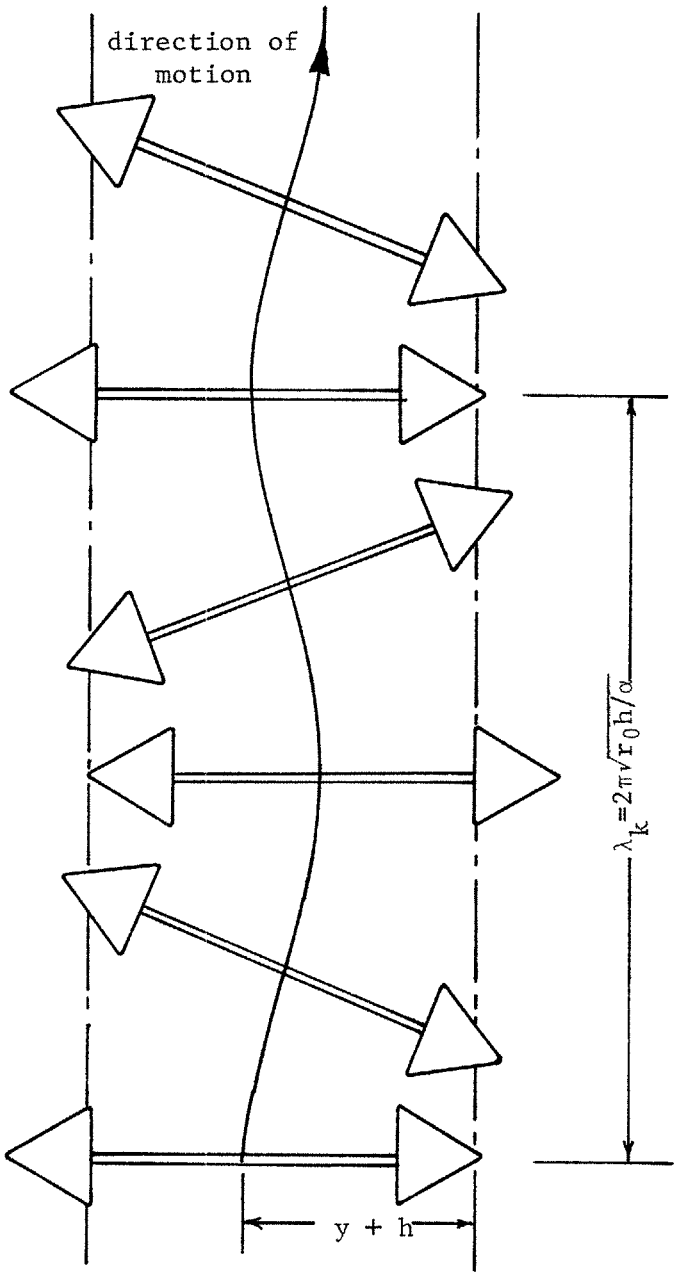

FIGURE 1-2

Kinematic Hunting of an Unrestrained Wheelset

$$r_- = r_0 - \alpha y \quad \text{for the right.} \tag{1.2.2}$$

Due to this difference in rolling radius, the wheelset is steered back toward the center of the track. Let ϕ be the yaw angle of the wheelset about a vertical axis; then if the angular velocity of spin of the wheelset about the axle is Ω,

$$d\phi/dt = -\Omega(r_+ - r_-) \,/\, 2h \;; \tag{1.2.3}$$

the track gauge is 2h. Substituting (1.2.1) and (1.2.2) gives

$$d\phi/dt = -V\alpha y \,/\, r_0 h \;, \tag{1.2.4}$$

where the substitution $V=\Omega r_0$ for the forward speed of the wheelset has been included. Finally, noting that $dy/dt=V\phi$,

$$\frac{d^2y}{dt^2} = \frac{-V^2\alpha}{r_0 h}\, y \;. \tag{1.2.5}$$

This is the equation of a linear, undamped, second - order oscillator whose frequency,

$$\omega_k = V\sqrt{\alpha/r_0 h} \;, \tag{1.2.6}$$

is called the kinematic hunting frequency. Notice that since this frequency is proportional to V, the wheelset will trace out a path of constant wavelength, regardless of speed.

The tendency of the wheelsets to oscillate at their kinematic hunting frequency manifests itself in two different types of vehicle motion, broadly termed <u>primary hunting</u> and <u>secondary hunting</u>. Primary hunting, so called because it is usually important at low

speeds, involves relatively large motions of the carbody with little wheelset motion. It occurs when the kinematic hunting frequency coincides with some natural frequency of the carbody-suspension system. Secondary hunting involves large-amplitude wheelset oscillations with little relative lateral carbody movement. Primary hunting can be unstable, but the term is used to apply to any large-amplitude carbody response due to resonance. Secondary hunting, similarly, refers to large wheelset oscillations whether stable or unstable. For most speeds, there exist lightly damped oscillatory modes which cannot be unambiguously identified as either primary or secondary hunting; such situations fall only into the generic category of kinematic hunting.

The pure rolling assumption made in the derivation of kinematic hunting provides no mechanism for either damping or growth of oscillations. The situation is different, however, when the effects of inertia and finite coefficient of friction are included. Since any slippage at the wheel / rail interface will result in imperfect steering action, the motion of a real wheelset can exhibit unstable growth in amplitude (limited, it is to be hoped, by impact of the wheel flanges against the rails). An unrestrained wheelset will be unstable at any forward speed. Attached to a vehicle, a wheelset may be stabilized in several ways -- the most usual one being to introduce a yaw stiffness between wheelset and carbody -- but any such stabilization through conventional means is effective for only

a limited range of speed. There exists a linear critical speed of forward vehicle motion, V_c, below which the motion is stable and above which it is unstable [6].

The rigid coned wheelset is also central to the quasi-steady curving mechanism of a conventional rail vehicle. Consider a single wheelset negotiating a curve of constant radius R in pure rolling, as in Figure 1-3. The yaw angular velocity of the wheelset must be

$$\dot{\phi} = -V / R \quad . \tag{1.2.7}$$

Equation 1.2.4 continues to apply; combining these two equations yields

$$y = r_0 h / \alpha R \tag{1.2.8}$$

as the lateral tracking error for kinematic curving of a single unrestrained wheelset. Observe that no mention has been made of centripetal force, slippage, or yaw restraint of the wheelset; these effects, if present, further increase the error and introduce yaw deviation away from the radial. Curving of conventional

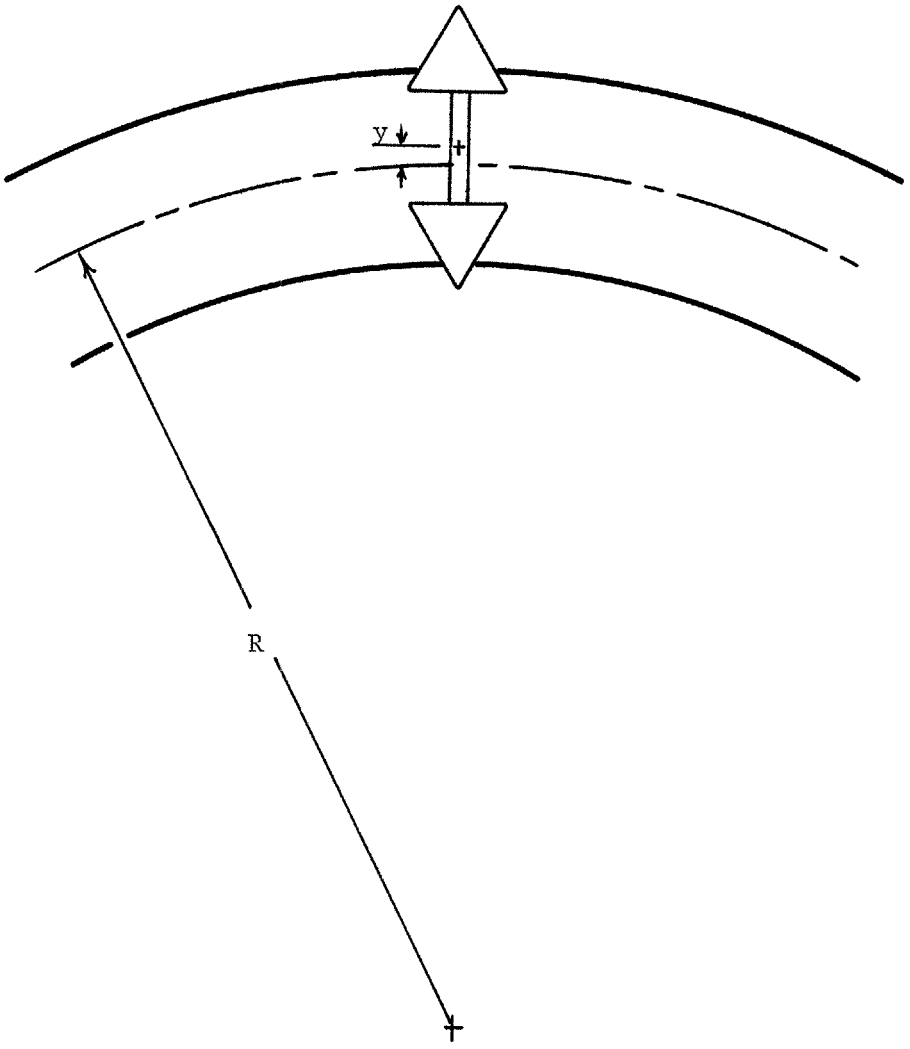

FIGURE 1-3

Quasi - Steady Curving of an Unrestrained Wheelset

vehicles will be examined in Chapter 10.

In summary, a rail vehicle derives lateral guidance not from any stiffness in the lateral direction, but rather from a steering action coupled with the vehicle's forward motion. (An exception is the independently - rotating wheel suspension which will be introduced in Chapter 3.) The resulting dynamic system is lightly damped and prone to instability. For these reasons it is of both interest and importance to study lateral dynamics and to bring them under control.

3. Design Considerations for Lateral Suspensions. The preceding section suggests that the requirements for a satisfactory lateral suspension may be quite different from those for a vertical suspension. The similarities and differences will now be briefly discussed.

A lateral suspension is not called upon to support the static weight of the vehicle. It shares with the vertical suspension, however, the function of negotiating the track while partially isolating the passenger compartment from the effects of track irregularities. The primary function of the suspension thus has two facets: tracking accuracy and ride comfort. Tracking accuracy in the lateral direction is important for several reasons. There is a limited amount of clearance beside the track, so the vehicle may only deviate so far from its nominal course without danger of interference. Similarly, tracking should be good enough that the wheel flanges very seldom contact the rails. Flange impact (flanging) is undesirable because it is felt by the passengers as a jolt, to the

detriment of comfort; because it accelerates wear of both wheel and rail; and because it increases the likelihood of wheel climb and possible derailment. Tracking error may be caused by the kinematic constraints and centripetal force encountered in curves, and by the suspension's dynamic response to track irregularities. Wind loading on the vehicle is another source of error, and one which may be expected to become more important with increasing speed.

The issue of ride comfort quantification has yet to be satisfactorily resolved, but it is generally accepted that acceleration experienced in the passenger compartment is an important -- if incomplete -- measure of discomfort [7,8]. One of the more satisfactory methods of expressing ride comfort is by displaying the acceleration power spectral density of the passenger compartment, given a specified track geometry and vehicle speed, in comparison with some standard spectrum which has been shown to be acceptable and which takes into consideration the variation of human sensitivity to vibration with frequency. Such a standard can of course be only a guideline until a better understanding of what determines comfort is obtained. The standard acceleration spectral density profile which will be referred to herein is one which was proposed by the U. S. Department of Transportation for the Urban Tracked Air Cushion Vehicle (UTACV -- now termed the Prototype TACV, or PTACV) and is based on measurements of the ride of a Metroliner coach [9] -- see Figure 1-4. Notice that the requirements are somewhat more strict in the lateral direction than in the vertical.

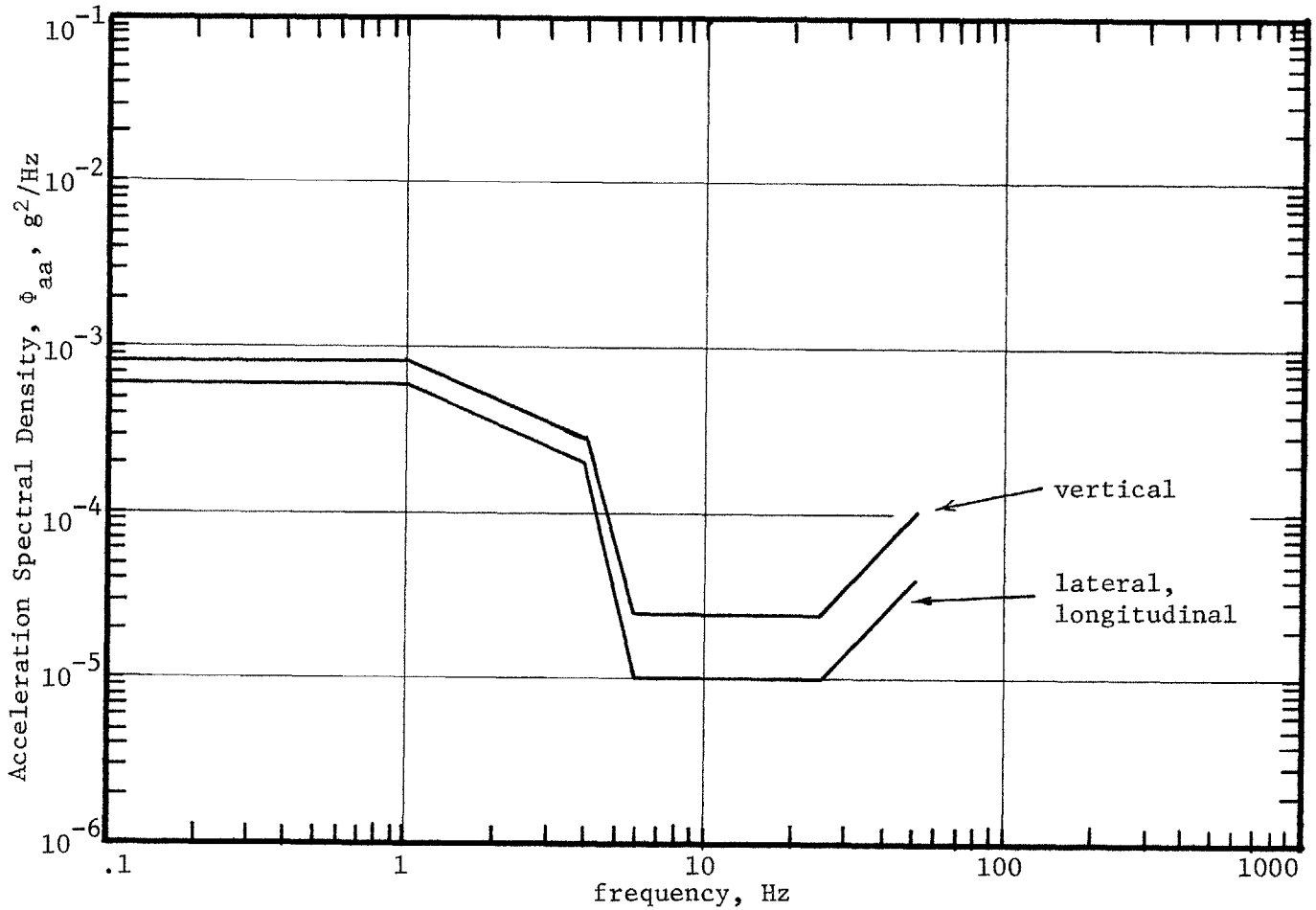

FIGURE 1-4

Recommended Standards for Acceleration Power Spectral Density

Stability is a vital aspect of suspension performance which, although it figures in both tracking error and ride comfort, deserves separate mention. The term "stable" as used in the context of this thesis refers to asymptotic stability of the linearized, small - disturbance model. It is possible for a real vehicle to be unstable in this sense but stable in the sense of Lyapunov because of the limiting action of flange impact [10].

Multiple - vehicle trains are also subject to coupling effects grouped into the classification of "train action". If the couplers transmit appreciable lateral force or yaw torque, the performance predicted by the analysis of a single vehicle may be significantly altered.

A final important consideration in the design of rail vehicles is compatibility with current practice. The railway systems of every country rely upon extensive standards to assure interchangeability of equipment, and it is only reasonable to comply with these standards in the design of advanced vehicles unless there is a strong reason to do otherwise. A vehicle designed with compatibility in mind can operate over existing track -- albeit perhaps at reduced speed -- over part or all of its route while improvements in the permanent way are made gradually.

4. High - Speed Rail Systems Proposed or In Service. Major strides have been taken in recent years toward practical high - speed (i.e., >100 mph) rail systems. The most notable achievement is probably the New Tokaido Line (NTL) of the Japanese National Railways.

That system required the construction of an entirely new guideway to achieve an operating speed of 130 mph. The new right - of - way is free of sharp curves and other encumbrances to high speed; rails are maintained in exceptionally good condition and alignment. The cars used on the NTL are of a conventional two - axle truck design [11], good riding quality being attributable more to the high track quality than to vehicle suspension innovations. New Shen Kansen extensions are being planned for 160 mph service.

New train design in Great Britain follows a different route. Rather than relying upon radical improvements to the permanent way, British engineers are requiring that the Advanced Passenger Train (APT) be capable of 150 mph operation over existing track; it should be noted, however, that mainline track in Great Britain is already well laid and maintained. The APT, when completed, will have tilting bodies and novel self - steering trucks to aid in curving at these high speeds [12]. In the meantime, British Rail will use the 125 mph High Speed Train -- a fast train of conventional design -- to phase in high speed operation.

In France, SNCF has placed into service a number of RTG gas turbine units on cross - country routes. These trains are designed to operate at 125 mph, and achieves 100 mph routinely over existing track. Two RTG turbotrains were leased by Amtrak recently for testing in the United States. The next generation of French high - speed trains is embodied in the TGV 001 five - car articulated set. The TGV 001 is intended for eventual 190 mph service over special

guideways, but for the present it will be operated up to 160 mph over existing routes [12].

In West Germany, development continues on the ET-403 electric locomotive for 125 mph service, but the emphasis there is on magnetic levitation for higher speeds [13]. Italy has also chosen electric power for its 160 mph ETR vehicles, which feature an ingenious tilting-body mechanism.

In the United States, there have been two recent attempts at increased speed. The Metroliner coaches, with top speed around 100 mph, are light vehicles of largely conventional design. The United Aircraft TurboTrains, on the other hand, are articulated trainsets with tilting bodies and represent a radical departure from tradition. The TurboTrains have been tested to 150 mph, but the condition of the track over which they operate between Boston and New York limits them to a top speed of around 90 mph.

5. Scope and Summary of This Work. This investigation was undertaken with three principal objectives in mind: (1) to develop rail vehicle models which would be useful for purposes of design -- accurate enough to predict the most important phenomena affecting dynamic performance, but simple enough to allow the effects of design modifications to be easily assessed; (2) to use these models to acquire information on the ride quality which may be expected from rail vehicles; and (3) to investigate possible methods of improving performance, especially using automatic control. Toward these ends, linear models have been used; single vehicles have been treated as isolated; and only lateral motions (translation, yaw) are included. Subsystems, such as

the trucks, have been taken as rigid bodies wherever possible.

In Chapter 2, prior work in the area of rail vehicle dynamics is reviewed. The models and methods which have gone before are assessed, and principal findings presented. The need for further modelling effort is pointed out.

Chapters 3, 4, and 5 taken as a group describe the performance of vehicles without any form of automatic control. In Chapter 3 the necessary models for vehicle, track, and interactions are presented. The equations of motion and some transfer functions are derived. Also, the parameter values which will be assumed for "baseline" values throughout the thesis are tabulated. Chapters 4 and 5 contain results obtained using the so-called "LMO" model, in which the yaw of the carbody is neglected, for the conventional rigid - axle wheelset and for the independently - rotating wheel truck respectively.

Chapters 6, 7, and 8 introduce the use of automatic control in an effort to extend stability and improve ride quality. The types of control which will be considered are defined in Chapter 6; certain important special cases are also noted there. The effects of two promising candidates are examined : active steering in Chapter 7, and a passive, asymmetric suspension in Chapter 8.

Chapters 9 and 10 concern the behavior of the more complete vehicle model, which includes the effects of carbody yaw, in comparison with the simpler LMO model. The differences can be significant, but Chapter 9 demonstrates that the LMO model can be an accurate and useful predictor of actual performance. Chapter 10 is on the subject

of quasi-static curving error, which can be adversely affected by some of the proposed control schemes.

Chapter 11 presents a group of conclusions arrived at in the course of this study. The LMO model is found to be an imperfect but highly useful design tool. Both active steering control and the passive asymmetric secondary have desirable dynamic effects, but the rigid truck with independently-rotating wheels offers such significant features unobtainable with the conventional rigid-wheelset truck that it merits strong consideration in future rail systems designed for either high or low speeds.

CHAPTER 2

SURVEY OF PRIOR RESEARCH

The lateral dynamic behavior of rail vehicles has long been the source of operational problems, and numerous studies have been undertaken in an effort to understand and control lateral motions. Some of the more important studies are cited in this chapter, together with results which are fundamental to the modelling effort. Significant gaps still remain, however: most work to date has considered only conventional, passive primary and secondary suspensions; and virtually no evaluation of ride quality has been carried out.

For the reader interested in a more complete literature survey, Law and Cooperrider [14] have compiled a critical summary of publications in the field of rail vehicle dynamics.

1. Fundamental Studies of Wheel - Rail Interactions. The assumption of pure rolling which was made in Chapter 1 to derive the equations of kinematic hunting is not adequate to describe all aspects of rail vehicle behavior. Beginning with Carter [15], various investigators have developed more elaborate theories to account for small slippage at the wheel - rail interface. Although the early impetus for these studies came from the need to drive locomotive wheels without slip, the resulting ideas are central to dynamic analyses even when gross slip is not an issue.

The small differential motions of two bodies in nominal rolling

contact are referred to as creep. After Carter, Vermeulen and Johnson [16], Johnson [17], and Ollerton [18] refined the theory of creep by modelling the wheel and rail as two bodies in Hertzian contact. If there are forces parallel to the contact plane, part of the elliptical contact patch will undergo slip at the coefficient of friction, μ (See Figure 2-1). The bodies accommodate to this partial slippby small elastic deformations in the slip region, which manifest themselves in a slightdifferenein overall rolling velocity (i.e., creep). When the tangent force reaches μN, where N is the normal contact force, the region of adhesion disappears and gross slippage begins. Figure 2-2 shows the relationship between tangential force and creepage, ξ, where

$$\xi = \frac{\text{relative velocity of patch}}{\text{rolling velocity of patch}} \qquad (2.1.1)$$

or, if V is the forward speed of the wheel hub and v_{cr} is the relative (creep) speed at the contact patch,

$$\xi = \frac{v_{cr}}{V} \quad . \qquad (2.1.2)$$

The normalizing factor, $\mu W/G\pi ab$, is typically of the order of 0.1%, with

μ = dynamic coefficient of friction,
W = normal load, per wheel,
G = shear modulus,
a = major axis of contact ellipse, and
b = minor axis of contact ellipse.

For small values of creepage, the exact creep relationship may be

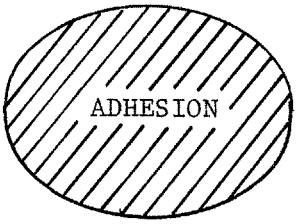

(a) Pure Rolling

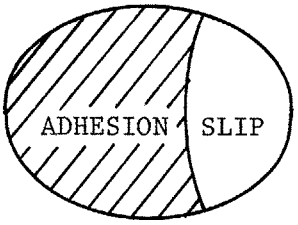

(b) Creep

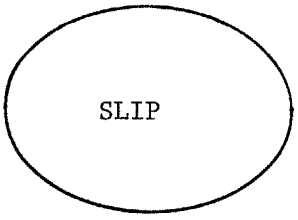

(c) Slip

FIGURE 2-1

Creep in the Contact Patch. Direction of Roll is from Right to Left.

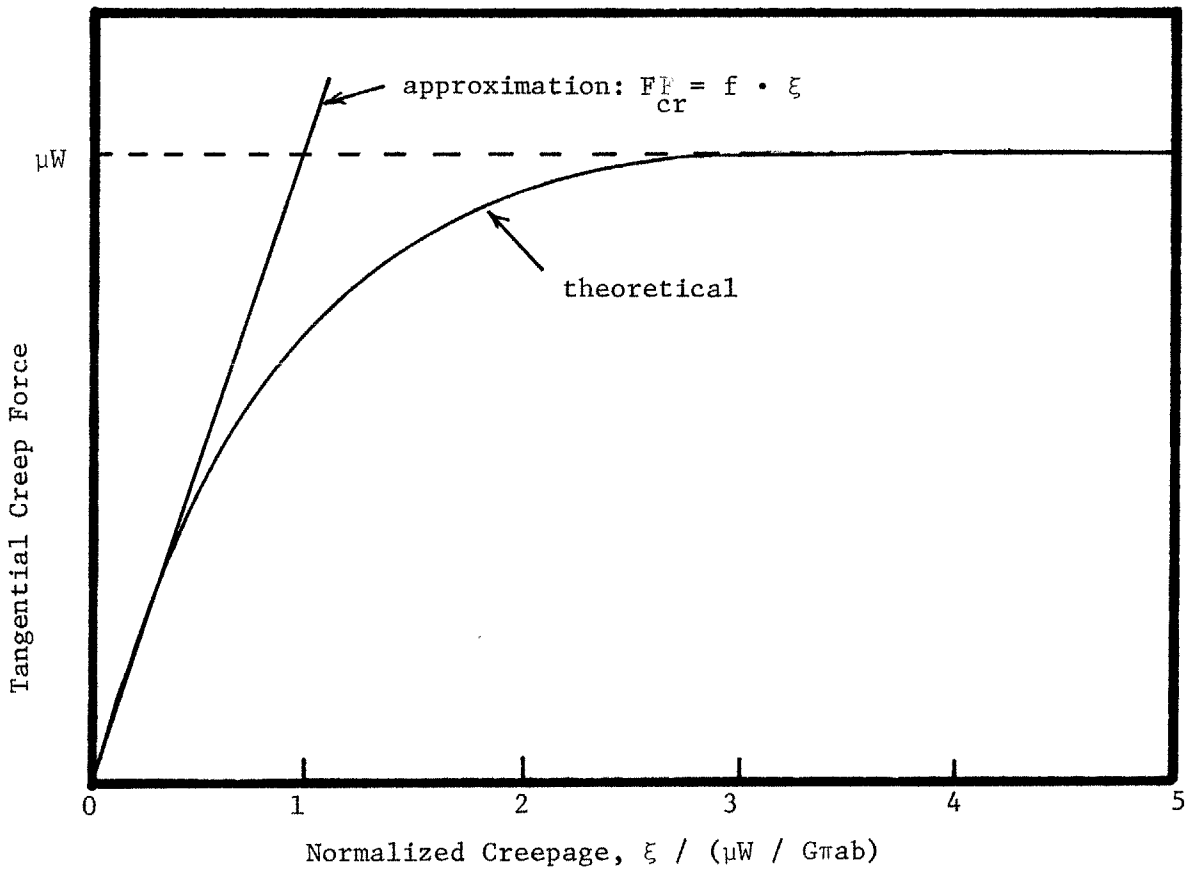

FIGURE 2-2

Creep Force Relation

approximated by

$$F_{cr} = f \cdot \frac{v_{cr}}{V} \quad , \tag{2.1.3}$$

where f is known as the creep coefficient. Cooperrider, in [10], gives the following approximation for f:

$$f\ [\text{lbf}] = 3500 \sqrt{\text{wheel dia.}[\text{ft}] \cdot \text{axle load}[\text{lbf}]} \quad . \tag{2.1.4}$$

Actually, the creep - force relationship is different for creep parallel to and perpendicular to the rolling direction, and at least two creep coefficients are necessary for precision. However, the so - called lateral and longitudinal creep coefficients are approximately equal in practice, and additionally are very imprecisely known. Therefore, a single value of f is commonly used to apply to motion in any direction.

Paul and Nayak [19] have carried out a series of experiments to show the relationship of surface finish to creep coefficient.

There is an additional mode of creep, called spin creep, in which rotation of the bodies in contact about an axis perpendicular to the contact plane give rise to resisting moments [20]. Spin creep has been shown to have a negligible effect on vehicle dynamics [30].

2. Properties of Track. The guideway structure, consisting of rails, ties, ballast, and subgrade, has generally been assumed rigid for the purposes of vehicle dynamic analyses. This assumption has given good results except in cases when hunting has been violent. The

elasticity of the track becomes important, however, when there is flange contact [21]. Several analyses [22, 23] have been carried out to test the stability of nonlinear oscillations with flange impact against elastic rails.

The dynamic properties of track are most imperfectly known, and they may naturally be expected to vary according to construction details. One significant parameter which has been measured [24] is the stiffness of a lain rail to a single lateral force, which appears to vary between $5x10^5$ and $5x10^6$ lbf/ft [10]. Such a measure ignores the continuous nature of the rail, due to which cross - coupling among axles through the rail might be expected to be significant.

Mechanisms of wheel and rail wear have received some attention [25]. It has been recommended [25] that the wheel tread and the rail crown be designed to a stable, "worn" set of profile which would exhibit lower stresses and be more immune to further wear than is the conventional new profile.

3. Curving Analyses. The quasi - steady guidance of a flexible truck around a curve of constant radius has been studied in depth by Newland [26]. He assumed that guidance forces would be provided entirely by creep -- i.e., no flanging -- and discovered that the tracking error in a curve is primarily geometry - constrained. That is, the lateral force required to produce centripetal acceleration contributes only a small additional error to that arising from rolling of coned wheelsets around a circle (see, for example, Equation 1.2.8), and that measures taken to reduce these forces (such as increasing the

superelevation) will be relatively ineffectual. Notice, however, that the contribution of centripetal force increases as V^2, whereas the geometric factor remains constant with speed, so the former may not be negligible for high - speed designs.

Curving with both creep and flanging has been treated by Müller [27], whose results show that flanging is the predominant mechanism of curve negotiation for virtually all conventional track.

4. Dynamic Models. The models which have been applied to rail car dynamics range from simple wheelsets to complete cars and even trains of cars. The complexity demanded of a model depends, first, upon the questions being asked of it (for example, a model in which carbody motions are neglected might yield information on flange forces, but obviously cannot predict carbody acceleration); and second, upon the frequency range of interest. In the case of conventional rail vehicles, the predominant forcing frequency is that of kinematic hunting, which is proportional to speed (Equation 1.2.6). Therefore, at higher speeds it becomes possible to neglect the overall motions of the more massive elements, such as the carbody.

The least massive component is the wheelset. Models of single wheelsets, suspended from "translating reference" carbodies which are assumed to move along the track at a constant speed V without moving laterally, are useful in predicting secondary hunting instability. Secondary hunting occurs at high speeds, and is characterized by large motions of the wheelsets or trucks but very little motion of the carbody. Wheelset models of this kind have been used by Wickens [28],

Law and Brand [29], and Law [30]. The last two involved the nonlinear dynamics of the wheelset.

The truck (or bogie) has received the most attention in dynamic studies. A truck consists of two (or occasionally more) wheelsets mounted in a frame, which is in turn suspended from the carbody. The frame has usually been treated as rigid, an assumption which appears adequate for most passenger trucks but less so for the typical three-piece freight truck which has little resistance to a form of deformation called "lozenging". The connection between wheelsets and frame may be rigid in all but the vertical direction (see the comments on the rigid truck below), or may have compliant primary suspension elements in any or all directions.

It may be shown [6] that a so-called rigid truck is dynamically equivalent to a single wheelset if gravitational stiffness (lateral restoring force due to static displacement) is neglected. The rigid truck is rigid only in the ground plane; the axles must be free to spin in their bearings, and must also roll if all four wheels are to stay in contact with the rails. The kinematic hunting frequency of a rigid truck is

$$\omega_k = V \sqrt{\alpha / (k^2+1) r_0 h} \quad , \qquad (2.4.1)$$

where the track gauge is 2h and the wheelbase of the truck is 2kh.

Benington [31] has proposed breaking the rigid axle of the wheelset and replacing it with a viscous coupling. This, he shows, would alleviate hunting without destroying the guidance action of the

coned wheelset.

The rigid truck has been extensively studied by de Pater [32], Clark and Law [33], Cooperrider [10], Jafar Shaghagi [34], and Wickens [35]. Flexible trucks have been analyzed by Weinstock [6], Matsudaira et al [36], Matsudaira [11], Yokose [37], Marcotte [38], Joly [39], and Cooperrider [10]. A number of interesting results have come from the flexible truck studies, but none as yet have been shown to be of general applicability. Small amounts of primary suspension flexibility have an effect only in the vicinity of secondary hunting instability, and do not appear to affect overall dynamic response appreciably.

A full vehicle, consisting of a carbody and two trucks (or, for some designs, two wheelsets), has at least six degrees of freedom in lateral modes -- seven if roll is included. This fact has generally prevented use of the more complicated flexible truck models for full - vehicle analyses. There has been a trend recently, however, toward the use of quite complete vehicle models simulated by numerical integration.

Matsudaira [11] examined a complete vehicle with two rigid trucks; he included carbody roll and yaw to yield a fourteenth - order system, of which he found the eigenvalues. Matsudaira found that for NTL prototype vehicles, the most significant mode of instability is yaw - dominated primary hunting. Primary hunting occurs when the kinematic frequency generated at the wheelsets coincides with some natural frequency of the system; a resonance is excited, and the resulting

motion may be truly unstable or merely lightly - damped, depending upon suspension parameters. In practice, the distinction between instability and resonance is somewhat academic, since a large amplitude oscillation is likely to cause flanging and subsequent nonlinear vibrations.

Matsudaira also investigated some simplifying assumptions about the carbody, but found them inadequate to predict the observed primary hunting. The assumptions tested were: (1) the body as a translating reference of infinite mass; and (2) a half - body, split at its center of mass and pivoted to allow yawing.

Others who have investigated full vehicles include Wickens [40, 41], Mauzin [42], Hobbs and Pearce [43], Weinstock [6], Marcotte [38], and Joly [39]. In most cases these analyses apply, with changes in parameters, to full vehicles with two rigid trucks or two wheelsets, and to single, unrestrained, flexible trucks.

A few analyses have considered the distributed nature of the long carbody [44].

A great deal of work has been done on carbody roll, which is a major problem in freight car operation. Typically the problem has been treated as a vibratory system (the carbody, center plate, side bearers, and secondary suspension) driven by kinematic hunting without back coupling [45, 46, 47, 48, 49].

From all the foregoing analyses, there are only a few results of general applicability. The first is that the motion of a rail car at any given speed consists mainly of a lightly - damped or unstable

oscillation at a frequency very near ω_k; the shape of the mode is more difficult to predict. Second, the onset of hunting instability, primary or secondary, may be pushed to higher speeds by reducing the constant of proportionality between ω_k and V:

$$\omega_k/V = \sqrt{\alpha / (k^2+1)r_0 h}$$

from Equation 2.4.1. Third, when other constraints prevent reducing this constant, hunting may be stabilized by increasing the yaw spring constant between truck and carbody. The large number of parameters required to characterize any but the simplest model have thus far made further generalizations difficult.

5. Novel Designs. The vehicles whose models have been discussed above may be termed conventional, in that (1) they employ more - or - less rigid wheelsets, (2) the vehicle is a distinct entity, which may or may not be coupled into a train, and (3) the components, other than distinct suspension elements, are intended to be approximately rigid. A number of unconventional vehicle configurations have been proposed as well, each of which is intended to overcome some of the problems inherent in the conventional type.

Because the mechanism of hunting is caused by the connection of two opposite wheels by an axle, some investigators have proposed eliminating hunting by eliminating the axle. With independently - rotating - wheels (IRW's), the guidance lost by discarding the action of coned wheelsets is supplied by one of two principal means. The Japanese National Railways are developing a trailing wheelset mech-

anism steered by a light central guide rail [50, 51, 52]. Alternatively, one may rely upon the gravitational stiffness of profiled wheels to generate steering force [53, 54]. The latter method, applied to a two - axle vehicle, eliminates hunting but introduces a new, lightly - damped (but stable) mode of its own.

Flowers and Flowers [55] designed and tested a unique IRW truck with a very flexible parallelogram linkage frame. Known as the Difco truck, it was originally intended to negotiate tight curves in mine service and was designed with cylindrical wheel treads. Fitted with concave profiled wheels with significant gravitational stiffness, however, the Difco truck might be suitable for high - speed applications.

The British have studied a self - steering flexible truck with two rigid wheelsets so linked as to decrease curving error by yawing into the curve [56, 57]. This truck is also said to offer certain desirable dynamic properties.

A final design innovation worth noting is the Calspan proposal for a flexible - spine unit train employing rigid wheelsets equally spaced along the length [58].

6. Automatic Control. To the author's knowledge, the techniques of active automatic control have rarely been applied to the problem of rail vehicle lateral motions. Sarma and Kozin [59] carried out an optimization of a rigid truck suspended from a translating reference body. They used as a performance index a weighted sum of mean square lateral error and control power. Some of the resulting optimal control

gains were heuristically selected to give a suboptimal controller, whose performance was found to be quite satisfactory. That suboptimal suspension corresponds to a conventional rigid truck with the additional feature of sizable gravitational stiffness at each wheel.

Active roll control devices intended to minimize passenger discomfort in curves have been investigated, most recently by Marcotte [38], and are being applied in the British APT.

Active suspensions have been applied frequently to solve the problem of vibration isolation in vehicle suspensions [3, 4, 60, 61, 62]. Such studies commonly use optimization techniques to minimize a weighted sum of mean square acceleration and displacement of the passenger compartment, thereby including the conflicting requirements of guidance and isolation. The difficulty in applying the results to rail vehicles comes from two sources. First, the available control studies have either assumed a spring - damper primary suspension or have allowed complete freedom as to the suspension between the carbody and the guideway; either assumption is unsuitable for a rail vehicle, whose primary suspension contributes its own peculiar dynamics to the problem. Second, the use of a mean - square performance index disregards the grave impact of a pure tone (at the hunting frequency) on passenger discomfort.

7. Systems Studies. Material on rail vehicle dynamics has been integrated with other pertinent aspects of system design in TRW's High Speed Rail Systems [1] and supporting studies. That report contains information on propulsion, track and structures, signalling,

economics, environmental constraints, and so forth. It is interesting that the system recommended by the TRW study is a light - weight electric train of essentially conventional design.

There is presently under way a cooperative effort among the American Association of Railroads, the Rail Progress Institute, the Federal Railway Administration, and other United States and Canadian groups to develop and organize a body of theory on track and train dynamics [63]. The main thrust of this program is toward generating computer models to aid in making up and handling long freight trains. Some of the tasks naturally involve modelling lateral dynamics, such as that dealing with freight truck optimization [69].

8. Overview; Gaps in the Literature. From the number of studies reviewed in this chapter, it should be evident that the lateral dynamics of rail vehicles has been a subject of intense analytical effort. The great bulk of prior work has attempted to find the linear critical speed, V_c, above which small disturbances do not damp out. Since large - amplitude hunting has been, and continues to be, the most troublesome source of wear, damage, and derailment in freight operations, it is to be expected that stability analyses would receive first priority. Many investigators have gone on to include the effects of nonlinearities on stability and on such large - amplitude problems as flange forces and wheel climb; nonlinear studies have been done by energy methods or, more recently, by computer simulation. Interest in the transmission of lateral vibrations to the carbody has been chiefly confined to some investigations of the gross rock - and -

roll resonances exhibited by high center-of-gravity freight cars.

Certain serious gaps remain, however, in the information available to the designer of high-speed rail vehicles. The issue of ride quality has very seldom been addressed (an exception is in Reference 1). The quality of the track and the sophistication of the suspension combine to determine ride quality. Economics almost invariably favor improvements to the suspension, so it is important to understand the limitations and capabilities of advanced suspension designs as they affect passenger comfort.

The possible application of automatic control to remedy the inherent problems of the conventional rail vehicle has received very little attention; neither has the use of independently-rotating wheels, which have promise of being a simple solution to a number of problems at both low and high speeds. Deliberate asymmetries in the secondary suspension are similarly promising and similarly neglected.

These and other issues should be addressed, however, as pressure for improved rail passenger service increases. Technically sophisticated approaches to suspension design, perhaps justifiably rejected as too expensive or too unreliable for freight operations, may appear more attractive in the passenger environment. It is likely, too, that there remain many improvements in freight car design which might be made without incurring economic penalties. For these reasons it is important that future studies of rail vehicle dynamics not be confined to the formulation of ever more elaborate models of existing systems, but should also point the way toward innovative and unconventional

design concepts.

CHAPTER 3

COMPONENT AND SYSTEM MODELS

This chapter contains the fundamental assumptions and models which will be used in the remainder of this thesis. The vehicle is divided into subsystems, and each subsystem (carbody, secondary suspension, truck) is analyzed. Two complete vehicle models are assembled from these subsystems, and their equations of motion derived. Baseline parameter values, representative of a real high-speed vehicle, are tabulated.

It was stated in Chapter 1 that the models developed here are intended to be useful in discovering new ways in which to design vehicles for better performance. Oversimplified models, which do not adequately approximate the behavior of real systems, are clearly not suitable; but neither are highly elaborate ones which, by including effects which are minute under any foreseeable operating conditions, become computationally unwieldy and opaque to physical insight. For the purposes of this study, it was deemed essential that any dynamic model reproduce the following three aspects of rail vehicle behavior: (1) the mechanism of lateral guidance through creep forces, and the possibility of instability due to hunting; (2) the influence of carbody vibration, especially near resonance, upon stability; and (3) the relationships between suspension design and the vibration transmitted to passengers or cargo.

1. Vehicle Subsystems and Coordinate System. A rail vehicle may be conveniently divided into components as in Figure 3-1: a carbody, supported on two trucks by means of two secondary suspensions. The carbody is the structure which holds the passenger compartment; in reality it also supports a collection of equipment, such as generators and compressors, which are massive and resiliently mounted and therefore may have significant dynamics of their own. Each truck consists of four wheels, which may or may not be in the form of two wheelsets (a pair of wheels connected by an axle is a wheelset), attached to a basically rectangular truck frame by means of primary suspensions (see Figure 3-2). The dimensions of the truck, measured between contact points when it is in equilibrium between the rails, is 2h (gauge) by 2kh (wheelbase). The length of the carbody between truck attachment points is 2L. The secondary suspensions consist of whatever assemblages of springs, dampers, and active devices connect the trucks to the carbody.

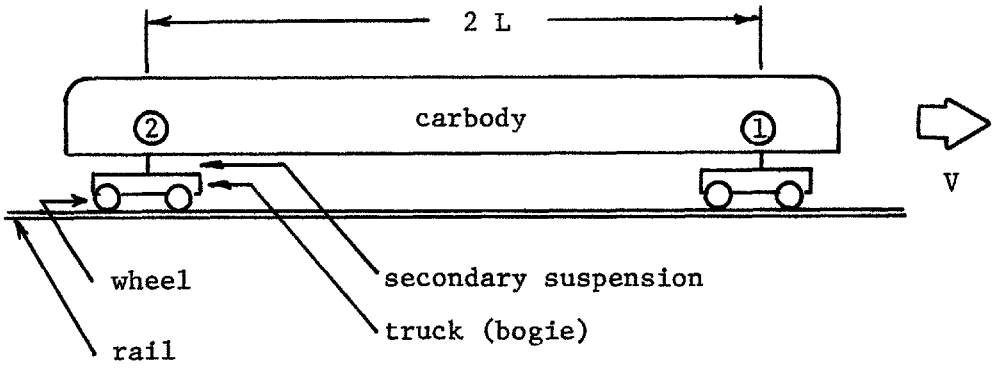

(a) Side View

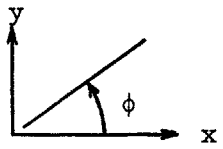

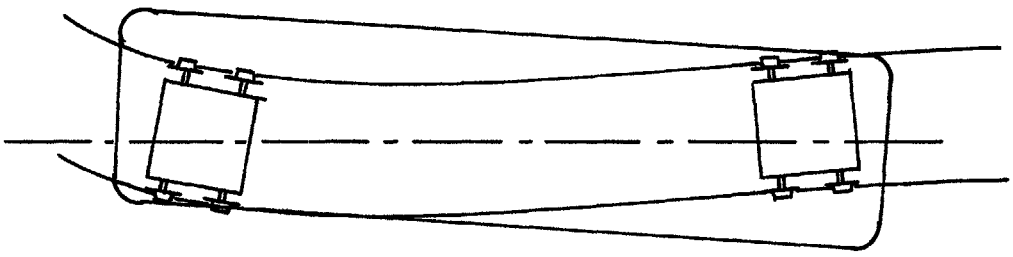

(b) Top View, Showing Rail Lateral Deviation and Coordinates

FIGURE 3-1

Nomenclature for Rail Vehicle Models

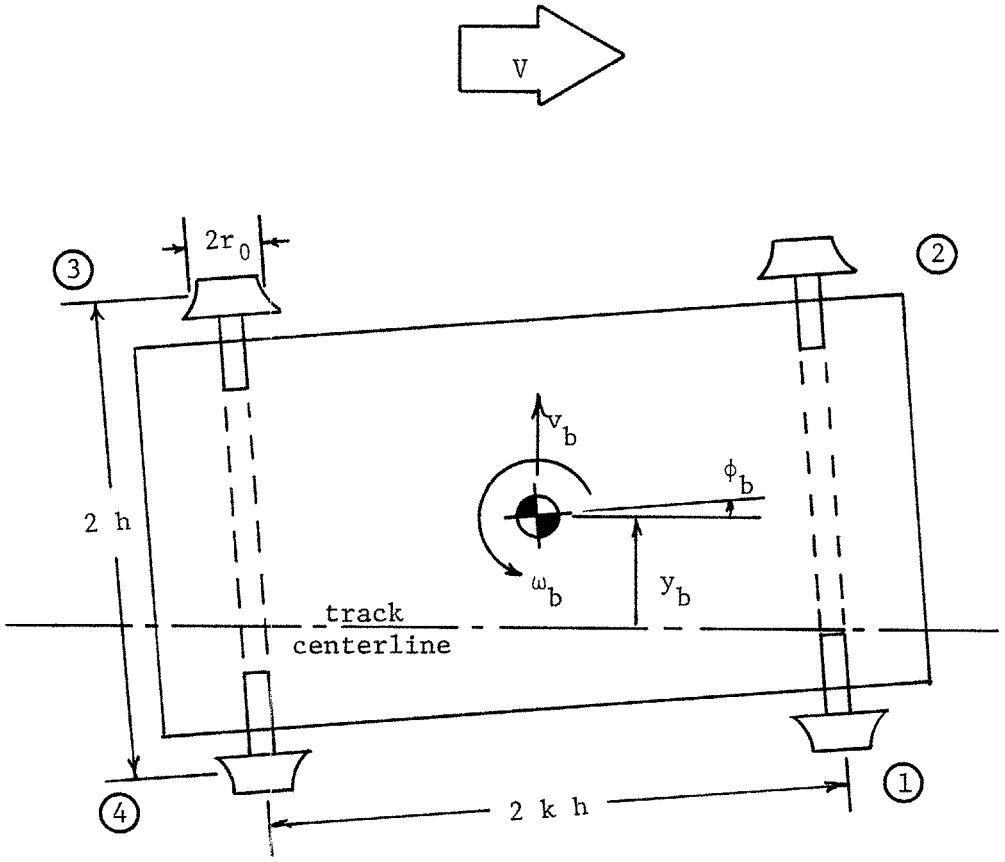

Axle positions shown dashed.

Circled numbers are wheel reference numbers.

FIGURE 3-2

Nomenclature for Truck Models

The coordinate system being used is shown in Figure 3-1. Lateral excursions from the nominal track centerline are termed "y", yaw angles are "ϕ", and the direction of forward motion is "x".

2. Modelling Assumptions. A number of assumptions are necessary at this point to constrain and simplify the analysis.

Rigidity. All trucks are rigid trucks as defined in §2.4. Axles, if present, are rigid. The carbody is a rigid unit and so may be characterized by its mass and moment of inertia.

Linearity. The equations of motion, in their final form, will be linear. The effective conicity of the wheels, defined by

$$\alpha = \partial r / \partial y \quad , \tag{3.2.1}$$

is assumed constant; the assumption of constant α is exact for conical wheel treads. The creep force relation is approximated by the linearization of Equation 2.1.3 which, in vector form, is

$$\vec{F}_{cr} = - f \vec{v}_{cr} / V \quad . \tag{3.2.2}$$

The lateral gravitational stiffness at each wheel,

$$K_L = -\partial F_y / \partial y \tag{3.2.3}$$

for static lateral displacements, is assumed constant (see Appendix B for a derivation of K_L under the assumption of constant radii of curvature). All suspension elements are assumed linear; in particular, no stops or flange impacts are permitted.

Symmetry. The carbody and trucks are assumed to be geo-

metrically symmetric about their centers of mass. Passive suspension elements (except as special cases of automatic controllers, as in Chapter 8) have no preferred direction of action.

Constant Speed. The forward speed of the vehicle along the track is assumed constant at V. If rigid wheelsets are used, their rotational speed is constant at

$$\Omega = V / r_0 \quad . \tag{3.2.4}$$

Small Motions. All linear and angular displacements are assumed to be small. Therefore first - order approximations to trigonometric functions ($\sin\phi \simeq \phi$, $\cos\phi \simeq 1$) may be used.

No Roll. The carbody is assumed not to roll at all. The roll of the axles, necessary to accommodate wheel conicity with lateral excursions, is assumed to be sufficiently slight not to affect the wheel - rail contact angle (and hence the gravitational stiffness) appreciably.

Notice that with all the foregoing assumptions, there are a maximum of six degrees of freedom for a complete vehicle: translation and yaw (y and ϕ) for the carbody and each of two trucks.

Single Input from Rail. The only inputs considered are those applied to the vehicle at the wheel - rail interface. This assumption excludes body forces (e.g., wind), coupler forces, and braking and acceleration.

The particular form of rail input being considered is of importance. In general, the two rails might be treated as two distinct

dynamic systems with different -- though correlated -- initial profiles. The first assumption made here is that the two rails are rigid. The second is that the rails do not deviate vertically from the ground plane, an assumption justified by the fact that vertical inputs do not couple to lateral motions in the absence of roll and of nonlinear effects. The third and final assumption is that the rails undergo lateral displacements while remaining parallel (i.e., at constant gauge). Refer to Figure 3-8. An arbitrary pair of rail profiles may, in the lateral direction, be decomposed into a component of gauge variation about a fixed centerline, and a component of centerline alignment variation at constant gauge. Under assumptions of linearity, symmetry, and small motions, the action of gauge variation may be seen always to be equal and opposite on opposite wheels. It therefore contributes no net lateral force and may be correctly dropped from further consideration. This thesis is concerned only with parallel, rigid rails with alignment error from a straight ("tangent") nominal centerline.

3. Carbody Models. Two models for the carbody will be used in this work. The more complete is the "Rigid Plane Body" (RPB) model, in which the body may both translate and yaw. A truck is at each end, at a distance L from the center. The equations of motion for the RPB model (using the force and moment direction conventions illustrated in Figure 3-4) are:

$$\ddot{y}_c = -(F_{b1}+F_{b2}) \;/\; 2m_c \quad , \text{ and} \qquad (3.3.1)$$

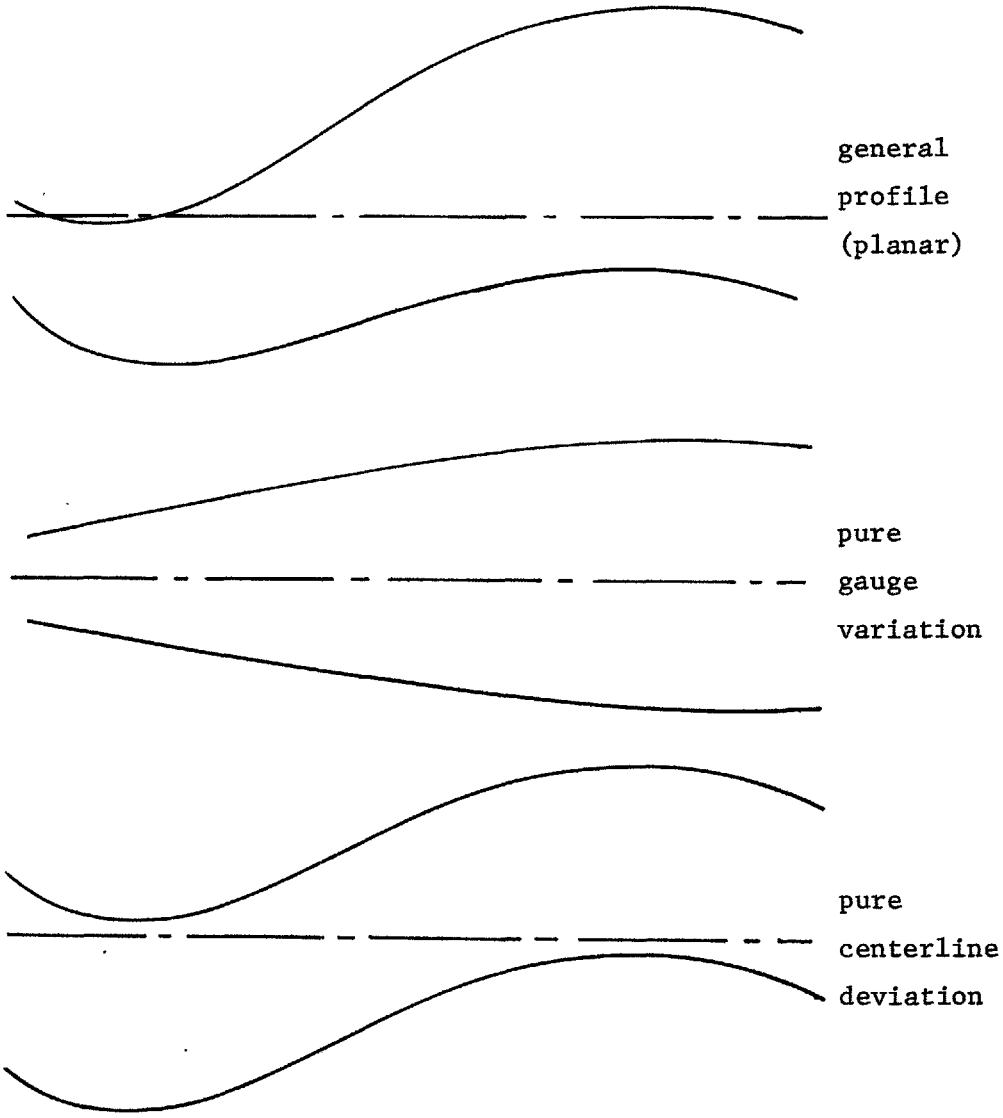

FIGURE 3-3

Decomposition of Lateral Rail Profile

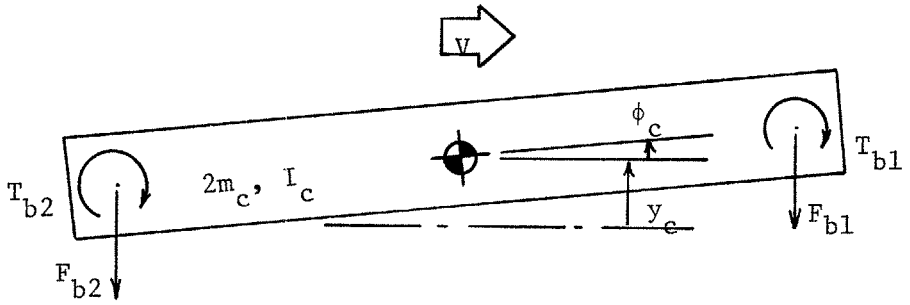

(a) Rigid Plane Body (RPB)

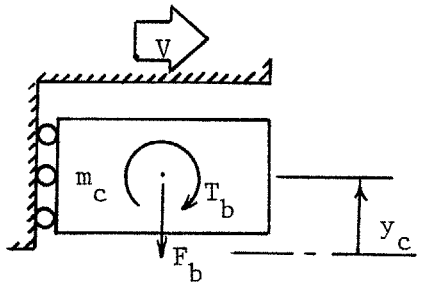

(b) Lateral Mass Only (LMØ)

Shaded reference translates along track at V.

FIGURE 3-4

Carbody Models

$$\ddot{\phi}_c = \frac{-(T_{b1}+T_{b2}) - L(F_{b1}-F_{b2})}{I_c} \quad . \qquad (3.3.2)$$

The RPB model has two degrees of freedom. More importantly from the standpoint of analytical complexity, it requires that the dynamics of two complete trucks and their suspensions be included in the complete vehicle model.

A simpler carbody model which preserves some important features of the RPB model is the "Lateral Mass Only" (LMO) model shown in Figure 3-4. The LMO model allows the carbody to translate but not to yaw; only one truck is required. The equation of motion is

$$\ddot{y}_c = -F_b / m_c \quad , \qquad (3.3.3)$$

with $\phi_c \equiv 0$. The LMO model is a limiting case of the RPB model with

$$L \to \infty \quad , \text{ and} \qquad (3.3.4)$$

$$I_c \to 2m_c L^2 \quad . \qquad (3.3.5)$$

Furthermore, the commonly used "translating reference" carbody model is a special case of the LMO model with $m_c \to \infty$.

The utility of the LMO carbody model lies in the fact that, without undue complexity, it takes into account the finite mass of the carbody. It is therefore capable of showing primary hunting, which occurs at a body resonance. It is also possible to examine the vibration isolation properties of the secondary suspension using the LMO model. The correspondence of LMO results to those obtained using more elaborate models -- especially the RPB -- depends upon the values

of system parameters. The latter issue will be examined in Chapter 9.

4. Secondary Suspension Models. The secondary suspension is the connection between the truck and the carbody. For the purposes of this work, the suspension acts in two directions, lateral and yaw. The suspension elements may be active or passive. Of the infinite variety of possible passive suspension configurations, the simple parallel and series connections illustrated in Figure 3-5 have been selected as representative. Inclusion of active elements will be deferred until Chapter 6; at that time, the active force and torque, F_{bc} and T_{bc}, will be assumed to act in addition to their passive counterparts, F_b and T_b.

In the lateral direction, the only passive suspension considered consists of a linear spring and damper connected in parallel as in Figure 3-5a. Such a parallel connection is necessary for there to be a static stiffness in the secondary. Static stiffness is required to resist side loads and to prevent lateral drift. It is defined by

$$F_b = -K_c(y_b - y_{cb}) - B_c(\dot{y}_b - \dot{y}_{cb}) \quad , \qquad (3.4.1)$$

where y_{cb} is the lateral displacement of the truck attachment point (as distinguished from y_c, the lateral displacement of the carbody center of mass). Notice that F_b acts <u>on</u> the truck in the y direction.

No static yaw stiffness is required in the secondary for a four-wheeled truck. The creep forces alone will keep the truck approximately aligned with the track, and the flanges will limit yaw excursion. The carbody, being supported at both ends, derives its yaw stiffness primarily from the lateral stiffness of the two secondaries. Therefore it

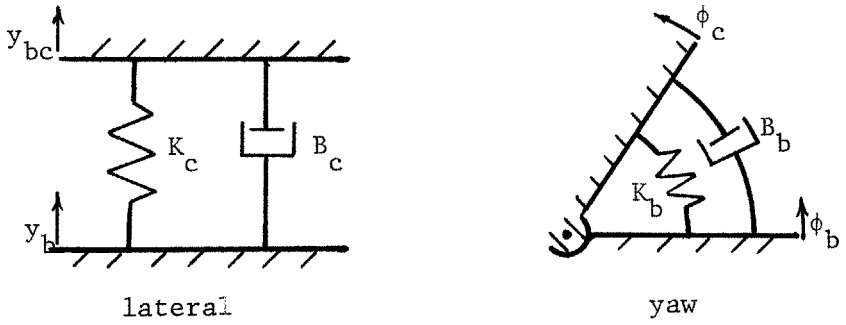

(a) Parallel Connection

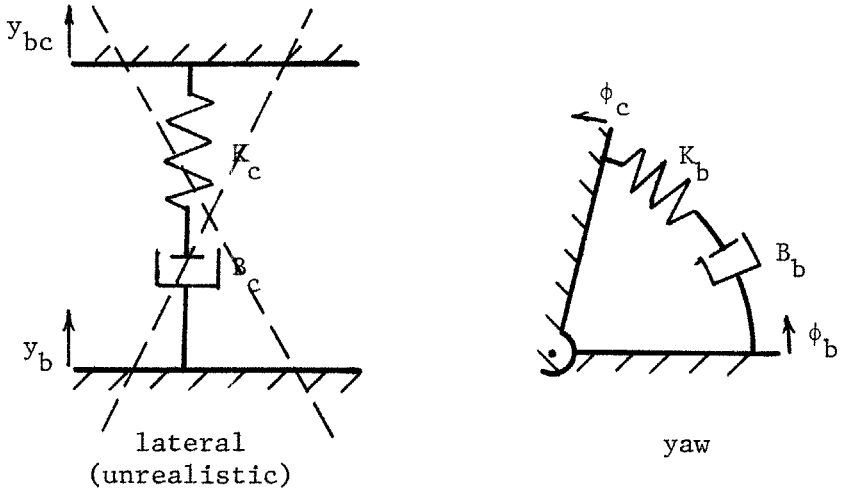

(b) Series Connection

FIGURE 3-5

Secondary Suspension Models

is reasonable to define two basic passive yaw suspensions as in Figure 3-5a and 3-5b. The first ("K-B parallel") has the spring and damper in parallel, so

$$T_b = -K_b(\phi_b-\phi_c) - B_b(\dot{\phi}_b-\dot{\phi}_c) \ , \qquad (3.4.2)$$

where again T_b is defined as positive acting on the truck. The second arrangement ("K-B series") has the spring and damper connected in mechanical series. This form of suspension introduces an additional order, viz.

$$\dot{T}_b = -K_b(\dot{\phi}_b-\dot{\phi}_c) - \frac{K_b}{B_b} T_b \ . \qquad (3.4.3)$$

The K-B series yaw secondary is of practical use when it is desired to have a high stiffness against dynamic (high - frequency) motions but a low stiffness against quasi - static motions (for example, curving).

5. Truck Models. It is the behavior of the trucks which gives the lateral motions of rail vehicle their unique character. Two types of rigid trucks will be considered here: the "rigid conventional" (RC) and the "rigid, independently - rotating wheeled"(RIW) trucks. As shown in Figure 3-6, both share essential geometric properties. It has already been stated that the trucks are rectangular and symmetric with gauge of 2h and wheelbase of 2kh. The effective conicity is α, and the equilibrium (centered) rolling wheel radius is r_0. The difference is that the RC truck has rigid axles which rotate at constant speed, and the RIW does not.

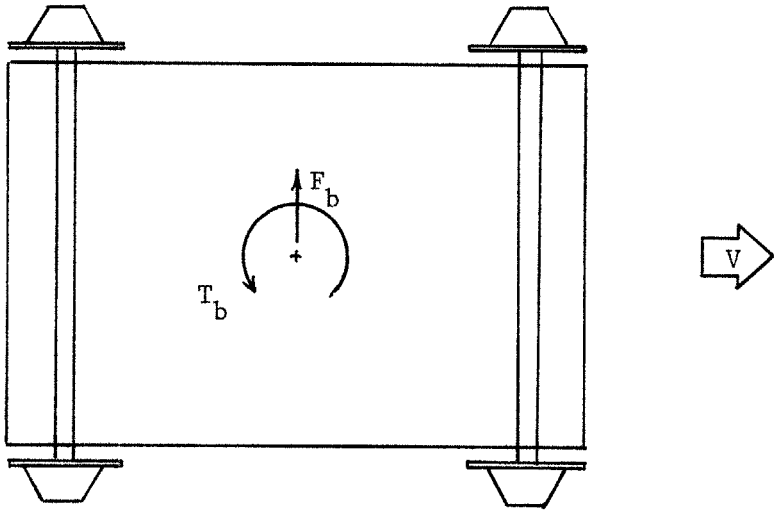

(a) Rigid conventional (RC)
(showing conical wheel treads)

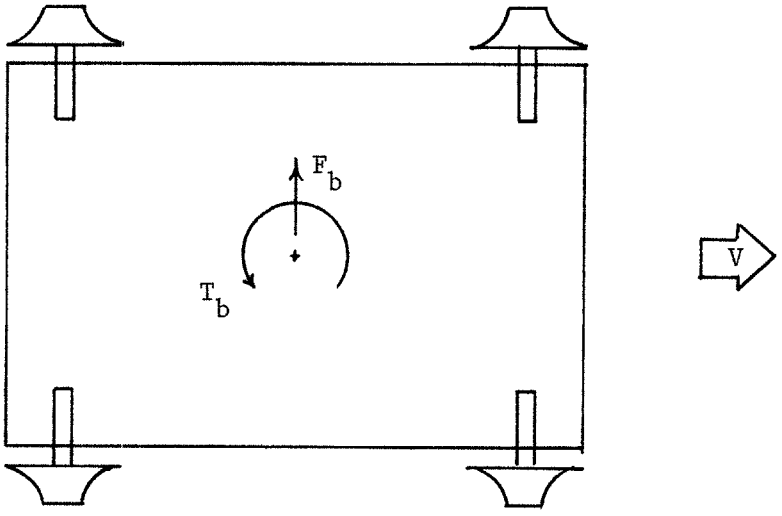

(b) Rigid with Independently - Rotating Wheels (RIW)
(showing concave wheel treads)

FIGURE 3-6
Rigid Truck Models

It is convenient at this point to introduce the following new variable definitions:

$$\begin{aligned} v_b &= \dot{y}_b \ , \\ \omega_b &= \dot{\phi}_b \ , \\ v_c &= \dot{y}_c \ , \text{ and} \\ \omega_c &= \dot{\phi}_c \ . \end{aligned}$$

For this section on truck models only, the subscript "b" will be dropped since just truck motions are of interest.

RC Truck. The RC truck is capable of deriving its guidance from creep forces alone, and does not depend upon gravitational stiffness. Consider Figure 3-7. Let $\vec{i}$ and $\vec{j}$ be unit vectors in the x and y directions respectively. Then the absolute hub velocities are:

$$\begin{aligned} \text{wheel 1:} \quad & \vec{i}\,(V + \omega h[\cos\phi - k\sin\phi]) + \vec{j}\,(v + \omega h[k\cos\phi + \sin\phi]) \\ \text{wheel 2:} \quad & \vec{i}\,(V - \omega h[\cos\phi + k\sin\phi]) + \vec{j}\,(v + \omega h[k\cos\phi - \sin\phi]) \\ \text{wheel 3:} \quad & \vec{i}\,(V - \omega h[\cos\phi - k\sin\phi]) + \vec{j}\,(v - \omega h[k\cos\phi + \sin\phi]) \\ \text{wheel 4:} \quad & \vec{i}\,(V + \omega h[\cos\phi + k\sin\phi]) + \vec{j}\,(v - \omega h[k\cos\phi - \sin\phi]) \ . \end{aligned}$$

(3.5.1)

Recall that from Equation 3.2.4, the spin or rolling angular speed of the axle is constant at $\Omega = V/r_0$, an assumption which is good to second order for a rigid wheelset. Then the velocity of the wheel rim at the contact point, relative to the hub, is:

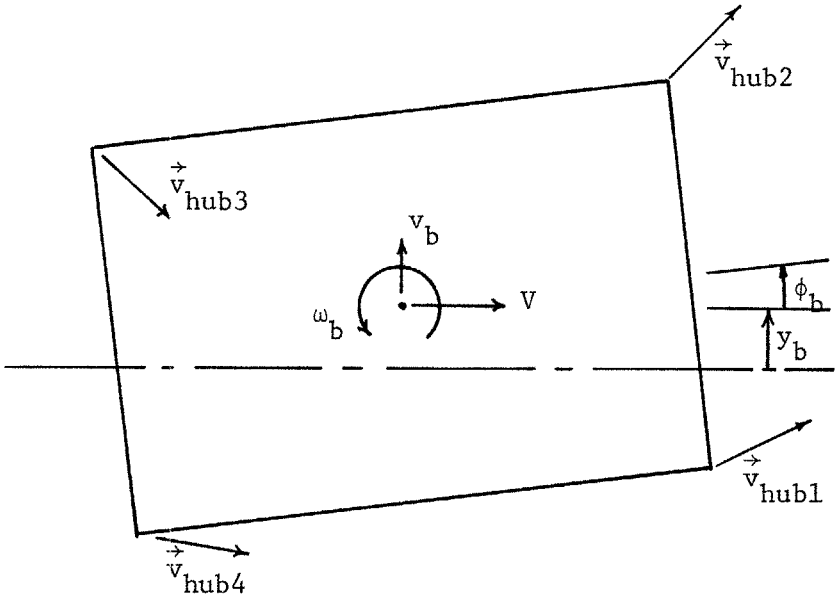

(a) Diagram for Hub Velocities

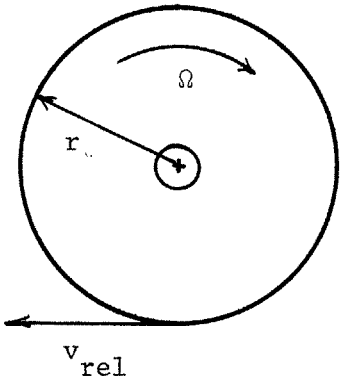

(b) Diagram for Rim Velocities Relative to Hubs

FIGURE 3-7

Diagrams for Derivation of Creep Velocities

$$
\begin{aligned}
&\underline{\text{wheel 1}}: \quad \vec{i}\,(-\Omega\, r_1 \cos\phi) + \vec{j}\,(-\Omega\, r_1 \sin\phi) \\
&\underline{\text{wheel 2}}: \quad \vec{i}\,(-\Omega\, r_2 \cos\phi) + \vec{j}\,(-\Omega\, r_2 \sin\phi) \\
&\underline{\text{wheel 3}}: \quad \vec{i}\,(-\Omega\, r_3 \cos\phi) + \vec{j}\,(-\Omega\, r_3 \sin\phi) \\
&\underline{\text{wheel 4}}: \quad \vec{i}\,(-\Omega\, r_4 \cos\phi) + \vec{j}\,(-\Omega\, r_4 \sin\phi) \quad .
\end{aligned}
\tag{3.5.2}
$$

The lateral position of the rail under each wheel -- assumed here to be equivalent to the lateral position of the contact point -- is measured from the nominal gauge as y_{ir} for the i^{th} wheel. Due to the linearized action of the effective conicity, the rolling radius r_i for each wheel is:

$$
\begin{aligned}
&\underline{\text{wheel 1}}: \quad r_1 = r_0 - \alpha(y+kh\phi-y_{1r}) \\
&\underline{\text{wheel 2}}: \quad r_2 = r_0 + \alpha(y+kh\phi-y_{2r}) \\
&\underline{\text{wheel 3}}: \quad r_3 = r_0 + \alpha(y-kh\phi-y_{3r}) \\
&\underline{\text{wheel 4}}: \quad r_4 = r_0 - \alpha(y-kh\phi-y_{4r}) \quad ,
\end{aligned}
\tag{3.5.3}
$$

where the small - angle assumptions have been made.

The absolute velocity of the wheel rim at the contact point is then the vector sum of the hub velocity and the relative rim velocity. The creep velocity is the vector difference of the wheel rim and rail velocities at the contact point. The rail velocity in the x direction is zero. In the y direction, the apparent rail velocity is due to the encounter of a spatial irregularity profile at the forward speed V, but in any case is the time derivative of y_{ir},

$$
v_{ir} = \dot{y}_{ir} \; . \tag{3.5.4}
$$

For the assumption of parallel rails and small displacements,

$$\begin{aligned} y_{1r} &= y_{2r} \equiv y_{rf} \quad , \\ y_{3r} &= y_{4r} \equiv y_{rb} \quad , \\ v_{1r} &= v_{2r} \equiv v_{rf} \quad , \text{ and} \\ v_{3r} &= v_{4r} \equiv v_{rb} \quad . \end{aligned} \tag{3.5.5}$$

Combining Equations 3.5.1, 3.5.2, 3.5.4, and 3.5.5 gives for the creep velocity at each wheel (with small - angle approximations):

$$\begin{aligned} &\underline{\text{wheel 1}}: \ \vec{i}\,(V + \omega h - \omega k h\phi - \Omega r_1) \\ &\qquad +\vec{j}\,(v + \omega k h + \omega h\phi - \Omega r_1\phi - v_{rf}) \\ &\underline{\text{wheel 2}}: \ \vec{i}\,(V - \omega h - \omega k h\phi - \Omega r_2) \\ &\qquad +\vec{j}\,(v + \omega k h - \omega h\phi - \Omega r_2\phi - v_{rf}) \\ &\underline{\text{wheel 3}}: \ \vec{i}\,(V - \omega h + \omega k h\phi - \Omega r_3) \\ &\qquad +\vec{j}\,(v - \omega k h - \omega h\phi - \Omega r_3\phi - v_{rb}) \\ &\underline{\text{wheel 4}}: \ \vec{i}\,(V + \omega h + \omega k h\phi - \Omega r_4) \\ &\qquad +\vec{j}\,(v - \omega k h + \omega h\phi - \Omega r_4\phi - v_{rb}) \quad . \end{aligned} \tag{3.5.6}$$

The total net creep force is:

$$F_{cr} = -\frac{f}{V}\,(\vec{v}_{cr1}+\vec{v}_{cr2}+\vec{v}_{cr3}+\vec{v}_{cr4})\cdot\vec{i} \quad , \tag{3.5.7}$$

where $\vec{v}_{cri}$ is the creep velocity of the i^{th} wheel. Similarly, the net creep torque is:

$$\begin{aligned} T_{cr} = &-\frac{f}{V}\,h\,(\vec{v}_{cr1}-\vec{v}_{cr2}-\vec{v}_{cr3}+\vec{v}_{cr4})\cdot\vec{i} \\ &-\frac{f}{V}\,kh\,(\vec{v}_{cr1}+\vec{v}_{cr2}-\vec{v}_{cr3}-\vec{v}_{cr4})\cdot\vec{j} \quad . \end{aligned} \tag{3.5.8}$$

Substituting Equations 3.5.3 and 3.5.6 into Equation 3.5.7 gives the following expression for creep force:

$$F_{cr} = -\frac{4f}{V} v_b + 4f\phi_b + \frac{4f}{V}\left(\frac{v_{rf}+v_{rb}}{2}\right) . \qquad (3.5.9)$$

The subscript "b" has been reintroduced for clarity. Notice that for the parallel - rails assumption, nonlinear terms in $\Omega\phi y_b$ vanish identically.

In a like manner, substituting Equations 3.5.3 and 3.5.6 into Equation 3.5.8 gives for creep torque:

$$T_{cr} = -\frac{4fh^2(k^2+1)}{V}\omega_b - \frac{4fh\alpha}{r_0} y_b + \frac{4fkh}{r_0}\left(\frac{v_{rf}-v_{rb}}{2}\right) + \frac{4fh\alpha}{r_0}\left(\frac{y_{rf}+y_{rb}}{2}\right) . \qquad (3.5.10)$$

In addition to the creep forces, forces act at each wheel due to the gravitational stiffness K_L. The net force and torque on the truck due to gravitational stiffness are:

$$F_g = -4K_L\left(y_b - \frac{y_{rf}+y_{rb}}{2}\right) , \text{ and} \qquad (3.5.11)$$

$$T_g = -4K_L kh\left(kh\phi_b - \frac{y_{rf}-y_{rb}}{2}\right) . \qquad (3.5.12)$$

Finally, the truck is acted upon by the secondary suspension with force F_b and torque T_b. If the truck has mass m_b and moment of inertia I_b, force and torque balance gives the following equations of motion for the RC truck model:

$$m_b \ddot{y}_b = F_{cr} + F_g + F_b$$
$$I_b \ddot{\phi}_b = T_{cr} + T_g + T_b \quad ,$$

which, after making the indicated substitutions and defining

$$k_s = (k^2 + 1) \tag{3.5.13}$$

are:

$$\begin{aligned}
\dot{y}_b &= v_b \\
\dot{v}_b &= (-4K_L/m_b)y_b + (-4f/m_b V)v_b + (4f/m_b)\phi_b \\
&\quad + (4K_L/m_b)([y_{rf}+y_{rb}]/2) + (4f/m_b V)([v_{rf}+v_{rb}]/2) + (1/m_b)F_b \\
\dot{\phi}_b &= \omega_b \\
\dot{\omega}_b &= (-4fh\alpha/I_b r_0)y_b + (-4K_L k^2 h^2/I_b)\phi_b + (-4fh^2 k_s/I_b V)\omega_b \\
&\quad + (4fh\alpha/I_b r_0)([y_{rf}+y_{rb}]/2) + (4K_L kh/I_b)([y_{rf}-y_{rb}]/2) \\
&\quad + (4fkh/I_b V)([v_{rf}-v_{rb}]/2) + (1/I_b)T_b \quad .
\end{aligned} \tag{3.5.14}$$

Notice that the rail inputs appear both in an "in - phase" form (e.g., $y_{rf}+y_{rb}$) and an "out - of - phase" form (e.g., $y_{rf}-y_{rb}$).

RIW Truck. The truck with independently - rotating wheels differs from the conventional truck in that there are no axles to develop a centering torque by creep. The RIW truck derives its centering action from the gravitational stiffness at the wheels; conical wheel treads are therefore unsuitable for use with independent wheels. The four wheels are assumed to roll without slip perpendicular to their axes of spin, but they may slip or creep parallel to those axes.

The hub velocities are as given in Equation 3.5.1. The wheels will not support creep along their spin direction; the direction of creep at each is along the axle. The values of the creep velocity in the direction

$$-\vec{i}\sin\phi + \vec{j}\cos\phi$$

for each wheel are:

$$\begin{aligned}
&\underline{\text{wheel 1}}: && (v-v_{rf})\cos\phi + \omega kh - V\sin\phi + \\
&\underline{\text{wheel 2}}: && (v-v_{rf})\cos\phi + \omega kh - V\sin\phi \\
&\underline{\text{wheel 3}}: && (v-v_{rb})\cos\phi - \omega kh - V\sin\phi \\
&\underline{\text{wheel 4}}: && (v-v_{rb})\cos\phi - \omega kh - V\sin\phi \quad .
\end{aligned} \tag{3.5.15}$$

Making the small - angle approximations, Equation 3.5.15 yields the following expressions for creep force and torque:

$$F_{cr} = -\frac{4f}{V}\left(v - \frac{v_{rf}+v_{rb}}{2}\right) + 4f\phi \tag{3.5.16}$$

$$\vec{T}_{cr} = -\frac{4fk^2h^2}{V}\omega + \frac{4fkh}{V}\left(\frac{v_{rf}-v_{rb}}{2}\right) \tag{3.5.17}$$

Gravitational force and torque are as in Equations 3.5.11 and 3.5.12. The resulting equations of motion for the RIW model are:

$$\begin{aligned}
\dot{y}_b &= v_b \\
\dot{v}_b &= (-4K_L/m_b)y_b + (-4f/m_bV)v_b + (4f/m_b)\phi_b \\
&\quad + (4K_L/m_b)([y_{rf}+y_{rb}]/2) + (4f/m_bV)([v_{rf}+v_{rb}]/2) + (1/m_b)F_b \\
\dot{\phi}_b &= \omega_b \\
\dot{\omega}_b &= (-4K_Lk^2h^2/I_b)\phi_b + (-4fk^2h^2/I_bV)\omega_b + \ldots
\end{aligned}$$

$$+ (4K_L kh/I_b)([y_{rf}-y_{rb}]/2) + (4fkh/I_b V)([v_{rf}-v_{rb}]/2) + (1/I_b)T_b \qquad (3.5.18)$$

Points of Commonality. Comparison of Equations 3.5.14 and 3.5.18 reveals that the RIW equations may be brought into correspondence with the RC equations by making the following parameter identifications:

$$k_s \leftarrow k^2 \quad , \text{ and} \qquad (3.5.19)$$

$$\alpha \leftarrow 0 \quad . \qquad (3.5.20)$$

This fact simplifies the analysis by enabling one to deal with only one set of formal equations (the more general RC set), the model of interest being determined solely by parameter values.

It is worthy of note at this point that the formal equating of conicity to zero in the RIW model eliminates the source of stable and unstable hunting action.

6. Equations of Motion: LMO Complete Vehicle. In this section, a vehicle model is introduced which will be the basis of much of the analytical work in the remainder of the thesis. It consists of the LMO carbody assembled with one RC (reducible to RIW) truck by means of a K-B-parallel secondary (both lateral and yaw). The same model with a K-B-series yaw secondary is also included for completeness. Full equations of motion are generated, and transfer functions for carbody lateral acceleration are derived.

K-B-Parallel Yaw Secondary. The vehicle model with secondary yaw spring and damper in parallel is illustrated in Figure 3-8. The

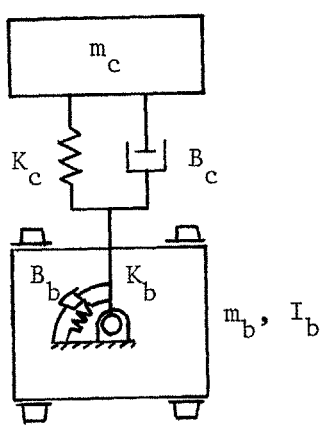

(a) LMO, K-B-Parallel Yaw

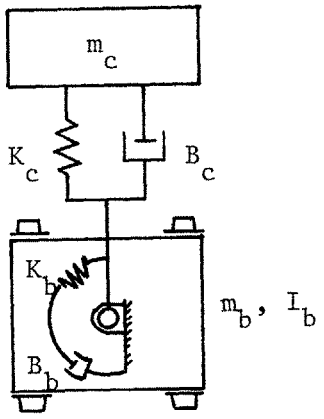

(b) LMO, K-B-Series Yaw

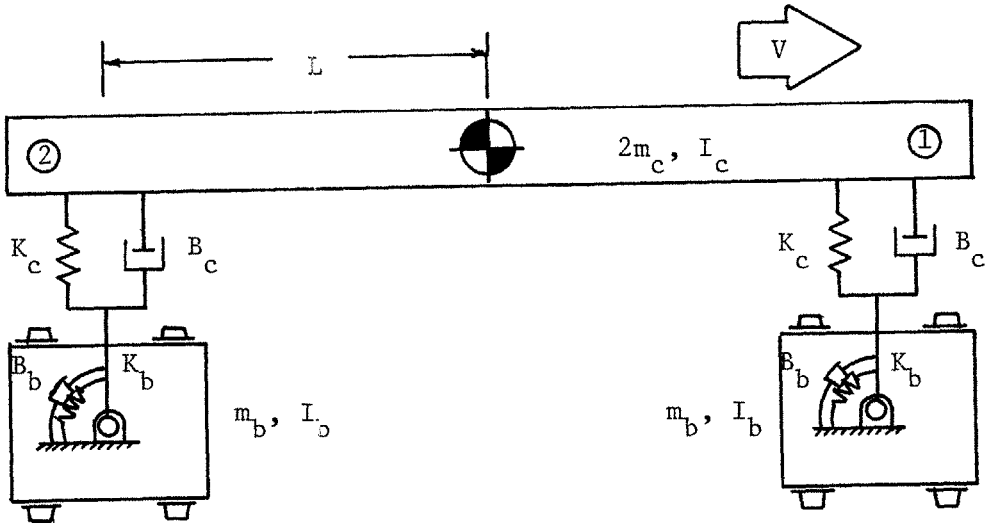

(c) RPB, K-B-Parallel Yaw

FIGURE 3-8

Complete Vehicle Models

(Exploded Laterally)

equations of motion may be obtained by combining Equations 3.3.3, 3.4.1, 3.4.2, and 3.5.14. For the LMO carbody, $\phi_c=0$ and $y_{cb}=y_c$.

The two rail inputs, y_{rf} and y_{rb}, and their derivatives are perfectly correlated under the rigid - rail assumption. Therefore, only one input (chosen as y_{rf}) is necessary to describe the system. Defining the truck time delay

$$\tau = 2\,k\,h\,/\,V \quad , \tag{3.6.1}$$

it is clear that

$$y_{rb} = y_{rf}\,\Delta[\tau] \quad , \tag{3.6.2}$$

where $\Delta[\tau]$ is the linear delay operator. Then using the time derivative operator P;

$$\begin{aligned} y_{rb} &= \Delta[\tau]\,y_{rf} \quad , \\ v_{rf} &= P\,y_{rf} \quad , \\ v_{rb} &= P\,\Delta[\tau]\,y_{rf} \quad . \end{aligned} \tag{3.6.3}$$

One may express the general linear single - input dynamic system equations thus:

$$\frac{d}{dt}\underline{x} = \underline{A}\,\underline{x} + \underline{b}\,y_{rf} \quad , \tag{3.6.4}$$

a vector equation in which $\underline{x}$ is the state variable vector, and $\underline{A}$ and $\underline{b}$ are matrices of dimension n by n and n by 1, respectively, containing constants and linear operators. The $\underline{A}$ and $\underline{b}$ matrices for the LMO system with K-B-parallel yaw secondary are in Figure 3-9.

MODEL: RC (RIW) - LMO, K-B-Parallel Yaw Secondary. n=6.

STATE VECTOR: $\underline{x}^T = [y_c, v_c, y_b, v_b, \phi_b, \omega_b]$

INPUT VECTOR: for y_{rf}, $\underline{b}$ =

$$\begin{bmatrix} 0 \\ 0 \\ 0 \\ (1+\Delta[\tau])([2K_L/m_b]+[2f/m_bV]P) \\ 0 \\ (1+\Delta[\tau])(2fh\alpha/I_b r_0) + (1-\Delta[\tau])([2K_Lkh/I_b]+[2fkh/I_bV]P) \end{bmatrix}$$

CHARACTERISTIC MATRIX: $\underline{A}$ =

$$\begin{bmatrix} 0 & 1 & 0 & 0 & 0 & 0 \\ (-K_c/m_c) & (-B_c/m_c) & (+K_c/m_c) & (+B_c/m_c) & 0 & 0 \\ 0 & 0 & 0 & 1 & 0 & 0 \\ (+K_c/m_b) & (+B_c/m_b) & \frac{-4K_L-K_c}{m_b} & \frac{-4f/V-B_c}{m_b} & (+4f/m_b) & 0 \\ 0 & 0 & 0 & 0 & 0 & 1 \\ 0 & 0 & \frac{-4fh\alpha}{I_b r_0} & 0 & \frac{-4K_Lk^2h^2-K_b}{I_b} & \frac{-4fh^2k_s/V-B_b}{I_b} \end{bmatrix}$$

FIGURE 3-9

System Matrices for the LMO Vehicle Model with K-B-Parallel Yaw Secondary

K-B-Series Yaw Secondary. The vehicle model with secondary yaw spring and damper in series is illustrated in Figure 3-8b. The development of equations of motion exactly parallels that above, except that Equation 3.4.3 is used in place of Equation 3.4.2. The resulting system is seventh order, with the matrices given in Figure 3-10.

7. Equations of Motion: RPB Complete Vehicle. The most complex model to be considered is shown in Figure 3-8c. It consists of an RPB carbody with an RC (or RIW) truck at each end. The only yaw secondary considered is of the K-B-Parallel type.

The development of equations of motion is similar to that of the preceding section, with differences arising from the presence of two spatially separated trucks. The truck attachment point lateral displacements used in Equation 3.4.1 are:

$$\begin{aligned} &\underline{\text{front truck}}: \quad y_{cb1} = y_c + \phi_c L \quad , \quad \text{and} \\ &\underline{\text{rear truck}}: \quad y_{cb2} = y_c - \phi_c L \ . \end{aligned} \tag{3.7.1}$$

Also, the rail inputs at the rear truck are delayed by the time

$$\tau_L = 2\,L\,/\,V \tag{3.7.2}$$

from the corresponding inputs at the front truck. It is useful to keep the rail input at the front axle of the front truck as the single input to the complete system. Therefore,

$$\begin{aligned} y_{rf1} &= y_{rf} \quad , \quad \text{and} \\ y_{rf2} &= y_{rf}\Delta[\tau_L] \quad , \end{aligned} \tag{3.7.3}$$

where the numerical subscript refers to the truck in question.

MODEL: RC (RIW) - LMO, K-B-Series Yaw Secondary, n=7

STATE VECTOR: $\underline{x}^T = [y_c, v_c, y_b, v_b, \phi_b, \omega_b, T_b]$

INPUT VECTOR: for y_{rf}, $\underline{b}$ =

$$\begin{bmatrix} 0 \\ 0 \\ 0 \\ (1+\Delta[\tau])([2K_L/m_b]+[2f/m_bV]P) \\ 0 \\ (1+\Delta[\tau])(2fh\alpha/I_br_0) + (1-\Delta[\tau])([2K_Lkh/I_b]+[2fkh/I_bV]P) \\ 0 \end{bmatrix}$$

CHARACTERISTIC MATRIX : $\underline{A}$ ... see next page

FIGURE 3-10

System Matrices for the LMO Vehicle Model with K-B-Series Yaw Secondary

$$
\begin{bmatrix}
0 & 1 & 0 & 0 & 0 & 0 & 0 \\
(-K_c/m_c) & (-B_c/m_c) & (+K_c/m_c) & (+B_c/m_c) & 0 & 0 & 0 \\
0 & 0 & 0 & 1 & 0 & 0 & 0 \\
(+K_c/m_b) & (+B_c/m_b) & \dfrac{-4K_L-K_c}{m_b} & \dfrac{-4f/V\ -B_c}{m_b} & (+4f/m_b) & 0 & 0 \\
0 & 0 & 0 & 0 & 0 & 1 & 0 \\
0 & 0 & (-4fh\alpha/I_b r_0) & 0 & \dfrac{-4K_L k^2 h^2}{I_b} & \dfrac{-4fh^2 k_s}{I_b V} & (+1/I_b) \\
0 & 0 & 0 & 0 & 0 & (-K_b) & (-K_b/B_b)
\end{bmatrix}
$$

FIGURE 3-10 (ctd.)

Characteristic Matrix (A) for the LMO Vehicle Model with K-B-Series Yaw Secondary

The resulting equations of motion are twelfth order, and some parameter group definitions will aid in presenting them. Define the mass and inertia ratios

$$\rho_m = m_b/m_c \tag{3.7.4}$$

$$\rho_i = I_b/I_c \quad , \tag{3.7.5}$$

and the length parameter

$$q_\ell = (m_b L)/I_c \quad . \tag{3.7.6}$$

These and other parameter groups (g_1, g_2, ... , g_{19}) are tabulated in Table 3-1. Groups g_{11} through g_{16} are reserved for later use in the context of automatic control gains.

With the nomenclature defined above, the RPB model with RC or RIW trucks obeys Equation 3.6.4 with the matrices of Figure 3-11.

8. Acceleration Transfer Functions: LMO Complete Vehicle. For studies of ride quality, the output variable of primary interest is the acceleration of a specified point in the passenger compartment, or carbody. In the case of the LMO carbody model, any point on the carbody is equivalent and its lateral acceleration is $\ddot{y}_c$. It has been possible to obtain analytical expressions for the transfer functions relating rail input, y_{rf}, and carbody acceleration for the two LMO models of Section 6 above.

For a single - input, single - output system, the transfer function for the selected state variable may be obtained [64] by the

TABLE 3-1

Parameter Groups for Rigid Plane Body Vehicle Model

parameter name	definition
ρ_m	m_b/m_c
ρ_i	I_b/I_c
q_ℓ	$m_b L/I_c$
g_1	B_c/m_b
g_2	K_c/m_b
g_3	B_b/I_b
g_4	K_b/I_b
g_5	$4f/(m_b V)$
g_6	$4K_L/m_b$
g_7	$4f/m_b$
g_8	$4fh\alpha/(I_b r_0)$
g_9	$4fh^2k_s/(I_b V)$
g_{10}	$4K_L k^2h^2/I_b$
$g_{11} - g_{16}$	[reserved]
g_{17}	$4fh^2k_s/I_b$
g_{18}	$1/(kh)$
g_{19}	$4fk^2h^2/I_b$

MODEL: RC (RIW) - RPB, K-B-Parallel Yaw Secondary, n=12

STATE VECTOR: $\underline{x}^T = [y_c, v_c, \phi_c, \omega_c, y_{b1}, v_{b1}, \phi_{b1}, \omega_{b1}, y_{b2}, v_{b2}, \phi_{b2}, \omega_{b2}]$

INPUT VECTOR: for y_{rf}, $\underline{b}$ =

$$\begin{bmatrix} 0 \\ 0 \\ 0 \\ 0 \\ 0 \\ [(1+\Delta[\tau])/2]\ [g_6 + g_5 P] \\ 0 \\ [(1+\Delta[\tau])/2]\ [g_8] \ + \ [(1-\Delta[\tau])/2]\ [g_{10}g_{18} + (g_{18}g_{19}/V)P] \\ 0 \\ \{\Delta[\tau_L]\}\ \{[(1+\Delta[\tau])/2]\ [g_6 + g_5 P]\} \\ 0 \\ \{\Delta[\tau_L]\}\ \{[(1+\Delta[\tau])/2]\ [g_8] \ + \ [(1-\Delta[\tau])/2]\ [g_{10}g_{18} + (g_{18}g_{19}/V)P]\} \end{bmatrix}$$

CHARACTERISTIC MATRIX: $\underline{A}$ ... see next page

FIGURE 3-11

System Matrices for the RPB Vehicle Model with K-B-Parallel Yaw Secondary

$$
\begin{bmatrix}
0 & 1 & 0 & 0 & 0 & 0 & 0 & 0 & 0 & 0 & 0 & 0 \\
-\rho_m g_2 & -\rho_m g_1 & 0 & 0 & \rho_m g_2/2 & \rho_m g_1/2 & 0 & 0 & \rho_m g_2/2 & \rho_m g_1/2 & 0 & 0 \\
0 & 0 & 0 & 1 & 0 & 0 & 0 & 0 & 0 & 0 & 0 & 0 \\
0 & 0 & \begin{matrix}-2\rho_i g_4 \\ -2Lq_\ell g_2\end{matrix} & \begin{matrix}-2\rho_i g_3 \\ -2Lq_\ell g_1\end{matrix} & q_\ell g_2 & q_\ell g_1 & \rho_i g_4 & \rho_i g_3 & -q_\ell g_2 & -q_\ell g_1 & \rho_i g_4 & \rho_i g_3 \\
0 & 0 & 0 & 0 & 0 & 1 & 0 & 0 & 0 & 0 & 0 & 0 \\
g_2 & g_1 & Lg_2 & Lg_1 & -g_2-g_6 & -g_1-g_5 & g_7 & 0 & 0 & 0 & 0 & 0 \\
0 & 0 & 0 & 0 & 0 & 0 & 0 & 1 & 0 & 0 & 0 & 0 \\
0 & 0 & g_4 & g_3 & -g_8 & 0 & -g_4-g_{10} & -g_3-g_9 & 0 & 0 & 0 & 0 \\
0 & 0 & 0 & 0 & 0 & 0 & 0 & 0 & 0 & 1 & 0 & 0 \\
g_2 & g_1 & -Lg_2 & -Lg_1 & 0 & 0 & 0 & 0 & -g_2-g_6 & -g_1-g_5 & g_7 & 0 \\
0 & 0 & 0 & 0 & 0 & 0 & 0 & 0 & 0 & 0 & 0 & 1 \\
0 & 0 & g_4 & g_3 & 0 & 0 & 0 & 0 & -g_8 & 0 & -g_4-g_{10} & -g_3-g_9
\end{bmatrix}
$$

FIGURE 3-11 (continued)

following procedure. First, apply the Laplace transform to Equation 3.6.4 to yield

$$s\,\underline{X}(s) = \underline{A}(s)\underline{X}(s) + \underline{B}(s)U(s) \quad , \tag{3.8.1}$$

where s is the Laplace variable and $\underline{X}$, $\underline{A}$, and $\underline{B}$ are matrices all of whose elements have been transformed. Of especial importance are the following transforms:

$$L(\Delta[\tau]) = e^{-\tau s} \quad , \text{ and} \tag{3.8.2}$$

$$L(P) = L(d/dt) = s \quad . \tag{3.8.3}$$

Second, solve Equation 3.8.1 algebraically for the required elements of the transformed state vector $\underline{X}$; Cramer's Rule may be used for this purpose. Third, combine the elements of $\underline{X}$ as required to produce the desired output. In the present case, the relationship between the output, $\ddot{y}_c$, and the state vector is a simple one, namely

$$\ddot{Y}_c(s) = s^2 Y_c(s) \quad . \tag{3.8.4}$$

This procedure may be further specialized for purposes of computation. Appendix B contains the methods used during this work to obtain transfer functions partially or wholly in symbolic form using the formal algebra computer languages Formac [65] and Macsyma [66].

Transfer functions of acceleration for the LMO carbody model involve only a single delay at the input -- the wheelbase transit time -- and may be written in the general form:

$$G_a(s) = \{s^2\} \frac{\sum_{i=0}^{m} \{ (\frac{1+e^{-\tau s}}{2}) b_{pi} + (\frac{1-e^{-\tau s}}{2}) b_{mi} \} s^i}{\sum_{i=0}^{n} c_i s^i} \qquad (3.8.5)$$

with

$$G_a(s) = \frac{L(\ddot{y}_c)}{L(y_{rf})} \quad . \qquad (3.8.6)$$

For sinusoidal inputs, the coefficients b_{pi} represent the influence of in-phase rail inputs at the front and rear axles, and the coefficients b_{mi} represent the influence of out-of-phase inputs. A useful simplification is obtained by forcing τ to zero -- i.e., neglecting the phase difference between axles. The resulting simplified transfer function will be termed the "envelope" approximation, since at low frequencies the wheelbase transit time is insignificant, and at high frequencies the out-of-phase inputs do not couple significantly to lateral displacement; at these extremes, then, the approximation follows and limits, respectively, the exact transfer function.

The parameter groups in Table 3-2 recur sufficiently often to merit being given names. The acceleration transfer function coefficients are tabulated in Table 3-3 (for K-B-parallel yaw secondary) and Table 3-4 (for K-B-series yaw secondary) using the new notation.

9. Baseline Parameter Values. The nominal values which will be used

TABLE 3-2

Parameter Groups for Transfer Functions, LMO Models

parameter name	definition
ρ_m	m_b/m_c
ρ_{bb}	$B_b V/(4fh^2k_s)$
ρ_{bc}	$B_c V/(4f)$
τ	$2kh/V$
g_5	$4f/(m_b V)$
S_1	$K_c(1+\rho_m) + 4K_L$
S_2	$K_b + 4K_L k^2 h^2$
S_3	$1 + \rho_{bc}(1+\rho_m)$
S_4	$K_c + 4K_L \rho_{bc}$
S_5	$4fh^2k_s/(I_b V)$
S_6	$4fh\alpha V/(I_b r_0)$
S_7	$B_b + 4fk^2h^2/V$

TABLE 3-3

Transfer Function Coefficients: RC (RIW), LMO, K-B-Parallel Yaw Secondary

n=6, m=4

DENOMINATOR

$$c_6 = 1$$

$$c_5 = g_5 S_3 + S_5(1+\rho_{bb})$$

$$c_4 = g_5 S_3 S_5(1+\rho_{bb}) + S_2/I_b + S_1/m_b + g_5^2 \rho_m \rho_{bc}$$

$$c_3 = g_5[(S_2 S_3/I_b)+(S_4 \rho_m/m_b)] + S_5(1+\rho_{bb})[(S_1/m_b)+g_5^2 \rho_m \rho_{bc}]$$

$$c_2 = g_5[S_6+(S_4 S_5 \rho_m\{1+\rho_{bb}\}/m_b)] + (S_2/I_b)[(S_1/m_b)+g_5^2 \rho_m \rho_{bc}] + (4K_c K_L \rho_m/m_b^2)$$

$$c_1 = g_5^2 \rho_m \rho_{bc} S_6 + [4K_c K_L \rho_m S_5(1+\rho_{bb})/m_b^2] + [g_5 \rho_m S_2 S_4/(m_b I_b)]$$

$$c_0 = g_5 K_c \rho_m S_6/m_b + [4K_c K_L \rho_m S_2/(m_b^2 I_b)$$

NUMERATOR (in-phase)

$$b_{p4} = g_5^2 \rho_m \rho_{bc}$$

$$b_{p3} = g_5 \rho_m S_4/m_b + g_5^2 \rho_m \rho_{bc}(1+\rho_{bb}) S_5$$

$$b_{p2} = g_5^2 \rho_m \rho_{bc} S_2/I_b + (\rho_m/m_b)[g_5 S_4 S_5(1+\rho_{bb})+(4K_c K_L/m_b)]$$

$$b_{p1} = g_5^2 \rho_m \rho_{bc} S_6 + (\rho_m/m_b)[(g_5 S_2 S_4/I_b)+(4K_c K_L S_5\{1+\rho_{bb}\}/m_b)]$$

$$b_{p0} = (\rho_m/m_b)[g_5 K_c S_6 + (4K_c K_L S_2/\{m_b I_b\})]$$

(continued)

TABLE 3-3 (continued)

NUMERATOR (out-of-phase)

$$b_{m4} = 0$$

$$b_{m3} = 0$$

$$b_{m2} = g_5{}^3 m_b V k h \rho_m \rho_{bc} \; / \; I_b$$

$$b_{m1} = g_5{}^2 V k h \rho_m S_4 \; / \; I_b$$

$$b_{m0} = g_5 (4 V k h K_c K_L \rho_m) / (m_b I_b)$$

TABLE 3-4

Transfer Function Coefficients: RC (RIW), LMO, K-B-Series Yaw Secondary

n=7, m=5

DENOMINATOR

$$c_7 = 1$$

$$c_6 = g_5 S_3 + S_5 + (K_b/B_b)$$

$$c_5 = (K_b/B_b)[g_5 S_3 + S_5] + g_5 S_3 S_5 + (S_1/m_b) + (S_2/I_b) + g_5^2 \rho_m \rho_{bc}$$

$$c_4 = [(K_b/B_b)+S_5][(S_1/m_b)+g_5^2 \rho_m \rho_{bc}] + g_5 S_3[(S_2/I_b)+S_5(K_b/B_b)] + (g_5 \rho_m S_4/m_b) + [4K_L k^2 h^2 K_b/(I_b B_b)]$$

$$c_3 = [S_5(K_b/B_b)+(S_2/I_b)][(S_1/m_b)+g_5^2 \rho_m \rho_{bc}] + (S_4 g_5 \rho_m/m_b)[S_5+(K_b/B_b)] + g_5[S_6+(4K_L k^2 h^2 S_3 K_b/\{I_b B_b\})] + 4\rho_m K_c K_L/m_b^2$$

$$c_2 = g_5 S_6[(K_b/B_b)+g_5 \rho_m \rho_{bc}] + (4K_c K_L \rho_m/m_b^2)[S_5+(K_b/B_b)] + (g_5 \rho_m S_4/m_b)[(S_2/I_b)+S_5(K_b/B_b)] + [4K_L k^2 h^2 K_b/(I_b B_b)][(S_1/m_b)+g_5^2 \rho_m \rho_{bc}]$$

$$c_1 = g_5 S_6 \rho_m[(K_c/m_b)+(g_5 \rho_{bc} K_b/B_b)] + [4\rho_m K_L/(m_b I_b)][(S_2 K_c/m_b)+(g_5 k^2 h^2 S_4 K_b/B_b)] + [4\rho_m K_c K_L S_5 K_b/(m_b^2 B_b)]$$

$$c_0 = (\rho_m K_c K_b/B_b)[(g_5 S_6/m_b) + (\{4K_L k\ h\ /m_b\}^2/I_b)]$$

NUMERATOR (in-phase)

$$b_{p5} = g_5^2 \rho_m \rho_{bc}$$

$$b_{p4} = (g_5 \rho_m S_4/m_b) + (g_5^2 \rho_m \rho_{bc})[S_5+(K_b/B_b)]$$

(continued)

TABLE 3-4 (continued)

$$b_{p3} = (g_5^2\rho_m\rho_{bc})[(S_2/I_b)+S_5(K_b/B_b)] + (g_5\rho_m S_4/m_b)[S_5+(K_b/B_b)] + (4K_cK_L\rho_m/m_b^2)$$

$$b_{p2} = (g_5^2\rho_m\rho_{bc})[S_6+(4K_Lk^2h^2K_b/\{I_bB_b\})] + (g_5\rho_m S_4/m_b)[(S_2/I_b)+S_5(K_b/B_b)] + (4K_cK_L\rho_m/m_b^2)[S_5+(K_b/B_b)]$$

$$b_{p1} = g_5\rho_m S_6[(K_c/m_b)+g_5\rho_{bc}(K_b/B_b)] + [4K_L\rho_m K_b/(m_bB_b)][(S_5K_c/m_b)+(S_4g_5k^2h^2/I_b)] + [4K_cK_L\rho_m S_2/(m_b^2I_b)]$$

$$b_{p0} = (\rho_m K_cK_b/B_b)[(S_6g_5/m_b)+(\{4K_Lkh/m_b\}^2/I_b)]$$

NUMERATOR (out-of-phase)

$$b_{m5} = 0$$

$$b_{m4} = 0$$

$$b_{m3} = g_5^3m_bVkh\rho_m\rho_{bc} \;/\; I_b$$

$$b_{m2} = (g_5^2Vkh\rho_m/I_b)[S_4+(g_5m_b\rho_{bc}K_b/B_b)]$$

$$b_{m1} = (g_5Vkh\rho_m/I_b)[(g_5S_4K_b/B_b)+(4K_cK_L/m_b)]$$

$$b_{m0} = (g_5Vkh\rho_m/I_b)[4K_cK_LK_b/(m_bB_b)]$$

for parameters in the numerical examples throughout this work are listed in Table 3-5. They are based on the measured data on the Japanese New Tokaido Line (NTL) car studied by Matsudaira [36], and are representative of U. S. practice for light rail vehicles. Two baseline values are listed for K_L, one of them zero. The zero value is for conical wheel treads (as on the NTL vehicle), and is standard for RC models. The nonzero value corresponds to concave treads with ΔR=5 inches (see Appendix A), and is used for RIW models.

10. Importance of Finite-Mass Vehicle Body Models. It has been remarked that the "translating reference" carbody models frequently used to study secondary hunting may not provide a satisfactory estimate of the critical speed, V_c, at which hunting becomes unstable. Such models are based on the assumption that the truck mass is negligible in comparison with the carbody mass -- an assumption which is not justified for most passenger cars (ρ_m=0.53 for the baseline NTL vehicle, whereas ρ_m=0 would be required for the translating reference model to be exact). An example will illustrate the discrepancy between results obtained from the finite-mass LMO model and from the infinite-mass model. Figure 3-12 shows the damping ratio, ξ, of the most lightly damped pair of roots of a rigid truck model studied by Clark and Law [33]; the frequency of these eigenvalues is very close to the kinematic hunting frequency. Both curves were generated using the parameters of Reference 33 in the LMO characteristic polynomial of Table 3-3. The solid line corresponds to setting ρ_m=0 to conform to the translating reference model used in the

TABLE 3-5

Baseline Parameter Values

parameter and definition		value	units
m_b	truck mass	684.05	slug
m_c	carbody half mass	1300.	slug
I_b	truck inertia	1.591×10^6	slug-in^2
I_c	carbody inertia	2.112×10^8	slug-in^2
h	half gauge	29.528	in
k	wheelbase/gauge ratio	1.6667	-
r_0	equilibrium wheel radius	17.91	in
α	conicity (effective)	0.025	-
L	half carbody length	25.	ft
ΔR	wheel-rail curvature difference (profiled)	5.	in
K_b	secondary yaw stiffness	4.196×10^8	slug-in^2/sec^2
B_b	secondary yaw damping	0	slug-in^2/sec
K_c	secondary lateral stiffness	4.834×10^4	slug/sec^2
B_c	secondary lateral damping	6.714×10^3	slug/sec
	grav. stiffness (RC)	0.	slug/sec^2
K_L	grav. stiffness (RIW)	3.8367×10^4	slug/sec^2
f	creep coefficient	2.896×10^6	lbf
V	forward speed (default)	100.	mph

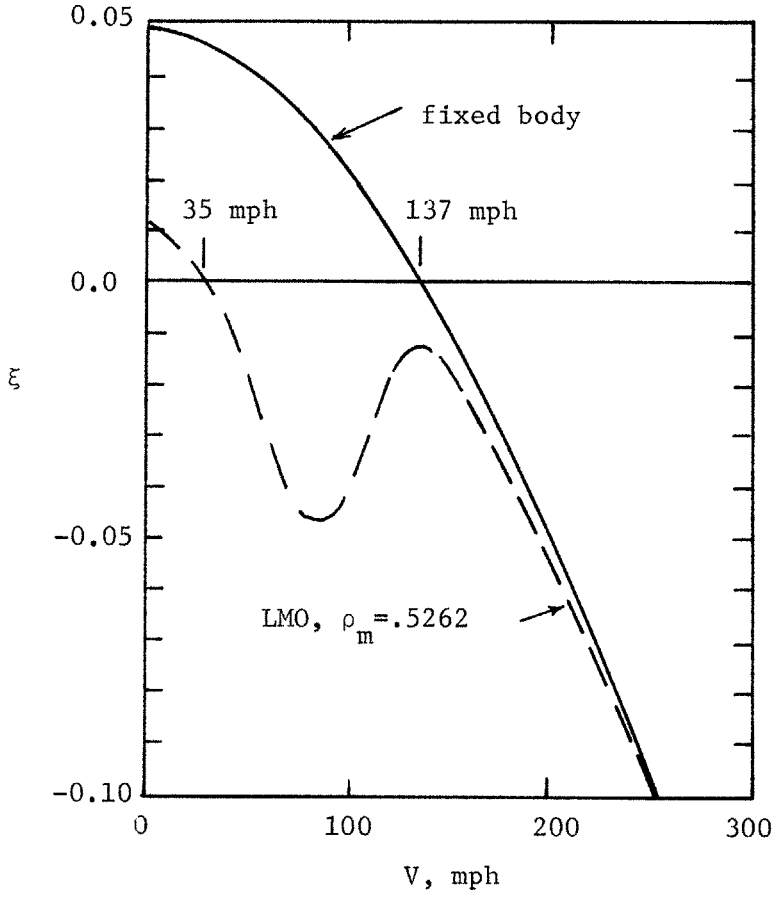

FIGURE 3-12

Comparison of LMO and Translating Reference Models

(Based on Clark and Law [33])

paper, and the dashed line to using the baseline value of ρ_m=0.5262. The introduction of finite carbody mass results in the reduction of critical speed from 137 to 35 mph. The curves approach one another in the high-speed limit, where the carbody may correctly be assumed to be nearly stationary. At low speeds and low ω_k, however, hunting is destabilized by finite carbody mass due to two mechanisms. First, truck and carbody masses add at very low frequencies, so that more stiffness is required to overcome dynamic inertial forces than would be if the carbody were stationary. Second, a broad resonance due to oscillation of the carbody on the secondary suspension is centered around 90 mph, contributing to a primary hunting instability completely absent in the translating reference model. It is clear that under some conditions, a dominant mode of instability can be entirely missed when carbody mass is not taken into account.

Figure 3-13 shows similar plots of damping ratio versus speed based on Matsudaira's published results [36]. Three curves of ξ for the least damped roots are shown, using the parameter values given in Reference 36 in three models of successively increasing complexity: (1) one truck attached to a translating reference (dashed); (2) one truck attached to an LMO carbody (solid); and (3) two trucks attached to a carbody with lateral, yaw, and roll freedom (solid-dashed). For this set of parameter values, the three models agree within 5% in their predictions of critical speed (about 250 mph). But in the range of 0-200 mph, both the LMO and the seven degree-of-freedom models show substantial reduction of damping due to carbody effects; the

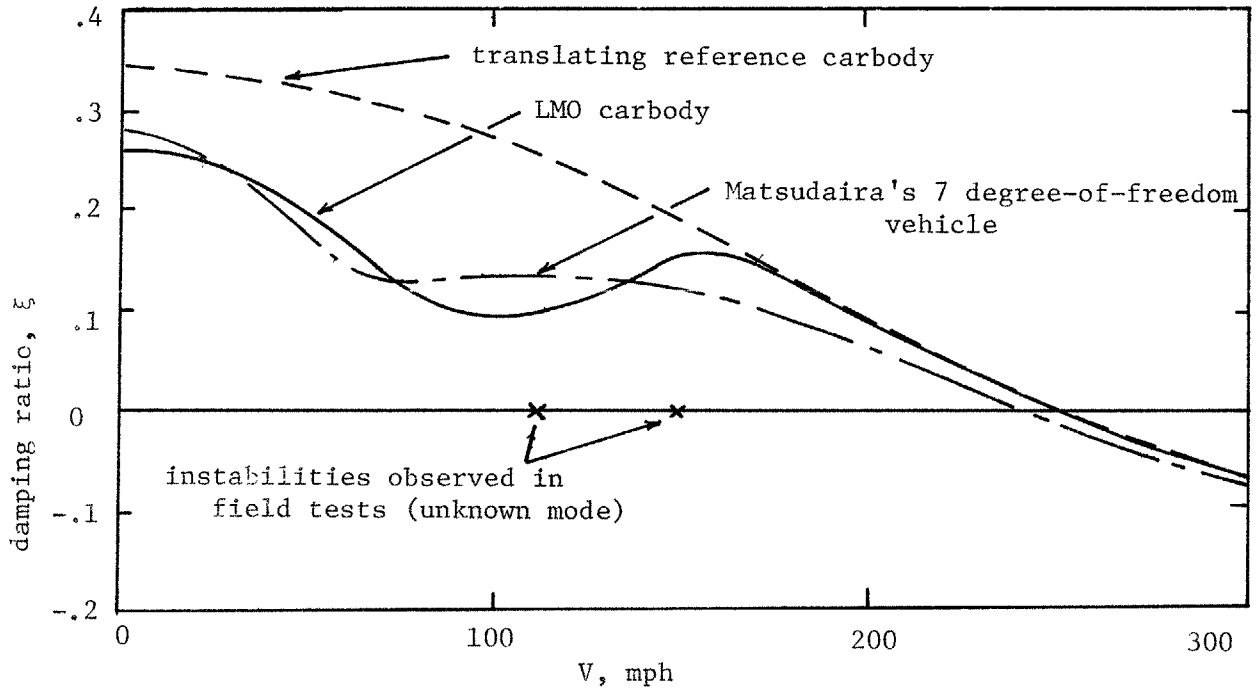

FIGURE 3-13

Comparison of Carbody Models -- Least-Damped Roots
(Parameters Based on Matsudaira [36])

fact that field tests showed instabilities (or perhaps resonances) in this speed range suggests that finite carbody mass cannot be correctly ignored.

It should be noted that the parameters used in [36] correspond to those of the baseline NTL vehicle with the exception of creep coefficient f, which was effectively 1.448×10^6 lbf in the reference. Use of the baseline value of f yields curves which are similar in shape to those of Figure 3-13, but displaced downward; V_c is reduced to approximately 200 mph.

11. Characterization of Rail Profile. Allowable lateral rail profiles have been restricted by Equations 3.5.5 to those involving parallel (or constant gauge) deviations of both rails from a straight nominal centerline. This assumption is imbedded in the equations of motion; any sort of function (e.g., steps, ramps, sinusoids) may be used for the input y_{rf}.

When a vehicle traverses a real guideway, however, it encounters rail inputs which are at least partially random in character. There may also be periodic components arising from such origins as rail joints and track supports. For the purposes of predicting vehicle response to this environment, it is necessary to find a statistical description of the input. It has been experimentally discovered [1,3] that for a wide variety of guideway types and over a broad band of component wavelengths, the amplitude of irregularities at a given wavelength (measured along the guideway) is roughly proportional to the

wavelength. When irregularities of this nature are encountered by a vehicle moving at speed V, the resulting temporal spectral density of input displacement impressed upon the vehicle suspension is

$$\Phi_{yy} = -\frac{A\,V}{s^2} \quad , \tag{3.11.1}$$

where A is a roughness parameter (with dimensions of length) and s is the Laplace variable; in this context

$$s \equiv j\,\omega \quad , \text{ where} \tag{3.11.2}$$

$$j \equiv \sqrt{-1} \quad .$$

If there are important periodic components in the input, or if it is necessary to deal with a very wide range of frequencies, this approximation is inadequate. In particular, notice that it gives an infinite mean square deviation because of the large excursions at long wavelength (low frequency). However, the expression of Equation 3.11.1 is a satisfactory approximation over the frequency range of interest to a guideway without periodic content, and due to its analytical simplicity it will be used exclusively in this work.

All spectral densities considered here are single - sided -- i.e., integration over positive values of frequencies only will yield the correct value of mean square. With this definition, a suitable value of the roughness parameter A is that for welded rail in good condition [1]:

$$A = 1.2566\text{x}10^{-6} \text{ ft.} \tag{3.11.3}$$

CHAPTER 4

PERFORMANCE OF CONVENTIONAL VEHICLE WITH LATERAL-MASS-ONLY CARBODY, UNCONTROLLED

In this chapter three important measures of the performance of a rigid conventional truck mounted on a lateral-mass-only carbody (RC-LMO) are examined: stability, ride quality, and tracking error. The most direct means of improving dynamic behavior is found to be increasing the stiffness resisting yaw of the truck; this may be accomplished either in the secondary by increasing the yaw stiffness K_b between truck and carbody, or at the wheels by using profiled treads to create a gravitational stiffness K_L. Putting a damper in series with the secondary yaw stiffness is suggested as a means of overcoming certain practical difficulties with the use of large K_b.

1. Stability. Stability of operation is essential to a vehicle, and has been the property most extensively studied in the past. In the context of this thesis, stability means asymptotic stability for small perturbations; it is also possible for a system to be stable for small perturbations but unstable for larger ones [30], a situation which requires nonlinearities and is not considered here. For linear or linearized systems, asymptotic stability depends only upon the characteristic polynomial, or denominator of the transfer functions. If any of the roots of the characteristic polynomial (C.P.) have positive real parts, the system is unstable. The presence of unstable roots may be determined in two ways: (1) by solving for the

roots explicitly (i.e., determining the system eigenvalues), or (2) by applying an indirect test such as the Routh-Hurwitz criterion [64]. Eigenvalues contain more information than is necessary to answer the simple question of stability, so the second method is used for the stability analysis.

Only parallel connection of K_b and B_b is considered in this section. Series connection is discussed in Section 5.

The C.P. which applies to the RC-LMO vehicle is given by the coefficients "c" in Table 3-3, with α nonzero and $k_s=k^2+1$. Some insight into the behavior of a conventional truck may be gained by considering the limit of these coefficients for low speed ($V\to 0$, or "crawl"). Restricting attention to a truck with coned wheels ($K_L=0$), and retaining only low-order terms in V^{-1}, gives:

$$
\begin{aligned}
c_6 &= 1 \\
c_5 &\simeq g_5(1 + m_b k_s h^2/I_b) \\
c_4 &\simeq g_5{}^2(m_b k_s h^2/I_b) \\
c_3 &\simeq g_5{}^2(\rho_m k_s h^2 B_c/I_b) \\
c_2 &\simeq g_5{}^2(\rho_m k_s h^2 K_c/I_b) \\
c_1 &\simeq g_5(\rho_m K_c/m_b I_b)\cdot K_b \\
c_0 &\simeq g_5{}^2 V^2(\rho_m K_c h/I_b r_0)\cdot\alpha \quad .
\end{aligned}
\tag{4.1.1}
$$

A necessary but insufficient condition for asymptotic stability is that each of these coefficients have the same sign [64], which in particular implies that K_c, B_c, K_b, and α must all be positive if the system is to be stable at even very low speeds. In the numerical

examples which follow, it will be shown that large yaw stiffness remains a primary means of stabilizing hunting at all speeds. The physical interpretation of this stabilizing role of K_b is that secondary yaw stiffness acts to align the truck with the carbody (which in turn is approximately aligned with the track), thereby opposing the buildup of kinematic oscillations. Yaw damping, B_b, has a negligible effect on stability at low speeds. At higher speeds damping retards the steering action of the truck and thereby makes hunting worse, although the contribution of the secondary damper is normally very small compared to that of creep friction. For the baseline vehicle, based on NTL parameters, $B_b=0$. Many actual vehicles, especially freight cars, use Coulomb friction yaw damping to stabilize hunting; the effect of friction damping, however, is radically different from that of linear damping and is beyond the scope of this thesis.

An alternative means of obtaining the effect of yaw stiffness is to use concave, rather than conical, wheel tread profiles. For such wheels it has been shown that there is a gravitational stiffness K_L. If there are four wheels, each with K_L, on a rectangular truck, the net effective yaw stiffness from their action is $4K_L(kh)^2$ -- a fact embodied in the expression for S_2. The use of gravitational stiffness has certain advantages over secondary yaw stiffness as a means of suppressing hunting. Since gravitational stiffness acts between rails and wheels, rather than between carbody and truck, it does not rely upon alignment of the carbody with the track for its proper effect.

A high secondary yaw stiffness can impede curving by resisting the truck's natural tendency to yaw with the curve; this problem does not exist if the yaw stiffness is relative to the track. The difficulty of aligning the truck in yaw so that there is no bias in the yaw spring is eliminated. The net effective rotational stiffness obtainable in this manner is considerable, arising as it does from a component of the vehicle weight applied with a sizable moment arm. There is no problem with transmitting torque through a flexible truck frame, since forces are applied directly at the wheels. The difficulty with concave wheel treads is that if they are poorly designed, or simply allowed to wear down, the effective conicity can increase markedly. This increasing conicity increases the kinematic hunting frequency (see Equation 2.4.1) and places added demands on yaw stiffness which may exceed the extra stiffness made available by K_L. (As an example, if the conicity of the baseline RC-LMO vehicle is increased to 0.05, total yaw stiffness must be nearly doubled to 8.1×10^8 slug-in^2/sec^2 in order to maintain critical speed at 200 mph.)

An idea of the potential added stiffness from worn or profiled wheels may be obtained by taking the RIW baseline value of K_L from Table 3-5. Then the added effective yaw stiffness is

$$4K_L(kh)^2 = 3.717 \times 10^8 \text{ slug-in}^2/\text{sec}^2,$$

a value comparable to the baseline K_b for a conventional truck.

Figure 4-1a shows, for an otherwise baseline RC-LMO vehicle, the loci of one of a complex conjugate pair of poles corresponding to truck

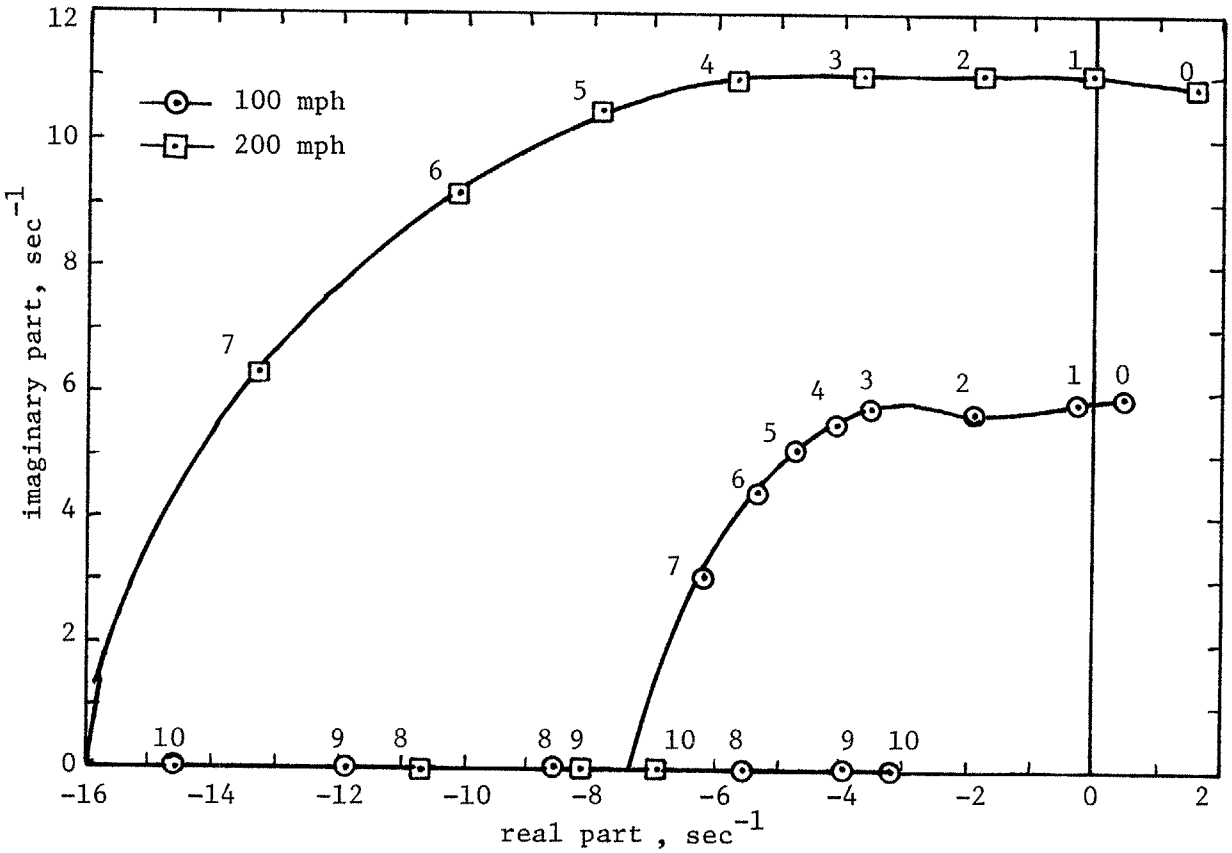

FIGURE 4-1 (a)

Root Loci of Hunting Pole, for Variations of Factor on K_b (Relative to Baseline)

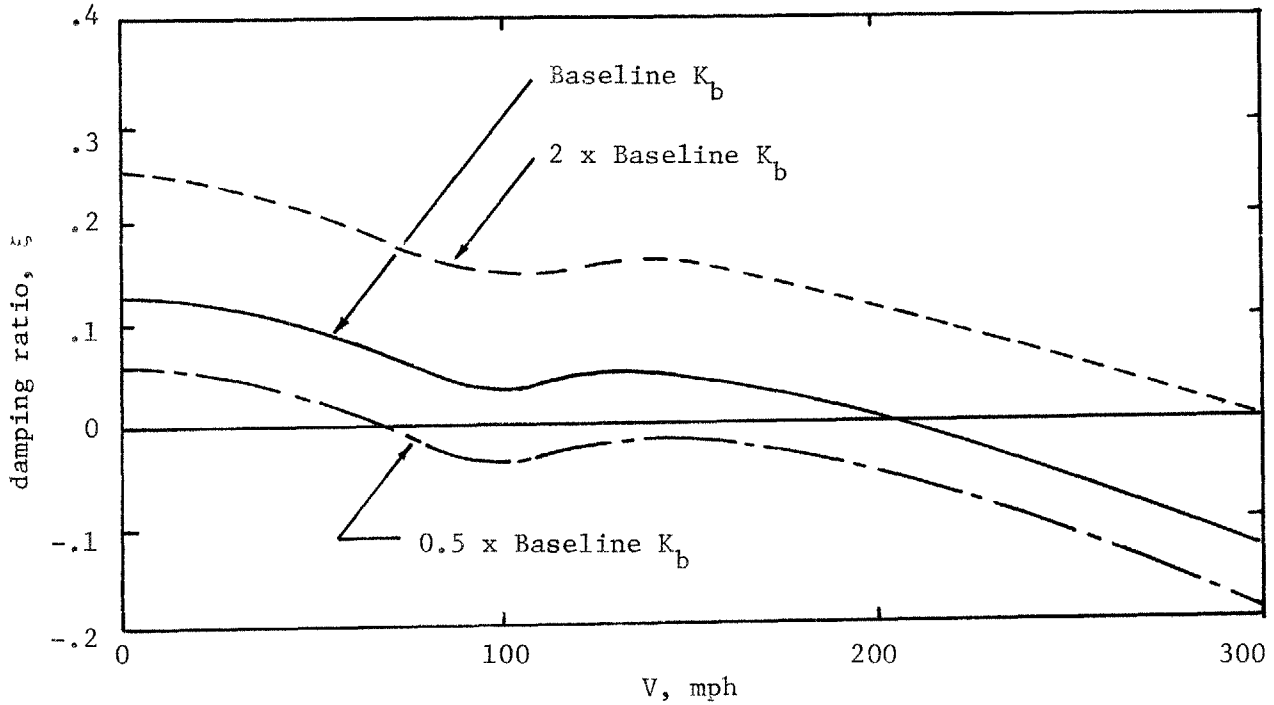

FIGURE 4-1 (b)

Variation with Speed of Damping Ratio of Least-Damped Roots, RC-LMO Model, Baseline Parameters with Variation of Yaw Stiffness K_b

hunting for each of two speeds (100 and 200 mph), as K_b is increased from zero to ten times its baseline value of 4.196×10^8 slug-in^2/sec^2. Both speeds are unstable (i.e., have poles in the right half-plane) at $K_b=0$. The nominal value of K_b stabilizes both, but the margin of stability at 200 mph is very small. Further increases in K_b increase the damping ratio significantly. The natural frequency increases slightly also, but the fact that it remains fairly constant over a wide range of yaw stiffness shows the strong influence of kinematic hunting on the dominant frequency. For comparison, Equation 2.4.1 predicts a kinematic frequency of 0.99 Hz (6.226 sec^{-1}) at 100 mph, and 1.98 Hz (12.452 sec^{-1}) at 200 mph. The somewhat erratic path of the 100 mph locus between stiffness factors 1 and 3 is due to a carbody resonance pole in the vicinity, already mentioned in §3.10. Figure 4-1b shows damping ratio versus speed for this case with three values of K_b. Notice that V_c for the baseline RC-LMO vehicle is just above 200 mph.

The trend of the hunting poles toward ever-higher damping, as in Figure 4-1, is an artifact of the LMO carbody model. If the carbody is allowed to yaw, damping increases up to a point along a similar path. At very high values of K_b, however, the trucks become so rigidly restrained that the entire vehicle begins to behave like an unrestrained truck of very long wheelbase, and damping decreases again. The stiffness values required for this type of behavior are well outside the practical range.

Figure 4-2 contains curves showing the boundary between stable and

(a) half baseline f

(b) baseline f

(c) twice baseline f

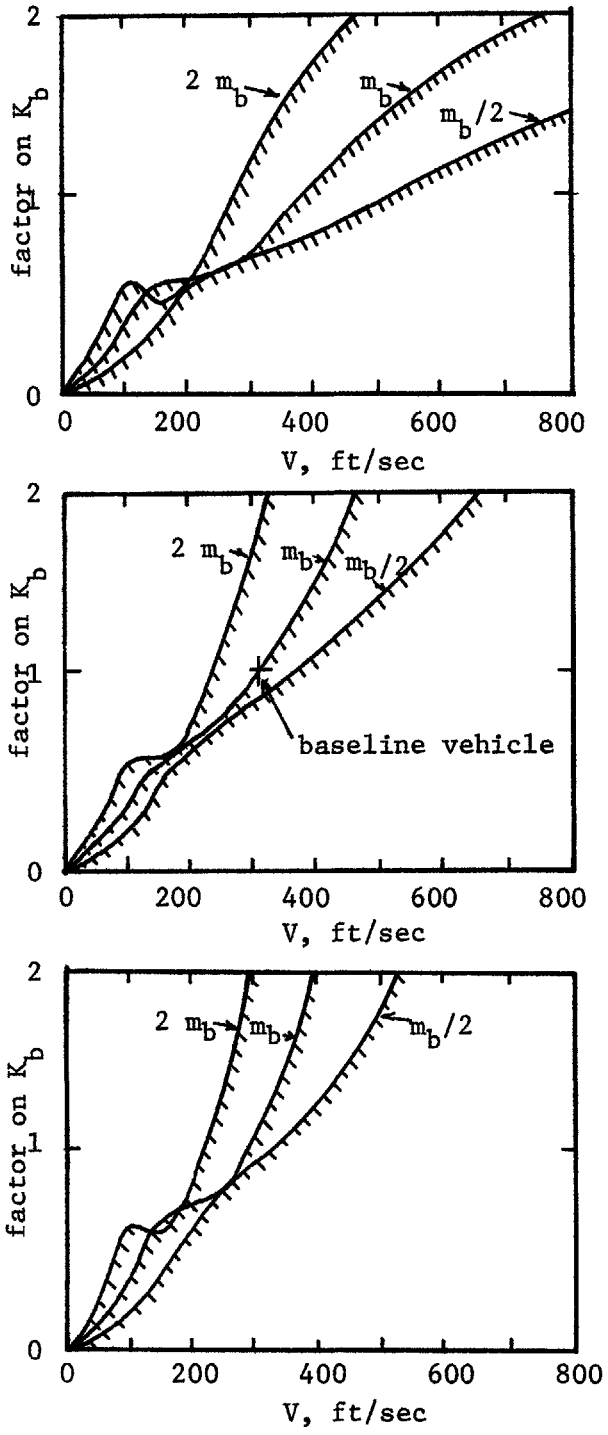

FIGURE 4-2

Variation of Critical Speed with Factors on K_b and m_b
(Relative to Baseline)
Shaded Side of Curve is Unstable.

unstable speeds as a function of K_b for various combinations of truck inertia (m_b and I_b) and creep coefficient f. The inertial properties have been assumed to vary proportionally, with

$$I_b = m_b \cdot (2.326 \times 10^3 \text{ in}^2) \quad . \qquad (4.1.2)$$

In the figure, m_b, f, and K_b are expressed as multiples of the baseline value. The system is stable to the upper left of the boundary, and unstable to the lower right. Notice that in some curves, particularly those with low m_b, it is possible to pass through one region of instability, through a region of stability, and into a second and final region of instability as V is increased; the two regions of instability correspond to primary and secondary hunting, respectively. The perturbations in the curves, even when not severe enough to cause two unstable regions, illustrate the importance of body resonances in vehicle dynamics. Figure 4-2 shows that the critical speed V_c may be extended indefinitely by increasing K_b, and that the K_b necessary to stabilize the system at a given V is approximately proportional to m_b. The dependency of yaw stiffness on creep coefficient f is relatively weak -- a fortunate circumstance, since f is known only approximately.

The baseline vehicle conditions are marked on Figure 4-2b with a cross. Its critical speed is about 305 ft/sec, or 208 mph.

2. Ride Quality. Recall that from §1.3, the perceived ride quality is assumed to depend upon the acceleration spectral density (A.S.D.) of the passenger compartment location of interest. The rail

centerline deviation is assumed to be a zero-mean Gaussian process with spectral density given by Equation 3.11.1. For a linear system, the output due to a Gaussian input process is also Gaussian, with a spectral density given by [67]:

$$\Phi_o = \Phi_i \, G(s) \cdot G^*(s) \quad , \tag{4.2.1}$$

where Φ_o and Φ_i are the spectral densities of output and input, respectively; G(s) is the complex transfer function relating output to input, and $G^*(s)$ is the complex conjugate of G. For the purposes of ride quality evaluation, the appropriate transfer function is the acceleration transfer function $G_a(s)$ given by Equation 3.8.6. The acceleration response to the assumed rail input spectrum may be computed and compared with the DOT/UTACV goal illustrated in Figure 1-4; the comparison gives a qualitative idea of whether the resulting ride would be considered "good". It is also possible to integrate the acceleration spectrum and take the square root to find root-mean-square (RMS) acceleration.

The A.S.D. for the baseline vehicle operating at 100 mph is shown in Figure 4-3. Several important features may be illustrated in this figure. There is a strong peak around 0.95 Hz, caused by a combination of kinematic hunting and a carbody natural frequency. The hunting frequency (neglecting dynamics) is given by Equation 2.4.1 and is proportional to speed V; at 100 mph, $\nu_k = \mu_k / 2\pi = 0.99$Hz. The secondary resonance is independent of V. Its frequency may be approximated by assuming the truck fixed, so that

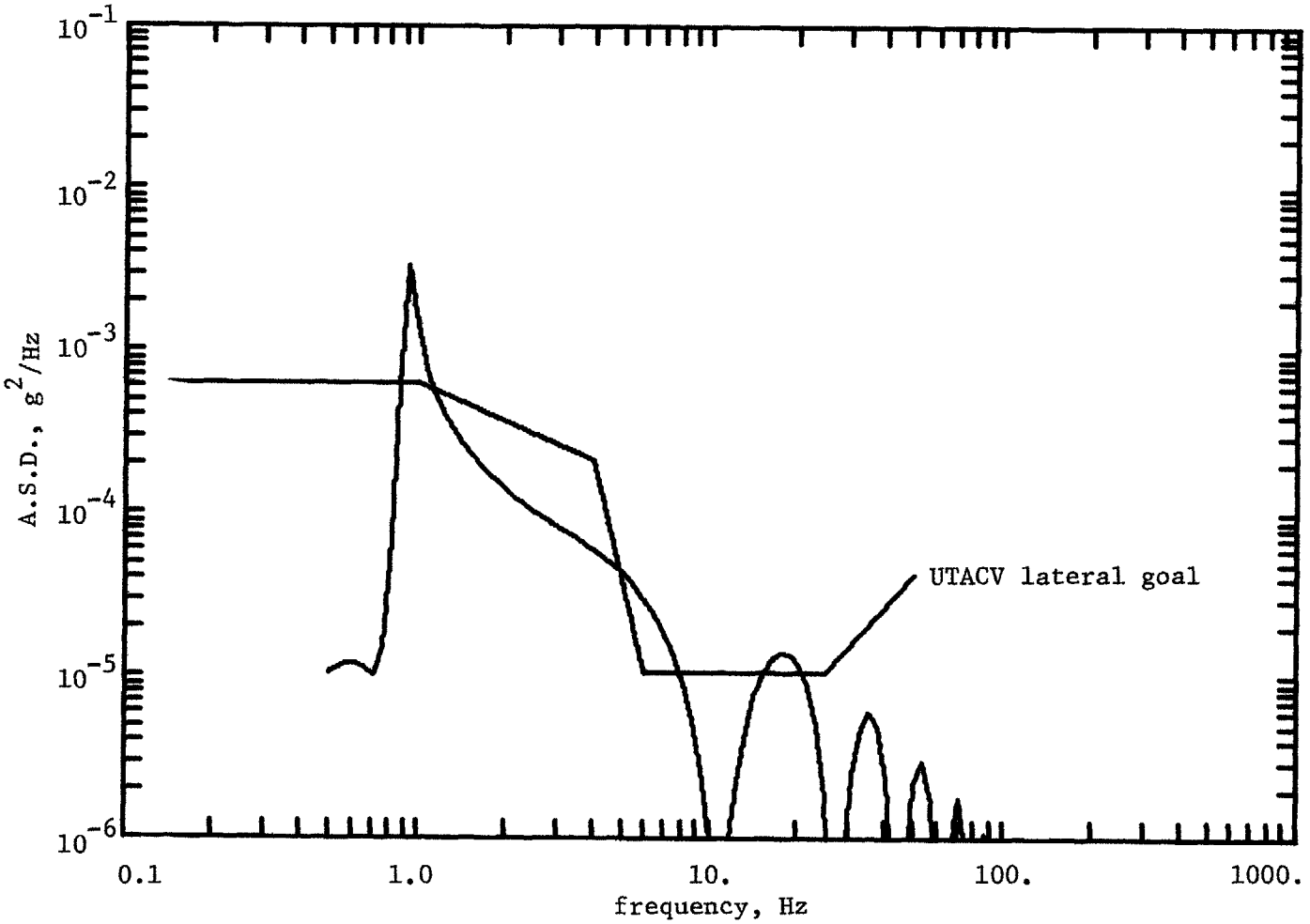

FIGURE 4-3

Acceleration Spectral Density of Baseline Vehicle at 100 mph (RC-LMO)

$$\nu_o = \sqrt{K_c/m_c}\ /2\pi = 0.97 \text{ Hz} \quad ;$$

coincidentally, this is close to the forcing (hunting) frequency at 100 mph, so a resonance condition is set up. The hunting peak exceeds the UTACV goal by an order of magnitude. A second important feature of Figure 4-3 is the succession of nodes and antinodes in the response at high frequencies. These are due to the wheelbase time delay, and will be examined in the next section.

The low- and high-frequency asymptotic behavior of the A.S.D. may be identified. At low frequencies, the vehicle follows the track centerline exactly, so that its A.S.D. approaches

$$\text{LFA} = (s^2)^2\ (-AV/s^2) = AV\omega^2 \quad . \qquad (4.2.2)$$

At frequencies well above that of kinematic hunting, the lateral creep force begins to dominate the tracking mechanism, as the difference in wheel and rail lateral velocity is resisted by a force $-f\Delta v/V$. Under this condition, the wheels may be replaced by equivalent dampers of constant

$$B_r = f/V \qquad (4.2.3)$$

as in Figure 4-4. Notice that the yaw restraints K_b and B_b have been omitted, since yaw of the truck does not couple significantly to lateral motion of the carbody at high frequencies; K_c has also been omitted for clarity, as its effect is overshadowed by that of B_c at high frequencies. The acceleration transfer function for this reduced system

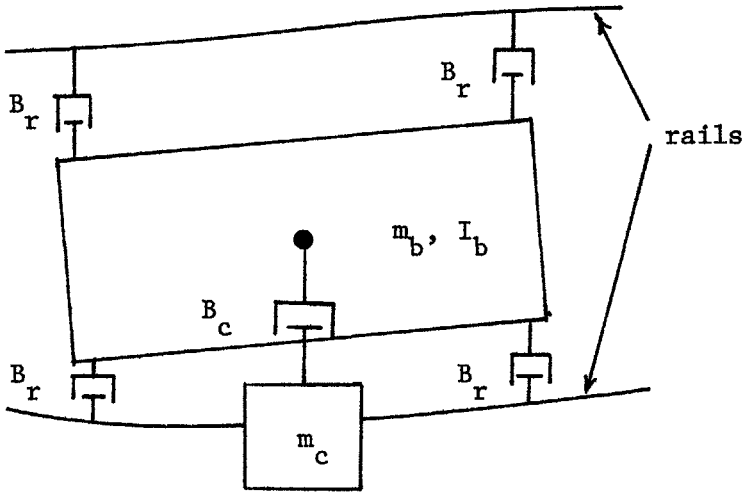

FIGURE 4-4

Equivalent LMO Model for High Frequencies

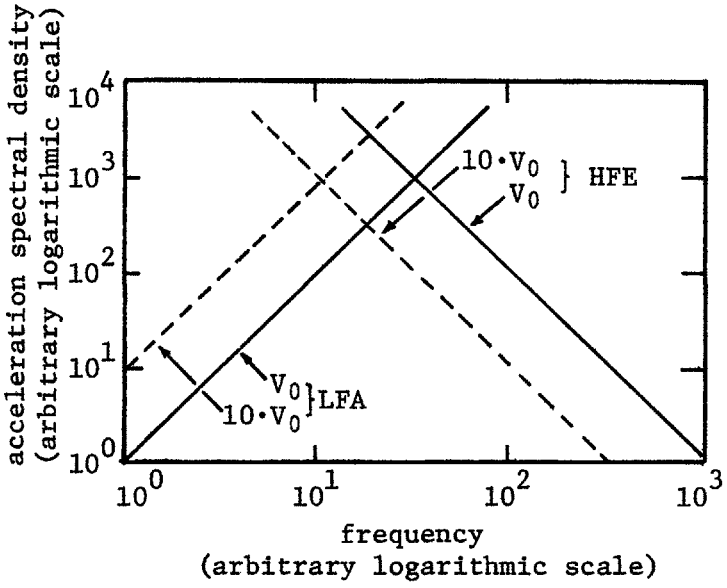

FIGURE 4-5

Variation of Low- and High-Frequency Asymptotes with Speed

is:

$$G_{a,HF} = \frac{\ddot{y}_c(s)}{y_{rf}(s)} = \left(\frac{1+e^{-\tau s}}{2}\right) \frac{4B_c B_r s^2}{m_b m_c s^2 + (m_b B_c + m_c B_c + 4m_c B_r)s + 4B_c B_r} \quad . \tag{4.2.4}$$

The high-frequency asymptote (HFA) of the actual system is thus:

$$HFA = (-AV/s^2)(4fB_c/[m_b m_c V])^2 \left(\frac{1+e^{-\tau s}}{2}\right)^2 . \tag{4.2.5}$$

The periodic component of this expression, due to wheelbase delay, is evident between 10 and 100 Hz in Figure 4-3. A more convenient expression, giving only the locus of the in-phase peaks (at $e^{-\tau s}=1$), is the high-frequency envelope (HFE):

$$HFE = (A/V)(4fB_c/[m_b m_c])^2(1/\omega^2) \quad . \tag{4.2.6}$$

The behavior of the LFA and HFE are illustrated in Figure 4-5 for two values of V. The LFA varies directly with V, whereas the HFE varies inversely. Also, the HFE is proportional to f^2; this fact, together with the HFE's importance in the region of highest human vibration sensitivity for typical present-day speeds, accounts for the observation that the ride is often smoother over wet rails (low f) than over dry rails (high f).

Figure 4-6 compares the LFA and HFE with the A.S.D. of the baseline conventional vehicle at 100 mph. Important deviation from the asymptotes is concentrated within the region from 0.3 to 30 Hz. The LFA at a given speed, being independent of suspension parameters,

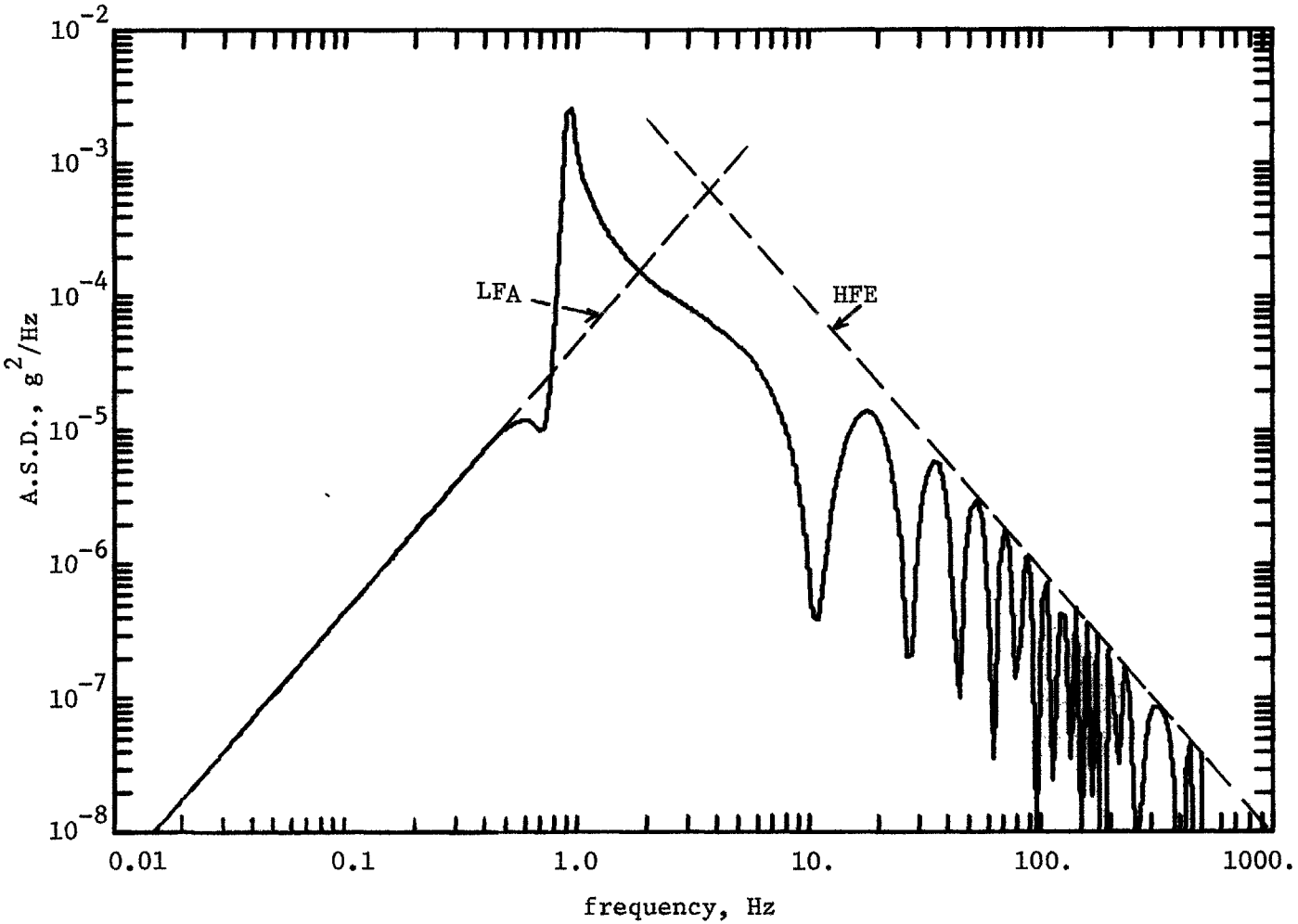

FIGURE 4-6

Comparison of Baseline Vehicle Response with Asymptotes

cannot be affected except by changing rail roughness A. The HFE may be altered by changing any of the small group of parameters in Equation 4.2.6 (notably B_c). Since the A.S.D. is governed by asymptotic behavior below 0.3 and above 30 Hz, the intermediate range should be the main focus of efforts toward improving ride quality.

The variation of A.S.D. with V is shown in Figure 4-7. The low- and high-frequency asymptotic behavior is clearly visible. Notice that the hunting peak occurs at a frequency proportional to V, and that its amplitude increases with V as V_c is approached. The UTACV goal is seriously exceeded by (1) the hunting peak, for V=100 and 150 mph, and (2) the shoulder at the beginning of the HFA, which occurs in the critical "dipper" range of the UTACV criterion.

Figure 4-8 shows the effect of varying the yaw stiffness K_b on the A.S.D. at 100 mph; K_b is given the values 0.5, 1.0, and 2.0 times its baseline value. Yaw secondary stiffness depressed the hunting peak without changing the asymptotic behavior.

The effect of gravitational stiffness K_L on A.S.D. at 100 mph is illustrated in Figure 4-9, in which the two curves are for the baseline vehicle with K_L=0, and the same vehicle with K_L=3.837x10^4 slug/sec^2. The latter curve shows a suppressed hunting peak indistinguishable from that which results from K_L=0 and a secondary yaw stiffness equal to the effective value

$$K_{b,eff} = K_b + 4K_L(kh)^2 \quad , \tag{4.2.7}$$
$$= 4.196\text{x}10^8 + 3.717\text{x}10^8$$
$$= 7.913\text{x}10^8 \text{slug-in}^2/\text{sec}^2$$

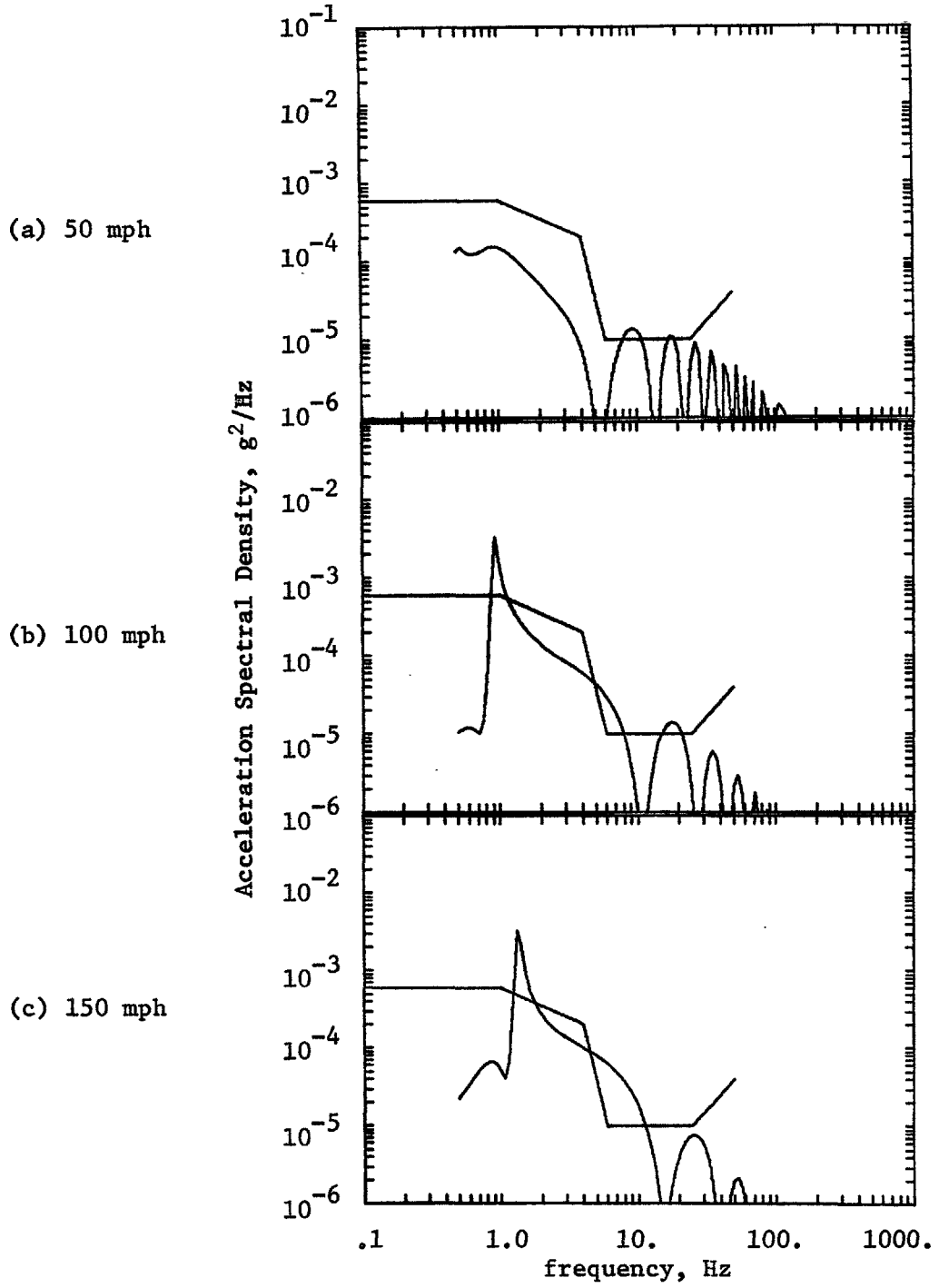

FIGURE 4-7

Carbody Acceleration Spectral Density at Three Speeds (Baseline)

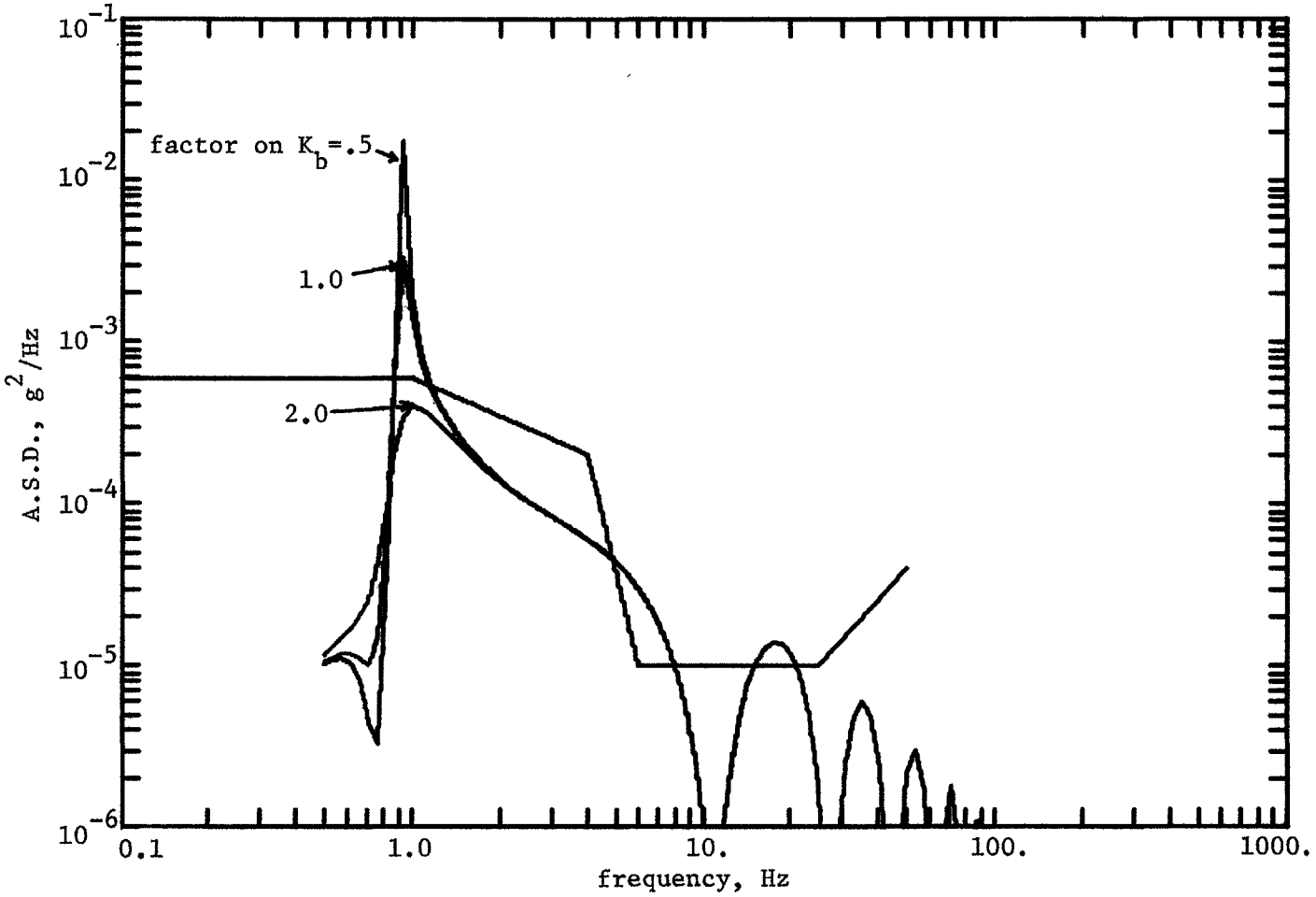

FIGURE 4-8

Effect on Response at 100 mph of Varying K_b

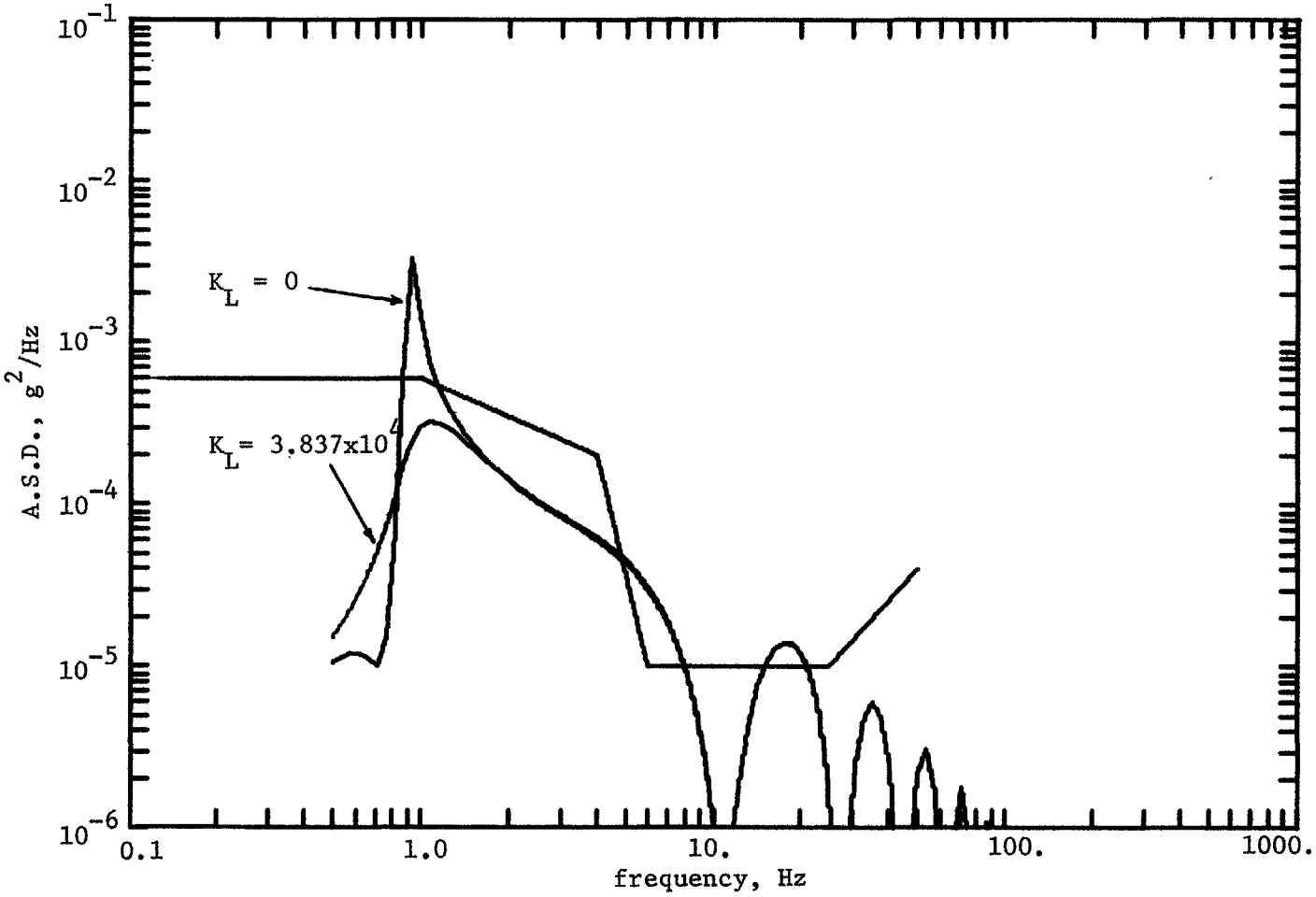

FIGURE 4-9

Effect of Gravitational Stiffness on Response at 100 mph.

for the present case. The asymptotes are unchanged.

Increasing K_b and K_L, then, reduce the carbody vibration at the kinematic hunting frequency at a given V, as well as extending the range of stability. High-frequency behavior of the A.S.D., however, may be affected only by (1) increasing m_b, m_c, or V, or (2) decreasing f, B_c, or A. Of all the preceding parameters, B_c is probably that which is most nearly under the designer's control; it should be reduced as far as is possible without causing excessively light damping in the secondary suspension.

3. Phasing of Inputs. Recall from Chapter 3 that the numerator of any of the transfer functions for the rectangular truck contain both "in-phase" and "out-of-phase" elements relating output to the rail input at the front and the rear axles. Above the kinematic hunting frequency, in-phase inputs tend to add, and out-of-phase inputs cancel, when the output is lateral motion. At lower frequencies, out-of-phase inputs become important; they tend to generate yaw motions, which in turn generate lateral translation by the action of the rigid axles.

In some studies [1], the effect of the wheelbase time delay τ has been neglected in an effort to reduce the complexity involved in evaluating spectral density or RMS values. The so-called "envelope" transfer function, defined in §3.8 by neglecting out-of-phase terms, is in the convenient form of a ratio of two polynomials. Straightforward methods exist [68] for the evaluation and optimization of performance indices based on such rational functions. Figure 4-10 compares the complete and the envelope A.S.D. for the baseline vehicle

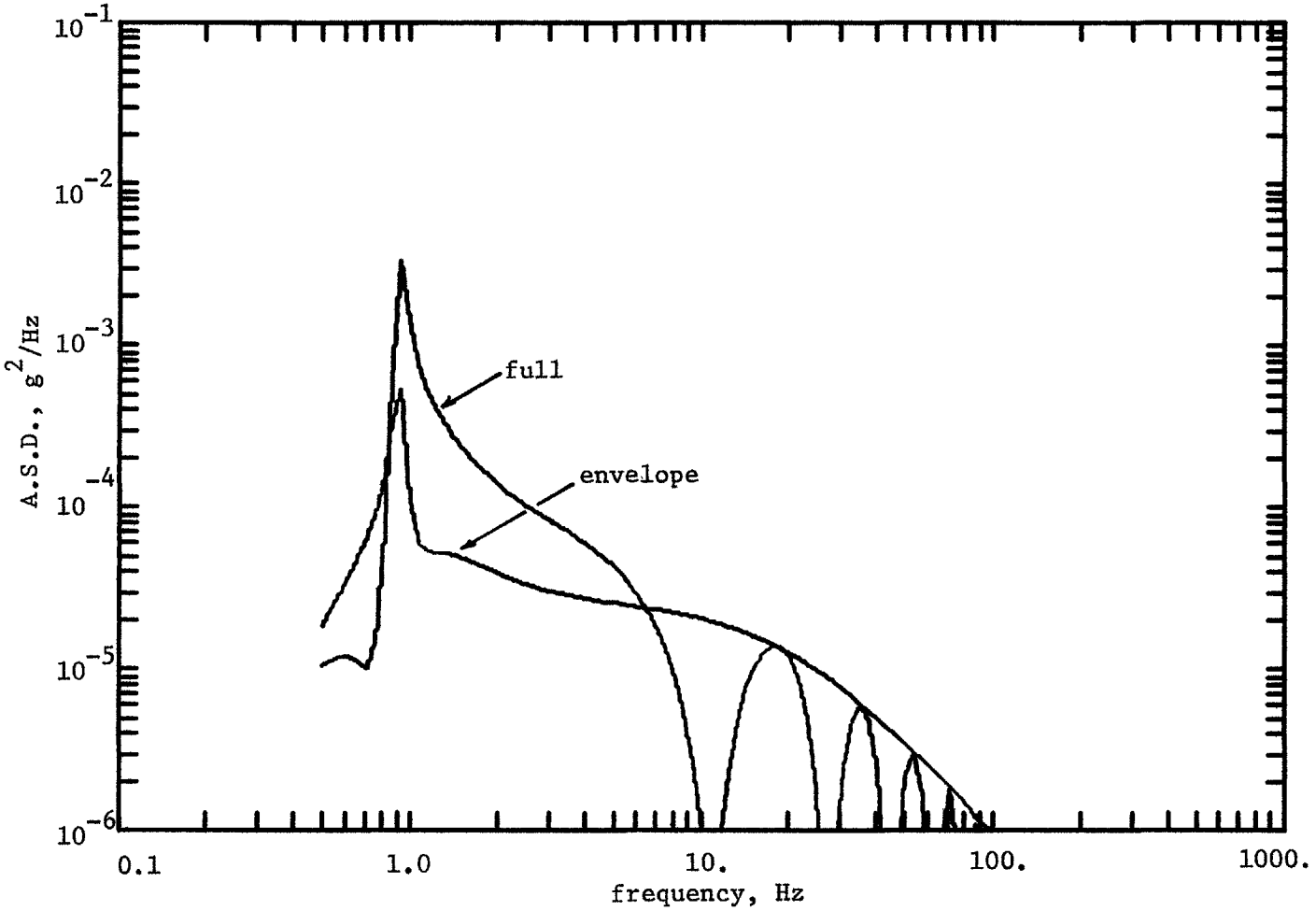

FIGURE 4-10

Comparison of Envelope A.S.D. with Full A.S.D., Baseline Vehicle at 100 mph

at 100 mph. The envelope reproduces the LFA and HFE correctly, and shows a hunting peak at the correct frequency. It suffers from the serious defect, however, of not reflecting accurately the behavior near the hunting peak (about 0.4 to 6 Hz, here) where out-of-phase inputs play an important role. The envelope cannot, of course, show the complex high-frequency pattern of nodes and antinodes due to the wheelbase time delay. In summary, the envelope approximation must be rejected as insufficiently accurate for the prediction of ride quality.

Notice that the envelope response is <u>not</u> the same as the response of a vehicle with two-wheeled trucks. The latter does have $\tau=0$, but it also has $k=0$, a different value of f, and a yaw gravitational stiffness which may no longer be negligible (see Appendix A, §A.6).

The spacing of the high-frequency nodes depends on the spatial irregularity wavelength and the wheelbase, 2kh. A minimum response is expected when the front and rear pairs of wheels are forced 180° out of phase, i.e. when

$$2kh = \lambda/2 + n\lambda \quad , \text{ or} \tag{4.3.1}$$

$$\lambda = 4kh/(2n+1), \quad n=0,1,2, \ldots \tag{4.3.2}$$

When the irregularity wavelength λ is encountered by a vehicle moving at speed V, the corresponding frequency is given by $\nu=V/\lambda$. Therefore a minimum response occurs when

$$\nu = (2n+1)V/4kh \quad , \quad n=0,1,2, \ldots \tag{4.3.3}$$

For the baseline vehicle, this means that nodes occur at odd multiples

of 8.94 Hz (at 100 mph).

4. Tracking Error. Along with good ride quality, low tracking error is a prime goal of suspension design. The truck should follow the track sufficiently well so that excessive clearances are not required to prevent frequent flange contact.

It has been shown that under the assumptions of linearity and stationary Gaussian input, all state variables also have Gaussian statistics. For a zero-mean Gaussian process, the standard deviation σ is identical to the RMS value:

$$\sigma = \text{RMS} = \sqrt{E[x^2]} \quad , \tag{4.4.1}$$

where x is the process and E[y] signifies the expected value of y. The standard deviation is a measure of the spread of the signal. It is possible, given σ, to specify the percentage of time during which the signal may be expected to stay within a given range of its mean (see Table 4-1). A signal will spend 99% of its time within the range $\pm 3\sigma$.

Standard deviation, or RMS, is therefore a suitable indicator of tracking error if the output variable is suitably chosen. An appropriate measure of tracking error is the difference between the truck center position, y_b, and the average of front and rear track centerline deviation, given by (in Laplace notation)

$$y_{r,ave} = y_{rf} \left(\frac{1+e^{-\tau s}}{2} \right) \quad . \tag{4.4.2}$$

Therefore, the transfer function for tracking error may be written:

$$G_{TE} = \frac{Y_b(s)}{Y_{rf}(s)} - \left(\frac{1+e^{-\tau s}}{2} \right) \quad . \tag{4.4.3}$$

TABLE 4-1

Percentage of Time Within Range
For Gaussian Signal

Range	Time Fraction in Range
$\pm\sigma$	68.26%
$\pm 2\sigma$	95.46%
$\pm 3\sigma$	99.74%
$\pm 4\sigma$	100.00%

Evaluating Equation 4.4.3, applying the usual input spectrum, and integrating numerically over a range approximating 0 to ∞, yields the curves for RMS tracking error versus speed in Figure 4-11. Three values of K_b (0.5, 1., and 2. times baseline) and two values of K_L (0 and 3.837×10^4 slug/sec^2) are shown. The tracking error becomes large at the critical speed, and shows an upward trend in the vicinity of body resonance, but otherwise decreases slightly with V. The baseline vehicle has an RMS tracking error of about 0.14 inches at 100 mph; decreases to less than 0.1 inches are possible with increasing K_b or K_L.

Depending on the detailed nature of the system, what happens when the allowable flange clearance is exceeded may range from a mild nonlinear limiting action, through a violent shock, to continued oscillations, breakage, or derailment. Although this issue will not be further discussed here, it is clear that a rail vehicle should be designed so that occasional flange impacts will not radically alter dynamic behavior.

5. K-B-Series Yaw Secondary. By connecting the secondary yaw spring and damper in series, rather than parallel, one may eliminate the static yaw stiffness. This is useful for two reasons. First, yaw stiffness impedes curving by acting to keep the truck aligned with the carbody rather than with the rails; therefore, eliminating static yaw stiffness reduces tracking error in curves. Second, a stiff damper in series with the spring allows the truck to compensate for any initial yaw misalignment by a process of gradual drift, yet does not reduce the

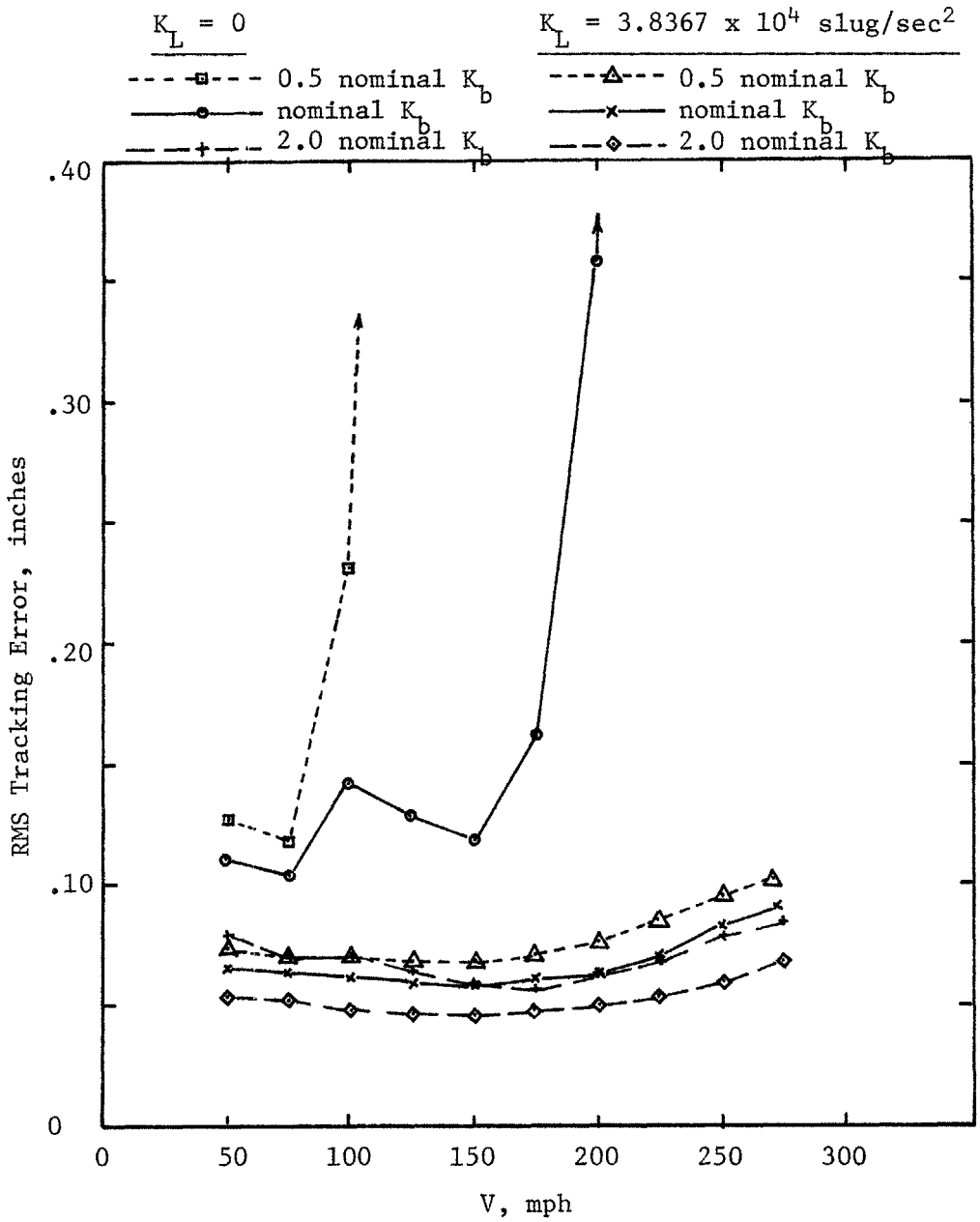

FIGURE 4-11

RMS Tracking Error versus Speed

high-frequency stiffness, necessary to avert instability. Conventional passenger trucks designed without series dampers must be frequently and precisely re-aligned to prevent them from being continually steered against one rail or the other.

The equations of motion for the RC-LMO vehicle with K-B-series yaw secondary are presented in Figure 3-10; the transfer function coefficients for carbody acceleration are given in Table 3-4. B_b should be chosen large enough so that the series combination acts essentially like a spring at the hunting frequency; i.e.,

$$K_b/B_b \ll \omega_k \quad . \tag{4.5.1}$$

Figure 4-12 compares the A.S.D.'s of the baseline vehicle (K-B-parallel yaw, B_b=0) and of two similar vehicles using the K-B-series yaw arrangement. For the latter, K_b retains its baseline value but B_b is taken arbitrarily as 4.196×10^8 slug-in^2/sec (K_b/B_b=1 sec^{-1}) and 8.392×10^7 slug-in^2/sec (K_b/B_b=5 sec^{-1}). Use of the larger value of B_b yields a spectrum almost identical to that for the baseline vehicle, but the smaller value leads to a higher hunting peak at this speed (ω_k=6.23 sec^{-1}).

The added complexity introduced by the K-B-series yaw model does not result in any significant alterations to vehicle dynamics when B_b is large enough to make series connection useful. Therefore, only parallel connection will be considered further. It is tacitly assumed throughout this work, however, that any yaw suspension considered may be connected in series to an additional, large yaw damper in order to

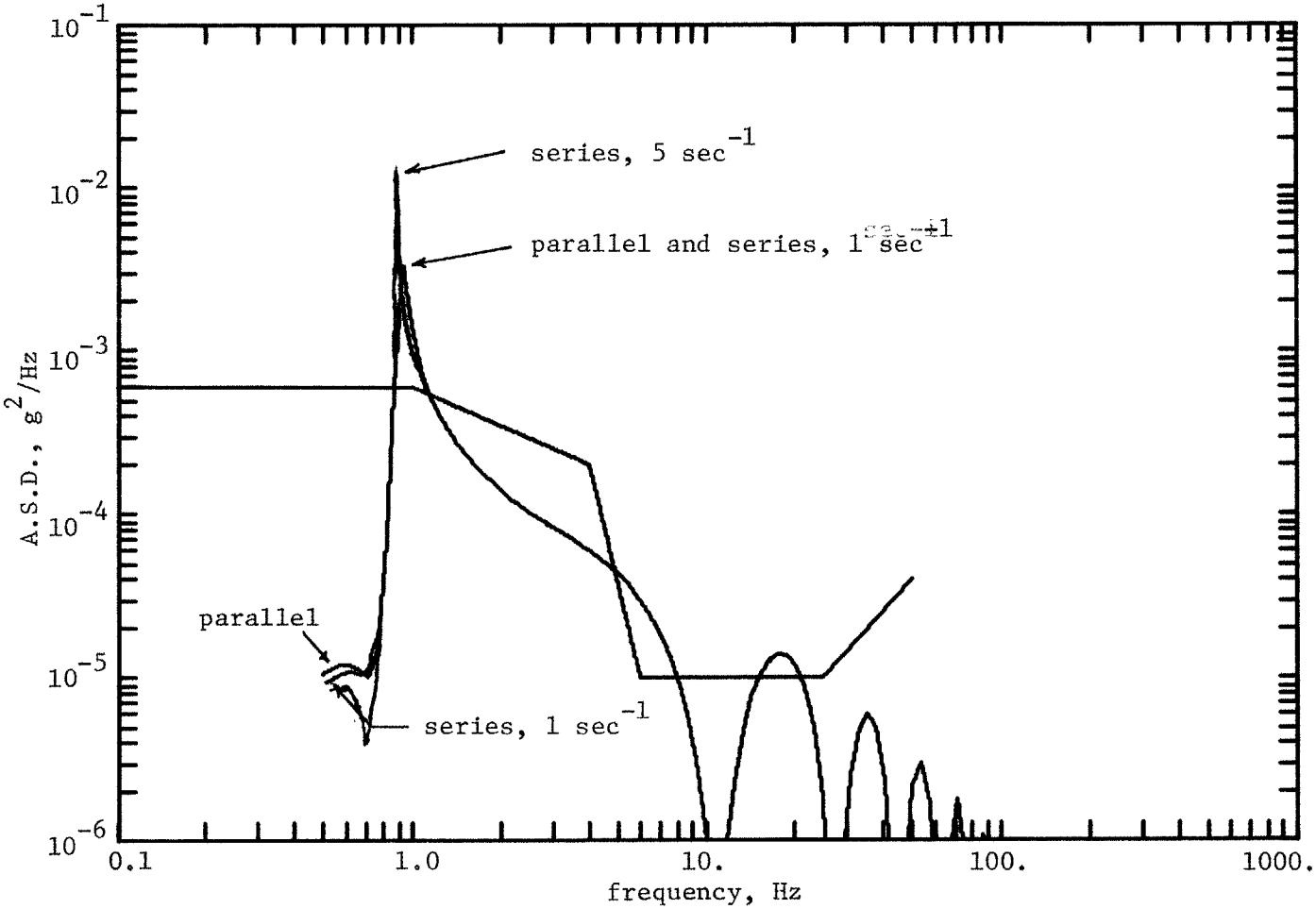

FIGURE 4-12

Comparison of K-B-Series and K-B-Parallel Yaw Secondary
at 100 mph

alleviate the practical problems of curving error and misalignment. Certain trucks, in fact, are now being manufactured with Coulomb friction dampers in series with the yaw springs for just such reasons.

6. Overview. This chapter has not been intended as an exhaustive survey of the influence of all the passive suspension parameters on stability, ride quality, and tracking error. Instead, it has established baseline measures of these characteristics based on a simple model of an unusually well - designed conventional passenger vehicle. The passive performance data of this chapter will be drawn upon as a basis for comparison with active and other unconventional suspension designs.

In addition, the effects of varying several of the most important suspension parameters have been explored, leading to some general conclusions:

- Secondary yaw stiffness, K_b, may be increased within practical limits as a means of extending the stable speed range and suppressing the hunting peak in the carbody acceleration response. The values of K_b required may be quite large, approaching the actual stiffness of components usually assumed rigid. If a large K_b is used, it is advisable to place it in series with a large damper to permit self - adjustment to curves and to misalignment.
- Lateral gravitational stiffness, K_L, has a similar effect to that of K_b for a rectangular truck, but is applied directly to the wheels and therefore does not depend on component stiffness. The potential problem with relying on gravitational stiffness is that nonzero K_L requires concave wheel treads, which may also have a large effective conicity offsetting the benefits of gravitational stiffness.
- The tracking error for all designs considered is

reasonably small, with RMS of less than 0.15 inches, except in the vicinity of instability. Flange impact on nominally straight track with random irregularities should not be a problem unless nonlinear effects after flanging are extreme. A gentle limiting action is recommended.

There are a number of fundamental problems with any vehicle using conventional trucks and suspensions. One is the decreasing margin of stability with speed, resulting in eventual instability. Another is the strong component of vibration transmitted to passengers at the kinematic hunting frequency. Each of these is a result of the creep steering mechanism of guidance. In the following chapters, various methods of modifying or supplanting the hunting mechanism will be explored.

CHAPTER 5

PERFORMANCE OF VEHICLE WITH LATERAL-MASS-ONLY CARBODY AND RIGID TRUCK WITH INDEPENDENTLY-ROTATING WHEELS

The equations of motion developed in Chapter 3 may be used to describe a vehicle with RIW trucks by the substitutions

$$\alpha \leftarrow 0 \quad , \quad \text{and}$$

$$k_s \leftarrow k^2 \ .$$

Eliminating the rigid axle between opposite wheels does away with yaw - lateral cross coupling, and hence with the root cause of hunting motion. This gain is offset by the loss of guidance from coned wheels, which must be made up for by the action of gravitational stiffness at the wheel - rail interfaces. The dynamic properties of the RIW - LMO vehicle model are examined in this chapter, and found to be highly attractive from the standpoints of stability, ride quality, and tracking error.

Throughout this chapter, the baseline value of K_L will be taken as 3.8367×10^4 slug/sec^2, based on the assumption of a five - inch difference in radius of curvature between wheel tread and rail crown (see Appendix A for derivations).

1. Equivalent RIW-LMO Mechanical System. The pertinent equations of motion are embodied in Equation 3.6.4 and Figure 3-9. They describe the equivalent system illustrated in Figure 5-1. The creep dampers, given by

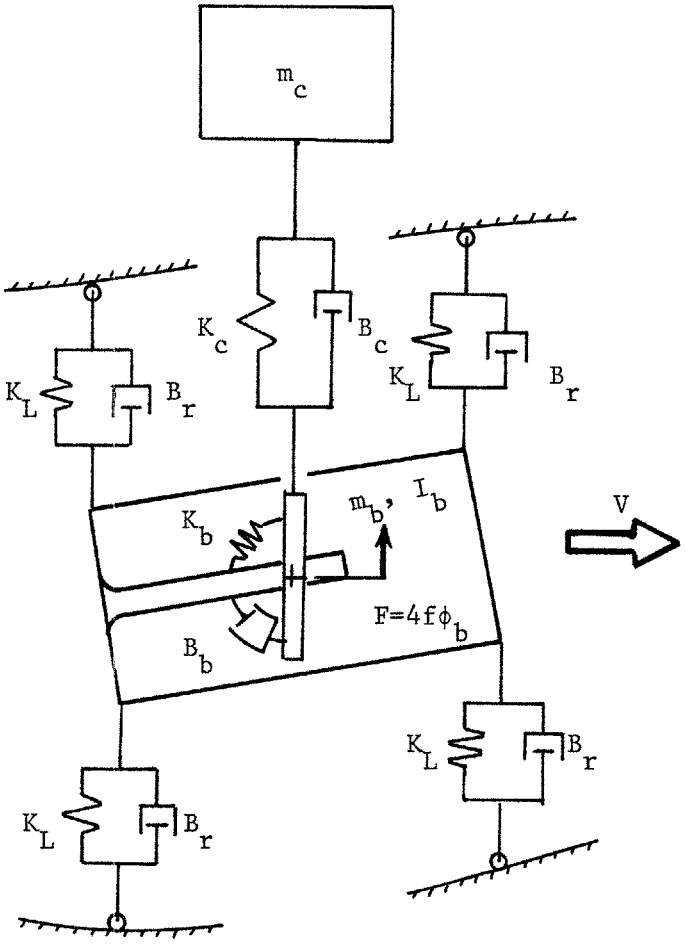

FIGURE 5-1 (a)

Equivalent Mechanical System for RIW-LMO Vehicle Model

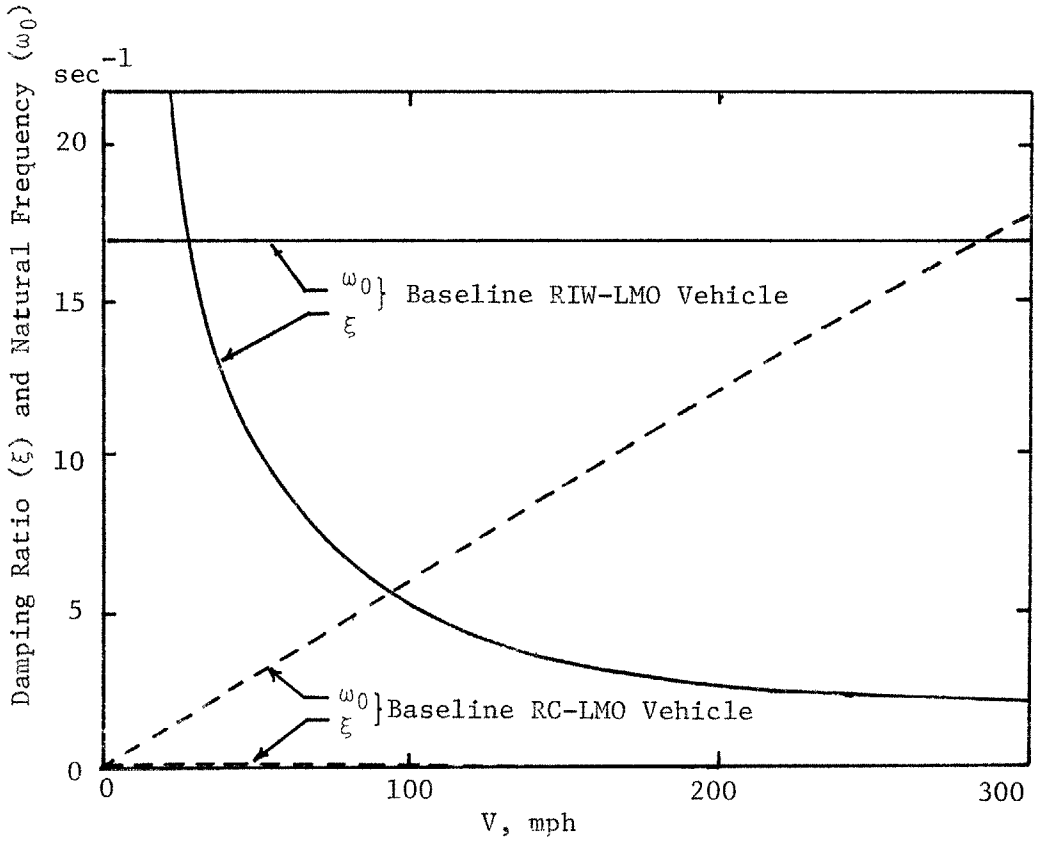

FIGURE 5-1 (b)

Variation of Natural Frequency and Damping Ratio with Speed, Baseline RIW-LMO Vehicle, Compared with Baseline RC-LMO.

$$B_r = f/V \quad , \tag{5.1.1}$$

are speed-dependent but always positive. Notice that truck yaw generates a lateral force (shown active in the figure), due to the preferred rolling direction of the wheels, of magnitude $+4f\phi_b$; this effect is the same for both RC and RIW models. Unlike the RC model, however, the linearized RIW model exhibits no back-coupling from lateral to yaw motions.

2. Stability. The absence of lateral-to-yaw coupling implies that the RIW-LMO system is stable at all speeds for non-degenerate parameter values (K_L, B_c, K_c, m_b, m_c, f, k, I_b, and h all positive and finite).

Consider an arbitrary set of initial conditions for the system of Figure 5-1. Truck yaw is independent of translation, and is a damped second-order system. Translation of the truck and carbody is described by a passive, damped, fourth-order system of equations subject to an input force equal to $4f\phi_b(t)$. This lateral input is bounded and tends to zero as yaw oscillations decay. Therefore, arbitrary lateral and yaw errors tend to zero and the system is asymptotically stable at any speed. Figure 5-1b shows the variation of natural frequency and damping ratio with speed for the least damped roots of the baseline RIW-LMO vehicle; those of the baseline RC-LMO model are included for comparison. In the RIW case, natural frequency is nearly constant with speed, and damping ratio decreases with speed but always remains positive.

3. Ride Quality. The RIW truck does not hunt. Therefore the strong peaks of acceleration spectral density at the kinematic hunting frequency, prominent in the RC curves of Chapter 4, are absent from the corresponding RIW responses. The asymptotic behavior, on the other hand, is as described in §4.2.

Figure 5-2 shows the A.S.D. of the baseline RIW-LMO vehicle at 100 mph, together with the response of the baseline RC-LMO model at the same speed (cf. Figure 4-3). Comparison illustrates the elimination of the 1 Hz hunting peak by the use of an RIW truck, and the fact that the asymptotes (governed by creep forces, masses, and secondary damping) are unchanged. Figure 5-3 compares RIW-LMO acceleration response at three speeds.

Figure 5-4 is a comparison of the full A.S.D. with the envelope approximation (cf. Figure 4-10). Again, the envelope is a poor representation of behavior at low frequencies where yaw-to-lateral coupling is important.

The fact that gravitational stiffness at the wheels alone provides substantial yaw stiffness to the truck suggests that the secondary yaw stiffness K_b may be entirely omitted. Figure 5-5 shows that setting $K_b=0$ raises the response slightly in the region of carbody resonance ($\sim$1 Hz), but does not alter it in the difficult band between 4 and 8 Hz.

The A.S.D. is relatively insensitive to the value of gravitational stiffness K_L, as Figure 5-6 shows. Reducing K_L increases response at low frequencies (<2 Hz in this case), but does not influence higher frequencies where creep damping becomes dominant. The major impact of

K_L is on tracking and curving error, not on ride quality. Ride quality of the RIW-LMO vehicle is improved (over that of an RC-LMO vehicle with the same secondary suspension) primarily in the elimination of the speed-dependent hunting peak. Use of the RIW truck, however, allows greater freedom in the choice of suspension components by guaranteeing stability. For example, the baseline vehicle was designed with a relatively large value of lateral damping B_c, needed to prevent unstable primary hunting at the carbody resonance frequency. Since the high-frequency asymptote fo the A.S.D. is proportional to B_c^2, performance in the 4 to 15 Hz range can be improved by using the RIW truck with a lower value of B_c instead of the baseline RC truck.

4. Tracking Error. The variation of RMS tracking error with speed is shown in Figure 5-7, for both nominal and zero yaw stiffness K_b and for various values of gravitational stiffness K_L. Numerical values for error range between 0.06 and 0.18 inches, and do not differ greatly from those obtained for the RC-LMO model well below instability (cf. Figure 4-11). Notice that for an RIW

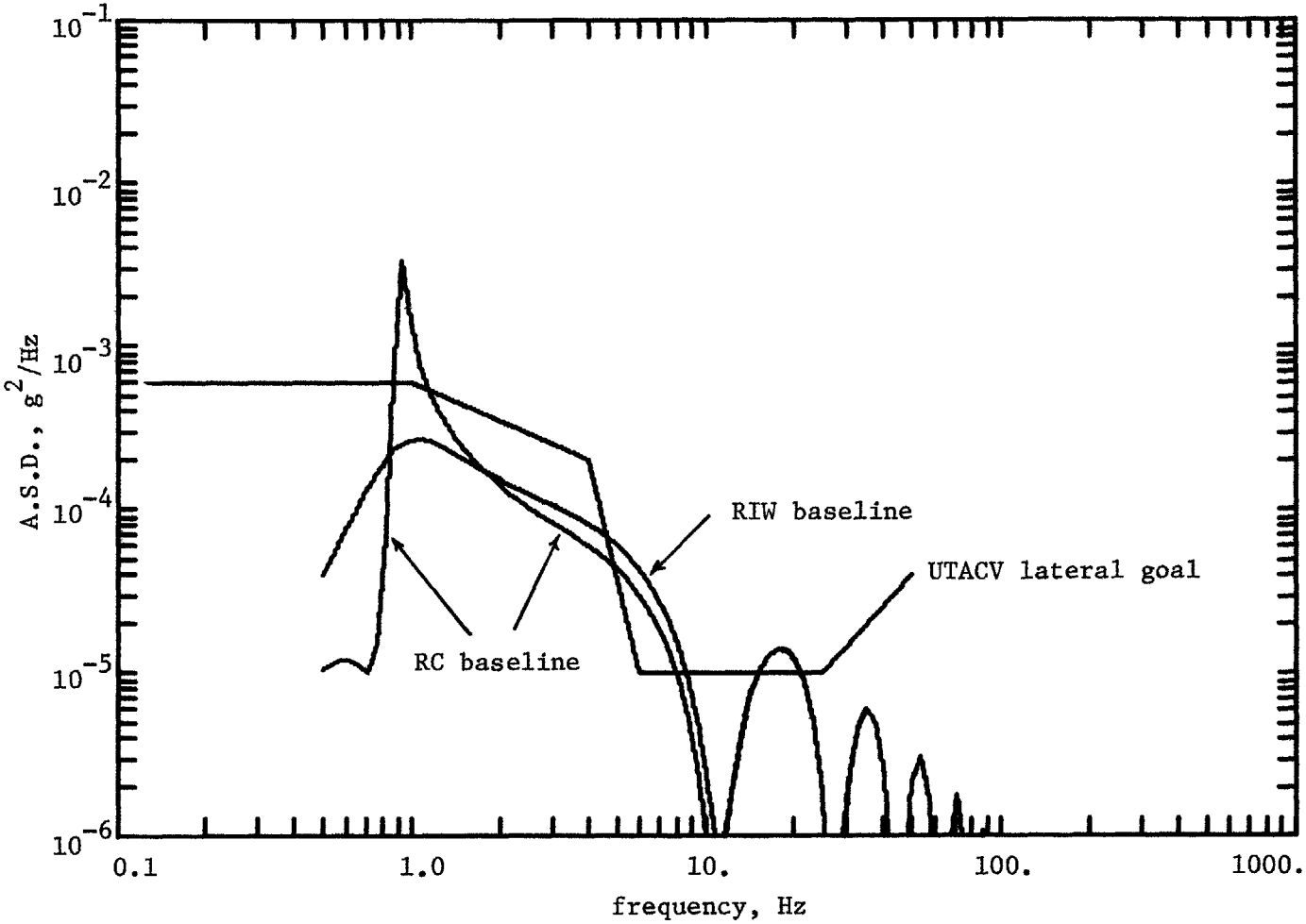

FIGURE 5-2

Comparison of Acceleration Spectral Density of RC and RIW Baseline Vehicles at 100 mph (LMO carbody)

(a) 50 mph

(b) 100 mph

(c) 150 mph

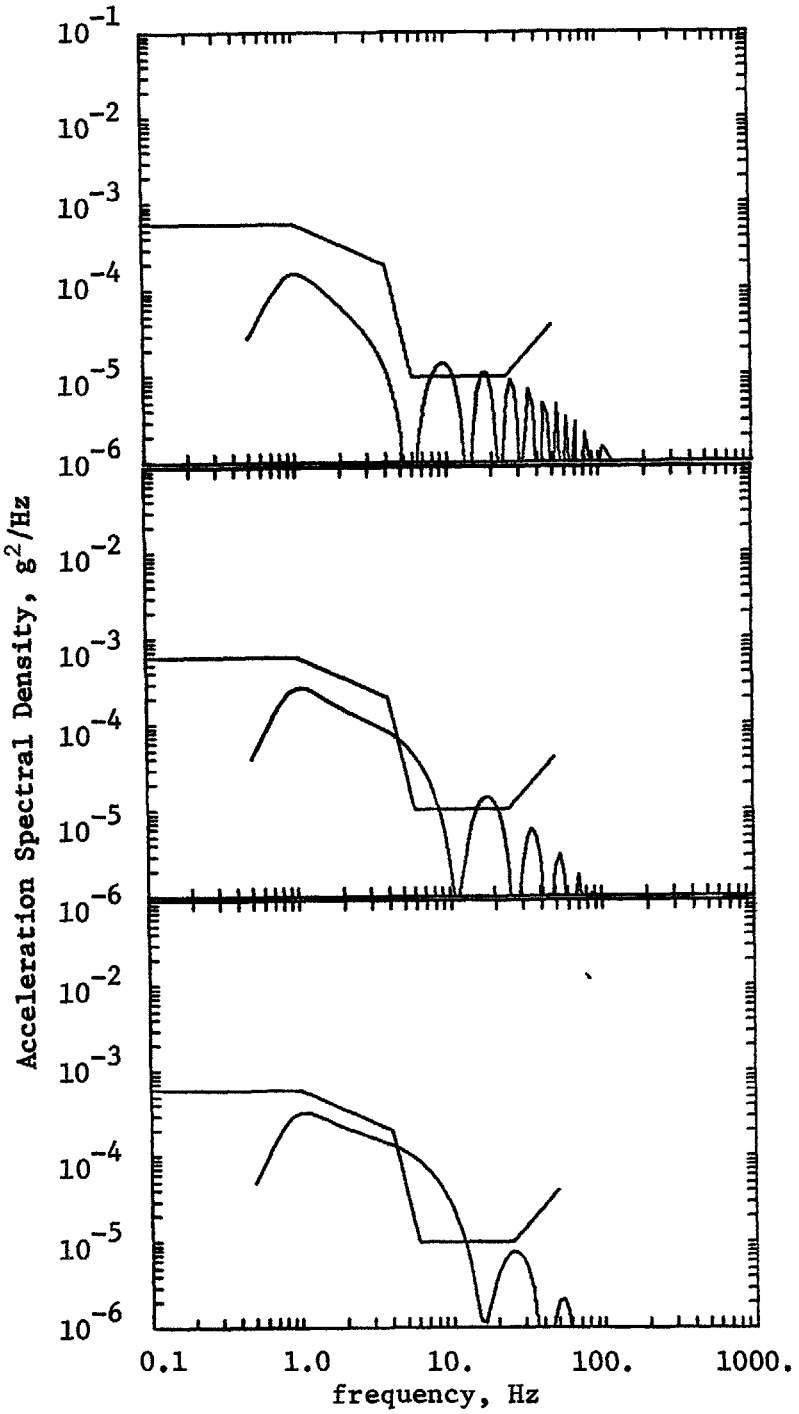

FIGURE 5-3

Carbody Acceleration Spectral Density at Three Speeds (RIW Baseline)

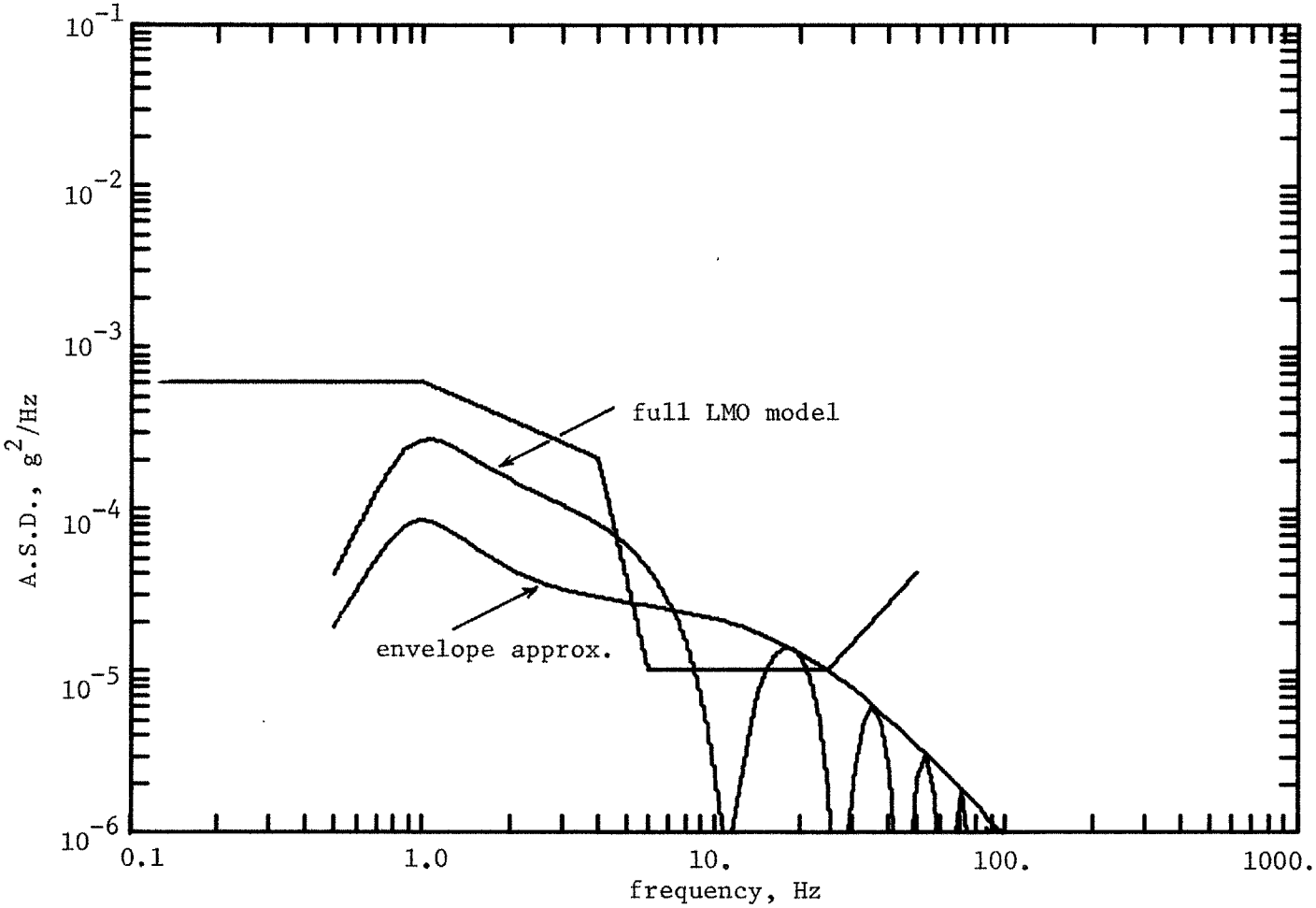

FIGURE 5-4

Comparison of Envelope Approximation with Full A.S.D. for RIW-LMO Vehicle at 100 mph

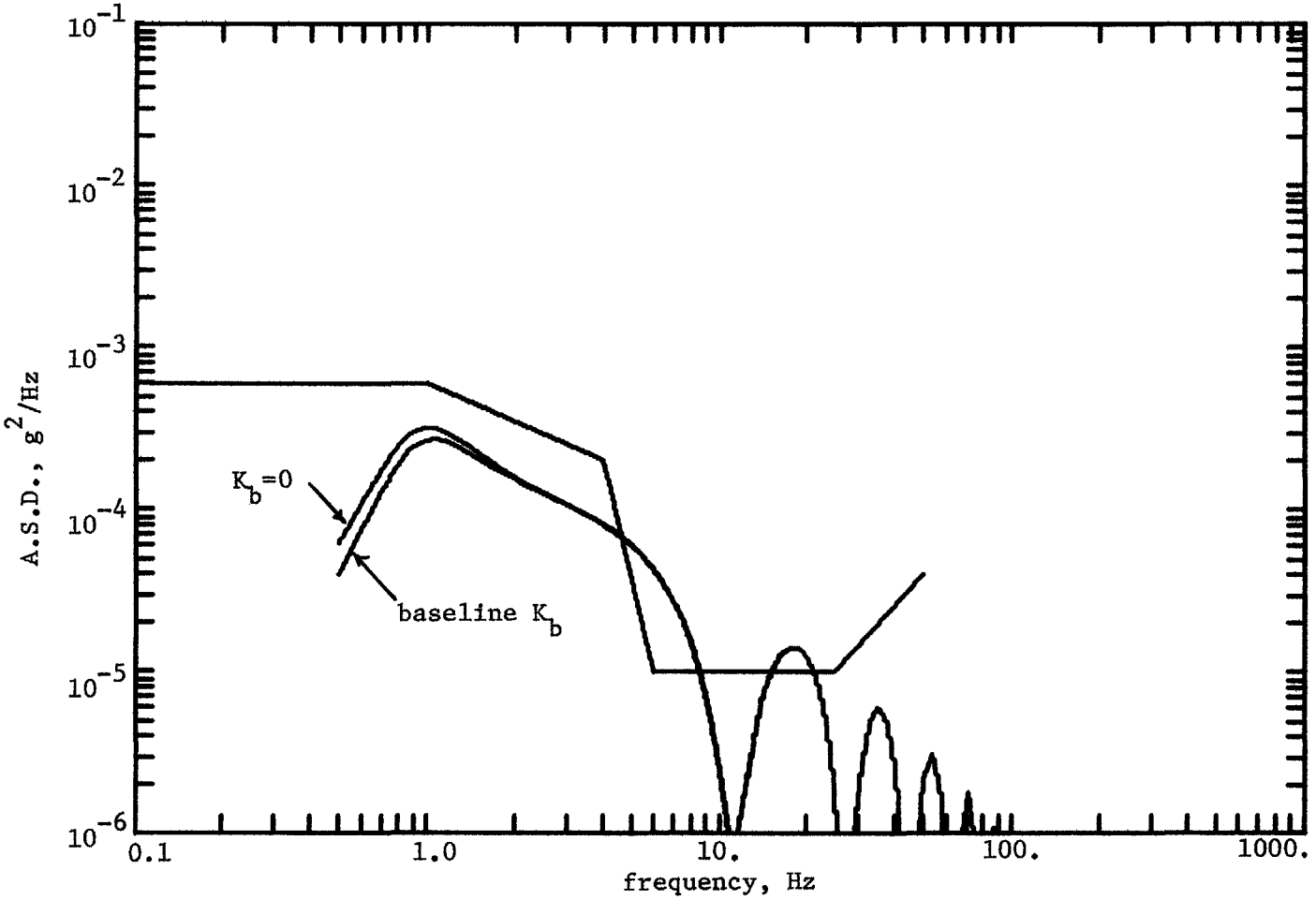

FIGURE 5-5

Effect on A.S.D. of Eliminating K_b, 100 mph

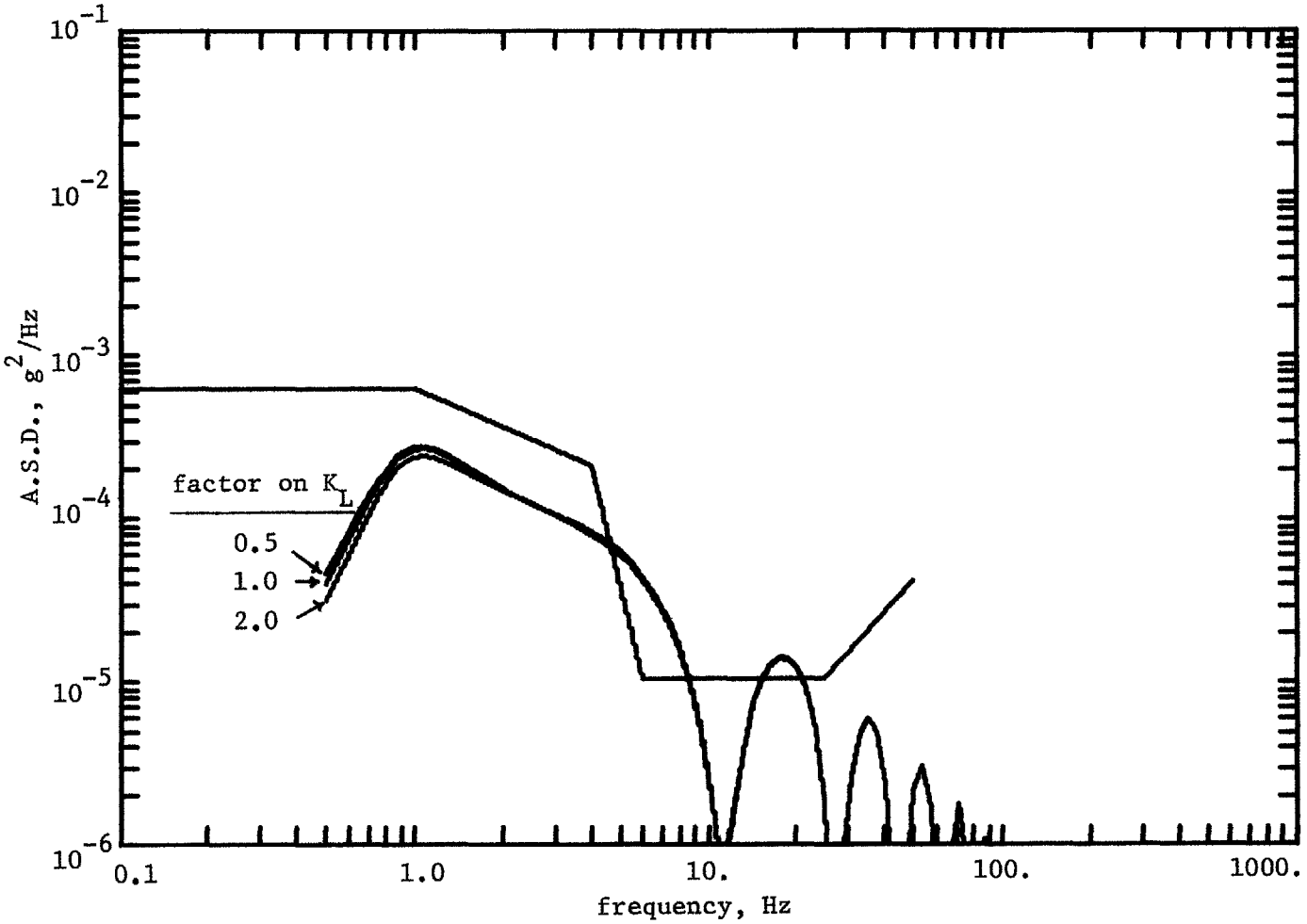

FIGURE 5-6

Effect of K_L on A.S.D., 100 mph

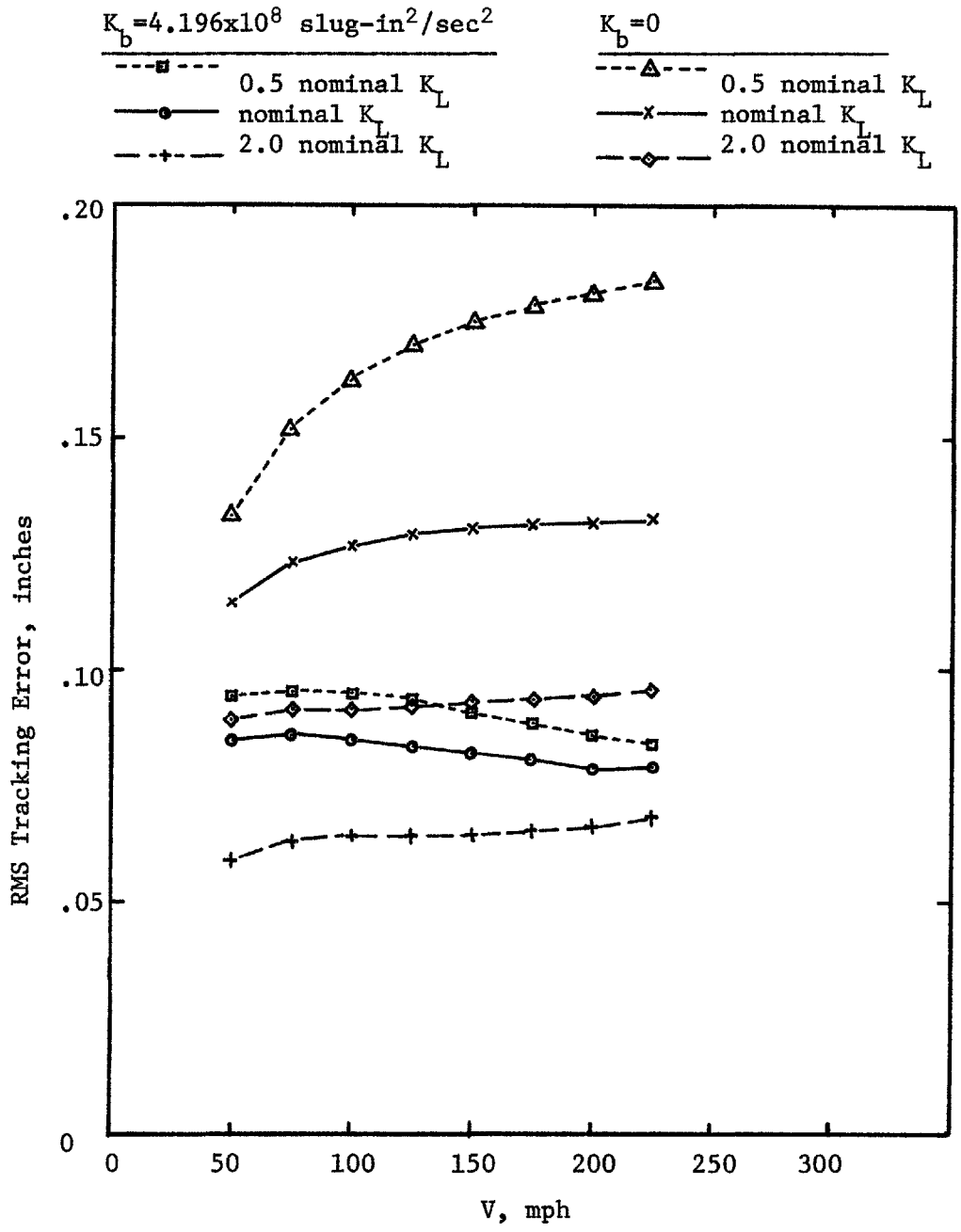

FIGURE 5-7

RMS Tracking Error versus Speed (RIW)

truck, there is no speed - dependent frequency to excite carbody resonance and increase tracking error in a particular speed range. Increasing K_b and/or K_L reduces error by suppressing low - frequency yaw.

5. Overview. The results of this chapter suggest that the RIW truck is an excellent candidate for high - speed rail systems, at least on the basis of dynamic considerations. Elimination of rigid axles leads to elimination of self - excited hunting instability; the RIW-LMO vehicle is stable at all speeds. No yaw restraint between carbody and truck is necessary for satisfactory operation. This guarantee of stability allows greater flexibility in choosing suspension parameters to improve ride quality and tracking error than is possible with an RC truck.

In contrast to the RC truck with concave wheel treads, recommended in Chapter 4, performance of an RIW truck is independent of conicity α and relatively insensitive to K_L. This means that wear of the wheels -- tending to increase both α and K_L -- is not a major problem.

The behavior of the RIW truck in a curve differs fundamentally from that of the RC truck. Curving is discussed in Chapter 10.

A truck with independently - rotating wheels will probably be more difficult to build than a conventional truck. The rigid wheelset serves the very practical function of maintaining opposite wheels separated by a fixed distance -- a requirement which must be met by the truck frame if the axle is eliminated. In addition, more and better bearings will be required to support the thrust and bending

loads encountered in the RIW system. It appears likely, however, that the potential of the truck for high speed passenger operation may justify the added complexity and initial cost of independent wheels.

CHAPTER 6

MODEL FOR AN AUTOMATICALLY CONTROLLED SECONDARY SUSPENSION

Up to this point, modelling and analysis have been confined to rail vehicle suspensions made up of passive elements. In this chapter, a restricted but very flexible class of active sensing and actuating elements are introduced in an attempt to achieve performance improvements not possible through more conventional means. Equations of motion with control are presented for both LMO and RPB carbody models. In the case of the LMO model, it has also been feasible to derive analytically an expression for the transfer function relating carbody acceleration to rail input. Practical considerations affecting controller design are discussed.

1. Rationale. The automatic controllers to be applied in this and succeeding chapters will be restricted at the outset in a way which takes into account the special nature of the rail vehicle suspension. Sarma and Kozin [59], in a paper on the subject, defined a broad class of controller which in general require forces and torques to be applied between trucks or carbody and a fixed inertial reference -- a system whose implementation would demand the use of something like jet action. (It is interesting to note, however, that the special case examined by Sarma and Kozin is equivalent to the use of gravitational stiffness at the wheels.) A more practical approach, however, is founded on two principles:

(1) any actuators should act internal to (i.e., between parts of) the vehicle, rather than directly on the environment; and (2) functions which may be implemented passively with springs and dampers should be so implemented. For the rail vehicle models being used here, the first principle requires that active force and torque be applied only between carbody and truck. The second means that the passive secondary suspension elements K_b, B_b, K_c, and B_c will be left in place, with active force and torque applied in parallel with them. The active force and torque will be referred to hereafter as F_{bc} and T_{bc}, respectively, as usual defined positive when acting positively on the truck. The actuators are idealized as massless, implying that any force or torque applied to the truck is applied oppositely to the carbody.

Figure 6-1 is a block diagram of the dynamics of the RPB vehicle model. Solid lines indicate interactions implicit in the passive case studied in previous chapters, while dashed lines show paths which cannot exist in general without active control. The latter paths may be grouped into three classes: (1) relations whereby yaw motions give rise to lateral forces and lateral motions give rise to yaw torques; (2) relations involving absolute, rather than relative, carbody displacement and yaw; and (3) relations involving acceleration feedback. Many other paths could be envisioned, but those in the Figure have been chosen as especially basic to the control of truck hunting motion. In particular, no active coupling among trucks is included.

2. Controller Definition. The most general controller to be

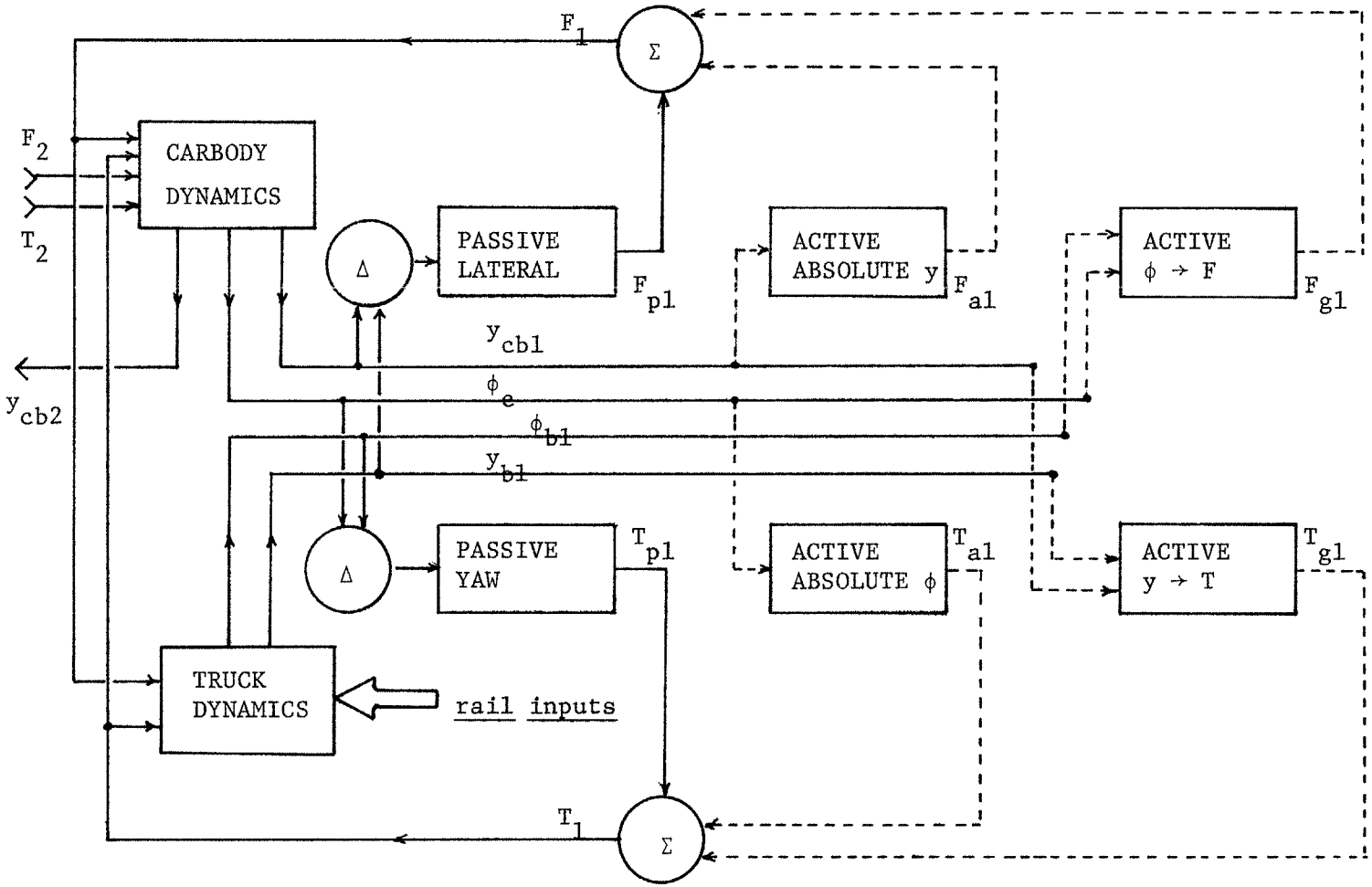

FIGURE 6-1

Block Diagram of Rail Vehicle Dynamics with Control. Front Truck Only is Shown.

studied is defined by the following relations:

$$T_{bci} = -D_1 y_{bi} + D_2 y_{cbi} - D_3 \dot{y}_{bi} + D_4 \dot{y}_{cbi} - D_5 \ddot{y}_{bi} + D_6 \ddot{y}_{cbi} - D_{16}\phi_c - D_{17}\dot{\phi}_c - D_{18}\ddot{\phi}_c \quad (6.2.1)$$

$$F_{bci} = -D_7 \phi_{bi} + D_8 \phi_c - D_9 \dot{\phi}_{bi} + D_{10} \dot{\phi}_c - D_{11} \ddot{\phi}_{bi} + D_{12} \ddot{\phi}_c - D_{13} y_{cbi} - D_{14} \dot{y}_{cbi} - D_{15} \ddot{y}_{cbi} \quad , \quad (6.2.2)$$

where i is a subscript denoting which end of the vehicle is being considered (i=1 for front, i=2 for rear, i is irrelevant to the LMO carbody model) and y_{cbi} is the lateral displacement of the carbody at the truck attachment point :

$$y_{cb1} = y_c + L \cdot \phi_c \quad (6.2.3)$$

$$y_{cb2} = y_c - L \cdot \phi_c \quad . \quad (6.2.4)$$

Equations 6.2.1 and 6.2.2 embody the relations set forth in Figure 6-1. Notice that the active force and torque at each end of the vehicle depend only on displacements and angles which can be measured at that end.

3. Special Cases. The control relations of Equations 6.2.1 and 6.2.2 are quite general in form. Practical considerations of power and ease of measurement suggest that three special cases of the control rule are particularly convenient to implement and should be singled out for study.

Relative Sensing. If the active secondary suspension elements, like the passive, depend only on the relative displacement

and yaw between truck and carbody, then:

$$\begin{aligned} D_1&=D_2 & D_7&=D_8 \\ D_3&=D_4 & D_9&=D_{10} \\ D_5&=D_6 & D_{11}&=D_{12} \\ D_{13}&=D_{14}=D_{15}=0 & D_{16}&=D_{17}=D_{18}=0 \end{aligned} \quad . \tag{6.3.1}$$

The relative sensing case is important because it is usually much easier to measure a relative quantity than an absolute one (although acceleration is an exception). Furthermore, absolute position becomes rather ambiguous when the track is not nominally straight. This controller in general must sense six quantities (relative position and angle, and derivatives), and is completely characterized by the six gains on these quantities.

Steering. There is a strong coupling between truck yaw and lateral motions arising from creep forces and forward motion. Therefore it is possible to obtain large power gains by acting on the truck in yaw alone. If $F_{bci}=0$, then:

$$D_7=D_8=D_9=D_{10}=D_{11}=D_{12}=D_{13}=D_{14}=D_{15}=0 \quad . \tag{6.3.2}$$

The steering controller also requires measurement of six quantities (car and truck displacements, and derivatives) and specification of six gains.

Passive-Asymmetric. It is possible to obtain coupling between lateral and yaw motions without active control. Consider Figure 6-2, which represents one truck with two purely lateral

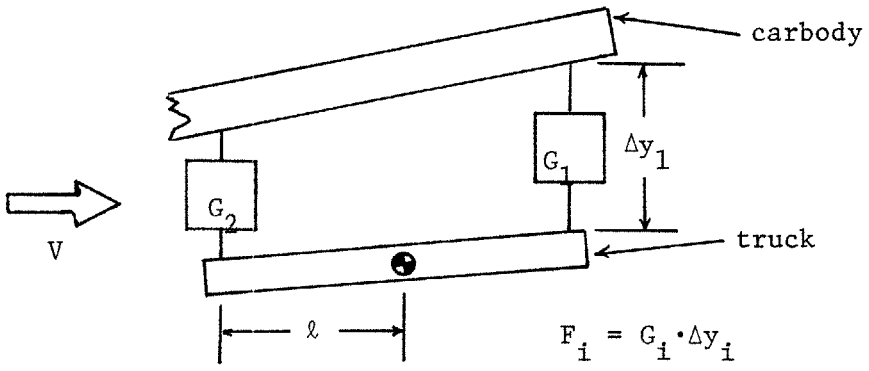

(a)
Principle of Asymmetric Suspension

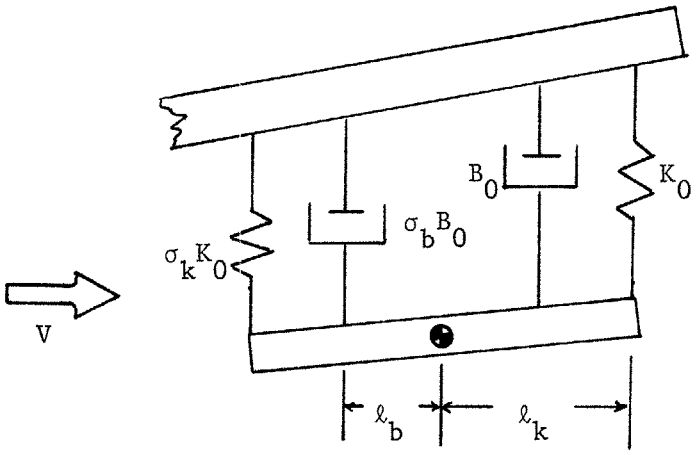

(b)
Passive - Asymmetric Suspension

FIGURE 6-2

Asymmetric Secondary Suspensions

suspensions, $G_1(s)$ and $G_2(s)$, situated symmetrically a distance ℓ from the truck center of mass. These suspensions respond only to the lateral relative displacements at their connection points,

$$\begin{aligned} \text{forward:} \quad \Delta y_1 &= (y_c - y_b) + \ell(\phi_c - \phi_b) \quad , \text{ and} \\ \text{rear:} \quad \Delta y_2 &= (y_c - y_b) - \ell(\phi_c - \phi_b) \quad . \end{aligned} \tag{6.3.3}$$

Therefore the net torque and force on the truck are

$$F_b = (G_1+G_2)(y_c - y_b) + \ell(G_1 - G_2)(\phi_c - \phi_b) \tag{6.3.4}$$

and

$$T_b = \ell(G_1 - G_2)(y_c - y_b) + \ell^2(G_1+G_2)(\phi_c - \phi_b) \quad . \tag{6.3.5}$$

Notice that such a system is of necessity relative sensing. The following parameter identifications may also be made (assuming parallel

yaw and lateral suspension notation from Chapter 3):

$$(G_1+G_2) = K_c+B_c s \quad , \tag{6.3.6}$$

$$(G_1+G_2)\ell^2 = K_b+B_b s \quad , \tag{6.3.7}$$

$$(G_1-G_2)\ell = D_1+D_3 s+D_5 s^2 \quad , \text{ and} \tag{6.3.8}$$

$$(G_1-G_2)\ell = D_7+D_9 s+D_{11} s^2 \quad . \tag{6.3.9}$$

More than two lateral suspensions may of course be used to obtain the desired combination of parameters. The important feature of this suspension configuration is that Equations 6.2.1 and 6.2.1 are implemented, with

$$\begin{aligned} &D_1=D_2=D_7=D_8 \\ &D_3=D_4=D_9=D_{10} \\ &D_5=D_6=D_{11}=D_{12} \\ &D_{13}=D_{14}=D_{15}=D_{16}=D_{17}=D_{18}=0 \quad . \end{aligned} \tag{6.3.10}$$

The suspension is termed asymmetric because it reduces to the conventional passive suspension if $G_1=G_2$. It may be implemented passively if the acceleration terms (D_5, etc.) are zero. Figure 6-2b illustrates such an implementation using two springs and two dampers, all of different constants as shown. Then

$$\begin{aligned} K_c &= K_0\ (1+\sigma_k) \quad , \\ B_c &= B_0\ (1+\sigma_b) \quad , \\ K_b &= K_0 \ell_k^2 (1+\sigma_k) \quad , \\ B_b &= B_0 \ell_b^2 (1+\sigma_b) \quad , \quad \ldots \end{aligned} \tag{6.3.11}$$

$$D_1=D_2=D_7=D_8 = K_0\ell_k(1-\sigma_k) \quad ,$$
$$D_3=D_4=D_9=D_{10}= B_0\ell_b(1-\sigma_b) \quad . \qquad \text{(6.3.11 ctd)}$$

4. Equations of Motion -- LMO Carbody. The system consisting of an RC or RIW truck, an LMO carbody, and K-B-parallel yaw and lateral secondary suspensions, together with active control in parallel, has equations of motion which may be obtained by assembling Equations 3.3.3, 3.4.1, 3.4.2, 3.5.14 (or 3.5.18), 6.2.1, and 6.2.2.

The use of compressed matrices will be introduced at this point, since their use will greatly simplify the writing of controlled equations of motion. The general linear system equations of Equation 3.6.4,

$$\dot{\underline{x}} = \underline{a}\,\underline{x} + \underline{b}\,y_{rf} \quad , \qquad (6.4.1)$$

may be Laplace transformed to give

$$s\,\underline{x} = \underline{A}(s)\,\underline{x} + \underline{B}(s)\,y_{rf} \quad . \qquad (6.4.2)$$

If Equation 6.4.2 can be partially solved -- e.g., if $x_2=\dot{x}_1$, then $x_2(s) = s\,x_1(s)$ -- it may be rewritten thus:

$$\underline{S}\,\hat{\underline{x}} = \hat{\underline{A}}\,\hat{\underline{x}} + \hat{\underline{B}}\,y_{rf} \quad , \qquad (6.4.3)$$

where $\hat{\underline{x}}$ is a reduced set of state variables and $\hat{\underline{A}}$ and $\hat{\underline{B}}$ are compressed matrices in s. $\underline{S}$ is also a matrix in s; when the original state variables $\underline{x}$ are related by derivatives only, $\underline{S}$ is diagonal in powers of s.

In compressed matrix notation, the equations of motion for the RC(RIW)-LMO controlled vehicle are given in Figure 6-3. The delay abbreviations,

$$\delta^{+} = \frac{1 + e^{-\tau s}}{2} \quad \text{and} \tag{6.4.4}$$

$$\delta^{-} = \frac{1 - e^{-\tau s}}{2} \quad , \tag{6.4.5}$$

have been introduced.

5. Equations of Motion -- RPB Carbody. The system consisting of two RC or RIW trucks, an RPB carbody, K-B-parallel yaw and lateral secondary suspensions, and active control, has equations of motion which may be obtained by assembling Equations 3.3.1, 3.3.2, 3.4.1, 3.4.2, 3.5.14, 6.2.1, and 6.2.2. The equations are presented in Figure 6-4, with the further definition

$$\delta^{L} = e^{-\tau_L s} \quad . \tag{6.4.6}$$

6. Acceleration Transfer Function: LMO Complete Vehicle. The coefficients of the transfer function relating carbody acceleration to parallel rail input, Equation 3.8.5, are tabulated in Table 3-1. Notice that active control does not change the order of the system.

7. Control Power. A highly important aspect of active controller design is the amount of power which must be supplied to the actuators. The actual power consumed depends on the hardware employed, but a consistent approximation to actual power may be obtained by computing the net mechanical power delivered by the actuator. Let x_1 and x_2 be

MODEL: RC (RIW) - LMO, Controlled, K-B-Parallel Yaw Secondary

REDUCED STATE VECTOR: $\hat{x}^T = [y_c, y_b, \phi_b]$

COMPRESSED INPUT VECTOR: for y_{rf}, $\hat{B} =$

$$\begin{bmatrix} 0 \\ \delta^+ ([4f/m_b V]s + [4K_L/m_b]) \\ \delta^+ (4fh\alpha/I_b r_0) + \delta^-([4fkh/I_b V]s + [4K_L kh/I_b]) \end{bmatrix}$$

DERIVATIVE MATRIX: $\underline{S} = \begin{bmatrix} s^2 & 0 & 0 \\ 0 & s^2 & 0 \\ 0 & 0 & s^2 \end{bmatrix}$

CHARACTERISTIC MATRIX: $\hat{A} = \begin{bmatrix} a_{11} & a_{12} & a_{13} \\ a_{21} & a_{22} & a_{23} \\ a_{31} & a_{32} & a_{33} \end{bmatrix}$

where:

$a_{11} = (D_{15}/m_c)s^2 + ([-B_c+D_{14}]/m_c)s + ([-K_c+D_{13}]/m_c)$

$a_{12} = (B_c/m_c)s + (K_c/m_c)$

$a_{13} = (D_{11}/m_c)s^2 + (D_9/m_c)s + (D_7/m_c)$

$a_{21} = (-D_{15}/m_b)s^2 + ([B_c-D_{14}]/m_b)s + ([K_c-D_{13}]/m_b)$

$a_{22} = ([-4f/V - B_c]/m_b)s + ([-4K_L-K_c]/m_b)$

(... continued ...)

FIGURE 6-3

System Matrices for the Controlled LMO Vehicle Model

$$a_{23} = (-D_{11}/m_b)s^2 + (-D_9/m_b)s + ([4f-D_7]/m_b)$$

$$a_{31} = (D_6/I_b)s^2 + (D_4/I_b)s + (D_2/I_b)$$

$$a_{32} = (-D_5/I_b)s^2 + (-D_3/I_b)s + ([-4fh\alpha/r_0 - D_1]/I_b)$$

$$a_{33} = ([-4fh^2k_s/V - B_b]/I_b)s + ([-4K_Lk^2h^2-K_b]/I_b)$$

FIGURE 6-3

(continued)

MODEL: RC (RIW) - RPB, Controlled, K-B-Parallel Yaw Secondary

REDUCED STATE VECTOR: $\hat{x}^T = [y_c, \phi_c, y_{b1}, \phi_{b1}, y_{b2}, \phi_{b2}]$

COMPRESSED INPUT VECTOR: for y_{rf}, $\hat{B} =$

$$\begin{bmatrix} 0 \\ 0 \\ \delta^+ ([4f/m_b V]s + [4K_L/m_b]) \\ \delta^+ (4fh\alpha/I_b r_0) + \delta^- ([4fkh/I_b V]s + [4K_L kh/I_b]) \\ \delta^L \delta^+ ([4f/m_b V]s + [4K_L/m_b]) \\ \delta^L \delta^+ (4fh\alpha/I_b r_0) + \delta^L \delta^- ([4fkh/I_b V]s + [4K_L kh/I_b]) \end{bmatrix}$$

DERIVATIVE MATRIX: $\underline{S} = \begin{bmatrix} s^2 & 0 & 0 & 0 & 0 & 0 \\ 0 & s^2 & 0 & 0 & 0 & 0 \\ 0 & 0 & s^2 & 0 & 0 & 0 \\ 0 & 0 & 0 & s^2 & 0 & 0 \\ 0 & 0 & 0 & 0 & s^2 & 0 \\ 0 & 0 & 0 & 0 & 0 & s^2 \end{bmatrix}$

CHARACTERISTIC MATRIX: $\hat{A} = \begin{bmatrix} a_{11} & a_{12} & a_{13} & a_{14} & a_{15} & a_{16} \\ a_{21} & a_{22} & a_{23} & a_{24} & a_{25} & a_{26} \\ a_{31} & a_{32} & a_{33} & a_{34} & a_{35} & a_{36} \\ a_{41} & a_{42} & a_{43} & a_{44} & a_{45} & a_{46} \\ a_{51} & a_{52} & a_{53} & a_{54} & a_{55} & a_{56} \\ a_{61} & a_{62} & a_{63} & a_{64} & a_{65} & a_{66} \end{bmatrix}$

where:

(... continued ...)

FIGURE 6-4

System Matrices for the Controlled RPB Vehicle Model

$$a_{11} = (D_{15}/m_c)s^2 + ([-B_c+D_{14}]/m_c)s + ([-K_c+D_{13}]/m_c)$$

$$a_{12} = (-D_{12}/m_c)s^2 + (-D_{10}/m_c)s + (-D_8/m_c)$$

$$a_{13} = (B_c/2m_c)s + (K_c/2m_c)$$

$$a_{14} = (D_{11}/2m_c)s^2 + (D_9/2m_c)s + (D_7/2m_c)$$

$$a_{15} = (B_c/2m_c)s + (K_c/2m_c)$$

$$a_{16} = (D_{11}/2m_c)s^2 + (D_9/2m_c)s + (D_7/2m_c)$$

$$a_{21} = (-2D_6/I_c)s^2 + (-2D_4/I_c)s + (-2D_2/I_c)$$

$$a_{22} = (2[D_{18}+L^2D_{15}]/I_c)s^2 + (2[-B_b-B_cL^2+D_{17}+L^2D_{14}]/I_c)s + (2[-K_b-K_cL^2+D_{16}+L^2D_{13}]/I_c)$$

$$a_{23} = (D_5/I_c)s^2 + ([B_cL+D_3]/I_c)s + ([K_cL+D_1]/I_c)$$

$$a_{24} = (D_{11}/I_c)s^2 + ([B_b+D_9]/I_c)s + ([K_b+D_7]/I_c)$$

$$a_{25} = (D_5/I_c)s^2 + ([-B_cL+D_3]/I_c)s + ([-K_cL+D_1]/I_c)$$

$$a_{26} = (-D_{11}/I_c)s^2 + ([B_b-D_9]/I_c)s + ([K_b-D_7]/I_c)$$

$$a_{31} = (-D_{15}/m_b)s^2 + ([B_c-D_{14}]/m_b)s + ([K_c-D_{13}]/m_b)$$

$$a_{32} = (-LD_{15}/m_b)s^2 + ([B_c-D_{14}]L/m_b)s + ([K_c-D_{13}]L/m_b)$$

$$a_{33} = ([-4f/V - B_c]/m_b)s + ([-4K_L-K_c]/m_b)$$

$$a_{34} = (-D_{11}/m_b)s^2 + (-D_9/m_b)s + ([4f-D_7]/m_b)$$

$$a_{35} = 0$$

$$a_{36} = 0$$

$$a_{41} = (D_6/I_b)s^2 + (D_4/I_b)s + (D_2/I_b)$$

$$a_{42} = ([-D_{18}+LD_6]/I_b)s^2 + ([B_b-D_{17}+LD_4]/I_b)s + ([K_b-D_{16}+LD_2]/I_b)$$

(... continued ...)

FIGURE 6-4
(continued)

$$a_{43} = (-D_5/I_b)s^2 + (-D_3/I_b)s + ([-4fh\alpha/r_0 - D_1]/I_b)$$

$$a_{44} = ([-4fh^2k_s/V - B_b]/I_b)s + ([-4K_Lk^2h^2-K_b]/I_b)$$

$$a_{45} = 0$$

$$a_{46} = 0$$

$$a_{51} = (-D_{15}/m_b)s^2 + ([B_c-D_{14}]/m_b)s + ([K_c-D_{13}]/m_b)$$

$$a_{52} = (LD_{15}/m_b)s^2 + ([-B_c+D_{14}]L/m_b)s + ([-K_c+D_{13}]L/m_b)$$

$$a_{53} = 0$$

$$a_{54} = 0$$

$$a_{55} = ([-4f/V - B_c]/m_b)s + ([-4K_L-K_c]/m_b)$$

$$a_{56} = (-D_{11}/m_b)s^2 + (-D_9/m_b)s + ([4f-D_7]/m_b)$$

$$a_{61} = (D_6/I_b)s^2 + (D_4/I_b)s + (D_2/I_b)$$

$$a_{62} = ([-D_{18}-LD_6]/I_b)s^2 + ([B_b-D_{17}-LD_4]/I_b)s + ([K_b-D_{16}-LD_2]/I_b)$$

$$a_{63} = 0$$

$$a_{64} = 0$$

$$a_{65} = (-D_5/I_b)s^2 + (-D_3/I_b)s + ([-4fh\alpha/r_0 - D_1]/I_b)$$

$$a_{66} = ([-4fh^2k_s/V - B_b]/I_b)s + ([-4K_Lk^2h^2-K_b]/I_b)$$

FIGURE 6-4
(continued)

TABLE 6-1

Transfer Function Coefficients: RC (RIW) - LMO, Controlled, K-B-Parallel Yaw Secondary

n=6, m=5

DENOMINATOR

$$c_6 = 1 - (D_5+\rho_m D_6)(D_{11}/m_b I_b) - (\rho_m D_{15}/m_b)$$

$$c_5 = g_5 S_3 + S_5(1+\rho_{bb})(1-[\rho_m D_{15}/m_b]) - (\rho_m g_5/m_b)(D_{15}+[D_6 D_{11}/I_b]) - (1/m_b I_b)([D_3 D_{11}+D_5 D_9] + \rho_m[D_4 D_{11}+D_6 D_9])$$

$$c_4 = S_5(1+\rho_{bb})(g_5 S_3-[\rho_m/m_b][D_{14}+g_5 D_{15}]) + S_2/I_b + S_1/m_b + g_5{}^2\rho_m\rho_{bc} - (\rho_m D_2 D_{11}/m_b I_b) + (g_5 V D_5/I_b)(1-[\rho_m D_{15}/m_b]) - (\rho_m D_4/m_b I_b)(D_9+g_5 D_{11}) - (\rho_m D_6/m_b I_b)(D_7+g_5 D_9+[4K_L D_{11}/m_b]) - (1/m_b I_b)(D_1 D_{11}+D_3 D_9+D_5 D_7) - (\rho_m/m_b)(D_{13}+g_5 D_{14}+[4K_L D_{15}/m_b]) - (\rho_m S_2 D_{15}/m_b I_b) - S_6 D_{11}/m_b V$$

$$c_3 = g_5([S_2 S_3/I_b]+[\rho_m S_4/m_b]) + S_5(1+\rho_{bb})([S_1/m_b]+g_5{}^2\rho_m\rho_{bc}-[\rho_m/m_b][D_{13}+g_5 D_{14}+4K_L D_{15}/m_b]) + (g_5 D_3 V/I_b)(1-[\rho_m D_{15}/m_b]) - (\rho_m D_2/m_b I_b)(D_9+g_5 D_{11}) - (\rho_m D_4/m_b I_b)(D_7+g_5 D_9+[4K_L D_{11}/m_b]) - (\rho_m D_6/m_b I_b)(g_5 D_7+[4K_L D_9/m_b]) - (1/m_b I_b)(D_1 D_9+D_3 D_7) - (g_5\rho_m V/I_b)([D_5 D_{14}/m_b]+g_5\rho_{bc}[D_6-D_5]) - (\rho_m/m_b)(g_5 D_{13}+[4K_L D_{14}/m_b]) - (\rho_m S_2/m_b I_b)(D_{14}+g_5 D_{15}) - S_6 D_9/m_b V$$

(... continued ...)

TABLE 6-1 (continued)

$$c_2 = g_5S_6 + S_5(1+\rho_{bb})(\rho_m/m_b)(g_5S_4-g_5D_{13}-[4K_LD_{14}/m_b]) + (S_2/I_b)(S_1/m_b + g_5^2\rho_m\rho_{bc})$$
$$+(4\rho_mK_cK_L/m_b^2) + (g_5VD_1/I_b)(1-\rho_mD_{15}/m_b) + (g_5V\rho_mD_5/m_bI_b)(K_c-D_{13})$$
$$+ (g_5^2V\rho_m\rho_{bc}/I_b)(D_3-D_4) - (\rho_mD_2/m_bI_b)(D_7+g_5D_9+[4K_LD_{11}/m_b])$$
$$- (\rho_mD_4/m_bI_b)(g_5D_7+[4K_LD_9/m_b]) - (4K_L\rho_mD_{13}/m_b^2)$$
$$- (\rho_mS_2/m_bI_b)(D_{13}+g_5D_{14}+[4K_LD_{15}/m_b]) - (S_6/m_bV)(D_7+g_5V\rho_mD_{15})$$
$$- (\rho_mg_5V/m_bI_b)(K_cD_6+D_3D_{14}) - (4\rho_mK_LD_6D_7/m_b^2I_b) - (D_1D_7/m_bI_b)$$

$$c_1 = g_5^2S_6\rho_m\rho_{bc} + (4K_L\rho_mS_5[1+\rho_{bb}]/m_b^2)(K_c-D_{13}) + g_5\rho_mS_2S_4/[m_bI_b] - (\rho_mS_2/m_bI_b)(g_5D_{13}+[4K_LD_{14}/m_b])$$
$$- (\rho_mD_2/m_bI_b)(g_5D_7+[4K_LD_9/m_b]) + (\rho_mg_5V/m_bI_b)(K_c[D_3-D_4]-D_1D_{14}-D_3D_{13})$$
$$+ (g_5^2V\rho_m\rho_{bc}/I_b)(D_1-D_2) - (4K_L\rho_mD_4D_7/m_b^2I_b) - g_5S_6\rho_mD_{14}/m_b$$

$$c_0 = (g_5\rho_mS_6/m_b)(K_c-D_{13}) + (4K_L\rho_m/m_b^2I_b)(S_2[K_c-D_{13}]-D_2D_7) + (g_5V\rho_m/m_bI_b)(K_c[D_1-D_2]-D_1D_{13})$$

NUMERATOR (in phase)

$$b_{p5} = -(\rho_mD_5/m_bI_b)(g_5D_{11})$$

$$b_{p4} = g_5^2\rho_m\rho_{bc} - (\rho_mD_5/m_bI_b)(g_5D_9+[4K_L/m_b]D_{11}) - (\rho_mD_3/m_bI_b)(g_5D_{11}) + (\rho_mS_6D_{11}/m_bV)$$

(... continued ...)

TABLE 6-1 (continued)

$$b_{p3} = (g_5\rho_m S_4/m_b) + g_5^2\rho_m\rho_{bc}S_5(1+\rho_{bb}) - (\rho_m D_5/m_b I_b)(g_5 D_7+[4K_L/m_b]D_9)$$
$$- (\rho_m D_3/m_b I_b)(g_5 D_9+[4K_L/m_b]D_{11}) - (\rho_m D_1/m_b I_b)(g_5 D_{11}) + (\rho_m S_6 D_9/m_b V)$$

$$b_{p2} = (g_5^2\rho_m\rho_{bc}S_2/I_b) + (\rho_m/m_b)(g_5 S_4 S_5[1+\rho_{bb}]+[4K_c K_L/m_b]) - (\rho_m D_5/m_b I_b)([4K_L/m_b]D_7)$$
$$- (\rho_m D_3/m_b I_b)(g_5 D_7+[4K_L/m_b]D_9) - (\rho_m D_1/m_b I_b)(g_5 D_9+[4K_L/m_b]D_{11}) + (\rho_m S_6 D_7/m_b V)$$

$$b_{p1} = g_5^2\rho_m\rho_{bc}S_6 + (\rho_m/m_b)([g_5 S_2 S_4/I_b]+[4K_c K_L S_5\{1+\rho_{bb}\}/m_b]) - (\rho_m D_3/m_b I_b)([4K_L/m_b]D_7)$$
$$- (\rho_m D_1/m_b I_b)(g_5 D_7+[4K_L/m_b]D_9)$$

$$b_{p0} = (\rho_m/m_b)(g_5 K_c S_6+[4K_c K_L S_2/m_b I_b]) - (\rho_m D_1/m_b I_b)([4K_L/m_b]D_7)$$

NUMERATOR (out of phase)

$$b_{m5} = (\rho_m kh/I_b)(g_5 D_{11})$$

$$b_{m4} = (\rho_m kh/I_b)(g_5 D_9+D_{11}[g_5^2 + 4K_L/m_b])$$

$$b_{m3} = (\rho_m kh/I_b)(g_5 D_7+D_9[g_5^2 + 4K_L/m_b]+D_{11}[8K_L g_5/m_b])$$

$$b_{m2} = (g_5^3 m_b Vkh\rho_m\rho_{bc}/I_b) + (\rho_m kh/I_b)(D_7[g_5^2 + 4K_L/m_b]+D_9[8K_L g_5/m_b]+D_{11}[4K_L/m_b]^2)$$

$$b_{m1} = (g_5^2 Vkh\rho_m S_4/I_b) + (\rho_m kh/I_b)(D_7[8K_L g_5/m_b]+D_9[4K_L/m_b]^2)$$

$$b_{m0} = (g_5 4VkhK_c K_L\rho_m/m_b I_b) + (\rho_m kh/I_b)(D_7[4K_L/m_b]^2)$$

a mechanical power pair (force and velocity, or torque and angular velocity). Then instantaneous power is given by

$$P = x_1 x_2 \quad . \tag{6.7.1}$$

If x_1 and x_2 are related to an input u by transfer functions $H_1(s)$ and $H_2(s)$, respectively, and if the spectral density of the input is given by $\Phi_u(s)$, then the spectral density of P may be written

$$\Phi_P = \Phi_u \frac{H_1 H_2^* + H_1^* H_2}{2} \quad , \tag{6.7.2}$$

where the asterisk denotes complex conjugate [67]. The net power is then obtained by integrating Φ_P between negative and positive infinity. If there are several power pairs, power is additive among them. For the active controller defined in this chapter, there are two pairs:

$$F_{bci} \text{ and } (\dot{y}_{cbi} - \dot{y}_{bi}) \quad , \text{ and}$$

$$T_{bci} \text{ and } (\dot{\phi}_c - \dot{\phi}_{bi}) \quad .$$

The fact that H_1 and H_2 must share a common denominator simplifies the analysis somewhat.

8. Other Practical Considerations. The expressions for F_{bc} and T_{bc} given in Equations 6.2.1 and 6.2.2 are convenient analytically, and will be shown to produce systems with good dynamic properties. When controller hardware is to be designed, however, their application must be tempered by considerations of practicality. Several such consider-

ations will be discussed briefly here.

The problem of forces arising from initial misalignment, mentioned in connection with the K-B-series yaw configuration in Chapter 4, is present also in the controlled vehicle when any of D_1, D_2, D_7, D_8, D_{13}, and D_{16} are nonzero. A different manifestation of essentially the same phenomenon is drift, a slow variation of parameter values or null settings. Since active control is used to improve dynamic response, it is not necessary at very low frequencies and measures should be taken to "high - pass" control action to prevent steady - state offset. A simple mechanical method of doing this is to place a stiff mechanical damper in series with yaw and lateral actuators; this method used alone can of course permit control power to be wasted at low frequencies, so it should be applied in conjunction with some system which would stop low - frequency control power flow at its source.

Controller action at very high frequencies can also be a problem. At such frequencies the contribution of the controller may be either insignificant or unnecessary, serving only to drain power. It is also possible for high - frequency instabilities to occur in a real system, due to the excitation of component bending modes for example, which would not be predicted by the simple rigid models being used here. It is therefore good practice to cut off controller response above the frequency range in which it plays a significant and beneficial role. Part of this function occurs naturally because of the mechanical, fluid, and/or electrical lags inherent in the sensing and actuation

hardware.

The two above considerations suggest that a practical control system should combine the basic properties of Equations 6.2.1 and 6.2.2 (or some more restricted case) with a band - pass characteristic to confine response to a desired region. The controller definitions are used unaltered for the purposes of this thesis, with a single exception: control power is computed by integrating only over the two decades between 0.3 and 30. Hz, which comprises the frequencies of greatest sensitivity to acceleration.

A relative - sensing controller is by far the easiest type to implement. Determination of absolute position and velocity would require either inertial navigation or a specialized external input, neither one of which seems worthwhile unless very great improvements in performance are to be had. The exception to this general conclusion is, of course, acceleration, which is more easily sensed absolutely than relatively.

The impact of an automatic controller on performance in curves should not be neglected. If response is band - passed as recommended above, there should be no effect on quasi - static curving. Beyond merely cutting off the control action at low frequencies, however, it is possible to use the same hardware to aid in curve negotiation by steering the truck into the curve. Further consideration of this possibility is beyond the scope of this thesis, but it points up one way in which active control can be used to achieve results difficult or impossible to achieve passively.

Two special cases of the general controller will be examined in Chapters 7 and 8. The relative-sensing steering controller (Chapter 7) requires only three gains (D_1, D_3, and D_5) and the sensing of only relative displacement and its derivatives. It acts directly on the hunting mechanism and so offers the possibility of an efficient cure for instability. The passive asymmetric secondary suspension (Chapter 8) offers features similar to those of active steering, but without its power requirements or complexity.

CHAPTER 7

PERFORMANCE OF ACTIVELY STEERED CONVENTIONAL VEHICLE MODEL WITH LATERAL-MASS-ONLY CARBODY

From the general class of controller introduced in Chapter 6, two special cases have been selected for detailed study. This chapter is devoted to a consideration of the relative-sensing, steering controller applied to the LMO carbody model, while the passive-asymmetric suspension is discussed in Chapter 8.

1. Controller Notation and Operation. The relative-steered controller type, defined in §§6.2 and 6.3, is a combination of the relative-sensing and steering special cases. Steering action has been identified as a potentially effective and low-power means of reducing the hunting of an RC truck. Relative sensing has been chosen because it can be readily implemented without any need for the sophisticated instrumentation necessary to keep track of absolute quantities; also relative displacements, unlike absolute displacements, are well-defined in curves. The combination of the two results in a system which acts to reduce the truck-carbody relative displacement and, under appropriate conditions, to counteract hunting.

The controller is characterized by three gains only: D_1 (position), D_3 (velocity), and D_5 (acceleration). The values of gains in the original control law (Equations 6.2.1 and 6.2.2) are:

$$D_1=D_2 \ , \quad D_3=D_4 \ , \quad D_5=D_6 \ , \tag{7.1.1}$$

$$D_7 = D_8 = D_9 = D_{10} = D_{11} = D_{12} = 0 \ , \text{ and} \tag{7.1.2}$$

$$D_{13} = D_{14} = D_{15} = D_{16} = D_{17} = D_{18} = 0 \ . \qquad (7.1.3)$$

A convenient scaling and abbreviation of these gains may be made by defining:

$$\varepsilon_1 = D_1 \ / \ (4fh\alpha/r_0) \ , \qquad (7.1.4)$$

$$\varepsilon_2 = D_3 \ / \ (4fh\alpha \ \sec/10r_0) \ , \text{ and} \qquad (7.1.5)$$

$$\varepsilon_3 = D_5 \ / \ (4fh\alpha \ \sec^2/100r_0) \ . \qquad (7.1.6)$$

For the ranges of gain to be considered, all ε's will be of order unity. Thus the relative-steered controller may be completely specified by the list

$$\varepsilon = (\varepsilon_1, \varepsilon_2, \varepsilon_3) \ . \qquad (7.1.7)$$

A steering controller is especially well-suited to use with a conventional truck because it acts directly on the lateral-yaw coupling which causes hunting. The "steering" for which it is named occurs when the truck, laterally displaced, receives a torque in a direction which causes it to roll closer to the carbody. This controller is inactive at low frequencies, where the carbody and truck move together, and unnecessary at high frequencies, where steering is ineffectual. It is active primarily in the regions of carbody resonance and of kinematic hunting -- i.e., for both primary and secondary hunting.

Figure 7-1 will illustrate the action of the steering controller. It shows the loci of the two least damped pairs of poles (normally identified with kinematic hunting and carbody resonance) for a 100 mph

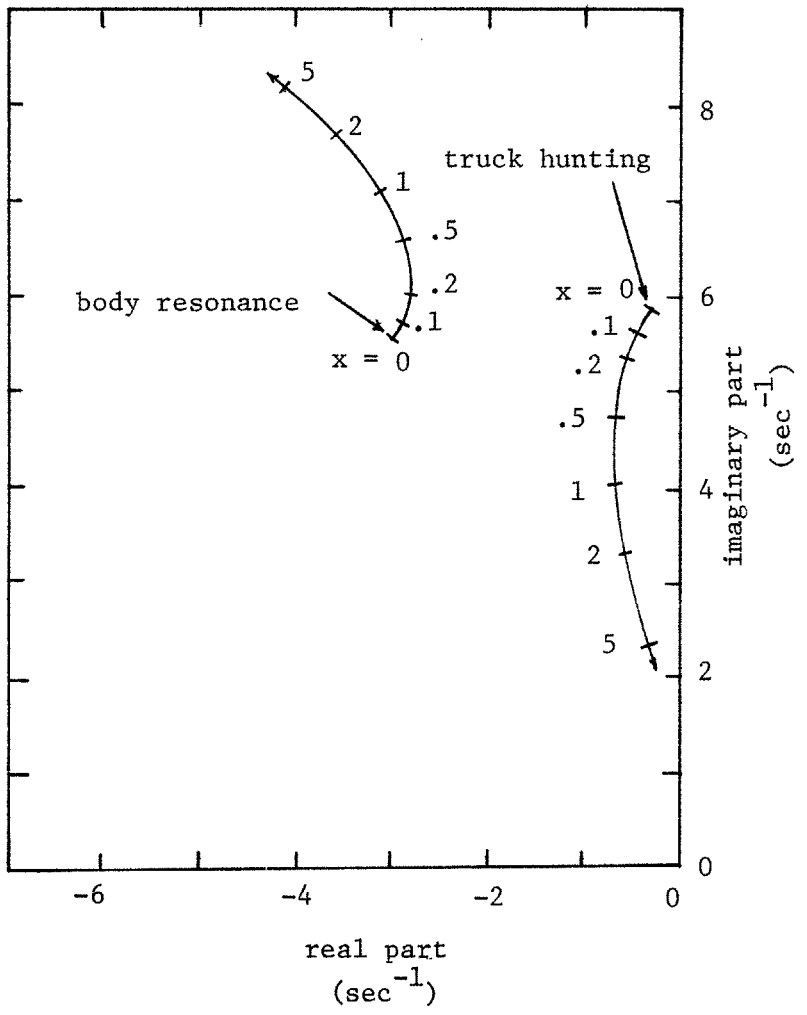

FIGURE 7-1

Locus of Least - Damped Poles of RC - LMO System with Relative - Steering Control, $\varepsilon=(x,x,x)$.

Baseline Parameters at 100 mph.

baseline RC-LMO model steering gain $\varepsilon=(x,x,x)$, as x is varied from zero to five. The case x=0 corresponds to the uncontrolled baseline vehicle. An examination of the eigenvectors corresponding to these poles reveals that below $x\approx0.2$, the poles of smaller modulus represent relatively small carbody motion with large truck oscillations (truck hunting); whereas those of larger modulus show large carbody amplitudes with little truck motion (carbody resonance). Above $x\approx0.2$, the low-modulus pole begins to represent the carbody and truck moving together in phase, with the high-modulus pole representing out-of-phase motion. The identification of modes is not, of course, completely clear-cut in this example, but it does show several significant features of steering control. As gain is increased, the truck follows the carbody more and more closely, reducing the effective lateral spring and damper rates; thus the carbody resonance frequency is decreased and the low-modulus locus is generated. If the carbody moves relatively little, as in the high-modulus locus, the controller acts similarly to increased conicity and thereby reduces response time. Notice that the low-modulus locus becomes unstable around $x\approx10$ due to oversteering.

2. Stability. Figure 7-2 consists of stability loci (planes) for an RC-LMO relative-steered vehicle model for various combinations of ε_1, ε_2, ε_3, and V; all other parameters have their baseline values as given in Table 3-5. The format of the figure is as follows: shaded areas represent regions of instability; within each graph, the

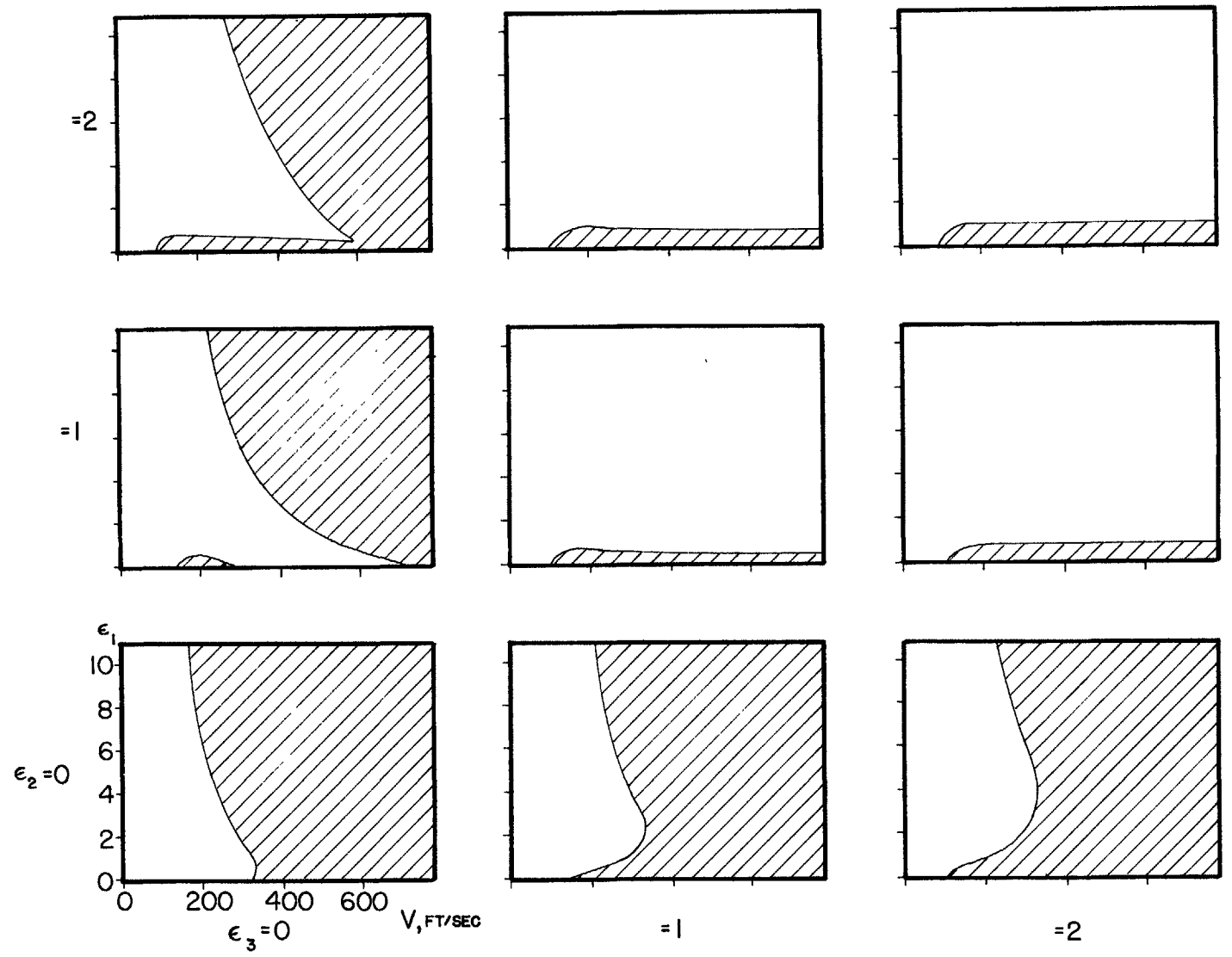

FIGURE 7-2

Stability Planes for RC - LMO Model with Relative - Steering Control. Baseline Parameters.

vertical axis is position gain ε_1 (0 - 11) and the horizontal is speed V (0 - 800 ft/sec); a horizontal row of graphs share a common velocity gain ε_2 (0, 1, or 2); and a vertical column share a common acceleration gain ε_3 (0, 1, or 2).

Figure 7-2 demonstrates that very significant increases in critical speed are possible with steering control. The uncontrolled baseline system shows $V_c \simeq 300$ ft/sec. Varying ε_1 alone can increase this only slightly, but $\varepsilon=(1,1,0)$ shows $V_c \simeq 600$ ft/sec, a 100% increase. Adding acceleration gain can extend V_c to infinity, according to this model: $\varepsilon=(1,1,1)$, for example, has an infinite critical speed. Such extremely high critical speeds are not useful in themselves; but the steering controller, by relaxing the stability constraint, allows more freedom in designing toward other goals, such as reducing secondary stiffness K_b or improving ride quality.

It should be noted that the stability planes for all three gains nonzero possess another region of instability at large ε_1 (>50) which does not show on the scale of the figure.

3. Ride Quality. Examination of the transfer function coefficients in Table 6-1 reveals that the relative - steering controller gains appear in a very simple manner due to the fact that $D_1=D_2$, $D_3=D_4$, and $D_5=D_6$. The numerator for carbody acceleration is unaltered. In the denominator, the effect of control is to add the following terms to c_2, c_3, and c_4:

$$\begin{aligned} &\text{to } c_2, \text{ add } D_1(4f/m_b I_b) \ , \\ &\text{to } c_3, \text{ add } D_3(4f/m_b I_b) \ , \text{ and} \\ &\text{to } c_4, \text{ add } D_5(4f/m_b I_b) \ . \end{aligned} \qquad (7.3.1)$$

These terms are speed - independent. Being confined to intermediate powers of s, they cannot affect either low - or high - frequency asymptotic behavior, but at intermediate frequencies can shift or suppress some resonances and introduce others. Whether this action improves or degrades ride quality depends on the magnitudes of the control gains.

Figure 7-3 illustrates the improvement in ride quality attainable with steering control. The four A.S.D. curves are all for a baseline RC-LMO vehicle model at 100 mph, with steering gains as follow:

1. $\varepsilon = (0,0,0)$ -- no control
2. $\varepsilon = (1,0,0)$
3. $\varepsilon = (1,1,0)$
4. $\varepsilon = (1,1,1)$.

Position gain alone (curve 2) reduces the hunting peak by an order of magnitude, and changes its location from about 1.0 to 1.8 Hz; the

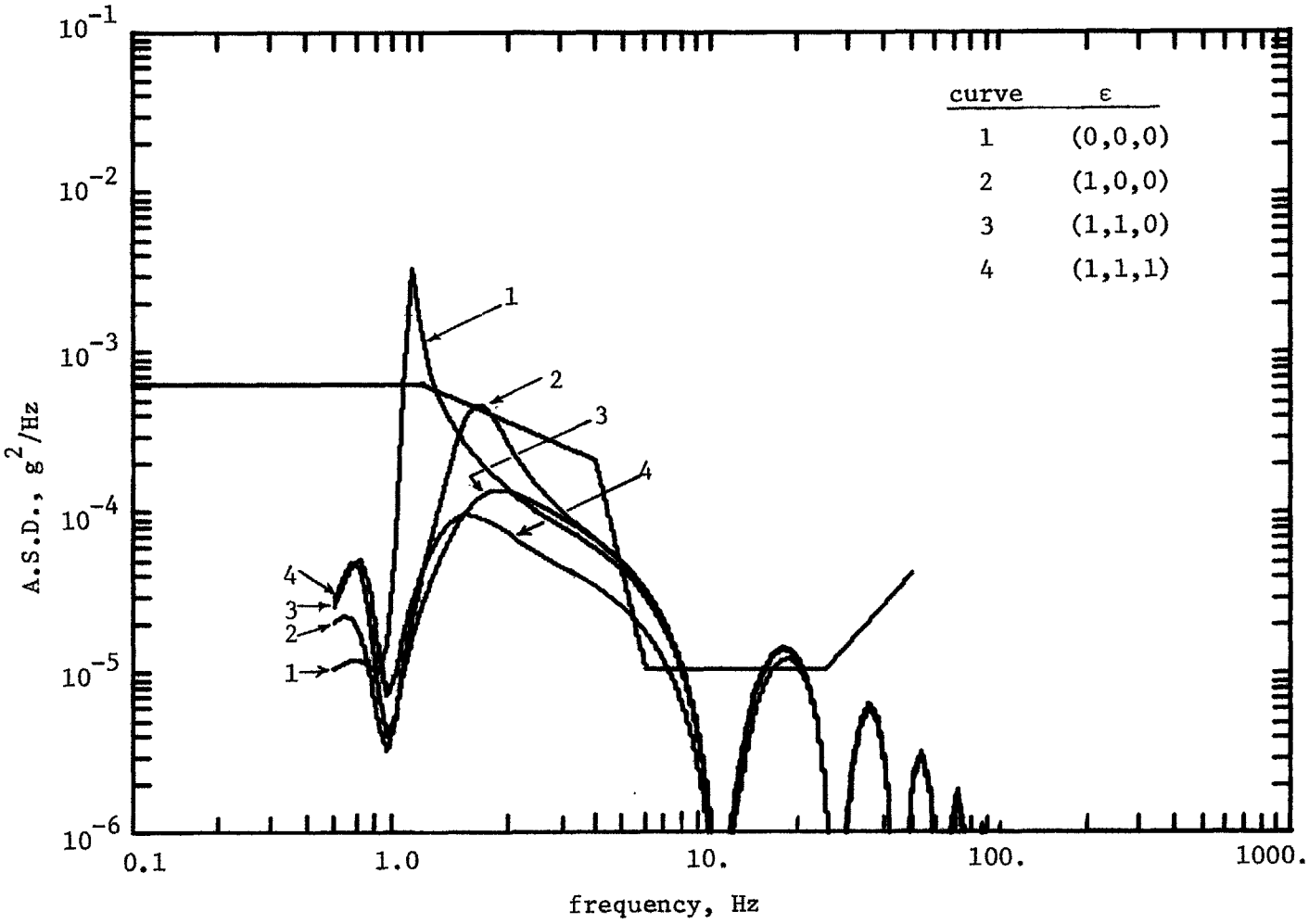

FIGURE 7-3

Acceleration Spectral Density for RC - LMO Model, Relative - Steered for Several Gain Combinations at 100 mph (Baseline Parameters)

comfort goal is very nearly met at this peak, although it is still exceeded by two high - frequency lobes. Velocity gain (curve 3) further depresses and displaces the peak. With acceleration gain (curve 4), the process is continued and extended to higher frequencies, so that the goal is exceeded only slightly at 6 Hz and 20 Hz.

Figure 7-3 shows clearly that ride quality may be greatly improved by active steering control. This fact, combined with the major increases in critical speed reflected in Figure 7-2, attests to the suitability of this type of controller for high - speed passenger systems.

If extremely high critical speed is not required, the steering controller permits substantial reductions in yaw secondary stiffness with only minor penalties in ride quality. Figure 7-4 shows A.S.D. curves for the baseline vehicle at 100 mph with $\varepsilon=(1,1,1)$, for K_b equal to 1.0, 0.5, and 0.1 times its baseline value. Reduction of K_b by a factor of ten is seen to have only a small negative effect on ride quality between 0.5 and 2 Hz. V_c is still infinite for each of these cases. Yaw stiffness may not be decreased to zero, however, without introducing a range of low unstable speeds at which the controller is inactive.

Figure 7-5 illustrates the variation of A.S.D. with gain for the particular form $\varepsilon=(x,0,0)$, as x is varied from zero to 1. The out - of - phase hunting peak is lowered and moved to higher frequencies, while the in - phase peak is increased in magnitude; it is the latter peak which eventually grows toward infinity as ε_1 approaches its stability limit. This figure is a good example of why the design of

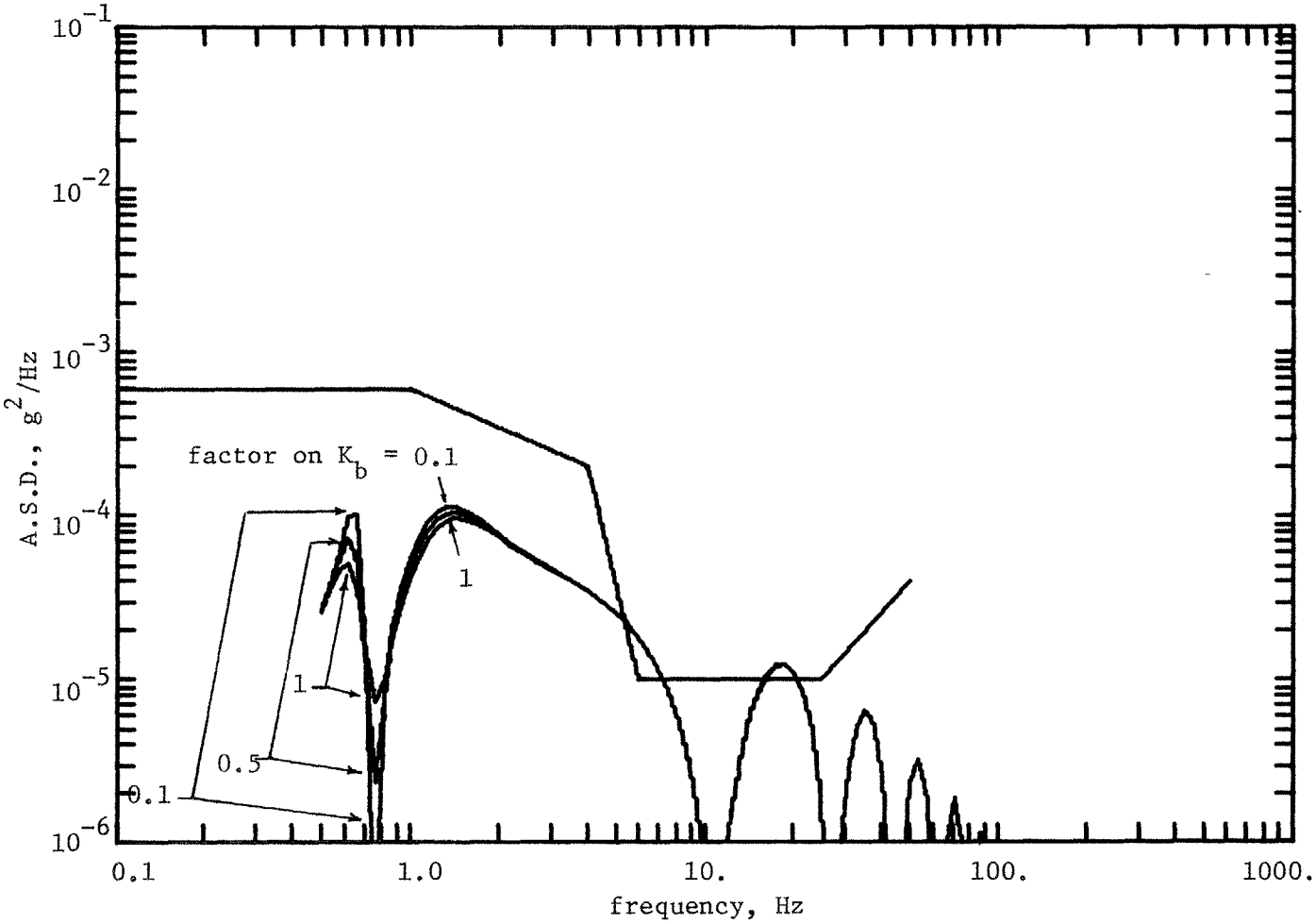

FIGURE 7-4

Effect on A.S.D. of Reducing K_b -- RC - LMO, Relative - Steered, ε=(1,1,1)
(Baseline Parameters, 100 mph)

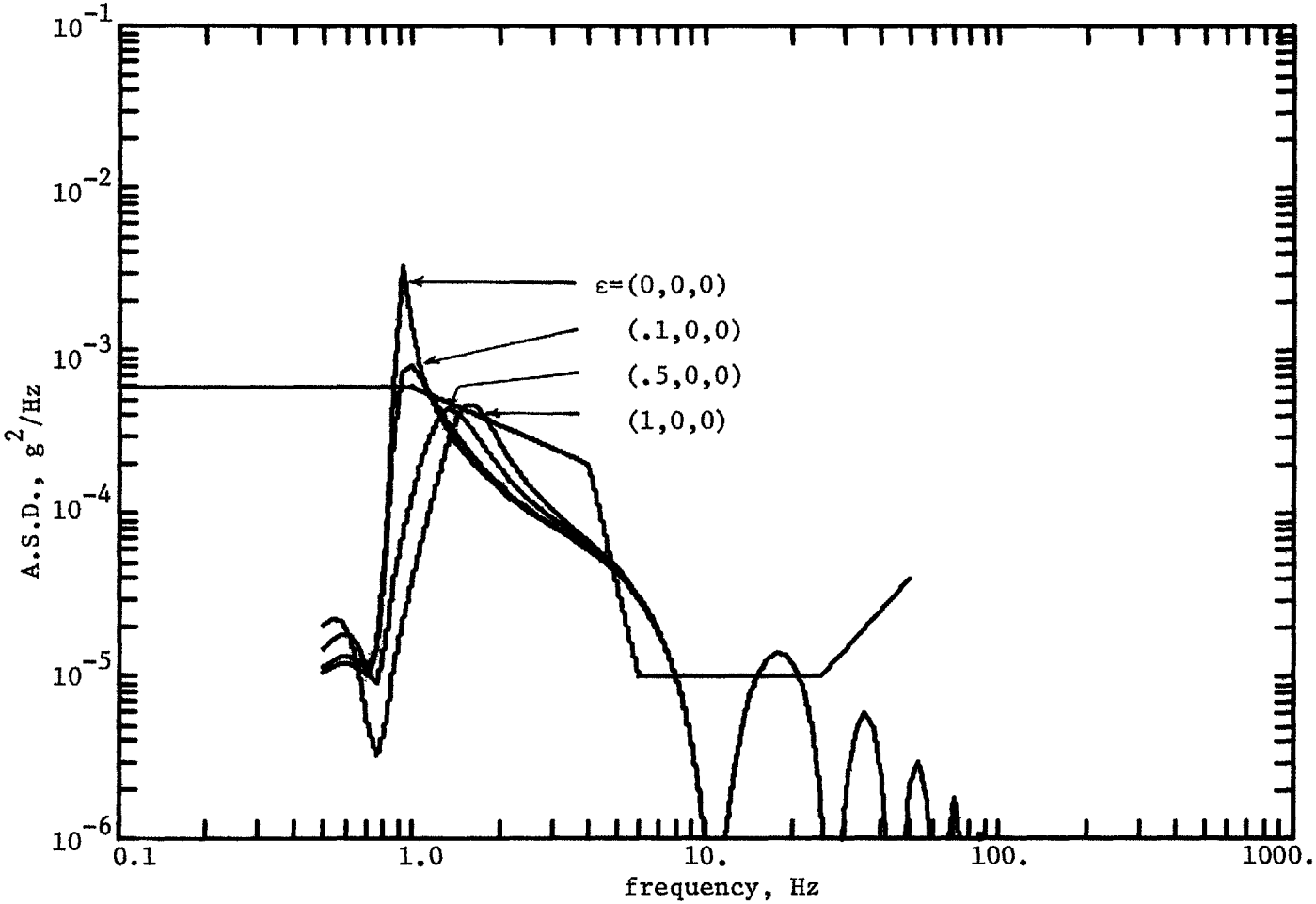

FIGURE 7-5

Effect on A.S.D. of Displacement Gain -- RC - LMO, Relative - Steered, ε=(x,0,0)
(Baseline Parameters, 100 mph)

a comfortable rail vehicle suspension requires (for the present, at least) that the entire acceleration spectrum, rather than a single figure of merit, be considered. One possible estimate of ride quality, RMS acceleration, increases monotonically with x for the example. Yet it seems clear that the system with x=0.1 would provide a better ride than that with x=0, because the hunting peak is so greatly reduced. Extending x much above 1, on the other hand, appears to be of little value; its main effect is to raise and spread the two resonance peaks, moving the higher one into a region of increased human vibration sensitivity.

Figure 7-6 shows the variation of A.S.D. with speed for the baseline vehicle with $\varepsilon=(1,1,1)$. Although the ideal choice of ε would depend on the planned operating speed, the figure shows that any particular choice can be effective in improving ride quality over a range of V.

4. Tracking Error. By suppressing hunting, the steering controller also reduces tracking error on nominally straight track. Figure 7-7 shows the tracking error versus speed for ε's of (0,0,0), (1,0,0), (1,1,0), and (1,1,1). Except for the (1,0,0) case, which shows an earlier onset of instability than does the uncontrolled vehicle (cf. Figure 7-2), increasing the order of feedback results in progressively smaller RMS error.

5. Control Power. The mathematical basis for estimation of power delivered by an active controller was given in §6.7. Recall that the frequency limits of integration of power spectral density

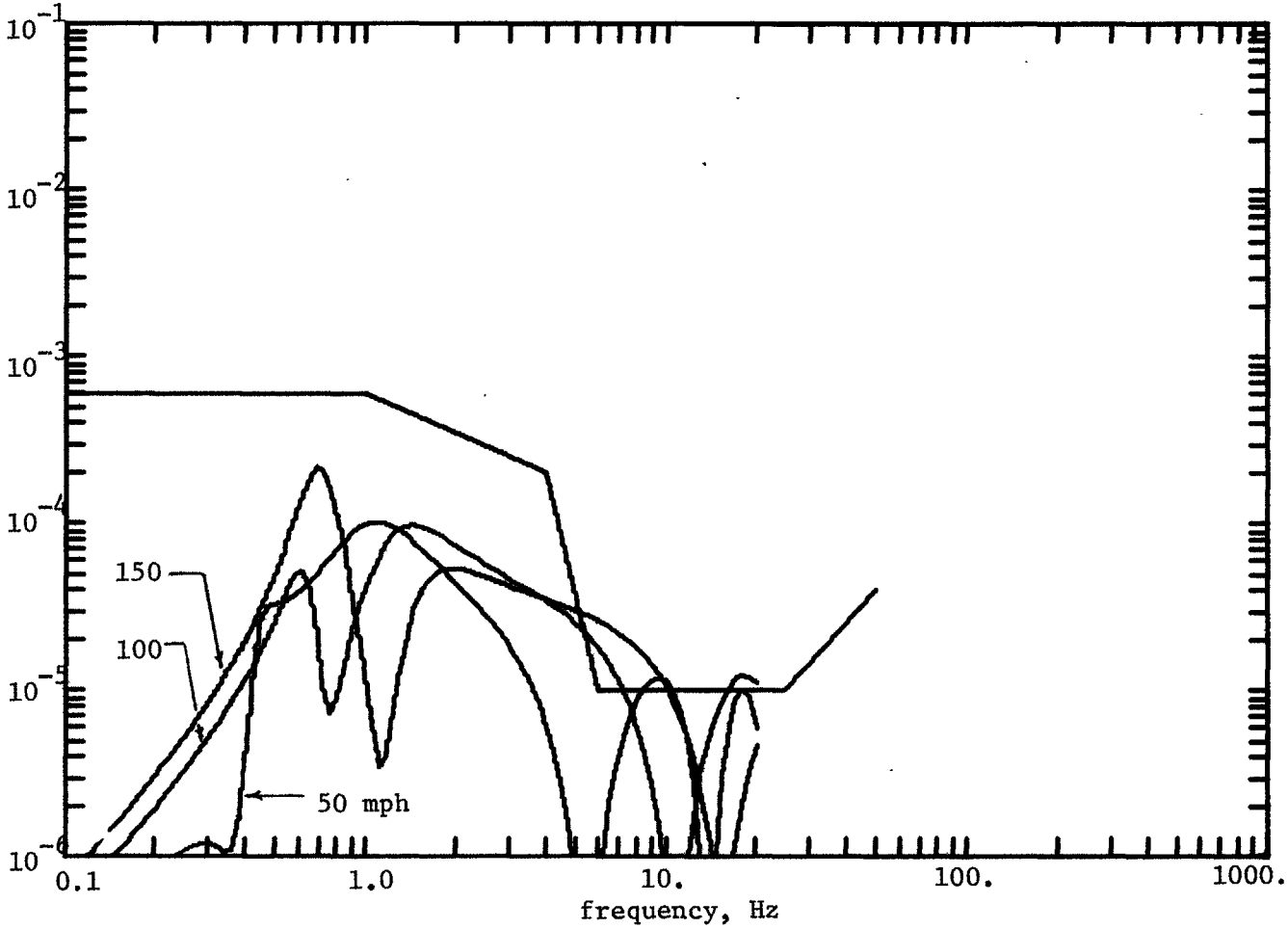

FIGURE 7-6

Effect of V on A.S.D. -- RC - LMO, Relative - Steered, $\varepsilon=(1,1,1)$
(Baseline Parameters)

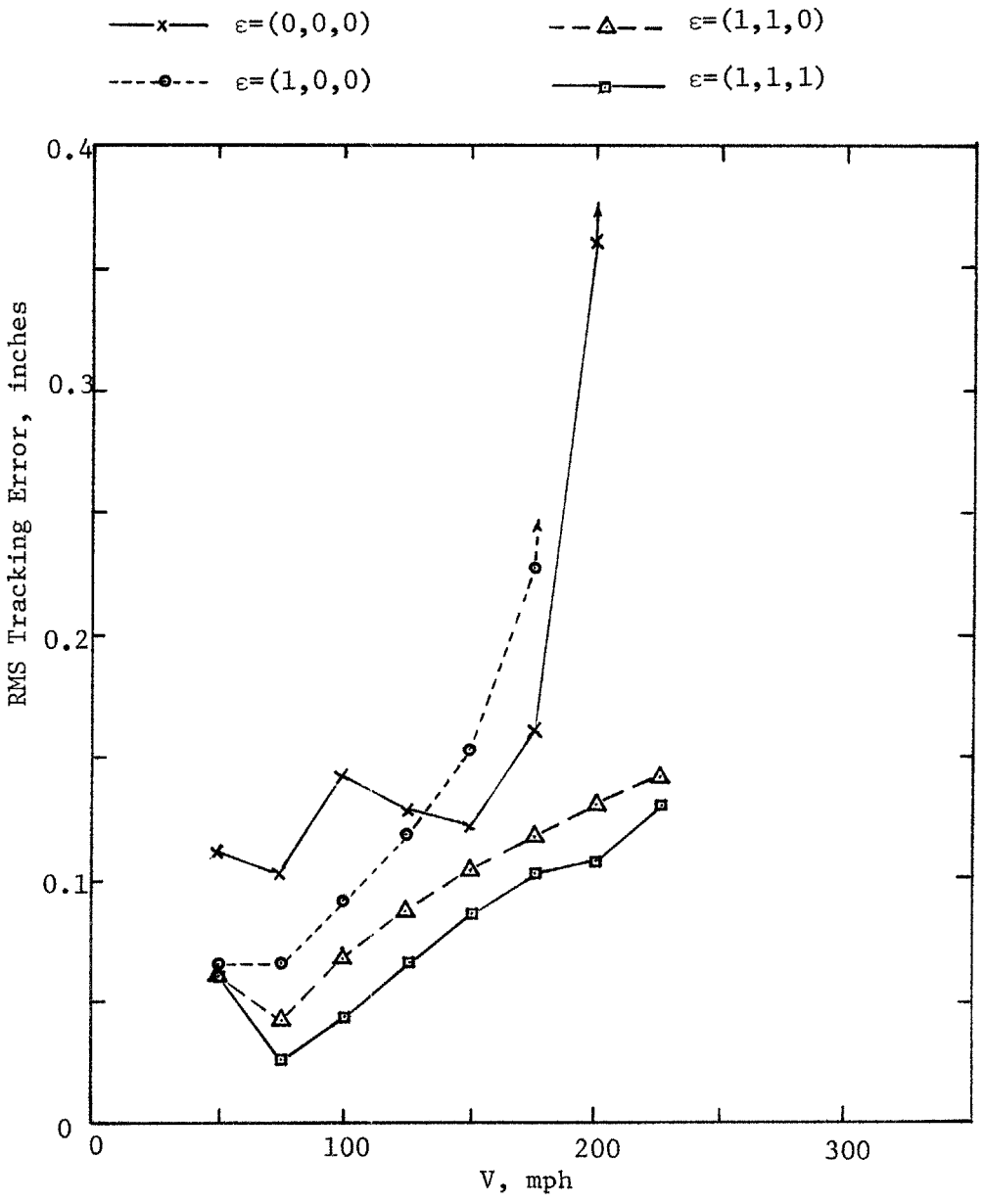

FIGURE 7-7

RMS Tracking Error versus Speed, RC - LMO, Relative - Steered
(Baseline Parameters)

have been fixed at 0.3 and 30 Hz, based on the practical necessity of bandpass filtering the controller output. Inspection of Figures 7-3 through 7-6 shows that all important contributions of active steering are confined to those two decades for all speed and gain combinations considered. Of course, filtering may be expected to have a significant effect at extreme speeds; in particular, the very high critical speeds shown in Figure 7-2 would not be correct.

Figure 7-8 contains net power delivered to the active part of the system in the 0.3 - 30 Hz band for three speeds and three sets of controller gains. In no case considered does control power exceed 0.6 horsepower. This modest figure should be applied with caution, however, because it represents only the minimum power required -- a real configuration may use significantly more.

6. Overview. This chapter has shown how the relative - steered active control scheme may be used to improve the performance of rail vehicles with conventional rigid trucks. Only the LMO carbody model has been used -- the RPB model will be applied in Chapter 9 -- but these results indicate that improvements may be substantial. Critical speed may be extended greatly. Ride quality, expressed as acceleration spectral density, may be improved, and tracking error may be reduced. In short, the hunting problem may be eliminated by the expenditure of roughly one horsepower per vehicle.

The steering approach is not the only reasonable method of actively controlling rail vehicles, but it has been selected for study because (1) it represents a direct attack on the hunting

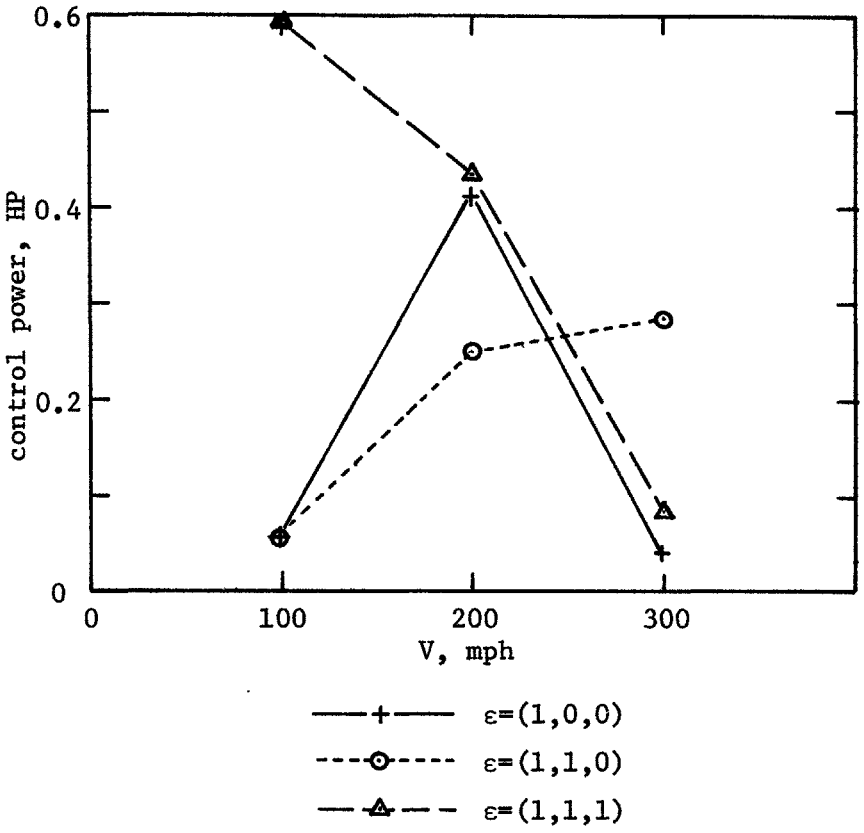

FIGURE 7-8

Net Control Power Delivered by Relative - Steering Controller

mechanism, and (2) it promises to be relatively simple to implement mechanically. An even simpler and lower - power "controller" -- the passive - asymmetric suspension -- will be treated in the next chapter.

CHAPTER 8

PERFORMANCE OF CONVENTIONAL VEHICLE MODEL WITH LATERAL - MASS - ONLY CARBODY AND ASYMMETRIC SECONDARY SUSPENSION

One special case of the general controller may be implemented passively. The passive-asymmetric suspension, described in Equations 6.3.11, achieves some of the benefits of the active steering controller through the use of unequal lineal springs and dampers in front of and behind the truck center of mass (see Figure 6-2). In this chapter, the passive-asymmetric suspension will be applied to the RC truck and LMO vehicle models. It has the advantages of being passive (thus requiring no additional power for operation) and mechanically simple. It will be shown to offer significant increases in critical speed compared to the conventional symmetric suspension, which may alternatively be traded for improved ride quality at lower speeds.

1. Physical Constraints. Recall from §6.3 that σ_k and σ_b represent the ratios of rear spring and damper constants, respectively, to those of the front spring and damper within the truck (K_0 and B_0). If σ_k and σ_b are both unity, there is no asymmetry and the suspension is referred to as conventional or symmetric. A realizable passive spring or damper must have a non-negative constant, which requires

$$\sigma_k \geq 0 \quad , \quad \text{and} \tag{8.1.1}$$

$$\sigma_b \geq 0 \quad . \tag{8.1.2}$$

Equations 6.3.11 are rewritten here for convenience:

$$K_c = K_0(1+\sigma_k) \qquad B_c = B_0(1+\sigma_b)$$
$$K_b = K_0\ell_k^2(1+\sigma_k) \qquad B_b = B_0\ell_b^2(1+\sigma_b) \qquad (8.1.3)$$
$$D_1=D_2=D_7=D_8 = K_0\ell_k(1-\sigma_k) \qquad D_3=D_4=D_9=D_{10} = B_0\ell_b(1-\sigma_b) \quad .$$

The following discussion will be limited to springs, but the form of Equations 8.1.3 shows that it applies equally well to dampers with the substitutions of "B" for "K" and "D_3" for "D_1".

First, note that

$$K_b/K_c = \ell_k^2 \quad . \qquad (8.1.4)$$

The available length ℓ_k is limited by truck size, and is unlikely much to exceed the wheelbase kh. This puts a limitation on the K_b attainable <u>from the lineal springs alone</u> at a given K_c:

$$K_{b\ max} \simeq K_{b0} + K_c(kh)^2 \quad , \qquad (8.1.5)$$

where K_{b0} is a purely torsional stiffness provided in some way other than by the lineal springs. The further requirement that σ_k be non-negative sets a bound on D_1 $(=D_2=D_7=D_8)$:

$$D_{1\ max} = K_c\ell_k \quad . \qquad (8.1.6)$$

K_c has been assumed as the primary variable because it is at least partially determined by considerations other than dynamics, such as suspension and trackside clearances.

Equation 8.1.5 includes a provision for a pure torsional spring of constant K_{b0}. Such a spring may be required in order to attain the very high yaw stiffness K_b needed to stabilize hunting at high speed,

without raising the lateral stiffness K_c excessively.

The numerical examples in this chapter are based on parameters for an "example vehicle", which differ from those for the "baseline vehicle" tabulated in Table 3-5 only in the value of B_b. K_c and B_c retain their baseline values,

$$K_c = 4.834 \times 10^4 \text{ slug/sec}^2, \text{ and} \qquad (8.1.7)$$

$$B_c = 6.714 \times 10^3 \text{ slug/sec} . \qquad (8.1.8)$$

It is further assumed that

$$\ell_k = \ell_b = kh = 49.213 \text{ inches} \ldots \qquad (8.1.9)$$

i.e., that springs and dampers are located over the wheels. The latter demands that B_b for the example vehicle cannot be zero as before, but rather has a lower bound (from the damping analog of Equation 8.1.5) of

$$B_b = B_c(kh)^2 = 1.626 \times 10^7 \text{ slug-in}^2/\text{sec}, \qquad (8.1.10)$$

which value will be used for the example vehicle. By contrast, K_b for the baseline vehicle is greater than $K_c(kh)^2$, and it may be obtained through the use of an auxiliary torsional spring K_{b0}:

$$K_b = 4.196 \times 10^8 \text{ slug-in}^2/\text{sec}^2, \text{ and} \qquad (8.1.11)$$

$$K_b = K_{b0} + K_c(kh)^2 , \qquad (8.1.5)$$

requiring that

$$K_{b0} = 3.025 \times 10^8 \text{ slug-in}^2/\text{sec}^2 . \qquad (8.1.12)$$

The higher value of B_b in the example vehicle results in a slightly

reduced critical speed relative to the baseline vehicle (292 ft/sec versus 294 ft/sec), but is required in order to demonstrate the effects of damper asymmetry.

2. Notation. After all other parameters are specified, it remains only to fix σ_k and σ_b. The degree of asymmetry in the suspension will be denoted by the list

$$\kappa = (\sigma_k, \sigma_b) \quad . \tag{8.2.1}$$

The symmetric (or conventional) secondary is thus denoted by $\kappa=(1,1)$.

3. Stability. The action of the asymmetric suspension is similar to that of the steering controller described in Chapter 7: lateral error produces a torque which, by virtue of forward motion and creep forces, steers the truck nearer the carbody. The asymmetric configuration has also a complementary mechanism whereby truck yaw generates lateral force. The contribution of asymmetry, like that of the relative-steering controller, is significant only at relatively high frequencies where the carbody undergoes little lateral motion.

Figure 8-1 is a plot of stability boundaries of the example vehicle, D_1 (or σ_k) versus V for several σ_b's. Any D_1 in excess of that corresponding to $\sigma_k=0$ cannot be achieved passively. The figure shows that asymmetry can extend V_c well beyond the 200 mph of the conventional suspension. For $\kappa=(.25,.5)$, for example, the system is stable from 0 to 300 mph.

The regions of instability in Figure 8-1 correspond to secondary

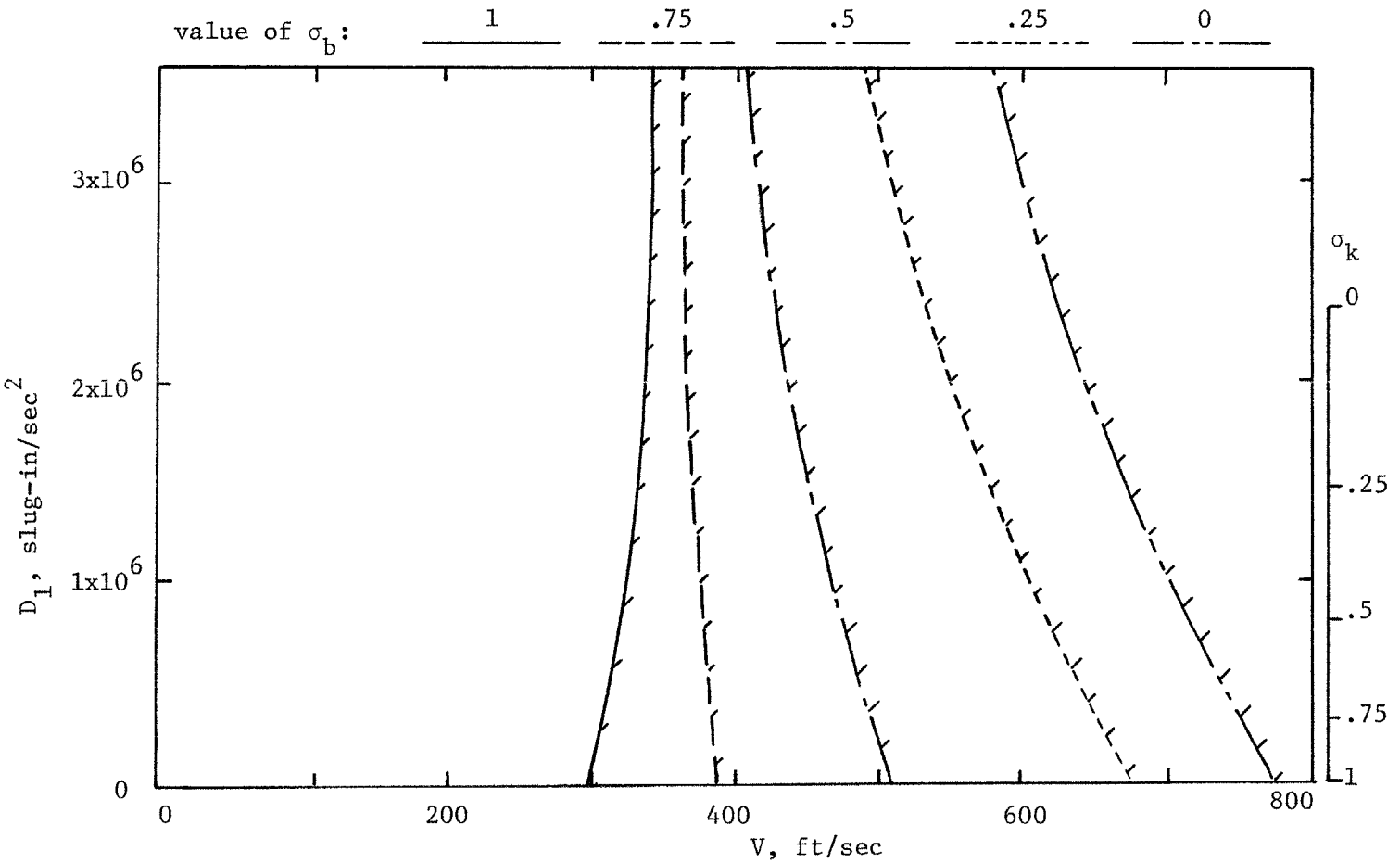

FIGURE 8-1

Stability Boundaries for RC-LMO Model with Passive-Asymmetric Suspension. (Example Vehicle Parameters). Shading Indicates Unstable Regions.

or truck hunting. Two other modes of instability resulting from asymmetric secondary suspensions have been observed in other numerical cases. In vehicles with low yaw stiffness K_b, it is possible for the onset frequency of hunting instability to be lower than the carbody resonance frequency; hunting occurs at low speed and there is little relative motion between truck and carbody. Since the asymmetric secondary relies upon relative lateral displacement between the truck and the carbody for its steering action, it is relatively ineffectual in suppressing this type of low-speed instability. Another region of instability may occur when K_{b0} is small or zero and σ_k approaches its limiting value of zero. Under these conditions and at low speeds, their is little resistance to fishtailing motion of the highly asymmetric truck, a motion which can become unstable at frequencies up to the carbody resonance.

4. Ride Quality. Figure 8-2 shows the A.S.D. for the example vehicle at 100 mph, for various degrees of asymmetry in the springs only ($\kappa=(x,1)$). The spectrum is unchanged at low and high frequencies, but the hunting peak is lowered (by as much as 90%) and broadened slightly.

Figure 8-3 is a similar set of spectra for variations of σ_b only ($\kappa=(1,x)$). The low-frequency behavior is unchanged. Reductions in σ_b tend to increase the amplitude of the hunting peak (up to 110%), reduce its frequency, and narrow it. The HFA is increased at out-of-phase frequencies due to coupling from yaw angle to lateral force; this may be seen by considering the high-order, out-of-phase

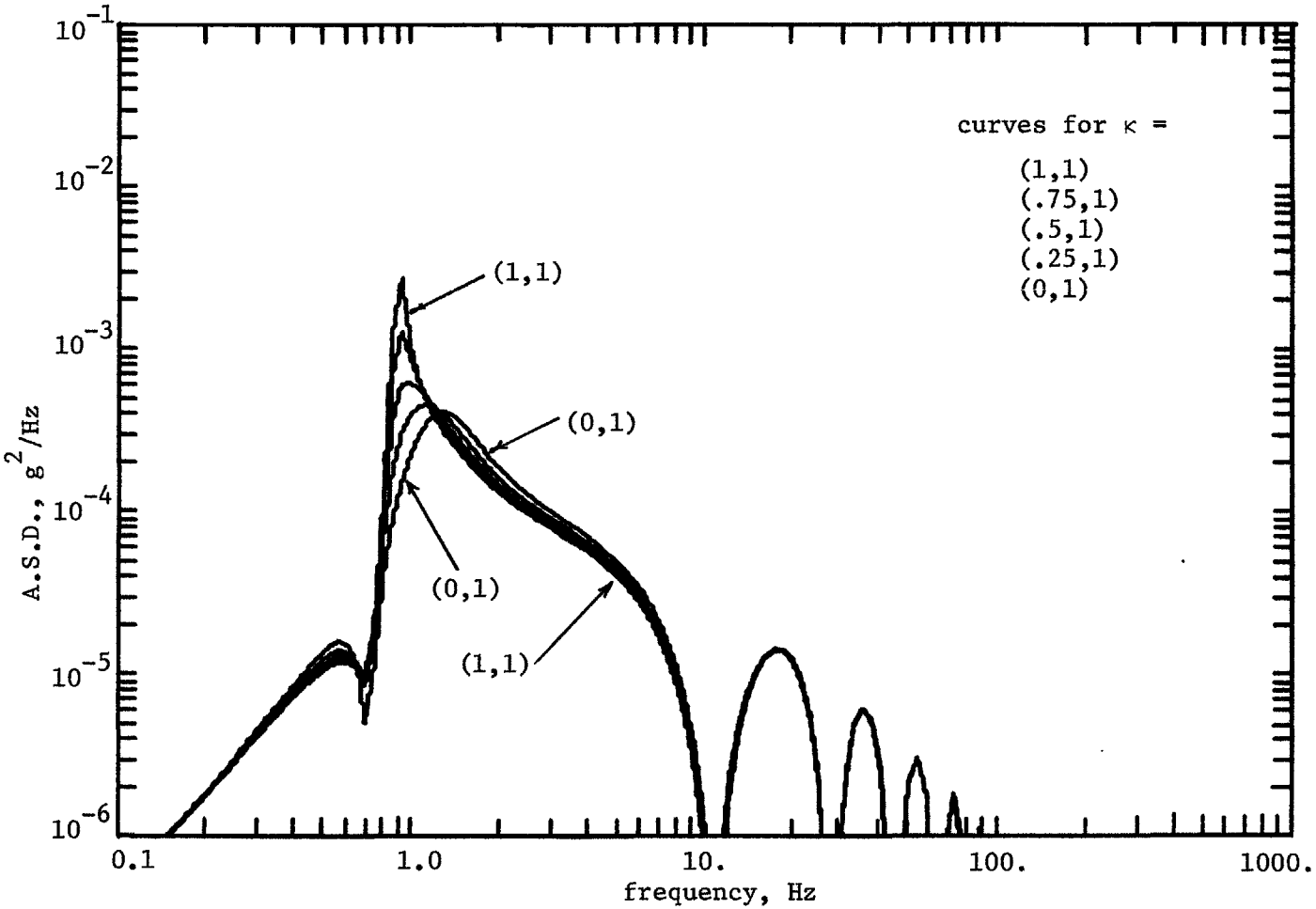

FIGURE 8-2

Effect of Spring Asymmetry at 100 mph. (RC-LMO, Example Vehicle).

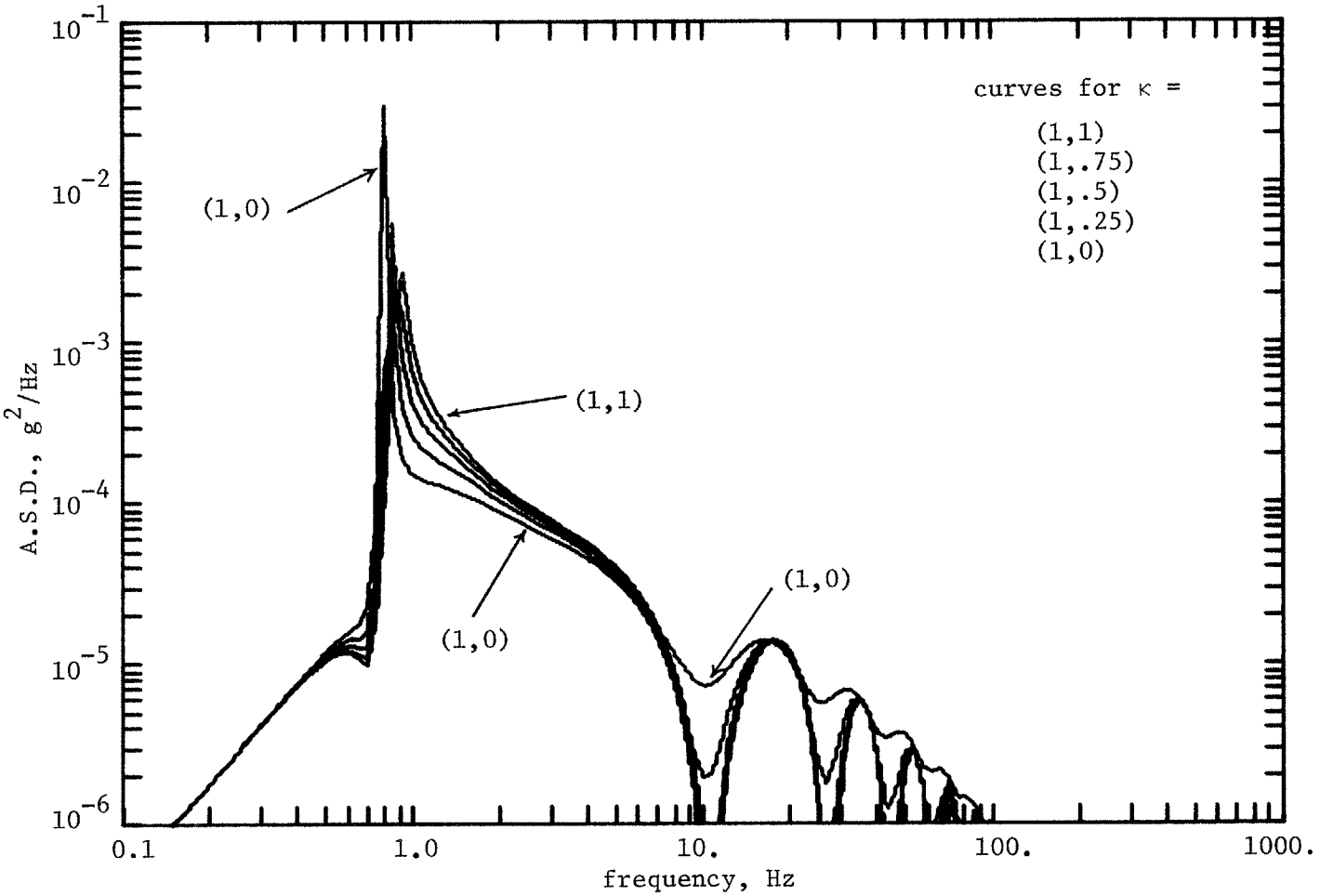

FIGURE 8-3

Effect of Damper Asymmetry at 100 mph. (RC-LMO, Example Vehicle).

numerator coefficient which for the asymmetric secondary is

$$b_{m4} = \frac{4f\rho_m khB_c \ell_b}{m_b I_b V} \left(\frac{1-\sigma_b}{1+\sigma_b} \right) \quad . \tag{8.4.1}$$

This out-of-phase contribution will exceed the in-phase HFE if

$$\frac{m_b kh\ell_b (1-\sigma_b)}{I_b (1+\sigma_b)} \quad > \quad 1 \quad . \tag{8.4.2}$$

Figure 8-4 shows the variation of A.S.D. with speed for κ=(.25,.5). It demonstrates that the asymmetric suspension is effective only when the hunting kinematic frequency is high relative to the carbody resonance frequency. At 50 mph, ω_k is about 0.5 Hz for the example vehicle, or half the carbody resonance; accordingly, the A.S.D. curve at 50 mph is almost identical to that for the conventional suspension. The curves for 100 and 150 mph and the asymmetric suspension, on the other hand, represent major improvements.

5. Tracking Error. RMS tracking error for the example vehicle is plotted against V in Figure 8-5. Again, asymmetry has little effect at low speeds, but reduces error significantly at higher V. There is the expected rise in the vicinity of 100 mph where carbody resonance is excited.

6. Overview. The passive-asymmetric secondary suspension has been found to be helpful in extending the stable speed range of an otherwise conventional rigid truck with given K_b, K_c, B_b, and B_c. It

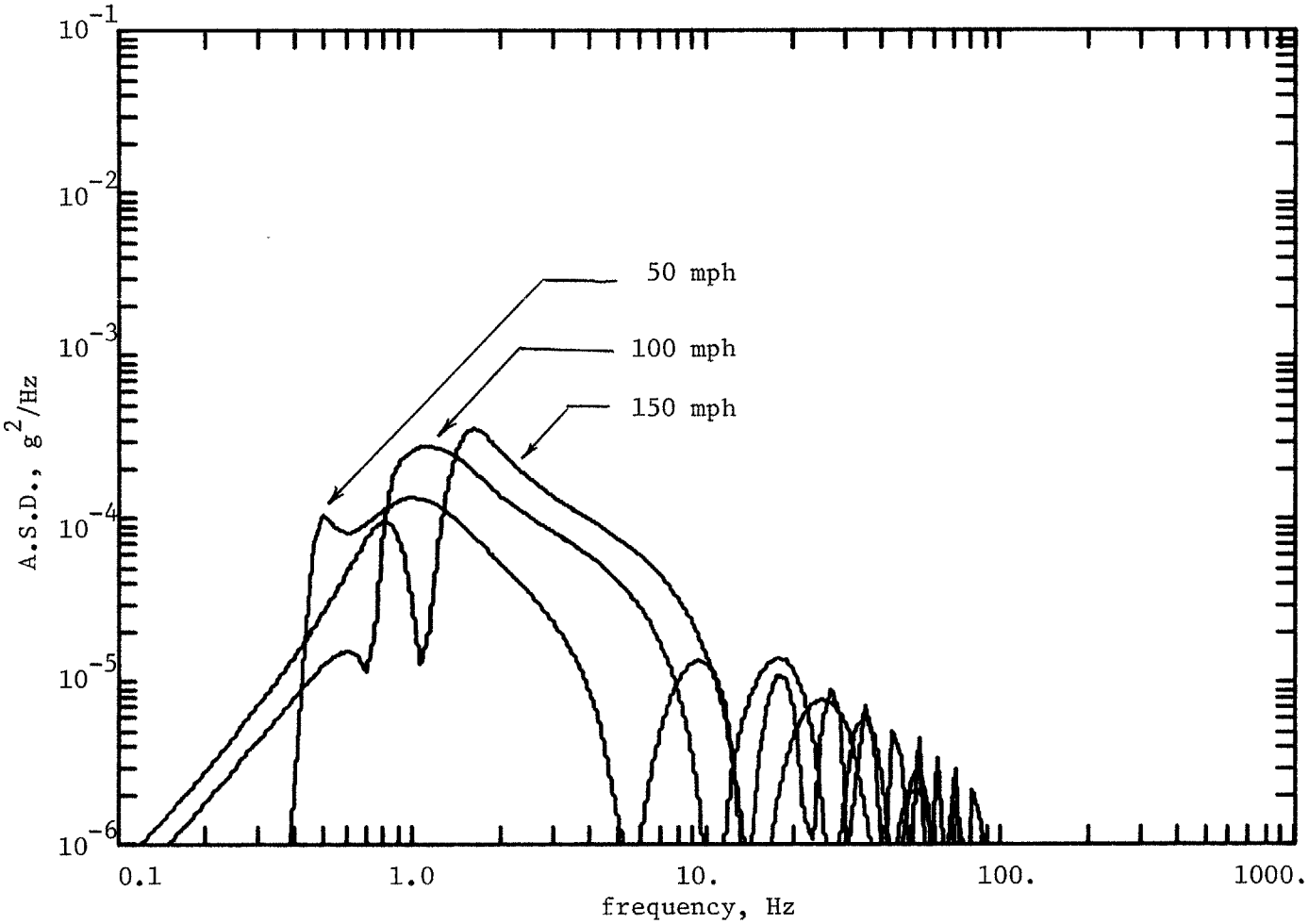

FIGURE 8-4

A.S.D. Variation with Speed, Passive-Asymmetric Secondary.
(RC-LMO, Example Vehicle, κ=(.25,.5)).

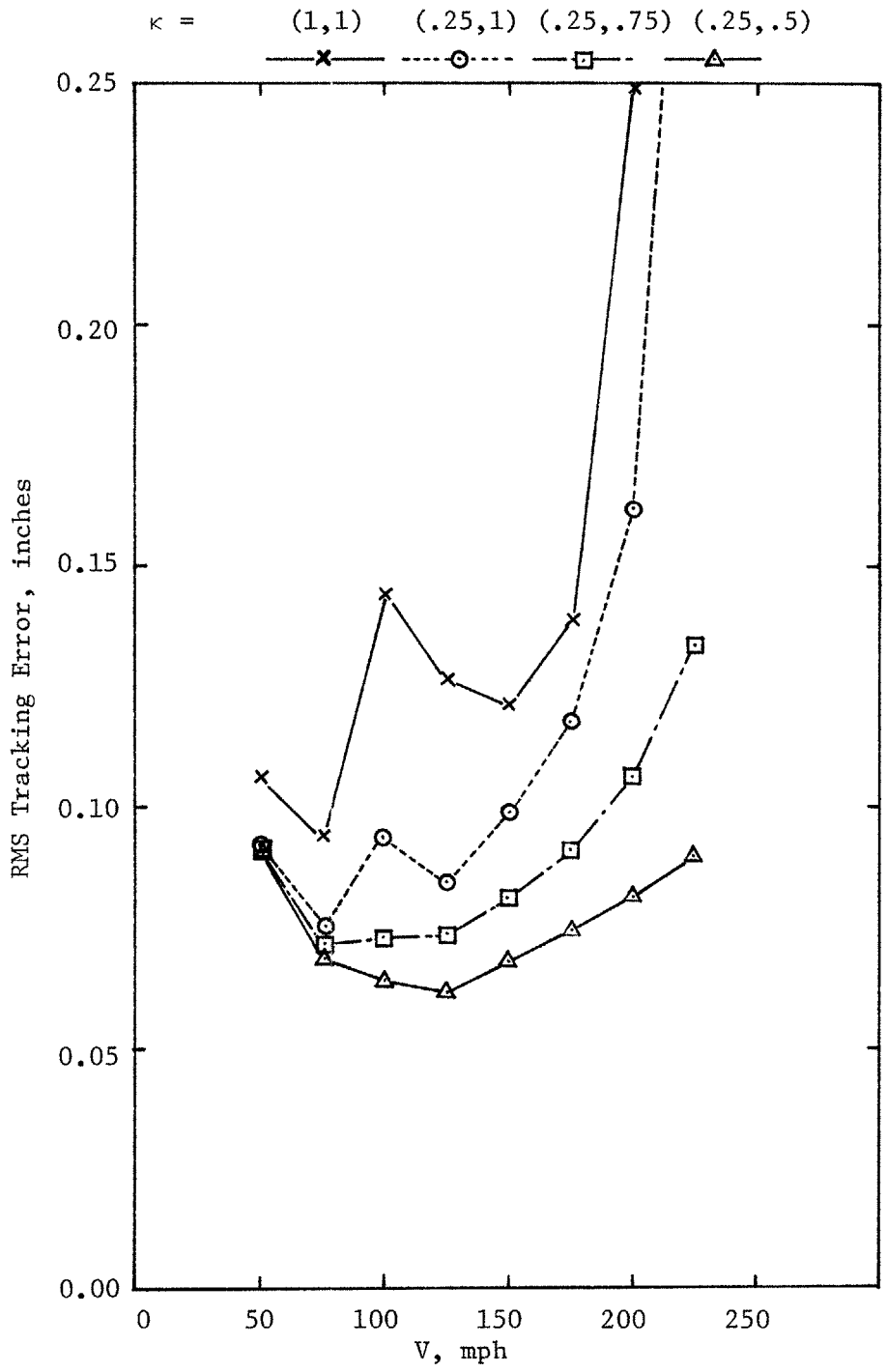

FIGURE 8-5

RMS Tracking Error versus Speed, RC-LMO, Passive-Asymmetric. (Example Vehicle).

allows for less flexibility in design than does an active controller, but has the advantage of requiring no control power. The stability at low speeds is determined mostly by yaw stiffness K_b, which should therefore be kept reasonably high. As speed increases, however, the asymmetry becomes important and permits faster operation than could be obtained from a symmetric suspension with comparable parameter values.

CHAPTER 9

PERFORMANCE OF VEHICLES USING RIGID - PLANE - BODY CARBODY MODEL

The Lateral - Mass - Only (LMO) carbody with a single truck attached has been used in previous chapters to approximate the dynamics of a complete rail vehicle. The approximation will be examined in this chapter by comparison with a considerably more complex model: the Rigid - Plane - Body (RPB) carbody with two trucks. Significant differences between the two models are noted, but the LMO model is shown to be a useful one from which to draw conclusions about the effects of proposed changes in suspension design. Certain general points concerning the influence of carbody length and inertia on stability and ride quality will also be demonstrated.

1. Response of a Symmetric Plane Body. The RPB carbody model, as defined in §3.3, is free to yaw and translate laterally, but cannot roll, pitch, heave, or deviate from a constant longitudinal speed V. The body is further assumed to be symmetric about its center of mass, and to be acted upon only at the truck attachment points. Such a carbody is illustrated in Figure 9-1, with forces and torques (F_{b1}, F_{b2}, T_{b1}, and T_{b2}) following the convention of §3.3.

Dynamic equations of motion for the RPB complete vehicle were derived in Chapter 3, and shown to be twelfth order, as compared with sixth order for the equivalent LMO vehicle. It is apparent that the

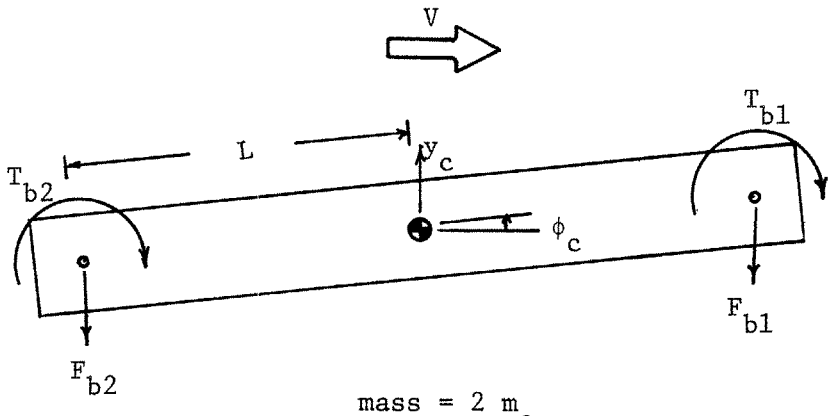

mass = 2 m_c

moment of inertia = I_c

FIGURE 9-1

Rigid Plane Body: Geometry and Interactions

use of the RPB model to improve accuracy results in a system which is much more difficult to analyze than was the LMO vehicle. The RPB model introduces two new sources of complexity not present in the LMO model. First, there are two trucks present, rather than one. Second, the carbody possesses a new degree of freedom -- yaw -- by which the trucks may be coupled. Such interaction of the two trucks has an impact on vibration transmitted to the passenger compartment, and may cause additional modes of instability or resonance.

The RPB model gives results identical to those obtained from the LMO model (1) directly over the trucks, when front and rear are decoupled, and (2) all along the carbody, when $\phi_c \equiv 0$ and the front and rear trucks move in phase with one another. The former situation holds in the limit as $L \to \infty$ and $I_c \to 2m_c L^2$ (mass concentrated over truck attachment points). In this case the car may be conceptually broken into two independent LMO systems. The second situation in which the correspondence is exact occurs when the rail inputs at the front and rear trucks are in phase and the secondary suspension torques (T_{b1} and T_{b2}) are zero. Under these conditions, the symmetry of the vehicle results in the carbody moving in pure translation, with $\phi_c = 0$. The requirement that T_{b1} and T_{b2} be zero would be met if all passive and active secondary restraint in the yaw direction were removed. Although there normally is some yaw restraint, yaw becomes insignificant relative to translation at high frequencies, causing the LMO approximation to be nearly exact at high frequencies which also correspond to

in-phase front and rear inputs.

The effect of carbody yaw on vibration transmission may be understood by writing the governing equations for the system in Figure 9-1:

$$2\, m_c\, \ddot{y}_c = -F_{b1} - F_{b2} \qquad (9.1.1)$$

$$I_c\, \ddot{\phi}_c = -T_{b1} - T_{b2} - F_{b1}L - F_{b2}L \quad . \qquad (9.1.2)$$

If a position along the length of the carbody measured from the center of mass is designated by $\rho_\ell L$ (ρ_ℓ=+1 for the front, ρ_ℓ=-1 for the rear attachment point), the net lateral acceleration at that position is

$$\ddot{y} = \ddot{y}_c + L\ddot{\phi}_c \quad . \qquad (9.1.3)$$

Therefore,

$$\ddot{y} = \frac{-(F_{b1}+F_{b2})}{2m_c} - \frac{(F_{b1}-F_{b2})\rho_\ell L^2}{I_c} - \frac{(T_{b1}+T_{b2})\rho_\ell L}{I_c} \quad . \qquad (9.1.4)$$

T_{b1} and T_{b2} are often small compared with $F_{bi}L$, particularly at high frequencies, and will be omitted in the following.

It is useful to normalize carbody inertia thus:

$$\bar{I}_c = I_c / (2m_c L^2). \qquad (9.1.5)$$

$\bar{I}_c$=1 corresponds to the carbody mass being concentrated directly over the trucks ("dumbell" carbody); $\bar{I}_c$=1/3 corresponds to the mass being uniformly distributed along the length 2L ("uniform rod" carbody). With this definition,

$$\ddot{y} = -\frac{1}{2m_c}\left[F_{b1}\left(1 + \frac{\rho_\ell}{\bar{I}_c}\right) + F_{b2}\left(1 - \frac{\rho_\ell}{\bar{I}_c}\right) \right] \quad . \qquad (9.1.6)$$

If F_{b1} and F_{b2} are sinusoidal at the same frequency and the same amplitude F_0, the acceleration response amplitude is bounded by the following limits:

$$\underline{\text{in-phase}}: \quad F_{b1}=F_{b2}=F_0,$$
$$\ddot{y} = -F_0/m_c \quad , \text{ for any } \rho_\ell; \qquad (9.1.7)$$

$$\underline{\text{out-of-phase}}: \quad F_{b1}=-F_{b2}=F_0,$$
$$\ddot{y} = (-F_0/m_c)\cdot(\rho_\ell/\bar{I}_c) \quad . \qquad (9.1.8)$$

The RPB carbody with negligible yaw restraint behaves like the LMO model for in-phase inputs, with constant acceleration (pure translation) along its length. For out-of-phase inputs, the carbody undergoes pure yaw. At the attachment points, the ratio of out-of-phase to in-phase acceleration amplitude is $(1/\bar{I}_c)$; this fact will be reflected in the high-frequency behavior of acceleration spectral density curves for RPB configurations for which $\bar{I}_c \neq 1$.

Carbody yaw has little effect on true secondary hunting instability, since by definition secondary hunting involves little motion of the carbody. The additional yaw degree of freedom can, however, have a significant role in primary hunting instability, which is due to carbody resonance. The natural frequencies of lateral and yaw carbody oscillations may be estimated by assuming the trucks to be fixed. Then,

$$\omega_{lat} = \sqrt{K_c/m_c} \quad , \text{ and} \tag{9.1.9}$$

$$\omega_{yaw} = \sqrt{(2K_cL^2+2K_b)/I_c}$$
$$= \sqrt{[K_c+(K_b/L^2)]/[m_c\bar{I}_c]} \quad . \tag{9.1.10}$$

Primary hunting is a potential source of instability when the kinematic hunting frequency approaches either of these natural frequencies. If the lateral and yaw frequencies happen to coincide ($\bar{I}_c$=1 and $K_b/L^2 << K_c$), primary hunting is especially difficult to avert; measures taken to suppress translational-mode hunting (e.g., increasing yaw stiffness, K_b) can aggravate yaw-mode hunting or "fishtailing".

For the baseline vehicle, $\bar{I}_c$=0.903. Also,

$$K_b/K_cL^2 = .0964 \ ,$$
$$\omega_{lat} = 6.098 \text{ sec}^{-1} \ , \text{ and}$$
$$\omega_{yaw} = 6.719 \text{ sec}^{-1} \ .$$

$\bar{I}_c$ is nearly unity, and the yaw and lateral natural frequencies are relatively close to one another, so primary hunting may be expected to be an important cause of instability for the baseline configuration.

2. Behavior of Conventional Vehicle. The baseline RPB vehicle with rigid conventional (RC) trucks shows a critical speed of 280 ft/sec (191 mph), slightly lower than the 300 ft/sec computed for the LMO carbody in Chapter 4. Eigenvector analysis shows this instability to be of the primary hunting type -- a fishtailing motion with large excursions at the rear of the vehicle only. Such asymmetric response is characteristic of a symmetric vehicle with yaw restraint in the

secondary suspensions.

Figure 9-2 shows the carbody acceleration spectral density (A.S.D.) of the baseline vehicle at 100 mph. Two locations are shown, one at the front (ρ_ℓ=+1) and one at the rear (ρ_ℓ=-1) truck attachment point. Due to the fishtailing motion, acceleration is more severe at the rear of the vehicle in the vicinity of the kinematic hunting frequency; both curves, however, approach common low- and high-frequency asymptotes.

In Figure 9-3, the curve for the rear A.S.D. is repeated for comparison with the LMO approximation to the same vehicle. RPB and LMO models show the same low-frequency asymptote. The RPB model shows a much higher hunting peak than does the LMO, due to yaw coupling. The high-frequency portions of the two models lie close to each other. Ripples of amplitude $(1/\overline{I}_c^{\,2})$=1.23 on the RPB curve exceed the in-phase (LMO) limit due to the vibration transmissibility effect discussed above; their close spacing corresponds to the long delay time τ_L.

Figure 9-4 is similar to Figure 9-3, except that $\overline{I}_c$ has been changed from 0.903 to 1/3 to illustrate the effect of carbody inertia on ride quality. In this case the high-frequency ripples due to out-of-phase inputs exceed the LMO limit by a factor of 9. Increasing $\overline{I}_c$ above 1 would cause the out-of-phase A.S.D. limit to fall below the LMO limit, but doing this would not seem to improve ride quality significantly.

The LMO approximation is most accurate when $\overline{I}_c \approx 1$. Since the

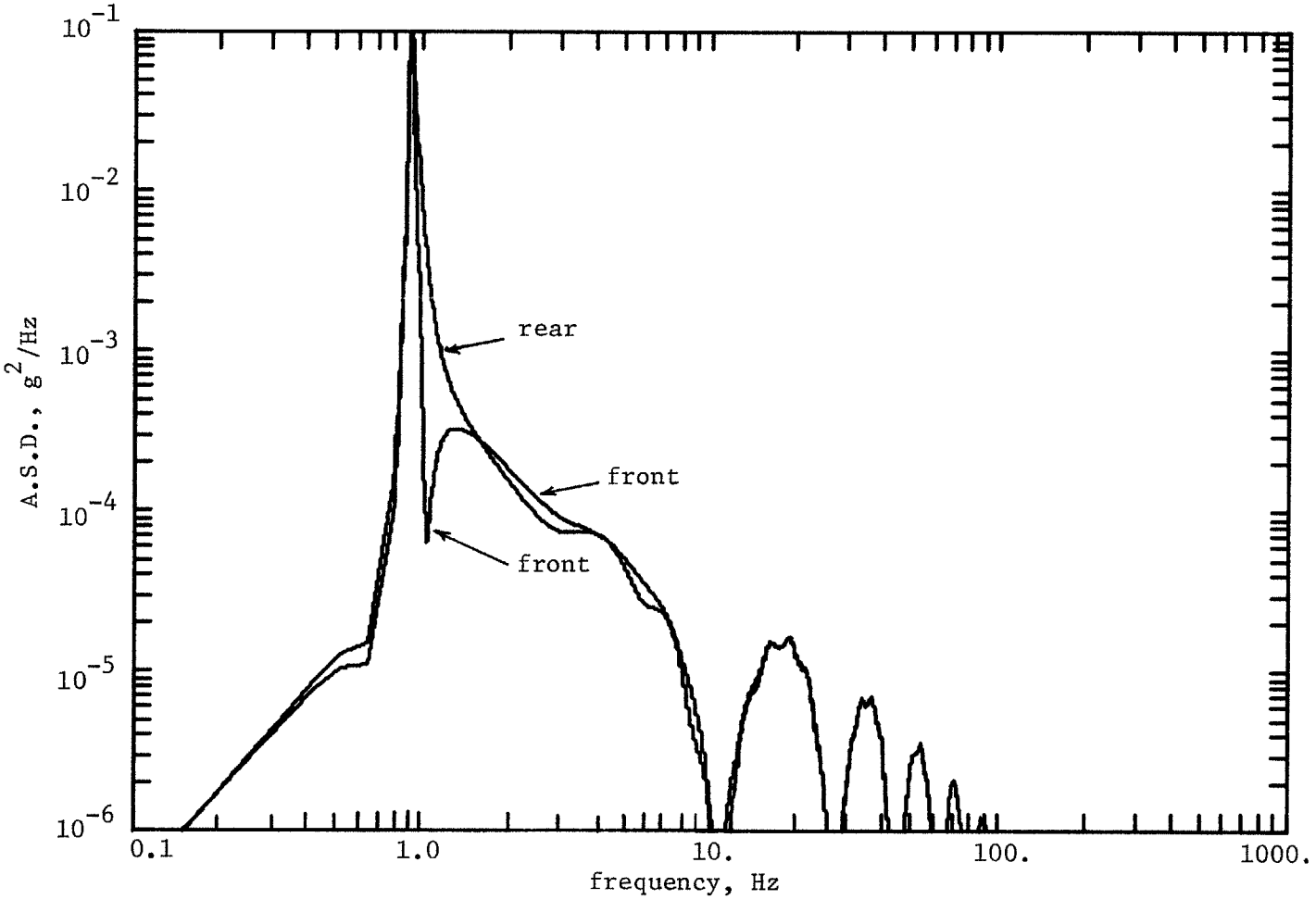

FIGURE 9-2

Acceleration Spectral Density at Front and Rear of Baseline RC-RPB Vehicle
(100 mph)

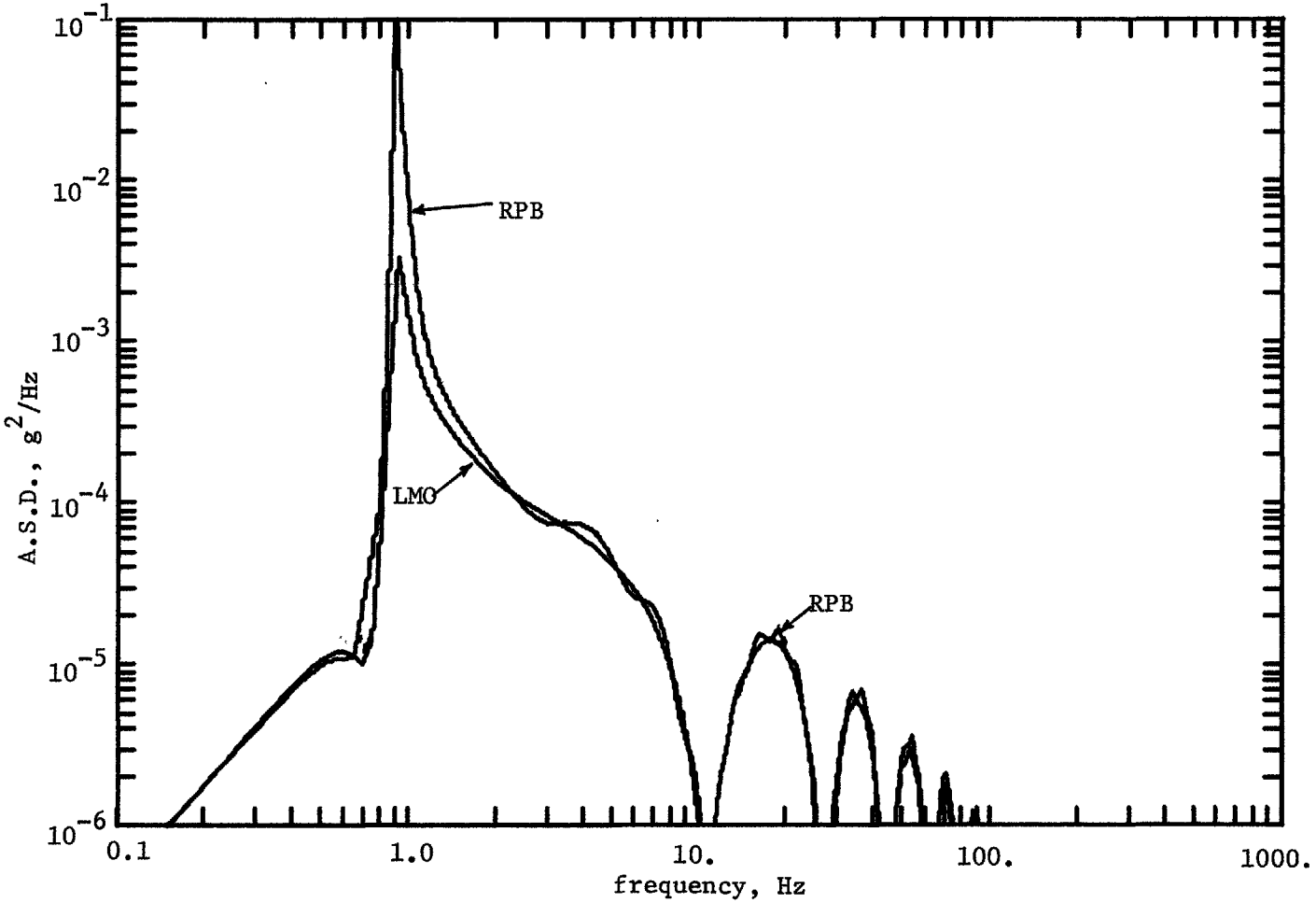

FIGURE 9-3

Comparison of A.S.D. using RPB and LMO Carbody Models (Rear)
(Baseline Vehicle, 100 mph)

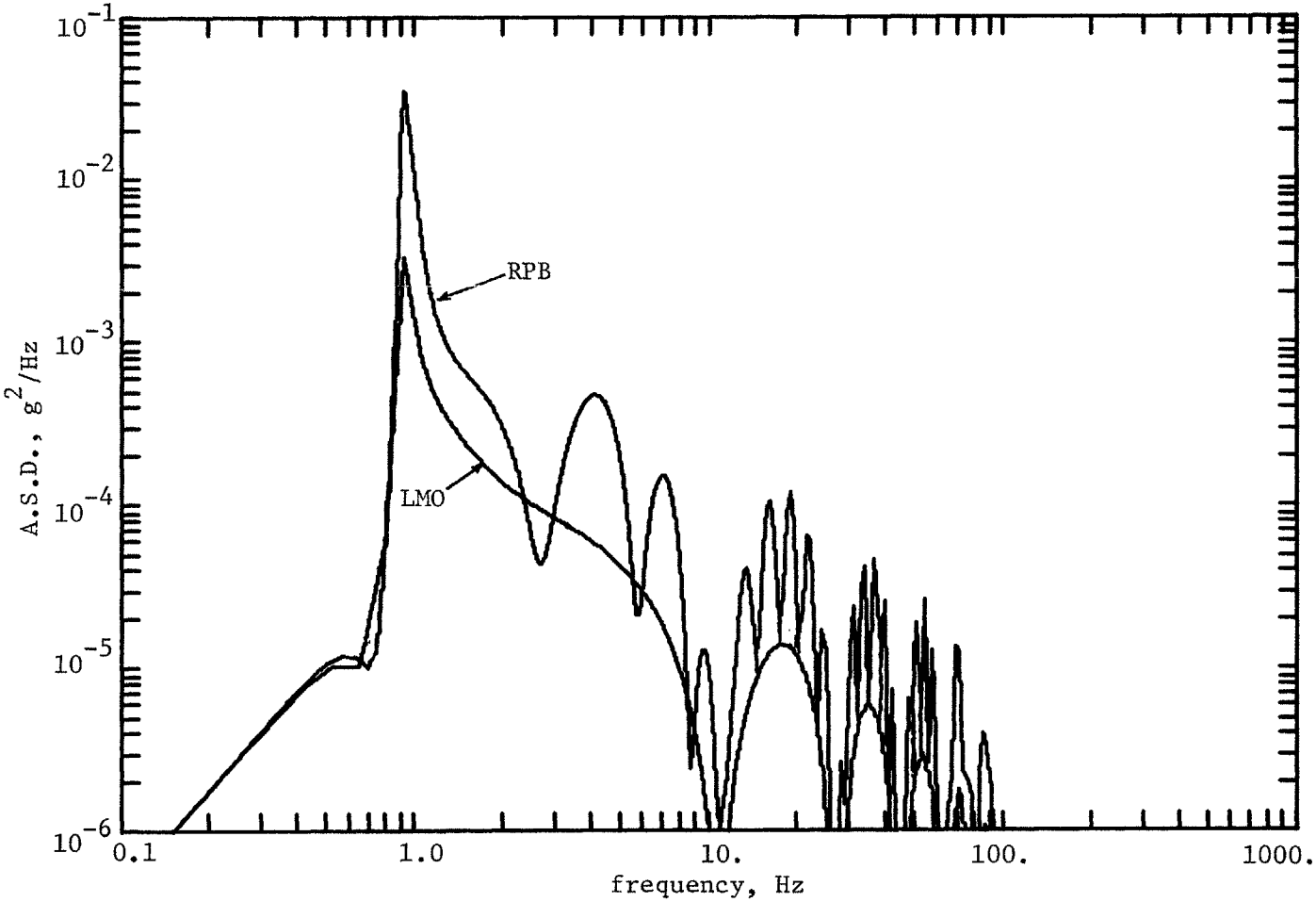

FIGURE 9-4

Effect of Carbody Inertia on A.S.D. using RC-RPB Model

(Baseline Vehicle Except $\overline{I}_c$=1/3, Rear, 100 mph)

amplitude and spacing of the high-frequency ripples may be easily predicted from first principles, however, it is a useful indicator of ride quality whenever front-to-rear yaw coupling is small.

3. Behavior of Vehicle with Independently-Rotating Wheels. The RPB vehicle with rigid independently-rotating-wheel (RIW) trucks is, like the RIW-LMO vehicle, stable for all speeds for any choice of parameter values considered (see Chapter 5). The A.S.D. for the rear of the baseline RIW-RPB vehicle at 100 mph is shown in Figure 9-5, along with the comparable RC-RPB curve from Figure 9-2. As for the LMO model, the hunting peak is eliminated but the asymptotes remain unchanged.

The only source of asymmetry in the response of a symmetrical vehicle is the yaw coupling between trucks and carbody. It was shown in Chapter 5 that there is no need for yaw secondary stiffness to stabilize the RIW truck. Figure 9-6 shows the front and rear A.S.D. for the baseline RIW-RPB case at 100 mph with $K_b=B_b=0$; the two curves are identical.

Use of the more complete RPB carbody model confirms the dynamic advantages of independently-rotating wheels. Hunting is eliminated, and with it the possibility of instability. Ride quality is significantly improved by suppression of the kinematic hunting peak. The effect of carbody yaw on vibration transmission at high frequencies is the same as that for the conventional truck discussed in the preceding section.

4. Behavior of Actively Steered RC-RPB Vehicle. In Chapter 7 it was shown that by using the steering, relative-sensing active control

system, major improvements could be made in the stable speed limit and in the ride quality of the RC-LMO vehicle model. Similar improvements are indicated when the RPB carbody model is used, but the interaction of control torque with carbody yaw introduces effects not observed in the LMO case.

Figures 9-7 through 9-9 are loci of stability for varying control gains $\varepsilon(\varepsilon=(\varepsilon_1,\varepsilon_2,\varepsilon_3))$, and may be compared with Figure 7-2, their counterpart for the LMO carbody model. Parameters are for the baseline vehicle ($\bar{I}_c=0.903$) in Figure 9-7; in Figure 9-8, $\bar{I}_c=2/3$; and in Figure 9-9, $\bar{I}_c=1/3$ (uniform rod carbody). The boundaries for all three values of $\bar{I}_c$, and also for the LMO model, are plotted together in Figure 9-10 for easy comparison. At the low values of $\bar{I}_c$, two fundamental regions of instability may be distinguished: a low-ε_1, high-V region which may be identified with translational hunting (primary or secondary); and a high-ε_1 region related to yaw-mode primary hunting. The former region in each case corresponds well to that previously obtained for the LMO approximation. The high-ε_1 region, however, is a new phenomenon which places additional limits on the feedback gains which may be used without causing instability. Notice that as $\bar{I}_c$ increases to unity, the regions tend to merge in a neck between 100 and 200 ft/sec. This can be ascribed to the fact that when $\bar{I}_c\simeq 1$, the lateral and yaw carbody natural frequencies coincide, and equal the kinematic hunting frequency ω_k at $V\simeq 150$ ft/sec.

That the two regions of stability are separated by an unstable region does not necessarily disqualify a control system from further

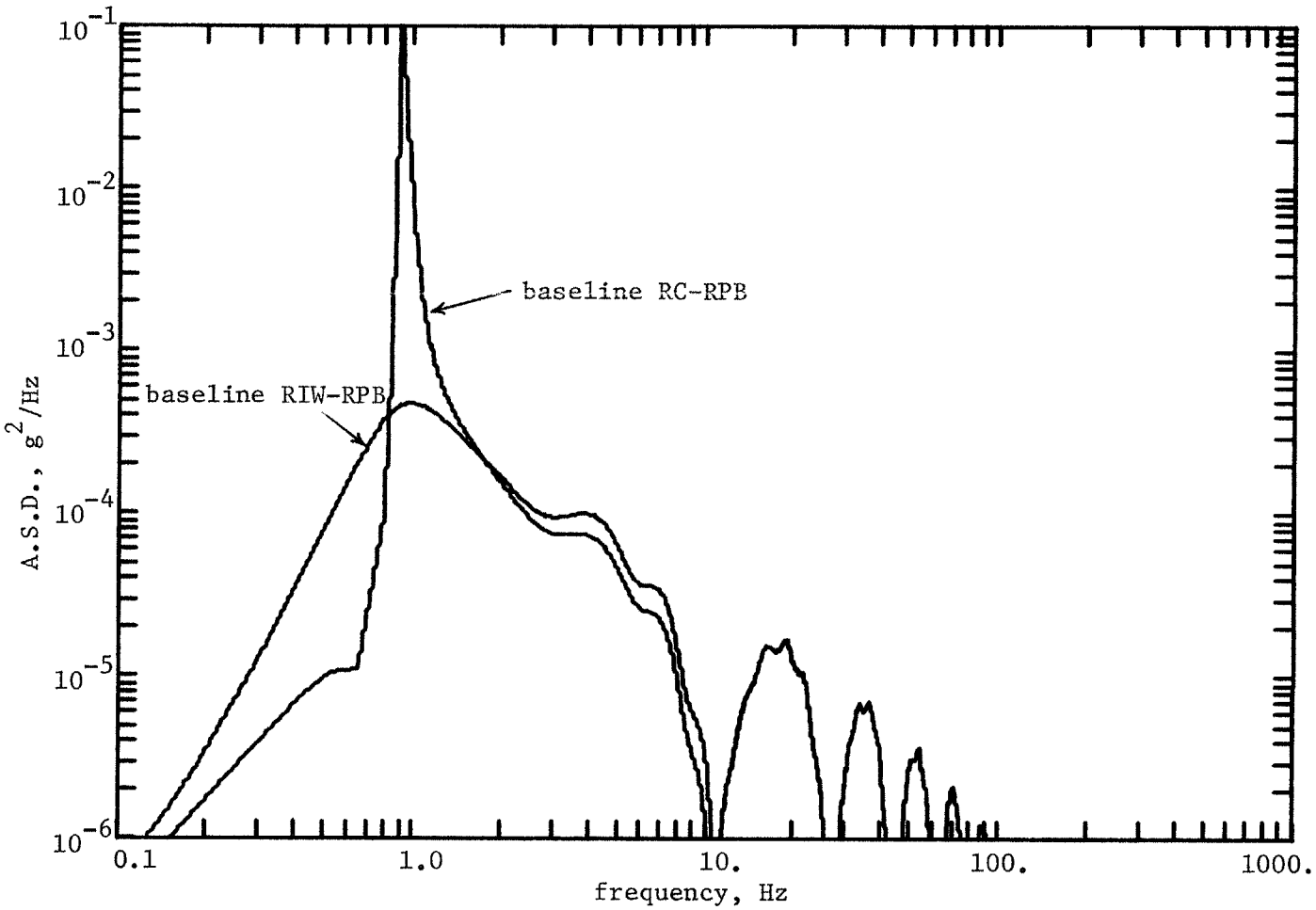

FIGURE 9-5

A.S.D. of Baseline RIW-RPB Vehicle, Compared with Baseline RC-RPB Vehicle (Rear, 100 mph)

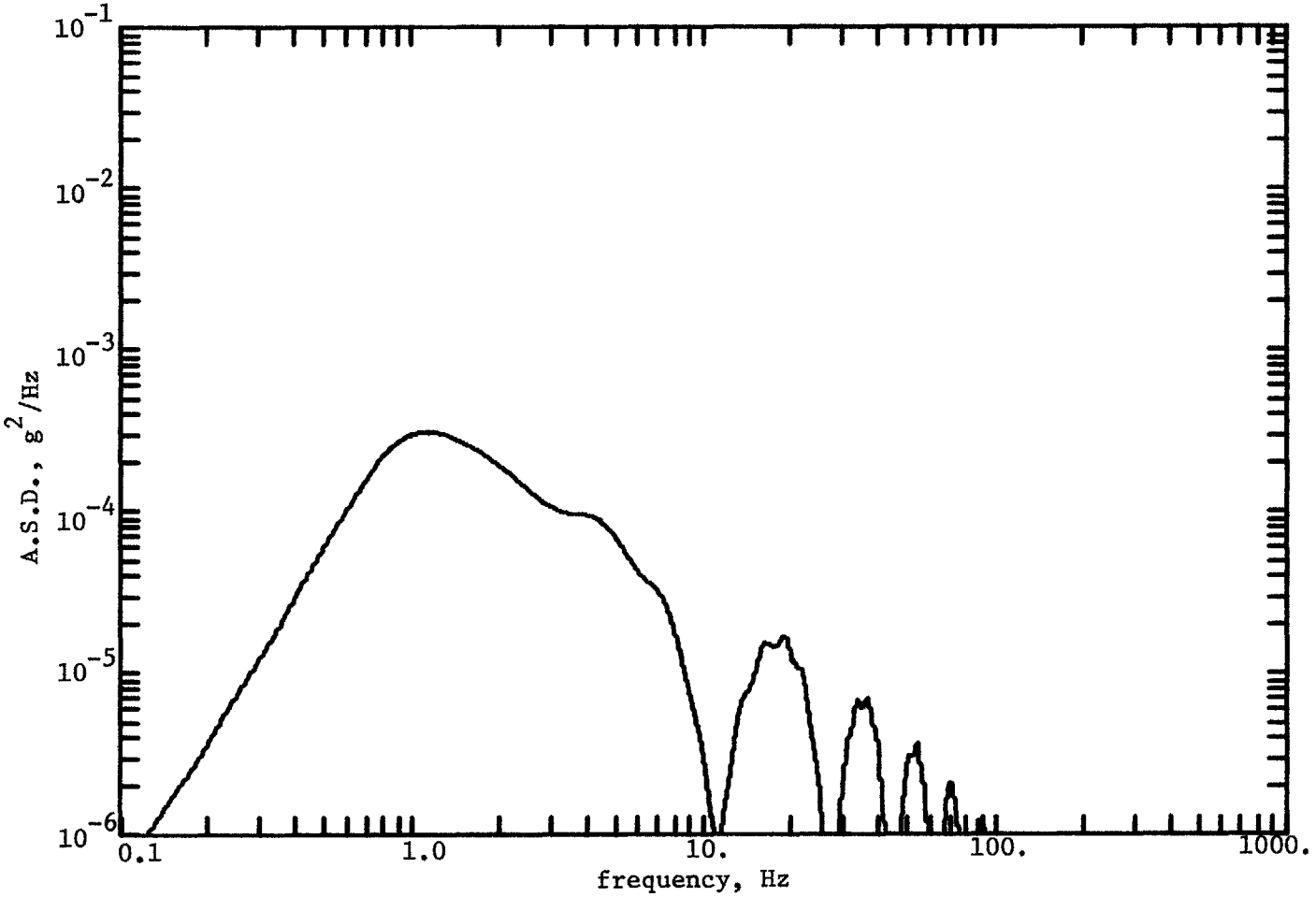

FIGURE 9-6

A.S.D. of RIW-RPB Vehicle with No Yaw Restraint. Front and Rear Identical.
(Baseline RIW, except K_b=0. 100 mph)

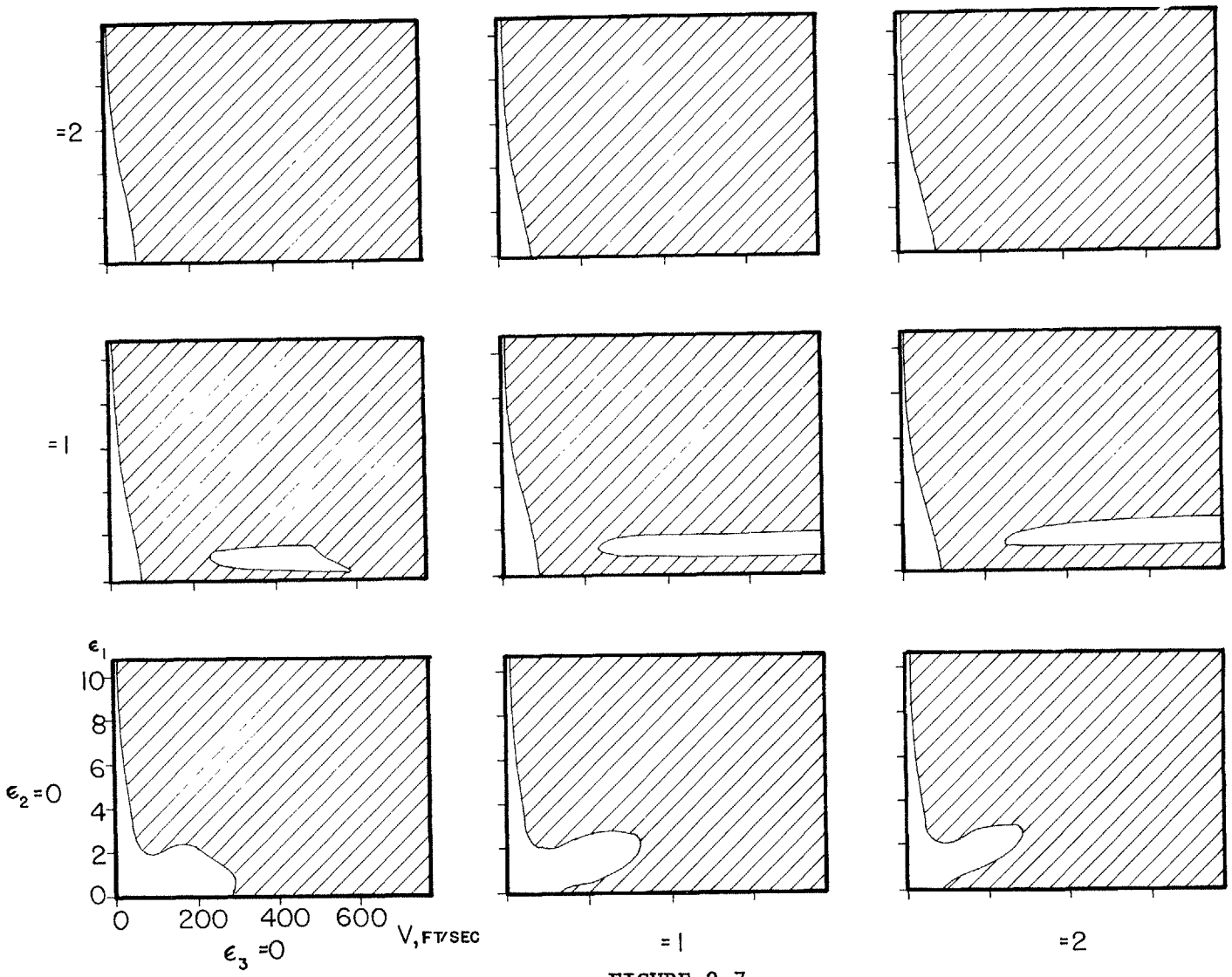

FIGURE 9-7

Stability Planes for RC-RPB Model with Relative-Steering Control (Baseline, $\overline{I}_c$=.903)

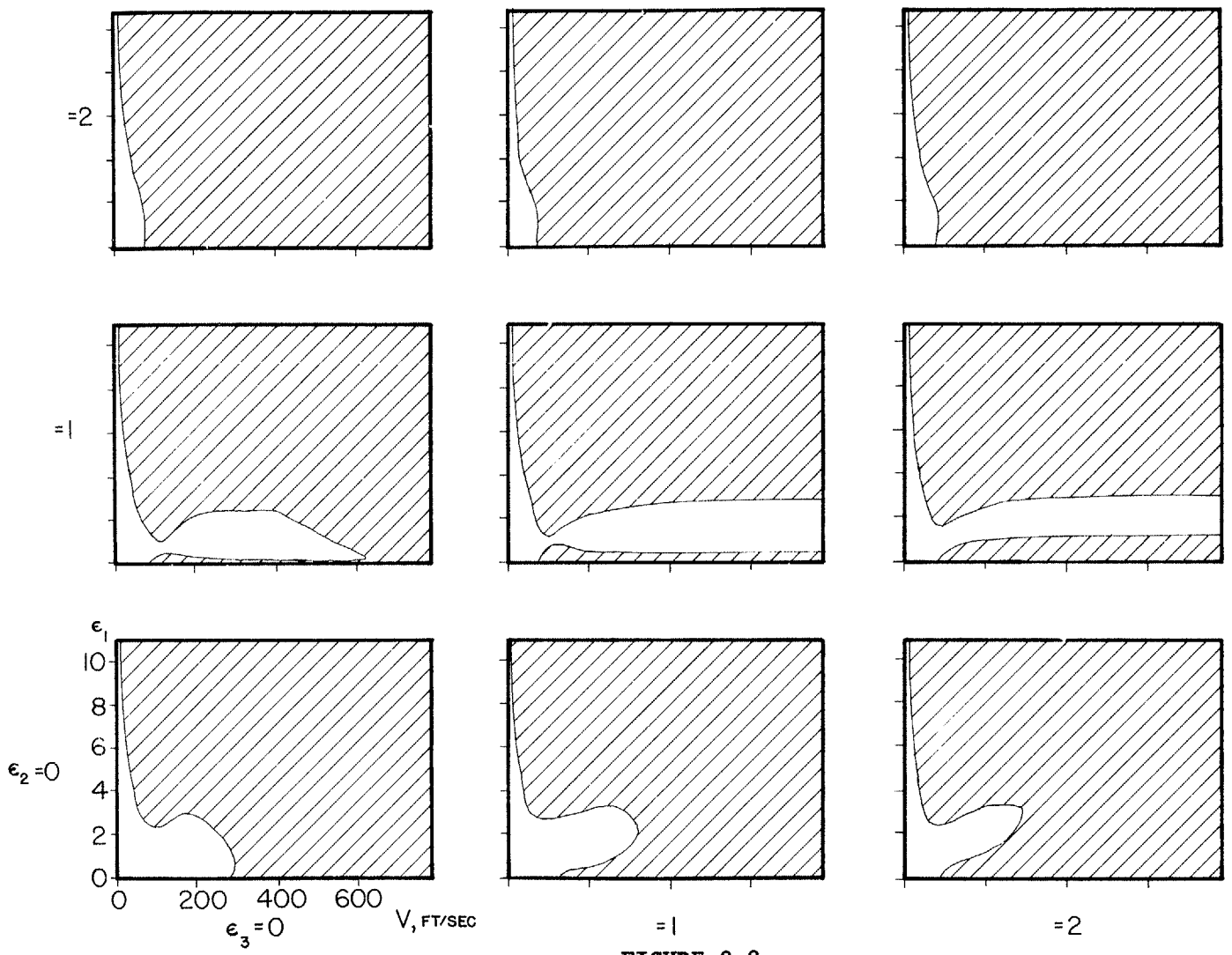

FIGURE 9-8

Stability Planes for RC-RPB Model with Relative-Steering Control (Baseline except $\overline{I}_c$=2/3)

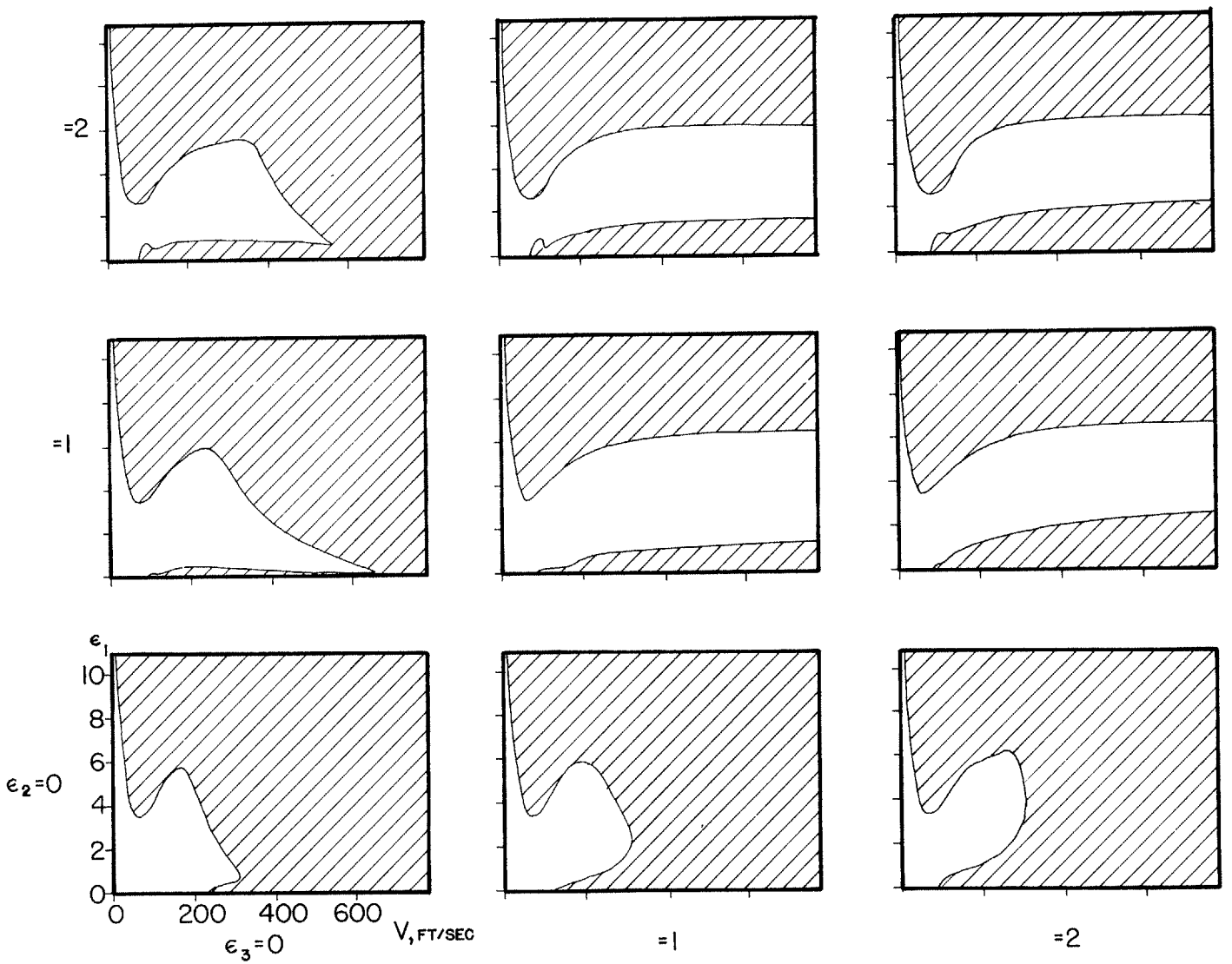

FIGURE 9-9

Stability Planes for RC-RPB Model with Relative-Steering Control (Baseline except $\overline{I}_c$=1/3)

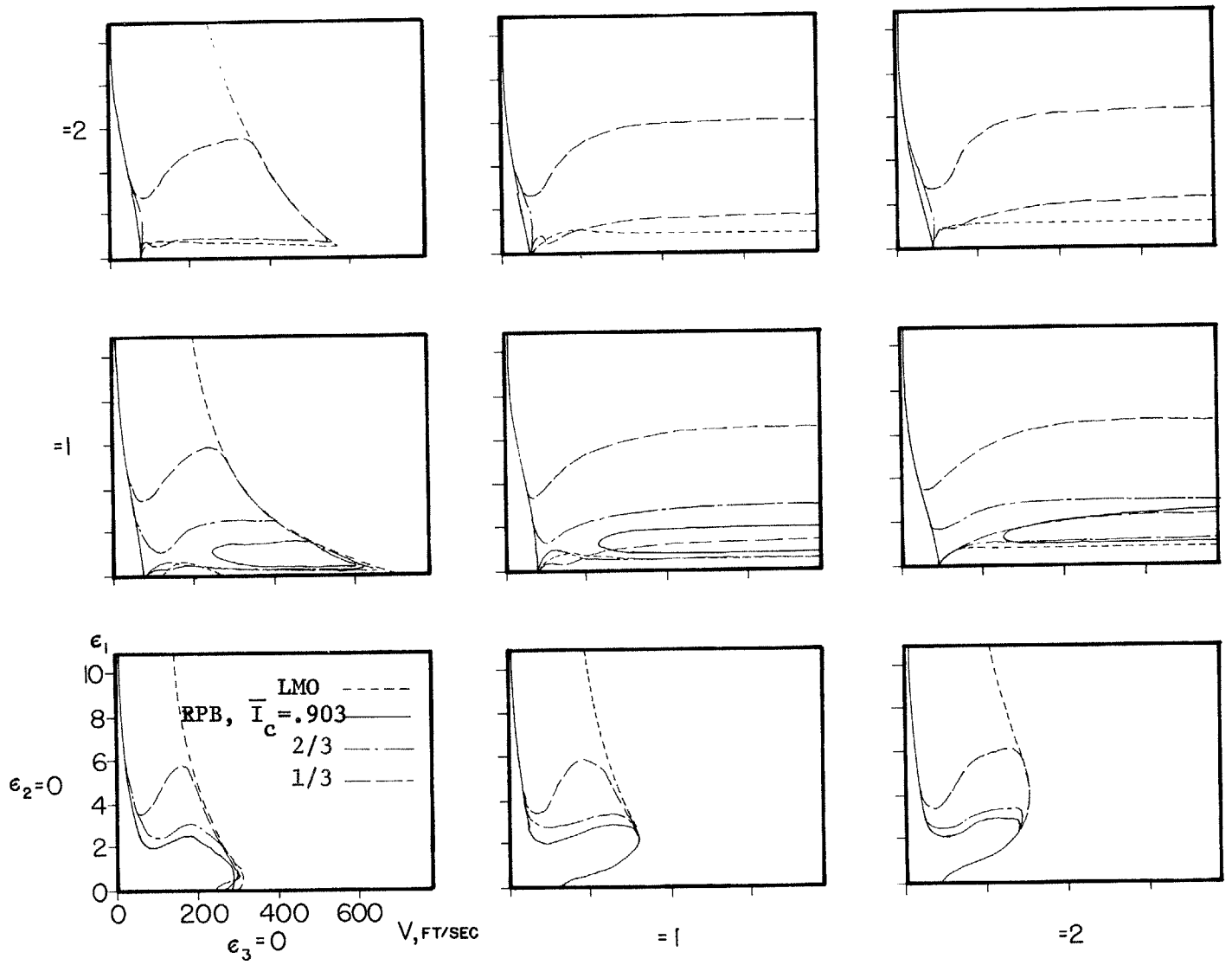

FIGURE 9-10

Stability Boundaries for Models with Relative-Steering Control (Baseline, several $\bar{I}_c$'s)

consideration. An example of such a system would be the $\varepsilon=(1,1,1)$ controller in Figure 9-7. If this system were intended for 400 ft/sec operation, it would need to accelerate through an unstable region between 100 and 250 ft/sec in order to reach that speed. Passing through the region could, however, result in acceptable performance if such passages were infrequent and brief and if the nonlinear behavior following the onset of linear instability were sufficiently mild. Another option available when active control is used is to make the feedback gains speed-dependent. Taking the same example of a 400 ft/sec vehicle, it would be possible to accelerate to 300 ft/sec using the $\varepsilon=(1,0,1)$ controller, and then to switch to $\varepsilon=(1,1,1)$ for the remainder of the acceleration. Instability would thereby be avoided entirely. It should be borne in mind that any of the relative-sensing controllers are useful primarily at high speeds, where carbody motion is small.

The A.S.D. at the rear of the 100 mph baseline vehicle is shown in Figure 9-11, for no control and for steering gain $\varepsilon=(1,0,0)$. Steering control significantly reduces the hunting peak and leaves the asymptotes unchanged. These effects were accurately predicted by the LMO analysis in Chapter 7 (see Figure 7-3). The other example cases from Chapter 7, $\varepsilon=(1,1,0)$ and $\varepsilon=(1,1,1)$, are unstable for the baseline RPB vehicle at 100 mph.

In summary, active steering control is beneficial in controlling oscillations of conventional trucks mounted on the RPB carbody. The stable operating speed limit can be extended, and the ride quality

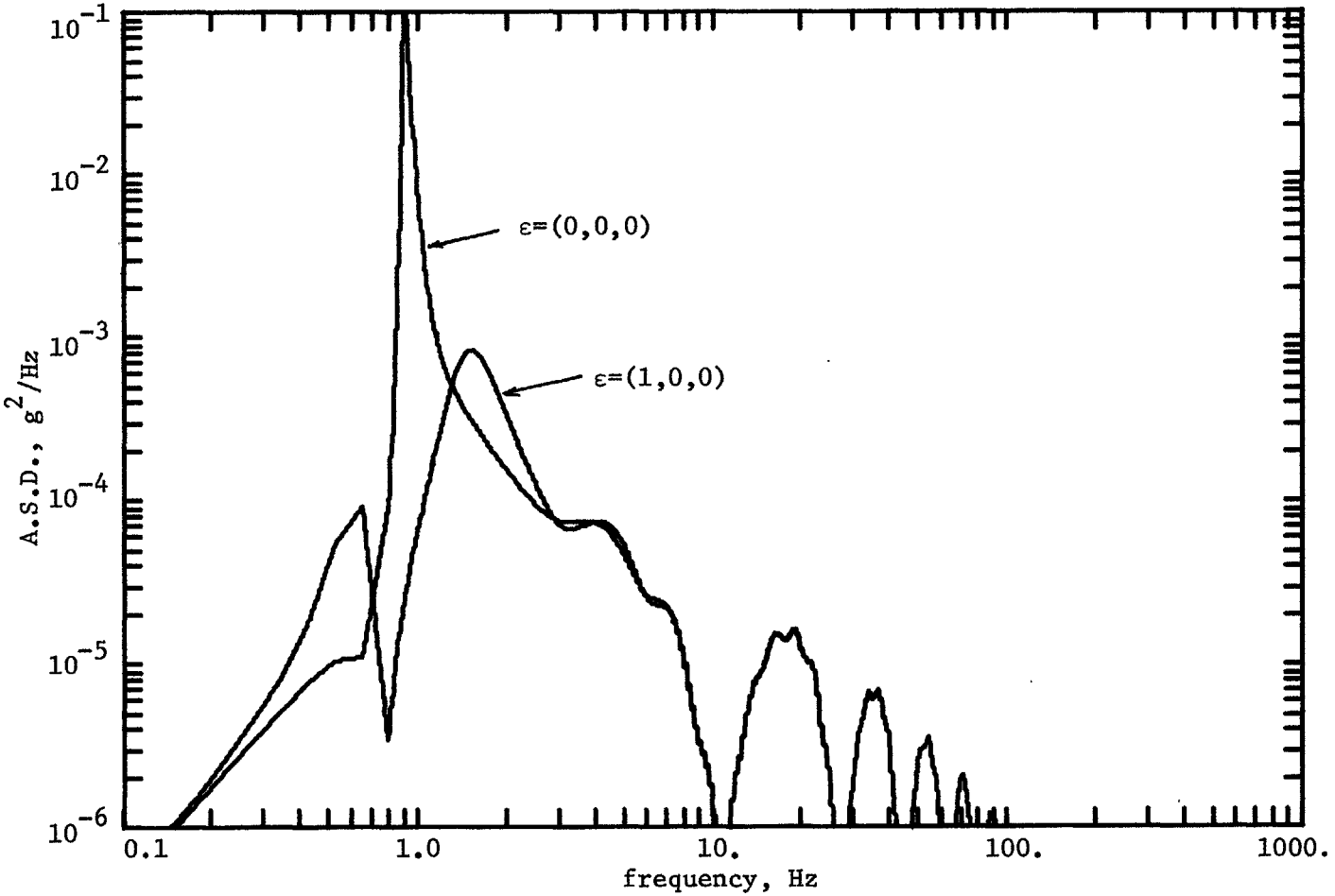

FIGURE 9-11

A.S.D. for RC-RPB Model with Relative-Steering Control (Baseline, Rear, 100 mph)

improved, at only a moderate cost in actuator power. The actuator for this type of controller acts in yaw between the truck and carbody, so that large controller gains which can excite yaw-mode instabilities must be avoided.

5. Behavior of RC-RPB Vehicle with Passive Asymmetric Secondary. The passive-asymmetric secondary suspension, examined in Chapter 8, was conceived as a mechanically simple way to accomplish steering action, and as a result it shares many features with the active relative-steering controller. In particular, yaw freedom of the carbody introduces an additional mode of primary hunting instability. The passive suspension does not have acceleration feedback, however, and is therefore not capable of the "infinite" critical speeds calculated for the active steering controller.

Figure 9-12 shows regions of stability for the example RPB vehicle ($B_b \neq 0$; cf. Figure 8-1) for damper asymmetries σ_b=1, 0.5, and 0. The stability boundaries correspond closely to those in Figure 8-1 for an LMO vehicle, except for an additional unstable region (for σ_k near 1 and V around 150 ft/sec) which corresponds to yaw-mode primary hunting.

Figure 9-13 shows the effect of the asymmetric configuration κ=(.25,.5) on rear A.S.D. of the example vehicle at 100 mph. The asymmetric suspension reduces the hunting peak amplitude to approximately 1% of its former value; the high-frequency asymptote is changed slightly by damper asymmetry.

The passive-asymmetric secondary suspension has been shown to

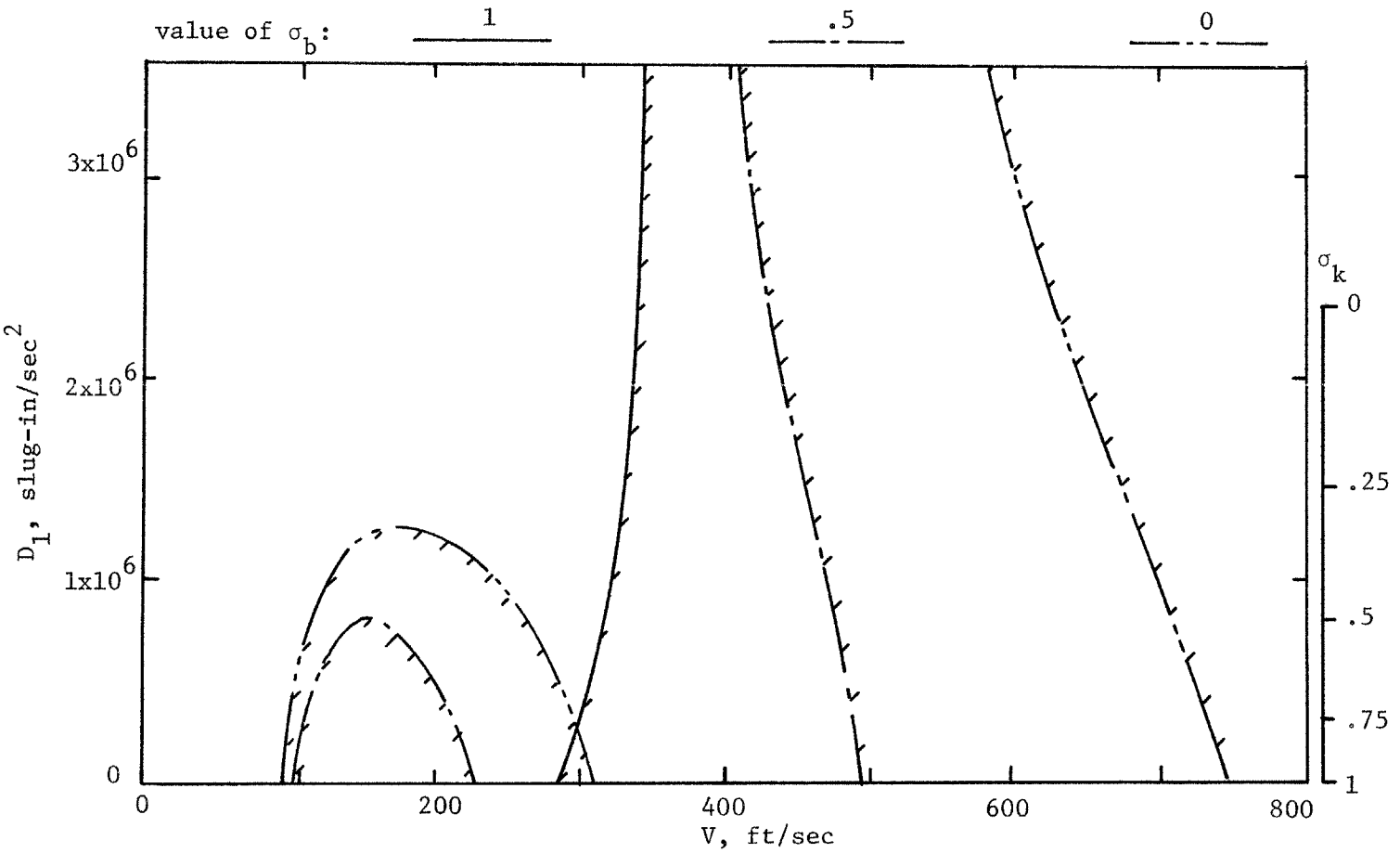

FIGURE 9-12

Stability Boundaries for RC-RPB Model with Passive-Asymmetric Secondary (Baseline Parameters)

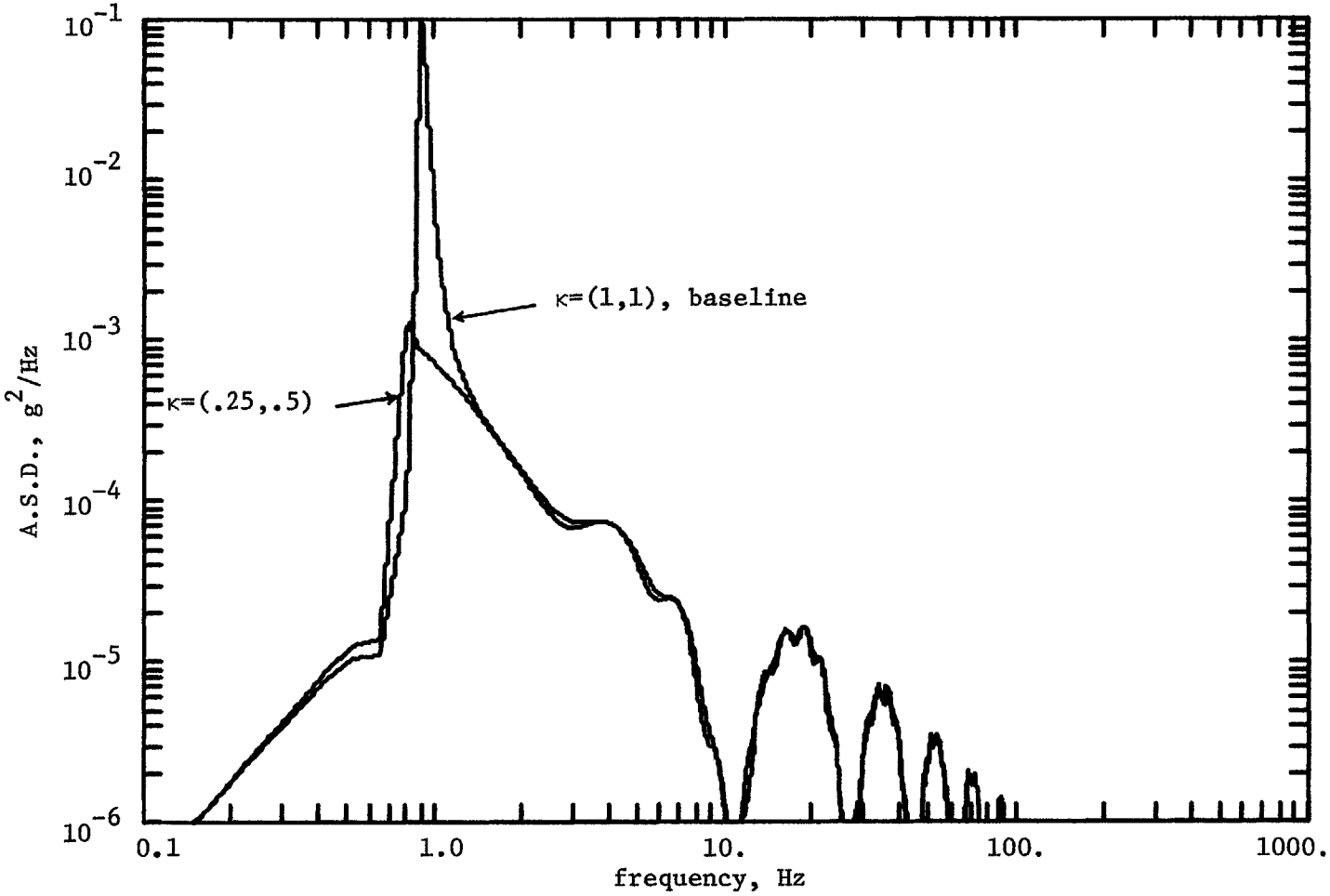

FIGURE 9-13

A.S.D. for RC-RPB Model with Passive-Asymmetric Secondary (Baseline, Rear, 100 mph)

improve the dynamic characteristics of the RC-RPB vehicle in much the same way as was predicted using the RC-LMO model in Chapter 8; the hunting acceleration peak is reduced, and critical speed increased. Like the active steering controller, however, the asymmetric secondary involves yaw coupling and so can excite unstable modes absent in the LMO carbody.

6. Discussion. The primary purpose of this chapter has been to verify that conclusions based on the LMO carbody model can be extrapolated to predict the performance of a vehicle which is in reality much more complicated. The basis for comparison has been taken to be the rigid plane body with two trucks, which, although it is a greatly simplified model, is yet so much more complex than the LMO approximation that symbolic results (such as the transfer function coefficients in Table 3-3) would be extremely difficult to obtain. The LMO model need not -- and cannot -- represent every aspect of RPB model behavior exactly, but it should give a good idea of how variation of a particular parameter will affect the performance of the more complete model. Evidence has been presented here to suggest that this is the case, at least for the particular vehicle configurations studied. In each case where a particular technique improved the ride quality of the LMO vehicle, the same technique (although not always the same parameter values) had a similar effect on RPB ride quality. The principal defect of the LMO model is its inherent inability to predict yaw-mode instabilities.

In addition to reinforcing the validity of the LMO model, work

with the RPB carbody model has pointed to two important roles of the carbody moment of inertia. To minimize transmission of vibration to the passengers, normalized inertia $\bar{I}_c$ should be unity or larger. To avoid instability due to coincidence of eigenvalues, $\bar{I}_c$ should be as far from 1 as possible, either larger or smaller. Taken together, these two considerations suggest that vehicles should be designed with $\bar{I}_c \to \infty$. Attainable values of $\bar{I}_c$ are limited by the need for structural integrity with reasonable overhang and load distribution; the physical implication, however, is that heavy body-mounted equipment should be kept near the ends of the car and beyond the truck attachments insofar as is possible. Effects of carbody asymmetry have not been included in this analysis.

All three of the unconventional approaches to rail suspension design which have been examined in detail -- the RIW truck, the relative-steering active controller, and the passive-asymmetric secondary suspension -- have been shown to perform well dynamically when applied to the RPB carbody. The next chapter will consider their effect on quasi-steady curve negotiation.

CHAPTER 10

TRACKING ERROR DUE TO STEADY CURVING

The primary focus of this thesis has been the dynamic behavior of rail vehicles moving along rough, but nominally straight, track. An equally important aspect of a vehicle's performance is its ability to negotiate curved track without excessive lateral tracking error. In this chapter, the steady-state lateral error of a rigid truck attached to a lateral-mass-only (LMO) carbody is calculated under the assumptions of constant curve radius and constant speed. The effects of various suspension parameters and of unconventional designs (independently-rotating wheels, active steering control, and the passive asymmetric secondary suspension) on the curving performance of this simple model are then illustrated. It will be shown that each of these techniques can adversely affect tracking error if the lateral component of "centrifugal force" is not balanced by banking (superelevation) of the track.

1. Simplifying Assumptions. A detailed, linearized study of the behavior of trucks in curves has been carried out by Newland [26], who included the effects of flexibility and of local curvature, but did not explicitly consider the carbody or secondary suspension. The present analysis will be confined to rigid trucks, either of the conventional (RC) or independently-rotating wheel (RIW) type. The vehicle is assumed to move at a constant circumferential speed V

along a plane track of constant gauge 2h whose centerline is a circular arc of radius R. R is assumed to be much larger than both the gauge (R>>2h) and the car length (R>>2L). The motion is assumed steady -- all time derivatives are zero. Any controller action present in the secondary suspension must be of the relative-sensing type (i.e., insensitive to absolute displacements or angles); a truly absolute-sensing system would not permit steady curving to occur.

Even with these assumptions, analysis of an RPB vehicle model (rigid-plane-body carbody plus two trucks) results in six simultaneous equations in y_c, ϕ_c, y_{b1}, ϕ_{b1}, y_{b2}, and ϕ_{b2}, whose solution is both difficult and obscure. For large R and small V, however, the lateral-mass-only (LMO) carbody with one truck provides a good estimate of tracking error, and will be used exclusively in this chapter.

For large R, the effect of local curvature along the length of the truck may be neglected. The approximate geometry is then as shown in Figure 10-1: the vehicle traverses two parallel rails whose speeds, as measured in the frame of reference moving with the vehicle, are:

$$v_{out} = V\left(1 + \frac{h}{R}\right) \quad , \quad \text{and} \qquad (10.1.1)$$

$$v_{in} = V\left(1 - \frac{h}{R}\right) \quad , \qquad (10.1.2)$$

for the outer and inner rails respectively. In order to use this rotating frame of reference, it is also necessary to introduce the fictitious centrifugal body forces

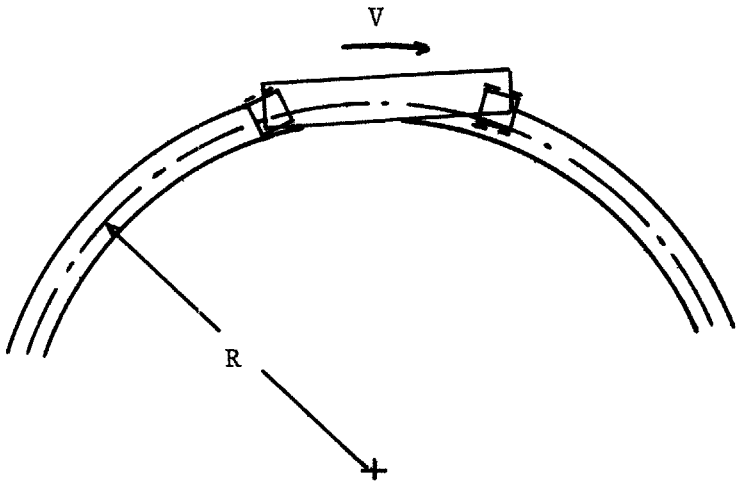

(a) General Curving Geometry

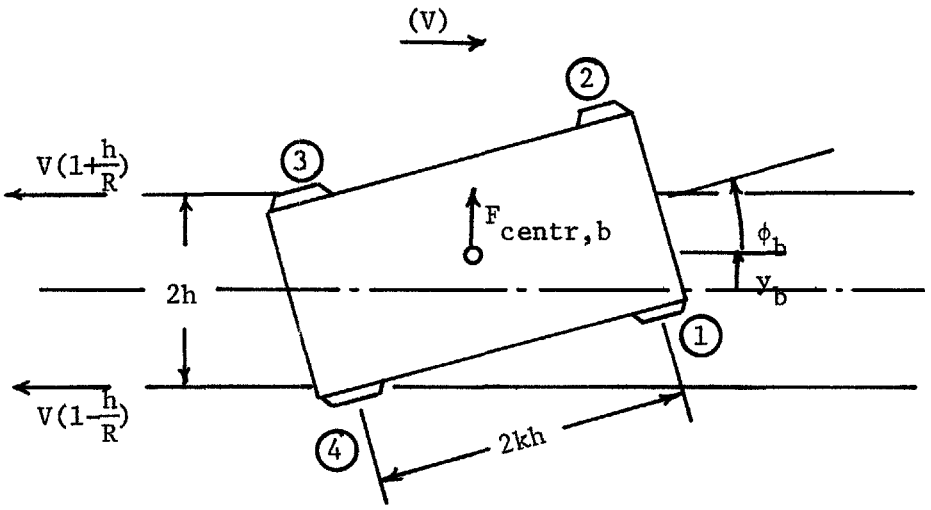

(b) Simplified Geometry. Frame of Reference of the Truck.

FIGURE 10-1

Geometry Used for Steady Curving Analysis

$$F_{centr,c} = m_c V^2/R \quad , \quad \text{and} \qquad (10.1.3)$$

$$F_{centr,b} = m_b V^2/R \quad , \qquad (10.1.4)$$

which appear to act outwardly on the carbody and truck.

Steady curving error will be defined as y_b, as illustrated in Figure 10-1. This definition is consistent with that used previously in the context of dynamic (RMS) tracking error. Another important index of curving performance which should be noted is the maximum wheel excursion, given by

$$y_{max} = \max \left| y_b \pm \phi_b kh \right| \quad . \qquad (10.1.5)$$

Notice that ϕ_b is positive when the truck yaws "out of" the curve. This excursion should be less than the flange clearance for smooth curving.

2. Governing Equations. The curving equations developed here follow the same assumptions of linearity presented in Chapter 3. There are only two new features in this analysis: (1) the presence of the centrifugal body forces so that calculations may be done in a reference frame revolving with the vehicle; and (2) a difference of $2Vh/R$ in the encounter speeds of the inner and outer rails.

The forces (real and fictitious) and torques acting on the truck are diagrammed in Figure 10-2. Letting i designate the wheel reference number as in the figure, they are:

centrifugal force, truck: $F_{centr,b} = m_b V^2/R$
lateral suspension force: F_b

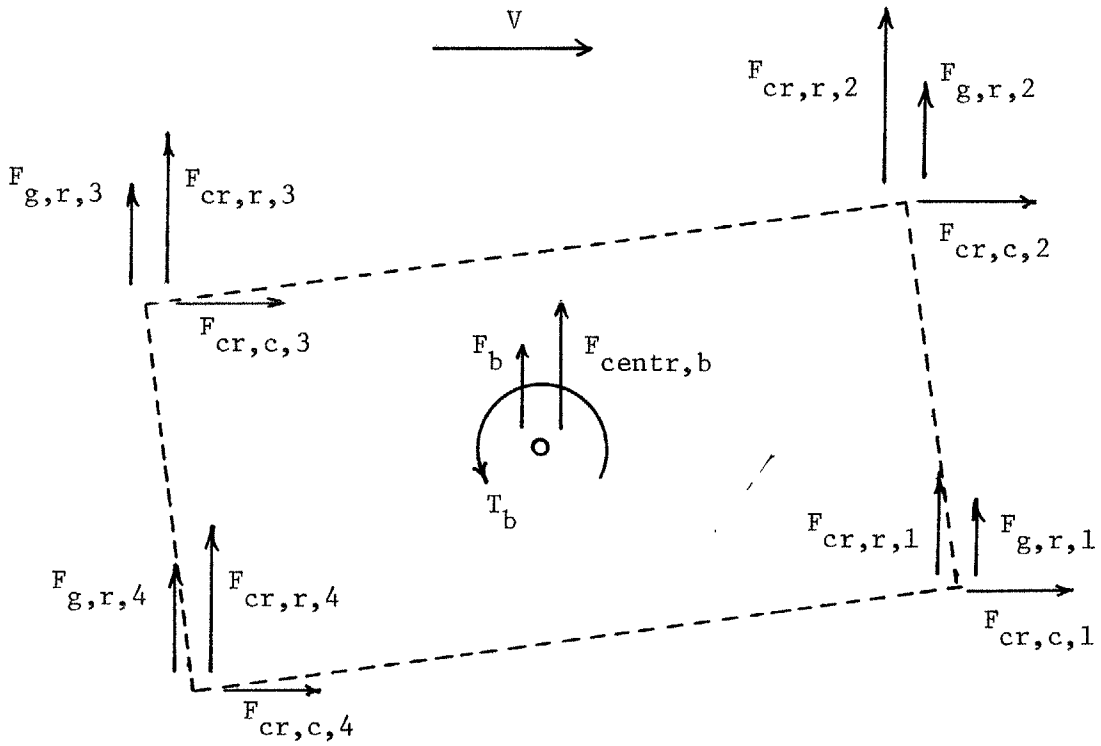

FIGURE 10-2

Forces Acting on Truck

yaw suspension torque: T_b
radial creep force, each wheel: $F_{cr,r,i}$
circumferential creep force, each wheel: $F_{cr,c,i}$
radial gravitational force, each wheel: $F_{g,r,i}$.

Steady curving requires that these forces and torques be in equilibrium.

Radial creep forces arise from truck yaw coupled with forward motion. They are:

RC: $$F_{cr,r,i} = f \phi_b (r_i/r_0) \qquad (10.2.1)$$

RIW: $$F_{cr,r,i} = f \phi_b \quad . \qquad (10.2.2)$$

Circumferential creep forces occur only in the RC model, and are due to a combination of unequal rolling radii and unequal rail encounter speed (Equations 10.1.1 and 10.1.2):

RC: $$F_{cr,c,1} = f \left(\frac{r_1}{r_0} - 1 + \frac{h}{R}\right) \qquad (10.2.3)$$

$$F_{cr,c,2} = f \left(\frac{r_2}{r_0} - 1 - \frac{h}{R}\right)$$

$$F_{cr,c,3} = f \left(\frac{r_3}{r_0} - 1 - \frac{h}{R}\right)$$

$$F_{cr,c,4} = f \left(\frac{r_4}{r_0} - 1 + \frac{h}{R}\right) \quad ,$$

RIW: $$F_{cr,c,i} = 0 \quad . \qquad (10.2.4)$$

Gravitational forces are due to wheel tread profile (see Appendix A). They act approximately radially. The difference between these forces and their balanced (centered) values are:

$$\underline{\text{RC and RIW}}: \quad F_{g,r,1}=F_{g,r,2}= -K_L(y_b+\phi_b kh)$$
$$F_{g,r,3}=F_{g,r,4}= -K_L(y_b-\phi_b kh) \quad . \tag{10.2.5}$$

The difference in rolling radii due to displacement of the wheels, of interest only in the RC model, is due to the effective conicity α:

$$\underline{\text{RC and RIW}}: \quad r_1 = r_0 - \alpha(y_b+\phi_b kh)$$
$$r_2 = r_0 + \alpha(y_b+\phi_b kh)$$
$$r_3 = r_0 + \alpha(y_b-\phi_b kh) \tag{10.2.6}$$
$$r_4 = r_0 - \alpha(y_b-\phi_b kh) \quad .$$

The K-B-parallel models for both lateral and yaw secondary suspensions are assumed, and the general control rule is restricted to relative sensing only. The assumption of steady curving implies that all time derivatives are zero at equilibrium. In that case the suspension forces due to both passive and active components (from Equations 3.4.1, 3.4.2, 6.2.1, 6.2.2, and 6.3.1) are:

$$F_b = K_c(y_c-y_b) - D_7\phi_b \quad , \text{ and} \tag{10.2.7}$$

$$T_b = D_1(y_c-y_b) - K_b\phi_b \quad . \tag{10.2.8}$$

The conditions for equilibrium of carbody and truck are:

$$\text{carbody force, lateral:} \quad F_b = m_c V^2/R \tag{10.2.9}$$

$$\text{truck force, lateral:} \quad F_b+F_{centr,b}+F_{g,r,1}+F_{g,r,2}$$
$$+F_{g,r,3}+F_{g,r,4}+F_{cr,r,1}+F_{cr,r,2}+F_{cr,r,3}$$
$$+F_{cr,r,4} = 0 \tag{10.2.10}$$

truck force, circumferential:

$$F_{cr,c,1}+F_{cr,c,2}+F_{cr,c,3}+F_{cr,c,4} = 0 \qquad (10.2.11)$$

truck torque: $T_b + (F_{g,r,1}+F_{g,r,2}-F_{g,r,3}-F_{g,r,4})kh$

$$+ (F_{cr,r,1}+F_{cr,r,2}-F_{cr,r,3}-F_{cr,r,4})kh$$

$$+ (F_{cr,c,1}+F_{cr,c,4}-F_{cr,c,2}-F_{cr,c,3})h = 0 \quad . \qquad (10.2.12)$$

Equation 10.2.11, for circumferential force, is satisfied identically for either model.

By combining all equations in this section except 10.2.7 and 10.2.8, one obtains:

RC and RIW:

$$(1+\rho_m)m_c V^2/R = 4K_L y_b - 4f\phi_b \qquad (10.2.13)$$

RC: $$T_b = 4K_L k^2h^2\phi_b + 4fh\alpha y_b/r_0 - 4fh^2/R \qquad (10.2.14)$$

RIW: $$T_b = 4K_L k^2h^2\phi_b \quad . \qquad (10.2.15)$$

Equations 10.2.14 and 10.2.15 may be put into the same form by use of the multiplier δ_I, defined thus:

$$\delta_I = 1 \quad \text{for RC truck}$$
$$\delta_I = 0 \quad \text{for RIW truck} \quad . \qquad (10.2.16)$$

Then

RC and RIW:

$$T_b = 4K_L k^2h^2\phi_b + \delta_I 4fh\alpha y_b/r_0 - \delta_I 4fh^2/R. \qquad (10.2.17)$$

Combining Equations 10.2.13, 10.2.17, 10.2.7, and 10.2.8 yields the steady curving lateral and yaw errors. It happens that the expressions for both contain a multiplicative factor of (1/R), showing that error is inversely proportional to R for a given vehicle at a given speed. It is therefore appropriate to deal with the groups $y_b R$ and $\phi_b R$, given by:

$$y_b R = \frac{\delta_I (4fh^2) + m_c V^2 \left[\frac{D_1}{K_c} + \frac{(1+\rho_m)}{4f} K_{eff} \right]}{\delta_I \left(\frac{4fh\alpha}{r_0}\right) + \frac{K_L}{f} K_{eff}} \qquad (10.2.18)$$

$$\phi_b R = - \frac{(1+\rho_m) m_c V^2}{4f} + \frac{K_L}{f} (y_b R) \quad , \qquad (10.2.19)$$

where K_{eff} is an effective yaw stiffness defined as

$$K_{eff} = K_b + 4K_L k^2 h^2 - \frac{D_1 D_7}{K_c} \quad . \qquad (10.2.20)$$

The numerator of equation 10.2.18 consists of a "geometric term", which is independent of V, and a "centrifugal term", proportional to V^2. Notice that the tracking error of the RIW vehicle is zero at zero speed, but that that of the RC vehicle with coned wheels (K_L=0) has as its low-speed limit

$$y_b \rightarrow \frac{r_0 h}{\alpha R} \quad . \qquad (10.2.21)$$

This value of lateral displacement allows the wheelsets to move around the curve in pure rolling. Equation 10.2.19 shows that the RC truck

with coned wheels tends to steer into the curve ($\phi_b<0$) so as to offset the centrifugal force with creep forces. The effects of α, K_L, K_b, D_1, and D_7 will be examined in succeeding sections.

3. RC Curving with Conventional Suspension. Figures 10-3 through 10-5 are plots of $y_b R$ versus V for the RC-LMO vehicle model with the conventional, K-B-parallel secondary suspension described in Chapter 3 ($D_1=D_7=0$). Figure 10-3 shows that the effect of varying yaw stiffness K_b is to increase error at all nonzero speeds. Yaw springing resists the tendency of the truck to steer into the curve and balance centrifugal force, so that a larger displacement is required to generate sufficient torque to produce the requisite ϕ_b. There is no effect of K_b at zero speed, where F_b is zero.

Figure 10-4 is a similar plot showing the effect of increasing gravitational stiffness K_L. At high speeds, the effect is similar to that due to increasing K_b. At low speeds (including V=0), gravitational stiffness reduces error by supplying some of the restoring torque which would otherwise be generated by creep alone.

The effect of conicity, α, on curving error is shown in Figure 10-5. A larger value of α results in a smaller error at all speeds, because a given amount of torque can be developed with less lateral displacement of the wheelsets.

4. RIW Curving with Conventional Suspension. The curving errors of the baseline RC-LMO and RIW-LMO vehicles are compared in Figure 10-6. That for the RIW truck is zero at V=0 (since it displaces due to centrifugal force only), then rises proportional to V^2. For these

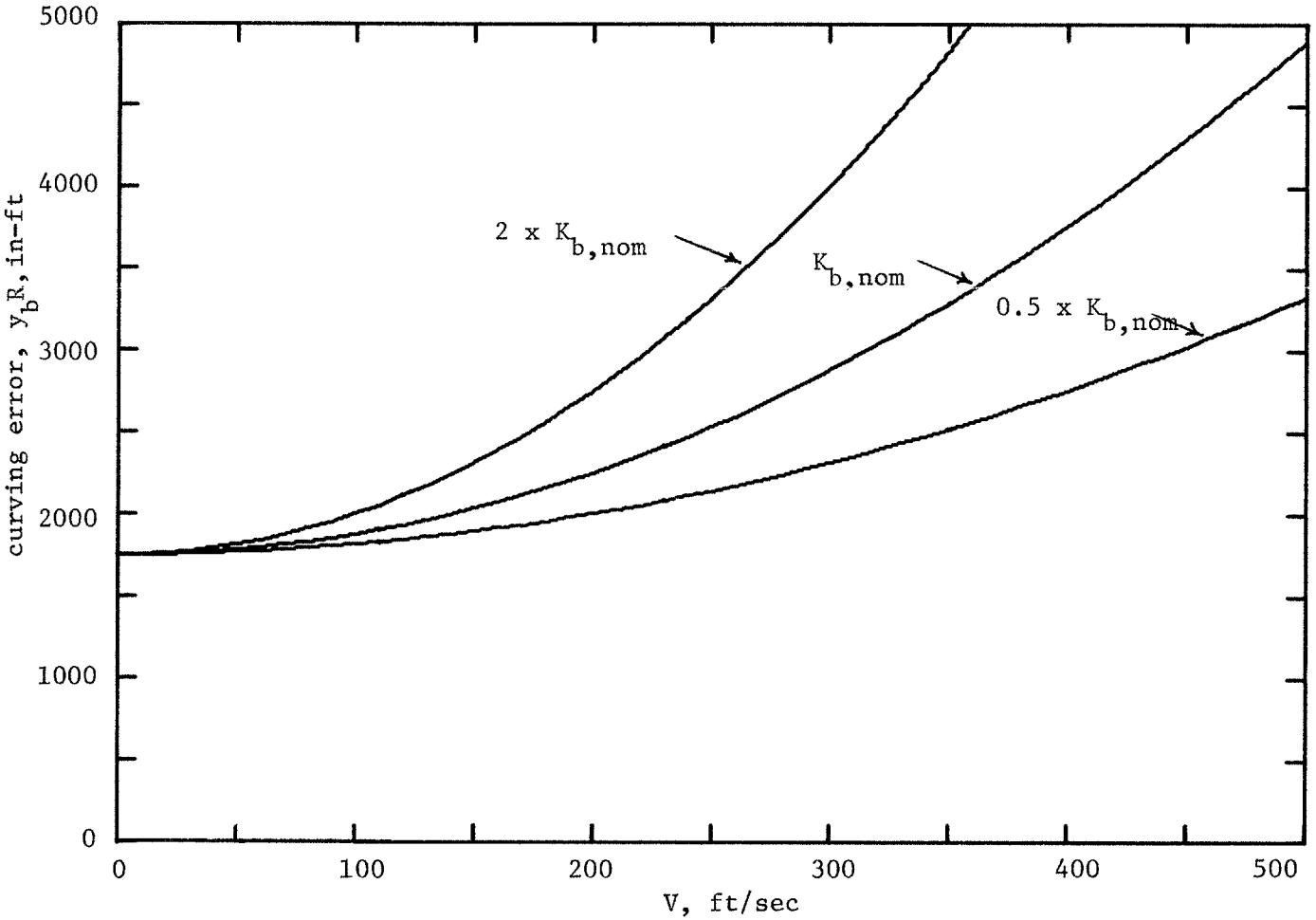

FIGURE 10-3

Steady Curving Error, RC-LMO. Effect of Varying K_b from Baseline Value $K_{b,nom}$.

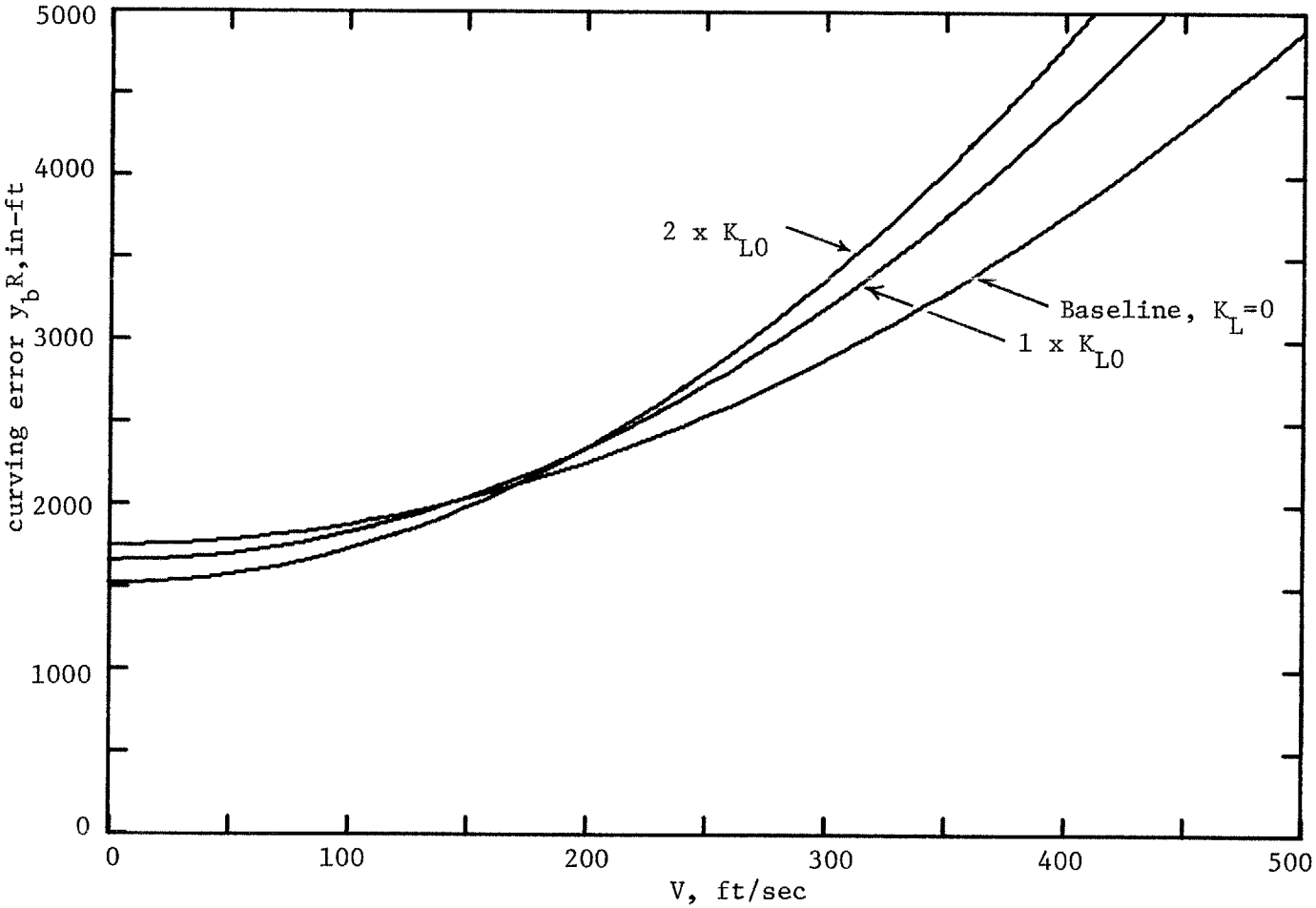

FIGURE 10-4

Steady Curving Error, RC-LMO. Effect of Varying K_L, in Multiples of $K_{L0}=3.837\times10^4$ slug/sec^2.

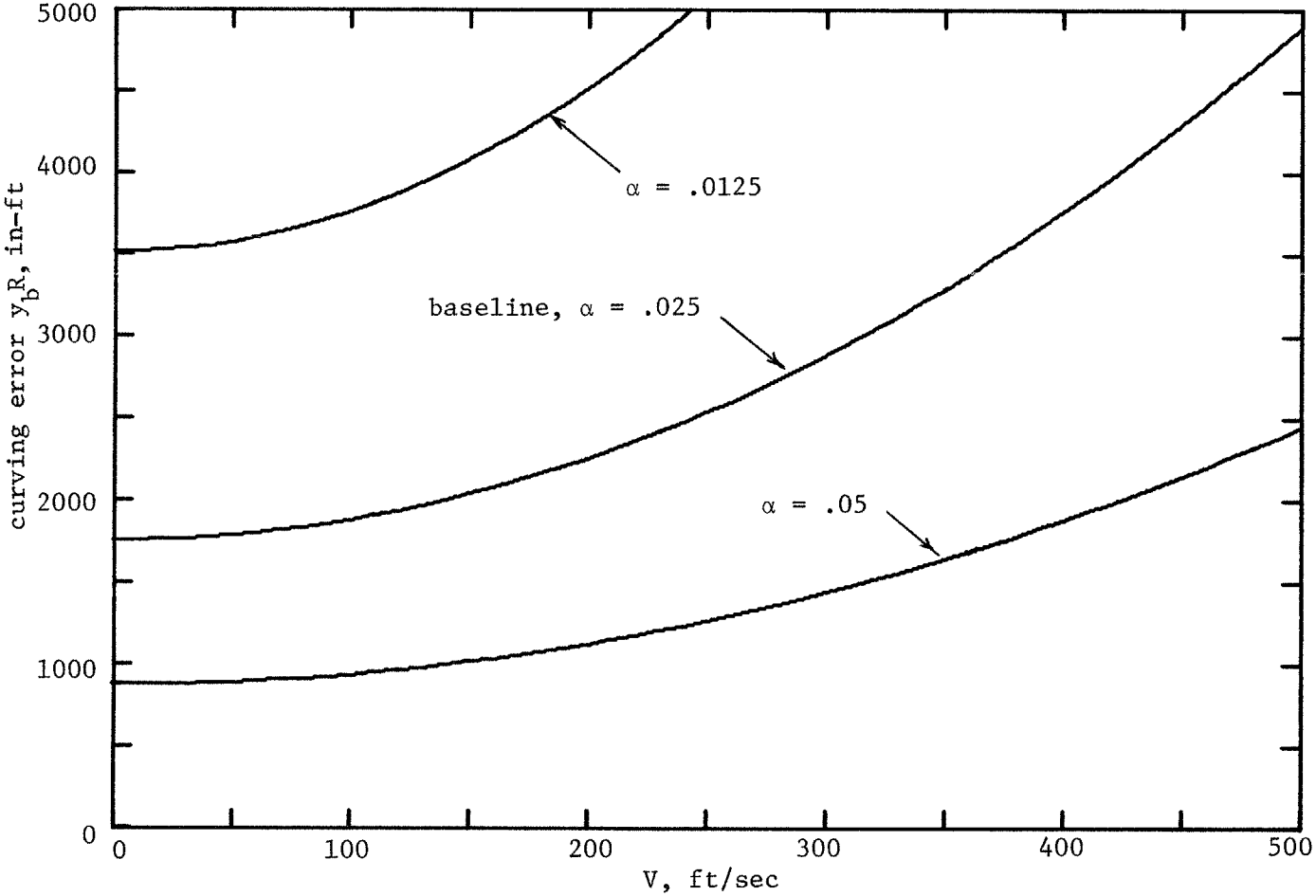

FIGURE 10-5

Steady Curving Error, RC-LMO. Effect of Varying Conicity α.

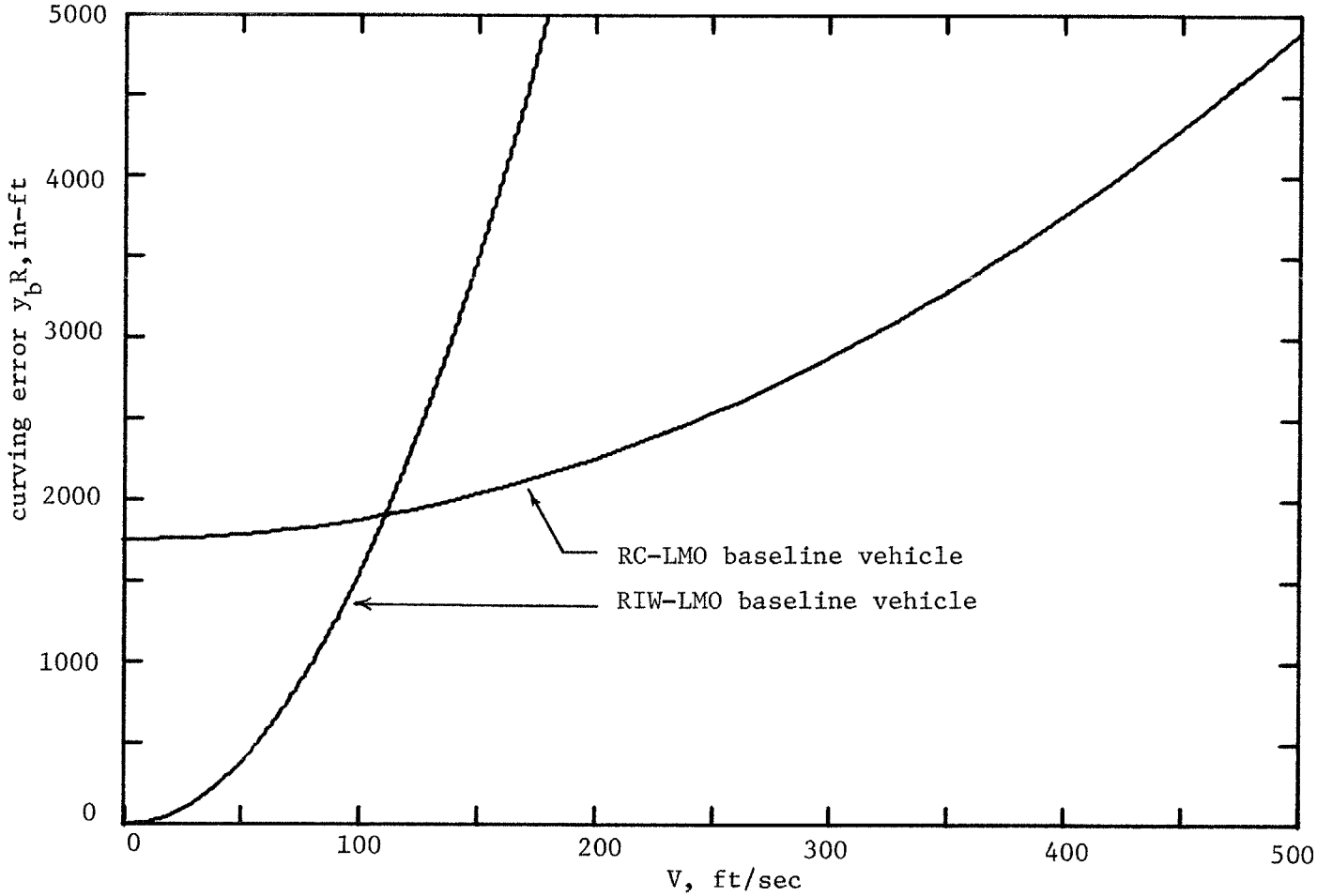

FIGURE 10-6

Steady Curving Error. Comparison of RC and RIW Vehicles.

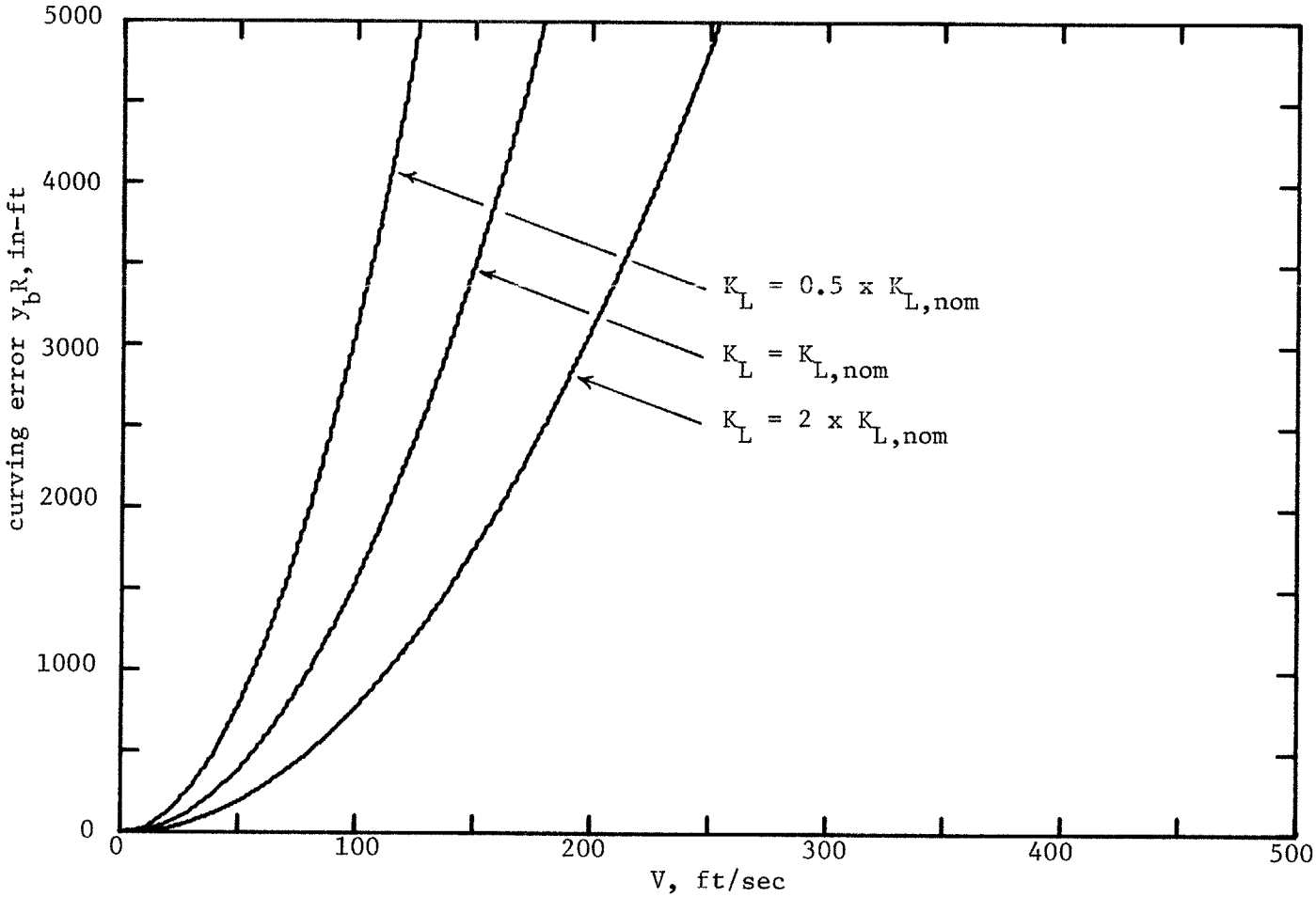

FIGURE 10-7

Steady Curving Error, RIW-LMO. Effect of Varying K_L from Baseline Value, $K_{L,nom}$.

particular parameter values, RIW error exceeds RC error for speeds above 110 ft/sec (75 mph). Figure 10-7 shows RIW curving error to be inversely proportional to K_L for all speeds. Notice from Equation 10.2.19 that $\phi_b=0$ if $K_b=0$; the RIW truck resists lateral force with gravitational, not creep, forces.

5. RC Curving with Steering Control. The relative-sensing, active steering controller was examined in Chapter 7. For the purposes of steady curving analysis, this controller is defined by the position gain D_1, where

$$D_1 = \varepsilon_1 \cdot (4fh\alpha/r_0) \quad . \tag{10.5.1}$$

D_7 is zero. As shown in Figure 10-8, increasing ε_1 leads to increased y_b for nonzero speed. For centrifugal force $m_c V^2/R$ to be transmitted through the lateral spring K_c, the relative lateral body-truck displacement y_c-y_b must be positive. According to Equation 10.2.8, such a displacement causes a positive control torque which steers the truck out of the curve. This effect was cited in Chapter 6 as one reason to high-pass filter or otherwise to modify the control rules of Equations 6.2.1 and 6.2.2.

6. RC Curving with Asymmetric Secondary. It was shown in Chapter 8 that some of the benefits of the actively steered suspension may be achieved passively by using an asymmetric arrangement of springs and dampers in the secondary suspension. In the notation of §6.3, σ_k represents the degree of spring asymmetry, and

$$D_1 = D_7 = K_0 \ell_k (1-\sigma_k) \quad . \tag{10.6.1}$$

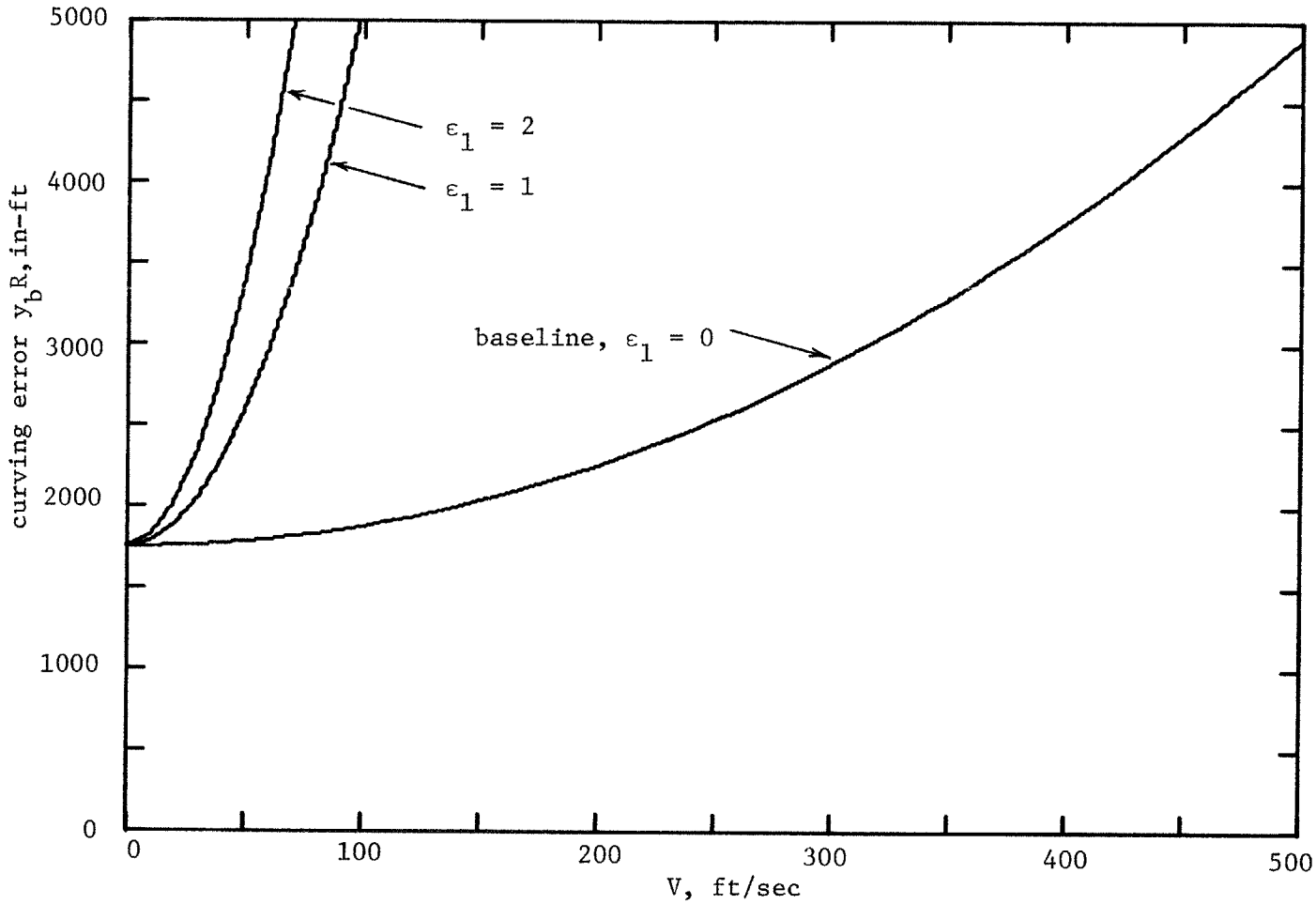

FIGURE 10-8

Steady Curving Error, RC-LMO. Baseline, Relative-Steered. Effect of ε_1.

Examination of Equation 10.2.18 reveals that use of an asymmetric secondary increases the curving error at nonzero speed if $D_1 < 4f/(1+\rho_m)$, and decreases it if $D_1 > 4f/(1+\rho_m)$; the latter condition is difficult to achieve in practice, however, so spring asymmetry will normally increase curving error. Figure 10-9 shows $y_b R$ versus V for the example vehicle of Chapter 8, for three values of σ_k.

7. Other Effects. The models used in this chapter are highly simplified to permit ready comparison of the effects of various suspension parameters on steady curving error. Some effects which could significantly influence the actual error, but which have been omitted in the foregoing analysis, are:

- Local curvature at small R tends to cause the truck to yaw out of the curve, increasing lateral error.
- Truck flexibility allows the wheelsets to yaw relative to one another. Such motion, even if very small, can be sufficient to change the calculated net creep forces greatly. Truck flexibility tends to reduce curving error [26].
- Finite coefficient of friction limits creep forces in tight curves. This may have one of several possible effects on lateral error, including gross slippage of one or more wheels.
- Wheel tread profile can have three types of effects. Concave treads give rise to a gravitational restoring force which is not generally proportional to displacement, but rather exhibits a stiffening characteristic; flanged conical treads are a special case of concave treads, with zero stiffness up to flange contact, and high stiffness thereafter. This fact tends to reduce or limit large

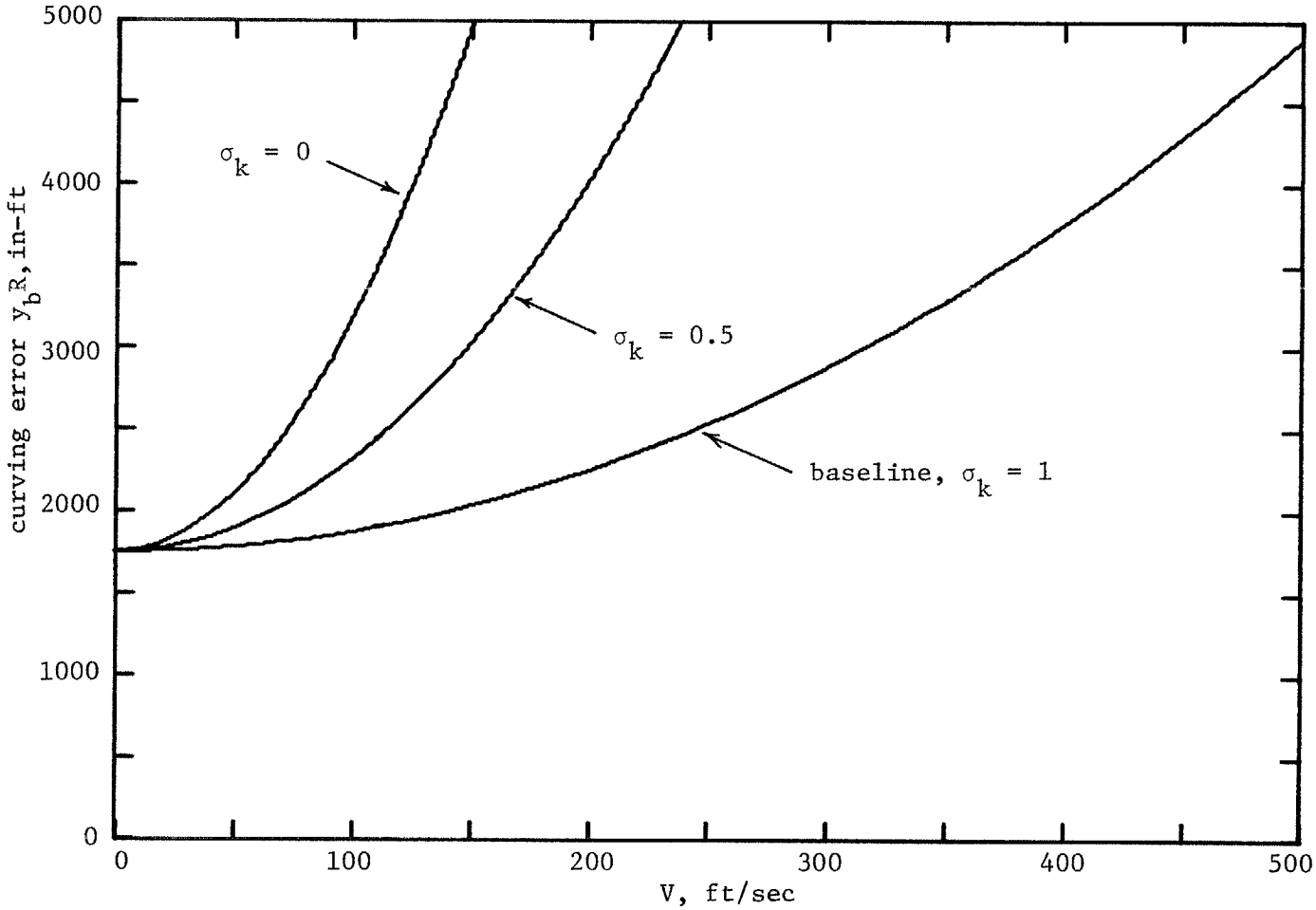

FIGURE 10-9

Steady Curving Error, RC-LMO. Example Vehicle, Passive-Asymmetric Secondary. Effect of Asymmetry, σ_k.

wheel-rail excursions. Secondly, concave treads show increasing local conicity α with displacement, which also reduces error of an RC truck. Finally, the inclination of the wheel-rail contact surface from the vertical due to tread profile can affect the assumed creep force relationw appreciably at large displacements.

- Vehicle length and second truck, present in the RPB vehicle models but absent in the LMO, become important at large L/R and large K_b. Under these conditions the carbody tends to yaw out of the curve, and both front and rear tracking errors are increased over the LMO estimate.
- Superelevation or banking of the track allows a component of the vehicle's weight vector, directed inward, to offset some or all of the centrifugal force, thereby reducing outward tracking error at all speeds (including V=0). A good choice of superelevation is crucial if a vehicle is to perform well in curves.

8. Observations on Steady Curving. The techniques studied to improve dynamic performance may be grouped into two categories: those which alter the primary suspension or truck (increasing K_L, the RIW truck); and those which alter the secondary suspension (increasing yaw stiffness K_b, active steering control, the passive-asymmetric secondary). In both groups, the underlying purpose of the suspension modifications is to cause the truck to follow the track more closely and with less oscillation. The difference between the two, however, is that the primary suspension responds to the actual relative error between the truck and the rails, whereas the secondary suspension senses the error between truck and carbody. For nominally straight

track and at high frequencies, the two errors are closely related, and techniques of either class may be applied successfully. In a curve, however, a method which causes the truck to follow the carbody more closely ipso facto reduces its ability to follow the rails. Hence, the approaches employing profiled wheel treads improve curving performance -- at low speeds, at least -- while those involving secondary suspension modifications degrade it. The reduction of α, a primary suspension modification, extends the range of dynamic stability but increases curving error.

The use of independently-rotating wheels should be seriously considered for applications, such as urban rapid transit, where speeds are low and curves are tight. Figure 10-6 illustrates how tracking error for an RIW vehicle may be lower than that for an RC vehicle at low speeds. Equally as important as the magnitude of excursions is the nature of wheel-rail contact when they become large. A conventional truck, negotiating a curve with insufficient flange clearance, undergoes flange contact and possibly gross slippage; the results are annoying squeal and rapid wear of both wheels and rails. An RIW truck, on the other hand, negotiates any curve in pure rolling if $K_b=0$. This fact suggests that the RIW truck may offer reduced wear as well as attractive dynamic characteristics.

CHAPTER 11

CONCLUSIONS AND RECOMMENDATIONS

Three types of rail vehicle suspension modifications -- independently-rotating wheels, active steering control, and the passive asymmetric secondary suspension -- have been examined in this thesis and shown to offer significant advantages in lateral dynamic performance over that normally obtainable using conventional methods. All have the potential of increasing the cruise speed of steel wheel / steel rail vehicles well above the present practical limit (about 160 mph), without adversely affecting passenger comfort or immunity to derailment. Each method may, depending on speed and other conditions, have an adverse effect on the ability of a vehicle to negotiate curves without flange impact. The relatively simple Lateral-Mass-Only (LMO) carbody model has been found to be a useful approximation for design purposes, preserving important features of more elaborate models without introducing undue analytical complexity.

Future work in the area of rail vehicle lateral dynamics should include: model refinement, linear and nonlinear; optimization studies; the use of other types of controller action; and design and testing of vehicles which embody the ideas proposed herein.

Conclusions

1. Usefulness of the LMO Carbody Model. Most of the results which

have been presented here were obtained using the Lateral-Mass-Only (LMO) carbody model. This represents a compromise between the simplicity of the "translating reference" assumption, frequently made in studies of truck hunting, and the accuracy obtainable when the length and inertia of the carbody and the presence of a second truck are taken into account. The equations of motion resulting from combining the LMO carbody with the rigid truck model are simple enough to allow system functions to be obtained explicitly in terms of the design parameters. Despite its simplicity, the model can show carbody resonance (primary hunting), a phenomenon of great importance in real vehicles which is entirely absent when the carbody is modelled as a translating reference. The finite mass of the carbody must also enter into any calculations of vibration transmitted to passengers or lading.

The LMO model was compared in Chapter 9 to a more complicated one -- the Rigid-Plane-Body (RPB) carbody with two trucks. The additional degree of freedom in the latter was found to introduce modes or oscillation, not predictable from the LMO model, which can become unstable due to yaw coupling between truck and carbody; by contrast, analysis based on the LMO model generally suggests that such yaw coupling improves dynamic performance. Despite this limitation, correspondence between the models was close for the cases examined. Suspensions which improved behavior of an LMO model had a similar effect (over some range of parameter values) on that of an RPB model. Any specific proposed design should be evaluated using the

most complete model available, but the LMO approximation appears a useful one with which to identify promising directions for inquiry.

2. Modifications to Conventional Suspension. Several modifications to the rigid conventional (RC) truck, examined in Chapter 4, can improve dynamic performance. The increase in critical speed V_c which comes from increasing yaw stiffness K_b or decreasing conicity α is well documented; either approach, however, impairs tracking ability, and K_b is further limited by considerations of practical component stiffnesses and tolerances. The possibility of placing a damper in series with the yaw spring was examined and shown to eliminate the misalignment and low-frequency tracking problems without adversely affecting critical speed or ride quality.

The inclusion of acceleration spectral density (ASD) as an index of ride quality leads to some constraints on performance not predictable from computations of critical speed alone. Low- and high-frequency ASD asymptotes may be identified which depend on only a few parameters. The high-frequency asymptote is proportional to the square of the lateral secondary damping, B_c; this damping should therefore be made as small as possible, consistent with the requirement for adequate damping of the carbody's natural modes.

Gravitational stiffness at the wheels, K_L, was identified as a means of extending V_c, improving ride quality, and reducing tracking error of an otherwise conventional rigid truck. Gravitational stiffness is effected by grinding wheels to a concave, rather than conical, tread profile; it is also possible to obtain a concave profile

through natural wear. The relationship between K_L and α for naturally worn treads, however, has not been established -- the increasing conicity which accompanies wear may offset the benefits of increasing K_L. Furthermore, profiled wheels may be expected to have very different effects depending upon whether they are mounted on rigid or flexible trucks. Nevertheless, there exists a strong possibility that designing with profiled wheels may offer both improved dynamics and lower regrinding costs relative to coned wheels.

3. The RC Truck with Active Steering Control. One type of active control device -- the relative-sensing steering controller -- has been studied. This system would measure relative displacement, velocity, and acceleration between the truck and the carbody in the lateral direction, and use them to generate a torque tending to steer the truck toward the carbody. It was found capable of extending stable operation to very high speeds, and of improving ride quality at a given speed, with the expenditure of a modest amount of control power. Applied to the RPB carbody model, the active steering controller had effects similar to those calculated for the LMO model except for the presence of new regions of instability due to yaw interaction. Tracking error in curves is increased by the controller in its pure form, but this problem can be circumvented by suitable filtering.

Active steering control is an attractive means of providing good dynamics at very high speeds. It is possible to implement the active controller in such a way that it can (1) perform ancillary functions

such as steering into curves to reduce error, in addition to its primary function; (2) be easily modified or tuned after installation; and (3) be made adaptive (e.g., speed- or load-dependent) so as to function well under a wide variety of conditions. The price of these advantages, in added cost, complexity, and maintenance, makes an active system probably better suited to passenger service than to freight.

4. The RC Truck with Asymmetric Secondary. The use of a secondary suspension with an asymmetric front and rear distribution of springs and dampers has been found to be a passive way of achieving some of the advantages of active steering control. Such a suspension requires no additional power for its operation; it would tend to be mechanically simple, inexpensive, rugged, and reliable. It is capable of extending the stable speed range considerably, while improving ride quality and dynamic tracking error at any given speed. Its two principal disadvantages are: (1) directionality -- an asymmetric truck can be operated at full speed in one direction only; and (2) increased steady curving error.

The features of the passive asymmetric secondary suggest that it might be conveniently retrofitted on existing passenger or freight cars for further evaluation.

5. The RIW Truck. The rigid truck with independently-rotating wheels represents a major departure from current practice. By eliminating the axle connecting opposite wheels, and relying on gravitational stiffness alone to guide the truck, hunting instabilities

are eliminated. The results are very high critical speed (infinite according to the assumptions in this thesis), improved ride quality, reduced dynamic (and at some speeds steady) tracking error, and increased flexibility in the choice of secondary suspension parameters. Drawbacks of the RIW truck include: (1) the necessity for a very rigid truck frame and for special bearings to keep wheels parallel and at constant gauge -- functions presently served by the axles; and (2) the added difficulty of properly accelerating and braking independent wheels.

The superior dynamic properties of the RIW truck recommend it for further consideration in high-speed applications. Its curving behavior also makes it especially suitable for rapid transit service.

Recommendations

6. Improvement of Models. This thesis has dealt only with relatively simple models for vehicles and inputs, in an effort to gain a physical understanding of the principal phenomena involved. Some ways in which the models may be further developed are summarized below.

- Carbody roll couples to lateral motions and can significantly affect dynamics in some situations. Its importance should be assessed.
- Nonlinear effects should be included where they are important, especially in freight car models. Important nonlinearities include flange impact, profiled wheel treads, friction damping, stops,

clearances, and the creep force relation.

- Additional flexibility may be introduced, especially between the wheelsets and truck frame. Conclusions based on a perfectly rigid truck become invalid at high frequencies.
- Freight truck models should be developed. The conventional three-piece freight truck is by no means rigid, and efforts to improve its performance should recognize this fact.
- Rail models should be developed which include their flexibility and distributed character.
- Inputs should be extended to include wind gusts, rail joints, and cross-level irregularities in order to obtain a more realistic picture of ride quality.
- Coupling effects between cars in a train should certainly be investigated. Models of long trains can be developed using modal approximations, and used to assess suspension designs.
- Acceleration and braking can affect lateral dynamics and should be examined.
- Profile of wheels is an important parameter which is not well understood. There is need for a means of predicting what pattern of tread wear will result from a given vehicle design and given operating conditions.

7. Further Control Studies. Active control was used successfully in this work to improve rail vehicle dynamics, but no attempt was made to optimize the suspensions using analytical control techniques. Such optimization is a desirable goal, however, as it may identify altogether new ways to improve dynamic behavior. The prerequisite for system optimization is a meaningful performance index; in the

case of rail vehicles, a suitable index must at least include measures of carbody vibration, tracking error, and control power. The strong but narrow hunting peak in the response of conventional vehicles is believed to affect ride quality more than its contribution to mean-square acceleration would suggest. and this fact has thus far prevented formulation of a workable comfort index. Further work in this area is required, both to ascertain the passenger's tolerance to random vibration with large pure-tone content, and to develop a convenient ride quality index which properly reflects human sensitivity to such vibration.

Only a small group of control laws were considered here, and others should be tried in the future. In particular, a rail vehicle is well suited to control with preview, either within the vehicle or along the length of a train.

8. Design and Experiment. The practical value of suspensions based on this work can be established only by detailed design and testing. Tradeoffs between active controller performance (sensitivity, bandwidth, reliability, etc.) and cost (capital, maintenance, power, etc.) should be investigated, as should constraints placed on new designs by the need for compatibility with existing practice. RIW systems as modelled have been shown to have excellent dynamics, but they must be carefully examined to determine their feasibility.

Controlled experiments on rail vehicle dynamics are badly needed. Efforts should be made to implement carefully scaled physical models on which new concepts might be conveniently tried. Full-scale

test facilities, such as that operated by the U.S. Department of Transportation at Pueblo, Colorado [6], are of great importance in the final stages of design.

LIST OF REFERENCES

1. High Speed Rail Systems, TRW Systems Group report for U.S. Department of Transportation, FRA-RT-70-36. Redondo Beach, Cal.: 1970.

2. Ward, J.D., "The Future Roles for Tracked Levitated Vehicle Systems", J. Dyn. Sys., Meas., and Ctl. (ASME), v.96-G, no.2, June 1974.

3. Shladover, S.E., "Optimal and Suboptimal Steering Control of Rubber-Tired Guideway Vehicles", S.B.-S.M. thesis, Department of Mechanical Engineering, M.I.T., Feb. 1974.

4. Sweet, L.M., "Analysis, Testing and Design of Plenum Air Cushion Suspensions, Including Feeding System Dynamics", Ph.D. thesis, Department of Mechanical Engineering, M.I.T., June 1974.

5. Borcherts, R.H., et. al., "Base Line Specifications for a Magnetically Suspended High Speed Vehicle," Proc. IEEE, May 1973.

6. Weinstock, H., "Analysis of Rail Vehicle Dynamics in Support of Development of the Wheel Rail Dynamics Research Facility", U.S. Department of Transportation report MA-06-0025-73 (PB 222 654), June 1973.

7. Lee, R.A., and Pradco, F., "Analytical Analysis of Human Vibration", Society of Automotive Engineers preprint 680091, 1968.

8. Borcherts, R.H., et. al., "Preliminary Design Studies of Magnetic Suspensions for High Speed Ground Transportation: Experimental Ride Simulation Studies", report of the Transportation Research and Planning Office, Ford Motor Company, under U.S. Department of Transportation contract DOT-FR-10026, June 1973.

9. "Performance Specification and Engineering Requirements for Urban Tracked Air Cushion Vehicle", research funding proposal, U.S. Department of Transportation, May 1971.

10. Cooperrider, N.K., "The Hunting Behavior of Conventional Railway Trucks", ASME paper 70-WA/RR-2, August 1970.

11. Matsudaira, T., "Hunting Problem of High-Speed Railway Vehicles with Special Reference to Bogie Design for the New Tokaido Line", Proc. I.M.E., v.180, part 3-F, p.58, 1965-1966.

12. "Hardware for High Speed in 1973", Railway Gazette International, v.129, no.9, p.336, September 1973.

13. Heumann, G.W., "German High-Speed Railroads", Machine Design, v.45, no.21, p.20, September 6, 1973.

14. Law, E.H., and Cooperrider, N.K., "Literature Survey of Railway Vehicle Dynamics Research", J. Dyn. Sys., Meas., and Ctl. (ASME), v.96-G, no.2, p.132, June 1974.

15. Carter, F.W., "On the Action of a Locomotive Driving Wheel", Proc. Royal Soc. of London, ser.A, v.112, p.151, 1926.

16. Vermeulen, P.J., and Johnson, K.L., "Contact of Nonspherical Elastic Bodies Transmitting Tangential Forces", J. Appl. Mech. (ASME), v.31-E, no.2, p.338, June 1964.

17. Johnson, K.L., "Effect of Spin Upon the Rolling Motion of an Elastic Sphere on a Plane", J. Appl. Mech. (ASME), v.25-E, no.2, p.332, June 1958.

18. Ollerton, E., "Stresses in the Contact Zone", Proc. I.M.E., v.178, part 3-E, p.161, 1964.

19. Paul, I.L., and Nayak, P.R., "Effects of Surface Roughness on Creep Rates in Rolling Metal Wheels", Proc. of the First International Conference on Vehicle Mechanics, Wayne State University, Detroit, Mich., p.36, July 1968.

20. Johnson, K.L., "Effect of Tangential Force Upon the Rolling Motion of an Elastic Sphere on a Plane", J. Appl. Mech. (ASME), v.25-E, no.2, p.338, June 1958.

21. Langer, B.F., "Dynamic Stability of Railway Trucks", Timoshenko Sixtieth Anniversary Volume, p.125. New York: MacMillan and Company, 1938.

22. Langer, B.F., and Shamberger, J.P., "Lateral Oscillations of Rail Vehicles", Trans. A.S.M.E., v.57, no.8, p.481, 1935.

23. Katz, E., and dePater, A.D., "Stability of Lateral Oscillations of a Railway Vehicle", Appl. Sci. Res., ser.A, v.7, p.393, 1958.

24. Birmann, F., "Track Parameters, Static and Dynamic", Proc. I.M.E., v.180, part 3-F, p.73, 1965-1966.

25. Meacham, H.C., and Ahlbeck, D.R., "A Computer Study of Dynamic Loads Caused by Vehicle-Track Interaction", ASME paper 69-RR-1, Jan. 1969.

26. Newland, D.E., "Steering a Flexible Railway Truck on Curved Track", J. Eng. for Ind. (ASME), v.91-B, p.908, Aug. 1969.

27. Müller, C. Th., "Dynamics of Railway Vehicles on Curved Track", Proc. I.M.E., v.180, part 3-F, p.45, 1965-1966.

28. Wickens, A.H., "The Dynamic Stability of Railway Vehicle Wheelsets and Bogies having Profiled Wheels", Int. J. Solids and Structures, v.1, p.319, 1965.

29. Law, E.H., and Brand, R.S., "Analysis of the Nonlinear Dynamics of a Railway Vehicle Wheelset", ASME paper 72-Aut-F, March 1973.

30. Law, E.H., "Nonlinear Wheelset Response to Random Lateral Rail Irregularities", ASME paper 73-WA/RT-1, November 1973.

31. Benington, C.K., "The Railway Wheelset and Suspension Unit as a Closed-Loop Guidance Control System: A Method for Performance Improvement", J. of Mech. Eng. Sci., v.10, no.2, p.91, April 1968.

32. dePater, A.D., "The Approximate Determination of the Hunting Movement of a Railway Vehicle by Aid of the Method of Krylov and Bogoljubov", Appl. Sci. Res., ser.A, v.10, p.205, 1961.

33. Clark, J.W., and Law, E.H., "Investigation of the Truck Hunting Instability Problem of High-Speed Trains", ASME paper 67-Tran-17, 1967.

34. Jafar Shaghaghi, K., "Hunting Motion of High Speed Tracked Vehicles", S.M. thesis, Department of Mechanical Engineering, M.I.T., August 1965.

35. Wickens, A.H., "The Dynamic Stability of Railway Vehicle Wheelsets and Bogies having Profiled Wheels", Int. J. Solids and Structures, v.1, no.3, p.319, July 1965.

36. Matsudaira, T., et. al., "Problems on Hunting of Railway Vehicle on Test Stand", J. Eng. for Ind. (ASME), v.91-B, p.879, August 1969.

37. Yokose, K., "Calculation of Hunting of High Speed Railway Truck -- Problems of Truck Design for SANYO SHIN KANSEN", Q. Repts. Tokyo Rwy. Tech. Res. Inst., v.11, no.2, p.108, 1970.

38. Marcotte, P.P., "Lateral Dynamic Stability of Railway Bogie Vehicles", M.Eng. thesis, Department of Mechanical Engineering, University of Sheffield, Sheffield, England, May 1972.

39. Joly, R., "Study of the transverse stability of a railway vehicle running at high speed", Rail International, v.3, no.2, p.83, February 1972.

40. Wickens, A.H., "The Dynamics of Railway Vehicles on Straight Track: Fundamental Considerations of Lateral Stability", Proc. I.M.E., v.180, part 3-F, p.29, 1966.

41. Wickens, A.H., "General Aspects of the Lateral Dynamics of Railway Vehicles", J. Eng. for Ind. (ASME), v.91-B, p.869, August 1969.

42. Mauzin, A., "The Static and Dynamic Parameters of Railway Coaches", Proc. I.M.E., v.180, part 3-F, p.120, 1965-1966.

43. Hobbs, A.E.W., and Pearce, T.G., "The Lateral Dynamics of the Linear Induction Motor Test Vehicle", J. Dyn. Sys., Meas., and Ctl. (ASME), v.96-G, no.2, p.147, June 1974.

44. Milner, J.L., Haight, E.C., and Hutchens, W.A., "A Normal Mode Analysis of Rail Research Car T-3", AIAA paper 72-336, 1972.

45. Diboll, W.B. Jr., and Bieniecki, H.S., "Suspension Dynamics by Computer Simulation", J. Eng. for Ind. (ASME), v.90-B, no.4, p.708, November 1968.

46. Liepins, A.A., "Digital Computer Simulation of Railroad Freight Car Rocking", J. Eng. for Ind. (ASME), v.90-B, no.4, p.701, November 1968.

47. Wiebe, D., "The Effects of the Lateral Instability of High Center of Gravity Freight Cars", J. Eng. for Ind. (ASME), v.90-B, no.4, p.727, November 1968.

48. Henderson, K.A., and Johnson, J., "A Criterion for the Control of 100 Ton Hopper Car Roll Motion", J. Eng.for Ind. (ASME), v.90-B, no.4, p.717, November 1968.

49. Manos, W.P., and Shang, J.C., "Dynamic Analysis of Rolling Freight Cars", ASME paper 65-WA/RR-8, 1965.

50. Williams, D., "A New Method of Dynamically Stabilizing Railway Bogies, Four-Wheel Wagons, and Road-Railers Against Undesirable Lateral Oscillations", Proc. I.M.E., v.180, part 3-F, p.125, 1965-1966.

51. Koyanagi, S., "The Motion of A Guided Railway Car with Independently Rotating Wheels -- Calculations Based on the SHIN KANSEN Car Model", Q. Repts. Tokyo Rwy. Tech. Res. Inst., v.14, no.3, p.168, 1973.

52. Koyanagi, S., "The Stability of Motion of the Independently-Rotating Wheel-Axle", Q. Repts. Tokyo Rwy. Tech. Res. Inst., v.12, no.1, p.29, 1971.

53. Kaplan, A., Hasselman, T.K., and Short, S.A., "Independently Rotating Wheels for High Speed Trains", SAE paper 700841, October 1970.

54. Kaplan, A., and Short, S.A., "Dynamics of Independently Rotating Wheel Systems", TRW Systems Group report for U.S. Department of Transportation, FRA-RT-71-47 (PB 194 000). Redondo Beach, Cal.: 1970.

55. Flowers, D.F., and Flowers, F.F., "An Axleless Railroad Truck", S.M. Thesis, Department of Mechanical Engineering, M.I.T., 1942.

56. List, H.A., "An Evaluation of Recent Developments in Rail Car Truck Design", ASME paper 71-RR-1, 1971.

57. Scales, B.T., "Behaviour of Bogies on Curves", Railway Engineering Journal, v.1, no.4, p.19, July 1972.

58. Newland, D.E., and Cassidy, R.J., "Fundamental Design Considerations for Multi-Wheeled Flexible Railway Vehicles", ASME paper 70-Tran-32, July 1970.

59. Sarma, G.N., and Kozin, F., "An Active Suspension System Design for the Lateral Dynamics of a High-Speed Wheel-Rail System", J. Dyn. Sys., Meas., and Ctl. (ASME), v.93-G, no.4, p.233, December 1971.

60. Bender, E.K., "Optimization of the Random Vibration Characteristics of Vehicle Suspensions", Sc.D. thesis, Department of Mechanical Engineering, M.I.T., June 1967.

61. Paul, I.L., and Bender, E.K., "Active Vibration Isolation and Active Vehicle Suspensions", report DSR-76109-1 (PB 173 648), Engineering Projects Laboratory, M.I.T., November 1966.

62. Hedrick, J.K., Billington, G.F., and Dreesbach, D.A., "Analysis, Design, and Optimization of High Speed Vehicle Suspensions Using State Variable Techniques", J. Dyn. Sys., Meas., and Ctl. (ASME), v.96-G, no.2, p.147, June 1974.

63. Lind, E.F., and Martin, G.C., "Track-Train Dynamics Research Planning and Progress", ASME paper 73-ICT-43, Sept. 1973.

64. Takahashi, Y., Rabins, M.J., and Auslander, D.M., Control and Dynamic Systems. Reading, Mass.: Addison-Wesley, 1972.

65. Xenakis, J., PL/I FORMAC Symbolid Math Formula Manipulation Interpreter. IBM program order number 360D-03.3.004. Cambridge: International Business Machines, 1971.

66. MACSYMA Reference Manual. Cambridge: The Mathlab Group, MIT Project MAC, 1974.

67. Crandall, S.H., and Mark, W.D., Random Vibration in Mechanical Systems. New York: Academic Press, 1963.

68. Newton, G.C. Jr., Gould, L.A., and Kaiser, J.F., Analytical Design of Linear Feedback Controls. New York: John Wiley and Sons, 1957.

69. "Freight Car Truck Design Optimization Project", report by the Southern Pacific Transportation Company for the U.S. Department of Transportation under contract DOT-FR-40023, July 1974.

APPENDIX A

GRAVITATIONAL STIFFNESS

When a loaded wheel rests on a rail, it is acted upon by a force vector at the contact point or points. The vertical component of this vector is necessary to support the weight of the vehicle; its lateral component, if unbalanced, will cause the wheel to accelerate laterally. A concave wheel tread profile gives rise to an increasing lateral restoring force with displacement from the centered position. By linearizing this force - displacement relationship, one can determine the linearized gravitational stiffness, K_L.

1. Idealized Wheel - Rail Contact Geometry. The exact geometry of the wheel tread - railhead system is complicated and variable. However, if only small motions in the plane normal to the direction of forward motion are considered, the wheel and rail may be characterized by their local radii of curvature in the region of contact.

Figure A-1 illustrates the geometry assumed for the purposes of this work. When viewed parallel to the rail, both tread and railhead are assumed to have constant radii, R_w and R_r respectively. Clearly $R_w > R_r$. The tread profile is assumed to be concave for two reasons: (1) a concave profile is necessary to provide a stable restoring force with displacement, and (2) any initial profile will

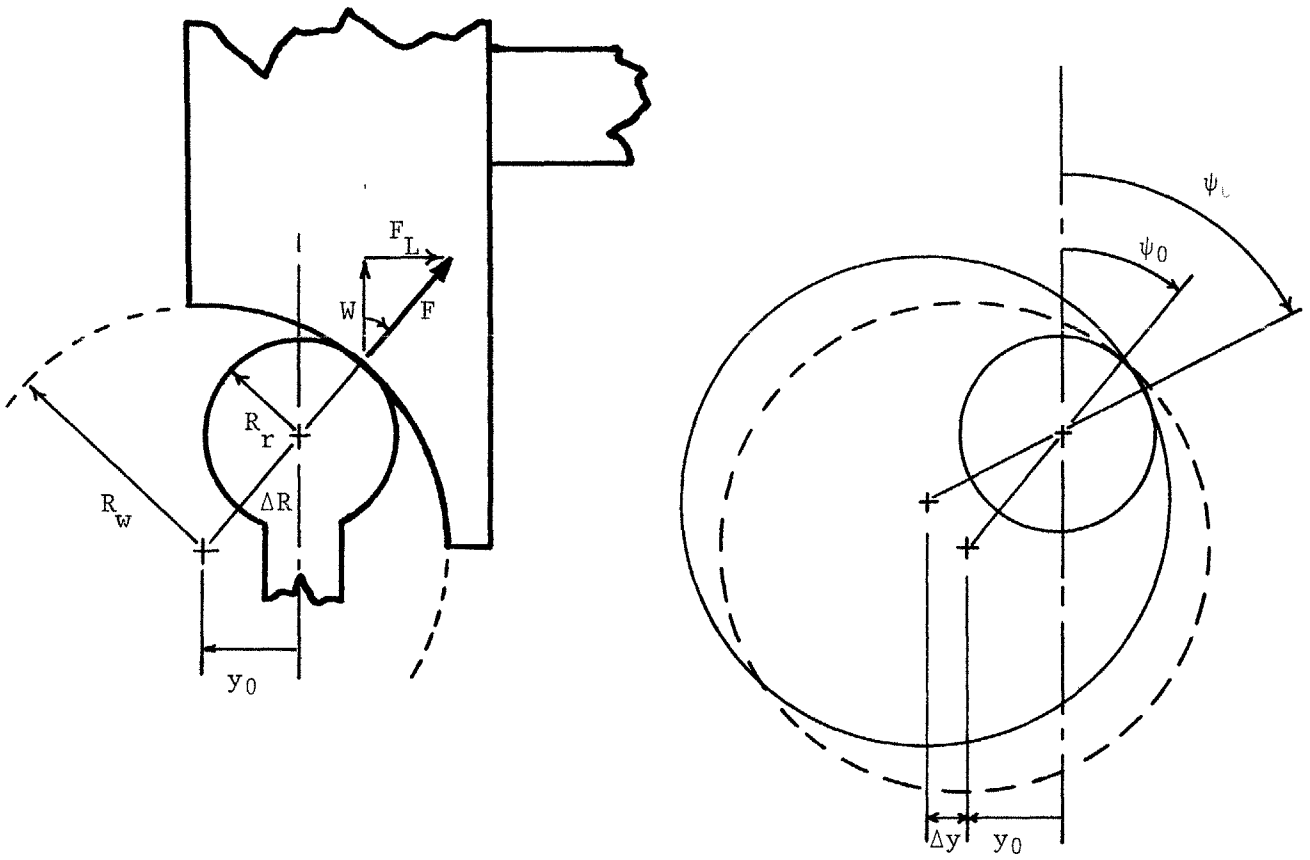

(a) Centered Position

(b) Geometry of Lateral Displacement

FIGURE A-1

Idealized Wheel - Rail Geometry with Concave Profile

wear to a concave one in service. Point contact is assumed.

When opposite wheels are centered between the rails, the center of each tread arc lies a distance y_0 outside that of each rail. This initial displacement should be zero or positive as shown; a negative value of y_0 causes the roll center of the wheelset to lie below the plane of the rails, a situation which tends toward static instability. The normal to both surfaces at the contact point is at an angle ψ_0 to the vertical, where

$$\psi_0 = \sin^{-1}(y_0/\Delta R) \ , \qquad (A.1.1)$$

and $\Delta R = R_w - R_r$. The initial contact force F_0 acts along this direction.

In most practical situations, it may be safely assumed that any vertical motions (i.e., roll) caused by lateral displacement of profiled wheels will not appreciably affect the contact geometry.

2. Forces at the Interface. It is assumed that each wheel experiences a vertical loading W; taking W to be constant neglects quasi-static (weight transfer or unbalance) and dynamic variations in wheel loading. Force balance in the vertical direction requires that the vertical component of F be equal to W, or

$$W = F \cos \psi \ . \qquad (A.2.1)$$

This implies that the lateral component is

$$F_L = W \tan \psi \ , \qquad (A.2.2)$$

or

$$F_L = W \frac{y}{\sqrt{(\Delta R)^2 - y^2}} \quad . \tag{A.2.3}$$

Differentiating with respect to y gives

$$K_L = \frac{dF_L}{dy} = \frac{W}{\Delta R} \left(\frac{1}{1 - (y_0/\Delta R)^2} \right)^{\frac{3}{2}} \quad . \tag{A.2.4}$$

3. Choice of Initial Displacement. Figure A-2 illustrates a constraint placed upon the choice of y_0 by conformity with current practice. Rails are laid so that their plane of symmetry is inclined from the vertical at an angle α. This is done so that a wheel of conicity α will transmit a normal load directly along the web of the rail. The same consideration demands that a profiled wheel designed for use over conventional track should have $\psi_0 = \alpha$. Applying this constraint gives

$$K_L = \frac{W}{\Delta R} \sec^3\alpha \quad . \tag{A.3.1}$$

4. Sensitivity to Initial Displacement. An important consideration in the use of profiled wheels is the sensitivity of K_L to gauge variation. If wheelset gauge remains constant, track gauge error is manifested in error in y_0. In Figure A-3, normalized lateral stiffness is plotted against the quantity $(y_0/\Delta R)$. K_L is seen to be insensitive to gauge error up to about $0.4\Delta R$.

5. Degree of Nonlinearity in Lateral Force Relationship. The use of a constant, K_L, to describe the lateral force relationship rests upon the assumption that the relationship may be usefully

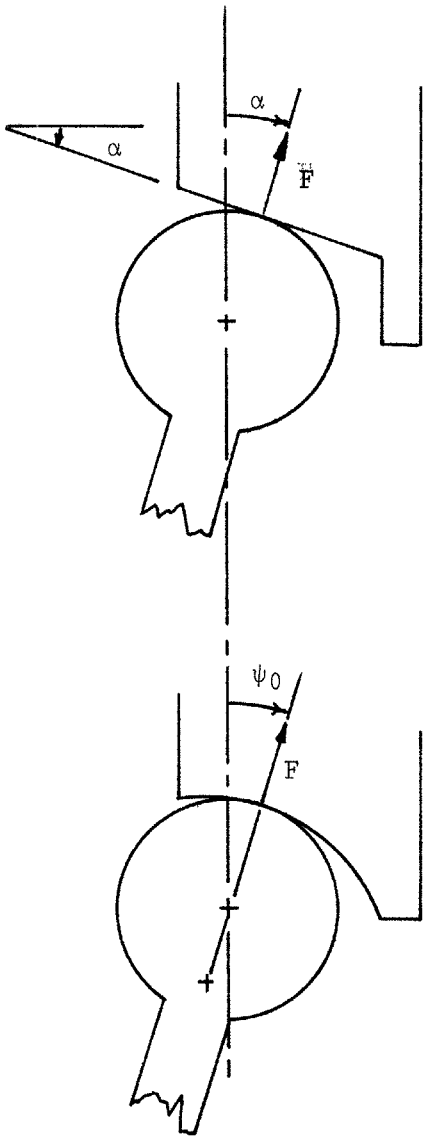

FIGURE A-2

Choice of Contact Angle to Conform to Standard Conicity

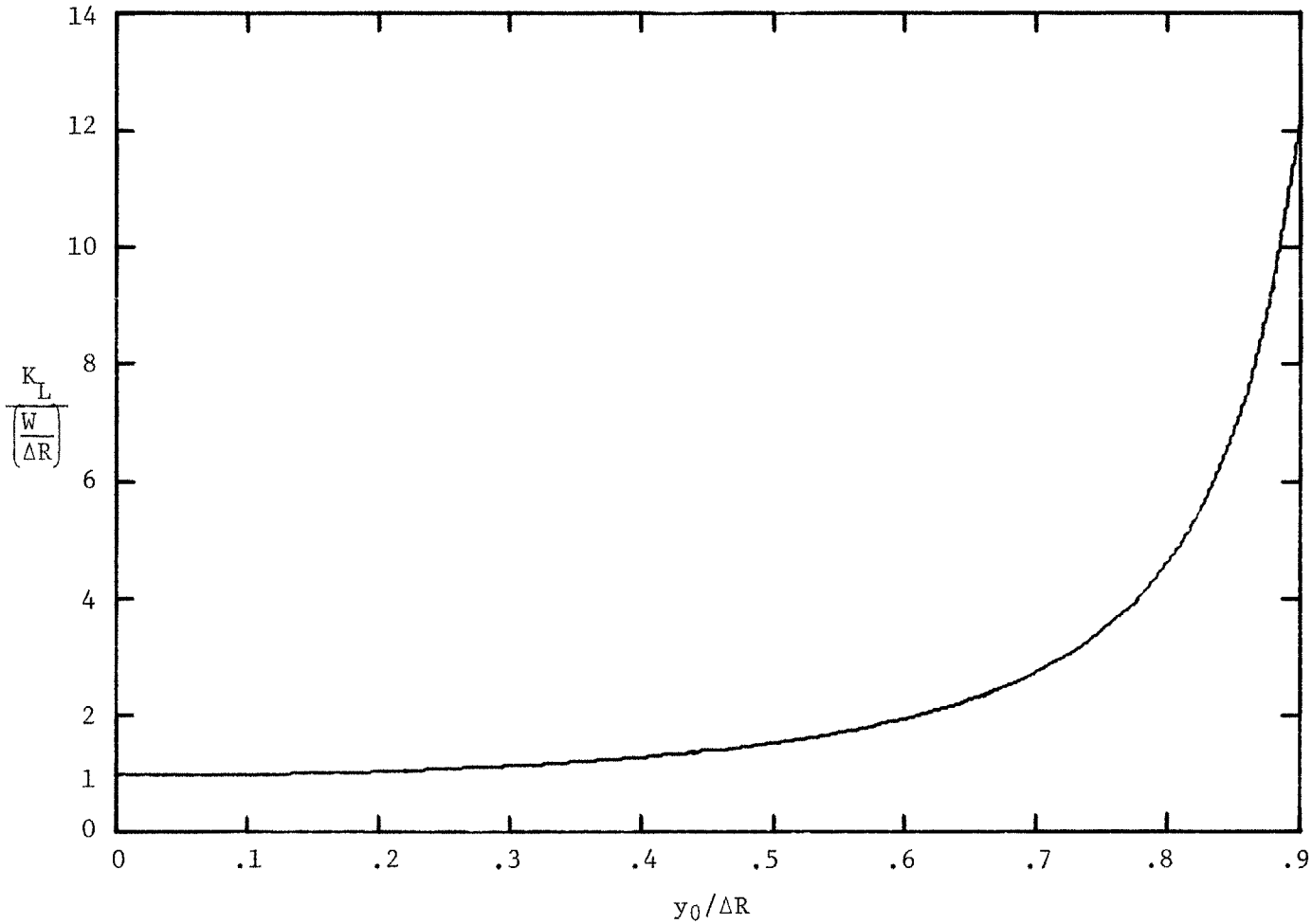

FIGURE A-3

Effect of Initial Displacement from Vertical On Linearized Lateral Stiffness

linearized about its operating point. The net restoring force due to the lateral displacement of a wheelset (pair of wheels) from its central position is plotted in Figure A-4 for three values of normalized initial displacement. The curves show a shape characteristic of a stiffening, nonlinear spring. This stiffening behavior is useful in that it gives a smoother limiting action than does a conventional flange; but the significant feature of the curves here is the extent of the nearly straight segments near the origin. For $y_0=0$, for example, the linearization is good to at least $\pm.4\Delta R$.

6. Yaw Gravitational Stiffness. When a wheelset yaws without lateral movement, it experiences a torque due to the preload F_0. To first order, F does not change with yaw; so the linearized yaw stiffness K_Y may be written as

$$K_Y = \frac{W}{\Delta R} \frac{(-2\ h\ y_0)}{\sqrt{1 - (y_0/\Delta R)^2}} \quad . \tag{A.6.1}$$

Notice that for positive y_0, K_Y is negative and therefore destabilizing. When a wheelset is rigidly mounted in a rectangular truck of dimensions $2kh$ by $2h$, however, the total effective yaw stiffness for the entire truck is $2K_Y+4K_L k^2h^2$. Comparison of equations (A.2.4) and (A.6.1) reveals that the destabilizing stiffness K_Y can be neglected when $y_0<<k^2h$. Since this is almost always the case for conventional trucks, K_Y is not used in the remainder of this work.

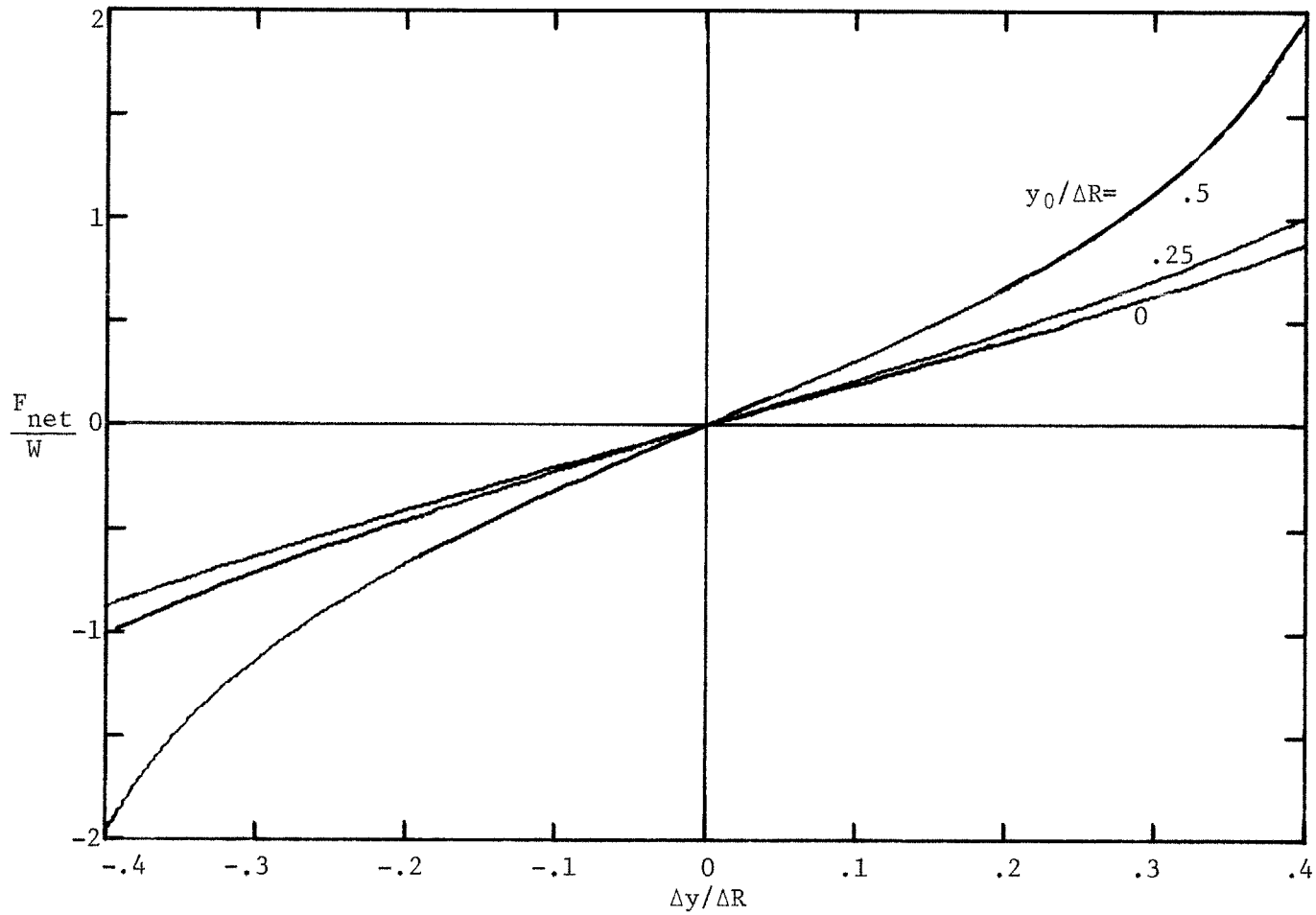

FIGURE A-4

Net Restoring Force due to an Opposed Pair of Profiled Wheels

APPENDIX B

MATRIX METHODS FOR FREQUENCY - DOMAIN ANALYSIS

Once the equations of motion of a system have been written in state - variable form, it is possible to obtain input - output relations in the Laplace (or frequency) domain using certain widely known techniques [64]. Important simplifications arise when only a single input and a single output are of concern. When it is possible to derive the transfer functions totally or partially symbolically (as opposed to numerically), one may take advantage of structural properties of the system matrices to reduce computation further.

1. System Representation in State Variable Form. A linear, time - invariant, single - input system may be represented thus:

$$\frac{d\underline{x}}{dt} = \underline{a}\,\underline{x} + \underline{b}\,u \quad , \tag{B.1.1}$$

where $\underline{x}$ is a vector of the state variables x_1, x_2, ... x_n; $\underline{a}$ is the n by n system matrix; $\underline{b}$ is the n x 1 input matrix; and u is the input variable. Throughout this thesis, u is identified with the lateral centerline deviation at the front axle, y_{rf}. The system responds not only to the front axle position, however, but also to its velocity and to the position and velocity of the rail as propagated (delayed) to the second and succeeding axle positions. The input matrix $\underline{b}$ must therefore include linear operators -- the time derivative, d/dt, and the delay, $\Delta(\tau)$ -- to account for these effects.

Equation (B.1.1) is linear and may be Laplace transformed (with the usual assumption of zero initial conditions) to give:

$$s\underline{X} = \underline{A}\,\underline{X} + \underline{B}\,U \quad , \tag{B.1.2}$$

where capitals denote Laplace transforms. The linear operators imbedded in $\underline{b}$, when transformed, become:

$$L[d/dt] = s \text{ , and} \tag{B.1.3}$$

$$L[\Delta(\tau)] = e^{-\tau s} \quad . \tag{B.1.4}$$

2. Compressed Matrices. There are many formulations of system equations which give rise to relatively sparse $\underline{a}$ matrices. An especially common case is that in which some of the state variables are derivatives of others. In such cases, it is straightforward to solve for some transformed variables in terms of the others by inspection. The result is a new set of equations which, although reduced in number, are equivalent to the original set. In particular, such compressed transformed equations of motion are n^{th} order in the Laplace variable s.

The compressed equivalent of Equation B.1.2 is

$$\underline{S}\,\hat{\underline{X}} = \hat{\underline{A}}\,\hat{\underline{X}} + \hat{\underline{B}}\,U \quad , \tag{B.2.1}$$

where $\hat{\underline{X}}$ is the reduced state variable vector, $\hat{A}$ and $\hat{B}$ are compressed matrices, and $\underline{S}$ is a diagonal matrix in powers of s.

As a simple example of this compression, consider a second - order system subject to an input and its derivative. The system equations

are:

$$\frac{d}{dt}\begin{bmatrix} x_1 \\ x_2 \end{bmatrix} = \begin{bmatrix} 0 & 1 \\ -\omega_n^2 & -2\xi\omega_n \end{bmatrix}\begin{bmatrix} x_1 \\ x_2 \end{bmatrix} + \begin{bmatrix} 0 \\ \omega_n^2 + 2\xi\omega_n(d/dt) \end{bmatrix} u \ . \qquad (B.2.2)$$

Since x_2 is the time derivative of x_1, compression of the matrices is possible. The 2 by 2 $\underline{A}$ matrix, the 2 by 1 $\underline{B}$ matrix, and the two - element $\underline{X}$ vector become scalar polynomials in s, with

$$\hat{\underline{A}} = -\omega_n^2 - 2\xi\omega_n s \ ,$$
$$\hat{\underline{B}} = \omega_n^2 + 2\xi\omega_n s \ ,$$
$$\underline{S} = s^2 \ , \text{ and}$$
$$\hat{\underline{X}} = x_1 \ .$$

The usefulness of compressing the system equations in this manner lies in the fact that the number of element multiplications required to solve for a transfer function given an n by n $\underline{A}$ matrix is approximately proportional to n!. The symbolic evaluation procedure must carry out or at least check all of these multiplications to be valid. A reduction in the size of the matrices which also reduces their sparseness therefore improves computational efficiency.

3. Solution for Transfer Functions. Given the set of n_c compressed and transformed system equations of Equation B.2.1, where $n_c \leq n$, any required transfer functions may be obtained. If the desired output is not among the state variables, it is first necessary to transform the state vector according to the following

linear combination:

$$\hat{\underline{X}}_o = \underline{T}\,\hat{\underline{X}} \quad , \tag{B.3.1}$$

where $\underline{T}$ is a square, nonsingular matrix. Under this transformation the i^{th} element of $\hat{\underline{X}}_o$ is the required output. Substituting (B.3.1) into (B.2.1) gives

$$(\underline{S}-\hat{\underline{A}})\,\underline{T}^{-1}\,\hat{\underline{X}}_o = \hat{\underline{B}}\,U \quad . \tag{B.3.2}$$

In this form, one may solve for the i^{th} element of $\hat{\underline{X}}_o$ using Cramer's Rule. The required transfer function is

$$G(s) = \frac{X_i(s)}{U(s)} = \frac{\text{numerator}}{\text{denominator}} \quad . \tag{B.3.3}$$

The denominator (or characteristic polynomial) has the value

$$\det\,[\,(\underline{S}-\hat{\underline{A}})\,T^{-1}\,]\;;$$

and the numerator is obtained by substituting the column vector $\hat{\underline{B}}$ for the i^{th} column of the matrix $[(\underline{S}-\hat{\underline{A}})T^{-1}]$ and taking the determinant of the resulting matrix.

4. Implementation of Symbolic Transfer Functions using Macsyma.

The procedure described above for the evaluation of transfer functions has been implemented using Macsyma, a symbolic mathematics computer facility developed by Project MAC [66]. The system allows for some or all of the symbolic names used in the matrices to be specified numerically, the transfer function being parametric in the unassigned variable names.

Figure B-1 illustrates the use of Macsyma to generate the transfer function for the system of Equation B.2.2. The block which computes the function is included in the figure. Input consists of the compressed matrix $(\underline{S}-\underline{\hat{A}})$ ("A" internally); the compressed input matrix $\underline{\hat{B}}$ ("B" internally); the transformation matrix $\underline{T}^{-1}$ ("T" internally); the size of the compressed system, n_c ("N" internally); and the index of the selected output variable, i ("J" internally). Notice that for the sake of illustration, the $\underline{A}$ matrix is not compressed to a scalar.

```
(C1) "example of macsyma use to evaluate transfer functions" $
(C2) "definition of routine tf which carries out computation" $
(C3) "s is the laplace variable.  etsp2, etsm2, etsl are
          exponentials in s which are used for delays" $
(C4) tf(a,b,t,n,j) := block( w:a.t , w:ev(w) , den:determinant(w) ,
                             den:rat(den,s) , for i:1 thru n do
                             w[i,j]:ev(b[i,1]) , num:determinant(w) ,
                             num:rat(num,etsm2,etsp2,etsl,s) ) $
(C5) "enter matrices for simple second-order system" $
(C6) a:matrix([s,-1],[omn**2,s+2*z*omn]) ;

                     [  S            -1     ]
                     [                      ]
(D6)                 [     2                ]
                     [ OMN     S + 2 Z OMN ]

(C7) b:matrix([0],[omn**2+2*z*omn*s]) ;

                     [          0         ]
                     [                    ]
(D7)                 [     2              ]
                     [ OMN  + 2 Z OMN S ]

(C8) t:ident(2) ;

                     [ 1  0 ]
(D8)                 [ 0  1 ]

(C9) "find transfer function for first element of x-vector" $
(C10) tf(a,b,t,2,1) $
(C11) num / den ;

                                        2
                       2 Z OMN S  +  OMN
(D11)                  ------------------------
                        2                      2
                       S   +  2 Z OMN S  +  OMN

(C12) "substitute a known value for z" $
(C13) z:.707 $
(C14) keepfloat:true $
(C15) tf(a,b,t,2,1) $
(C16) num / den ;
                                        2
                     1.414 OMN S  +  OMN
(D16)                ------------------------
                      2                      2
                     S   +  1.414 OMN S  +  OMN
```

FIGURE B-1

BIOGRAPHICAL NOTE

Robert Lee Jeffcoat was born on March 14, 1948, in Spartanburg, South Carolina, and educated in the Spartanburg city schools. He entered the Massachusetts Institute of Technology in September 1966 and received the degrees of Bachelor of Science in Mechanical Engineering, Master of Science in Mechanical Engineering, and Mechanical Engineer simultaneously in June 1972. He is a member of the American Society of Mechanical Engineers, Tau Beta Pi, Pi Tau Sigma, and Sigma Xi.

He was married to Marjorie Kaplan Jeffcoat on August 12, 1973. Both have been resident tutors in an M.I.T. undergraduate dormitory since September 1973.